

Journal of Environmental & Earth Sciences

Volume 5 • Issue 2 • October 2023 ISSN 2661-3190(Online)



Editor-in-Chief

Prof. Shuanggen Jin

Henan Polytechnic University; Shanghai Astronomical Observatory, China

Editorial Board Members

Fengtai Zhang, China	Nimal Shantha Abeysingha, Sri Lanka
Junfeng Wang, China	Senlin Zhu, China
Chin H. Wu, United States	Bing Xu, China
Faming Huang, China	Shaoliang Zhang, China
Carmine Apollaro, Italy	Kebede Wolka Wolancho, Ethiopia
Eugen Victor Cristian Rusu, Romania	Carla Patrícia Silva, Portugal
Lampros Vasiliades, Greece	Jixiang Yang, China
Karoly Nemeth, Hungary	Marco Kondracki Alcântara, Brazil
Vincenzo Convertito, Italy	Senthil Kumar Ramalinghm, Sultanate of Oman
Shaoyong Lu, China	Gino Dardanelli, Italy
Souhila Ait Hamoudi, Algeria	Ronglin Tang, China
Maria Barbara Zygadlo, Poland	Masoud Masoudi, Iran
Abdeltif Amrane, France	Jingying Fu, China
Aqil Tariq, United States	Miklas Scholz, South Africa
Rossana Sanfilippo, Italy	Ayad M. Fadhil Al-Quraishi, Iraq
Yazan Mohammad Taamneh, Jordan	Ramayah Thurasamy, Malaysia
Teodosio Lacava, Italy	Ram Kishor Fagodiya, India

Volume 5 Issue 2 • October 2023 • ISSN 2661-3190 (Online)

Journal of Environmental & Earth Sciences

Editor-in-Chief

Prof. Shuanggen Jin

Contents

Articles

- 1 Effects of Different Cations on the Flocculation and Sedimentation of Static Fine-Grained Sediments**
Xiaomin Liu, Yaotian Yang, Rui Wang, Wenjuan Wang, Qiang Luo
- 15 The Relationship between Water Resources Use Efficiency and Scientific and Technological Innovation Level: Case Study of Yangtze River Basin in China**
Guangming Yang, Qingqing Gui, Junyue Liu, Fengtai Zhang, Siyi Cheng
- 36 Sustainability Evaluation of Mangrove Forest Management System of Tagbanua Tribe in Bgy. Manalo, Puerto Princesa City, Palawan, Philippines**
Mark Joseph J. Buncag, Jaybie S. Arzaga, Liezl F. Tangonan, Jeffrey H. de Castro, Mary Claire M. Villanueva, Lilia Margallo, Imelda R. Lactuan, Sheryl G. Docto, Angelo V. Garcia, Princes Eunice C. Denosta, Sweet Angelikate L. Villaruel
- 50 Energy Emissions Profile and Floating Solar Mitigation Potential for a Malaysia's State**
Suraya Nabilah Zaini, Azlin Mohd Azmi, Annie Syazrin Ismail
- 76 Hyperspectral Inversion and Analysis of Zinc Concentration in Urban Soil in the Urumqi City of China**
Qing Zhong, Mamattursun Eziz, Mireguli Ainiwaer, Rukeya Sawut
- 88 SAR Change Detection Algorithm Combined with FFDNet Spatial Denoising**
Yuqing Wu, Qing Xu, Zheng Zhang, Jingzhen Ma, Tianming Zhao, Xinming Zhu
- 102 Hydrogeological Investigations of Groundwater and Surface Water Interactions in the Berg River Catchment, Western Cape, South Africa**
Seiphi Prudence Mabokela, Ntokozo Malaza
- 118 Comparison of Machine Learning Methods for Satellite Image Classification: A Case Study of Casablanca Using Landsat Imagery and Google Earth Engine**
Hafsa Ouchra, Abdessamad Belangour, Allae Erraissi

Review

- 61 Maximizing Oil Palm Yield: Innovative Replanting Strategies for Sustainable Productivity**
Ahmed Abubakar, Susilawati Kasim, Mohd Yusoff Ishak, Md Kamal Uddin

ARTICLE

Effects of Different Cations on the Flocculation and Sedimentation of Static Fine-Grained Sediments

Xiaomin Liu^{1,2}, Yaotian Yang^{2,3*}, Rui Wang⁴, Wenjuan Wang^{2,3}, Qiang Luo⁵

¹ College of Water Conservancy and Civil Engineering, Inner Mongolia Agricultural University, Hohhot, Inner Mongolia, 010018, China

² Collaborative Innovation Center for Integrated Management of Water Resources and Water Environment in the Inner Mongolia Reaches of the Yellow River, Hohhot, Inner Mongolia, 010018, China

³ Inner Mongolia JinHua Yuan Environmental Resource Engineering Consulting Co., Ltd, Hohhot, Inner Mongolia, 010020, China

⁴ Wuhai Wuda District Agriculture of Animal Husbandry and Water Affairs Bureau, Wuhai, Inner Mongolia, 016000, China

⁵ Yellow River Hai Bo-Wan Water Conservancy Project Development Center, Wuhai, Inner Mongolia, 016000, China

ABSTRACT

Natural water bodies mostly contain cations, and the type and content of these cations are the main factors affecting the flocculation of fine-grained cohesive sediments and the floc sedimentation rate at the interface between clear and turbid water. From the microscopic aspect, this study examined the changing patterns of porosity and the fractal dimension of the flocs of fine-grained cohesive sediments. Sedimentation experiments under different sediment contents and electrolyte conditions were conducted, and microscopic images of the flocs were analysed using Image-Pro Plus (IPP) and MATLAB based on the fractal theory. From the macroscopic aspect, this study experimentally investigated the flocculation and sedimentation of fine-grained cohesive sediments and proposed a sedimentation rate equation by introducing an ion concentration-related parameter into an existing sedimentation rate equation (stagnation zone) based on the adsorption isotherm equation. The equation proposed in this study was validated with measured data. The calculated values were in good agreement with the measured values, with a relative error of 16%. The findings of this study provide a reference for further research on the flocculation and sedimentation of fine-grained cohesive sediments in different water bodies.

Keywords: Flocs; Electrolyte; Fractal dimension; Porosity; Sedimentation rate

*CORRESPONDING AUTHOR:

Yaotian Yang, Collaborative Innovation Center for Integrated Management of Water Resources and Water Environment in the Inner Mongolia Reaches of the Yellow River, Hohhot, Inner Mongolia, 010018, China; Inner Mongolia JinHua Yuan Environmental Resource Engineering Consulting Co., Ltd, Hohhot, Inner Mongolia, 010020, China; Email: 645347148@qq.com

ARTICLE INFO

Received: 29 May 2023 | Revised: 15 July 2023 | Accepted: 19 July 2023 | Published Online: 9 August 2023

DOI: <https://doi.org/10.30564/jees.v5i2.5747>

CITATION

Liu, X.M., Yang, Y.T., Wang, R., et al., 2023. Effects of Different Cations on the Flocculation and Sedimentation of Static Fine-Grained Sediments. *Journal of Environmental & Earth Sciences*. 5(2): 1-14. DOI: <https://doi.org/10.30564/jees.v5i2.5747>

COPYRIGHT

Copyright © 2023 by the author(s). Published by Bilingual Publishing Group. This is an open access article under the Creative Commons Attribution-NonCommercial 4.0 International (CC BY-NC 4.0) License. (<https://creativecommons.org/licenses/by-nc/4.0/>).

1. Introduction

The Yellow River carries a higher proportion of sediment than water. Due to the mismatch between water and sediment fluxes, the Yellow River is famous for its high proneness to siltation, levee breaches, and channel migration. Water and sediment changes have always been a focus and challenge of fluvial research. Sediment-laden rivers often carry a certain proportion of cohesive sediment. Compared with noncohesive sediments, fine-grained cohesive sediments has special electrochemical properties and are thus highly prone to form flocs in water^[1]. Sediment flocculation and sedimentation have important effects on sediment transport, lake water quality, siltation in reservoirs and canals, and migrations of channels and estuaries of the Yellow River^[2]. Therefore, research on the flocculation of cohesive fine-grained sediment is of great importance for analysing changes in riverbed erosion and siltation and improving the ecological environment of water bodies.

According to the basic principle of flocculation, small particle size is the basic condition for sediments to form flocs, cations are the fundamental driver for floc formation, and the ion concentration also determines the degree of flocculation and floc size^[3]. Some studies have investigated the effects of different cation types and concentrations on sediment flocculation and sedimentation. For example, Wang et al.^[4-11] have experimentally demonstrated that flocculation is more likely to occur in an ion-rich environment than in a freshwater environment and that the ions with higher valence are more likely to cause flocculation. Qiao^[12], Zhang^[13], and Lee et al.^[14] introduced the Extended Derjaguin-Landau-Verwey-Overbeek (XDLVO) theory in colloidal chemistry into the 3D lattice Boltzmann model of particle sedimentation and used numerical simulation to analyse the effect of salt ion concentration on the sedimentation of fine-grained cohesive sediments. These studies have found that increasing salinity in freshwater environments is more likely to produce flocculation and that as the salt ion concentration increases, salt ions initially appear to promote the flocculation of sediments and the formation of larger flocs. However, when the salt ion concentration exceeds a cer-

tain value, a counter-ion layer is formed on the outer surface of fine-grained sediment, thus inhibiting sediment flocculation^[15], and consequently, the fine-grained sediment tends to be stable and deposits only due to its own weight. Through MATLAB programming, Chai et al.^[16] reconstructed the 3D images of the fine-grained sediment flocs with the grey values of the SEM images using MATLAB's surf function (with the pixel positions in planar images as X and Y axes and the grey values of images as Z axis), calculated the 3D fractal dimension of the flocs using the box-counting method through MATLAB programming, and deduced an equation for the floc sedimentation rate of the fine-grained sediment at the interface between turbid and clear water during hydrostatic sedimentation based on the calculated 3D fractal dimension of the without incorporating an ion concentration-related parameter.

In summary, many studies have investigated the effect of cation concentration on sediment flocculation and sedimentation. However, only a few studies have analysed the structural characteristics of flocs, and most of these studies segmented the images of flocs through the single-threshold method^[17], which resulted in a certain subjectivity. In addition, there are relatively few studies on the flocculation and sedimentation of fine-grained sediment from the perspectives of floc porosity and fractal dimension. To this end, this study used Image-Pro Plus (IPP), which is an image processing software that can directly import the floc images obtained by microscopy to extract the floc features, use the scales in the microscopic images for spatial scale calibration, and automatically track and measure object properties, thus reducing the influence of human error during image processing and improving the accuracy of the results. Furthermore, this study used MATLAB to analyse the effects of different cation concentrations, sediment concentrations, and electrolyte strength on the flocculation and sedimentation of cohesive sediments based on the fractal theory and then established a sedimentation rate equation for cohesive sediments incorporating an electrolyte concentration-related parameter based on the analysis results.

2. Materials and methods

2.1 Experimental equipment

The main equipment used in this experiment included an AE200 electronic balance, a graduated cylinder (1000 mL), a beaker, a syringe, a pipette, and a dropper. A Winner-2008A fully automatic wet laser particle size analyser was used for sediment sample grading, and an Olympus BX51 fluorescence microscope was used to capture the floc images. The images were then analysed and measured with IPP, which is an imaging software that can automatically track and measure the properties of imported objects, thus improving the image processing accuracy compared with the currently used image processing methods and reducing subjective human errors, allowing the internal structures of flocs to be better analysed and processed.

2.2 Experimental materials

The cohesive fine-grained sediment samples used in this experiment were sampled from the surface silt (0-20 cm) of the Haibowan reservoir during the implementation of the Reservoir Ecological Management Pilot Project of the Haibowan Conservancy Hub over the Yellow River in April 2020. Litter impurities and coarse grains were removed from the cooled and air-dried sediment. Before the experiment, a 0.074-mm standard sieve was used to remove large sediment particles and impurities, and then the sedimentation method was used for further sorting and sampling. The grading curves of the sediment samples were measured using a HELOS/OA-SIS intelligent, fully automatic, full-range dry laser particle size analyser, and the median particle sizes of the sediment samples were 0.01 and 0.02 mm, as shown in Figure 1.

2.3 Experimental methods

Hydrostatic sedimentation experiment

The experiment was carried out in a graduated cylinder with a height of 30 cm, a diameter of 6 cm, and a volume of 1000 mL. Before the experiment, a

scale ruler was attached to the outer wall of the graduated cylinder to record the position of the interface during the sedimentation, and then deionized (DI) water, quantitative cation concentration electrolytes (Na^+ , Ca^{2+} , Al^{3+}), and quantitative sediment sample concentrations (50 kg/m^3 , 70 kg/m^3 , 100 kg/m^3 , 150 kg/m^3) were added. The solution was fully stirred with a stirrer for approximately 1 min to evenly distribute the sediment. The distance and time of the uniform sedimentation section at the interface of clear and turbid water were recorded, the uniform sedimentation rate of the floc was calculated, and the changing pattern of the sedimentation rate was analysed. The specific experimental process is shown in Figure 2.

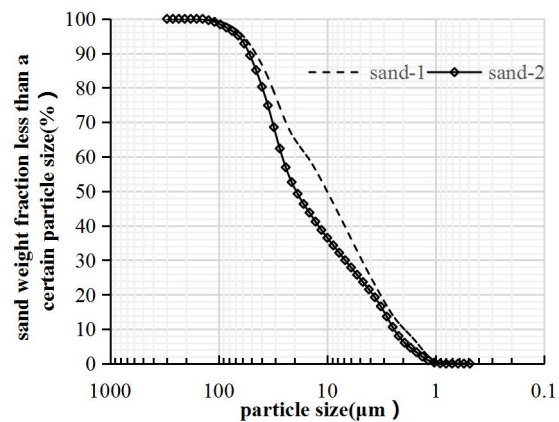
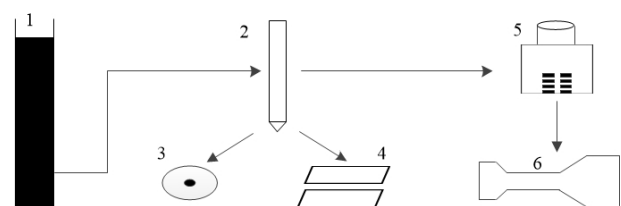


Figure 1. Experimental sand grading curve.



1-Settling cylinder 2-pipette 3-Petri dish 4-slide 5-Freeze dryer 6-microscope

Figure 2. Experimental instrument and workflow diagram.

Collection of floc samples

When collecting floc samples, to completely obtain the floc structure that is easily broken, a pipette with a larger inner diameter was used to gently transfer the flocs from the graduated cylinder to the glass slide. Subsequently, the slides were placed into a freezer for 8 hours and then freeze-dried, and the dried floc samples were used for follow-up research.

The sampling temperature was controlled at 15 ± 1 °C to reduce the effect of temperature on sedimentation, and each test was repeated three times.

Image data extraction and analysis

In image data extraction and analysis, the single-threshold method is commonly used to segment the floc image^[17]. In this paper, a BX51+DP70 microscope was used to scan and observe the floc samples, and the microscopic images of flocs at different magnifications (10, 20, and 40 times) were compared and analysed. Finally, the microscopic images at a magnification of 20 times were used for subsequent studies (**Figure 3**). First, IPP software was used to adjust the image to greyscale, adjust the brightness and contrast of the image, weaken the image background, and strengthen the floc boundary (**Figure 4**), and then the image processing function in the software was used to analyse the floc diameter, area, and perimeter and the pore diameter, area, and perimeter of the floc to calculate the floc porosity (**Figure 5**). The 2D digital images of the flocs formed under different conditions were analysed with the box-counting method through MATLAB to calculate the fractal dimensions and to analyse the changing pattern of the fractal dimensions of the flocs.

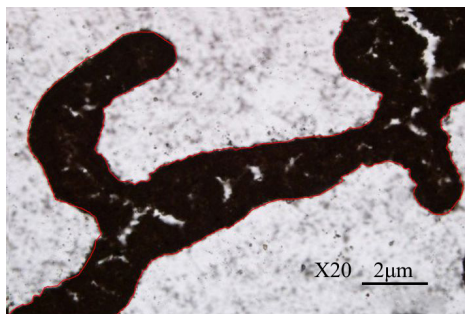


Figure 3. SEM image of the flocs (20x).

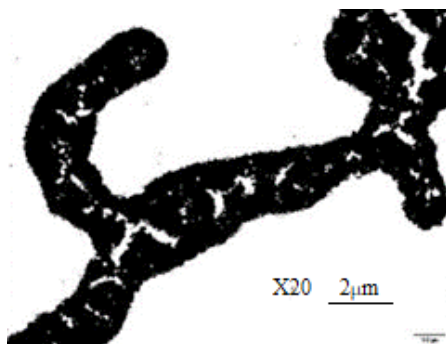


Figure 4. Floc image after IPP treatment.

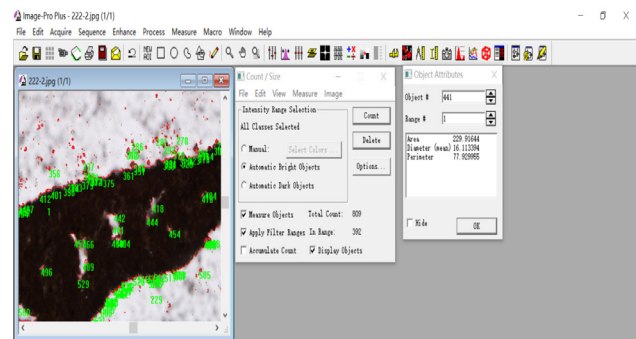


Figure 5. Data extraction.

3. Results and analysis

3.1 Analysis of floc sedimentation rate

Analysis of the change in the sedimentation rate of flocs with different particle sizes

The physical and chemical properties of sediment particles are the decisive factors for water and sediment control in the Yellow River, and the median particle size is the most important parameter^[18]. Therefore, this paper mainly studied the sedimentation of flocs formed by sediments with different particle sizes when other conditions are fixed.

According to the test results of sediment samples (1) and (2) under the same initial sediment content and electrolyte conditions, the sedimentation rate curves of flocs formed by sediments with different particle sizes were obtained, as shown in **Figure 6**.

Figure 6a indicates that when other conditions are fixed, the sedimentation curves of flocs formed by sediments with different particle sizes with the change in sediment concentration almost overlap, but as the particle size increases, flocculation decreases, and the floc sedimentation rate decreases, mainly because the finer the sediment particles are, the larger the specific surface area, and the easier the adhesion between the sediment particles.

When the sediment content is 150 g/L, the fluctuation range of the sedimentation rate of flocs formed by sediments with different particle sizes is not very large. Alternatively, when the sediment concentration reaches a certain value, the change in particle size can be considered to have little effect on the floc

sedimentation rate.

Figure 6b reveals that when other conditions are fixed, the sedimentation rate of flocs formed by sediments with different particle sizes increases with increasing electrolyte concentration, mainly because with increasing electrolyte concentration, the potential of sediment particles gradually decreases; that gradual decrease is conducive to mutual bonding between particles, and the change in electrolyte concentration plays a major role in the sedimentation of cohesive sediments. When the electrolyte concentration is too large, the decrease in the floc sedimentation rate of sediment sample (2) is faster than that of sediment sample (1). The preliminary analysis indicates that when the electrolyte concentration exceeds a certain value, the effect of electrolyte on flocculation decreases, and the formed flocs capture the surrounding sediment particles in the sedimentation. The smaller the particle size is, the larger the specific surface area and the stronger the adsorption effect, which supports the electrochemical properties of fine-grained sediments [19].

In summary, the effect of sediment particle size on floc sedimentation is not independent but depends on the electrolyte strength, initial sediment content, and cation valence. When the particle size of the sediment is less than 0.01 mm, the physical and chemical effects on the particle surface can produce microstructures between the particles [18]. Therefore, this paper mainly studied the change in the floc sedimentation rate of sediment sample (1) under different sediment concentrations, electrolyte concentrations, and cation valences.

Analysis of the change in the sedimentation rate of the flocs with different particle sizes

Figure 7 indicates that the sedimentation curve of flocs can be roughly divided into two stages, floc sedimentation and gel-like network sedimentation, possibly because initially, the particles collide and bond with each other to form flocs, and the sedimentation is fast, whereas in the later sedimentation, the flocs further flocculate to form a gel-like network structure, and the sedimentation is slow. When the sediment content

is large enough (150 g/L), the transition from the fast stage to the slow stage is more obvious because the sedimentation rate of the floc is much larger than that of the gel-like network. When the sediment content is 50 g/L and 70 g/L, the sedimentation curves deviate significantly from those of other sediment contents, which shows that when the initial sediment content is low, the floc sedimentation is faster than when the sediment content is higher, possibly because when the number of original sediment particles is small, the average distance between particles is large; because such large distances are not conducive to the further formation of the gel-like network structure, particles sediment faster due to flocculation.

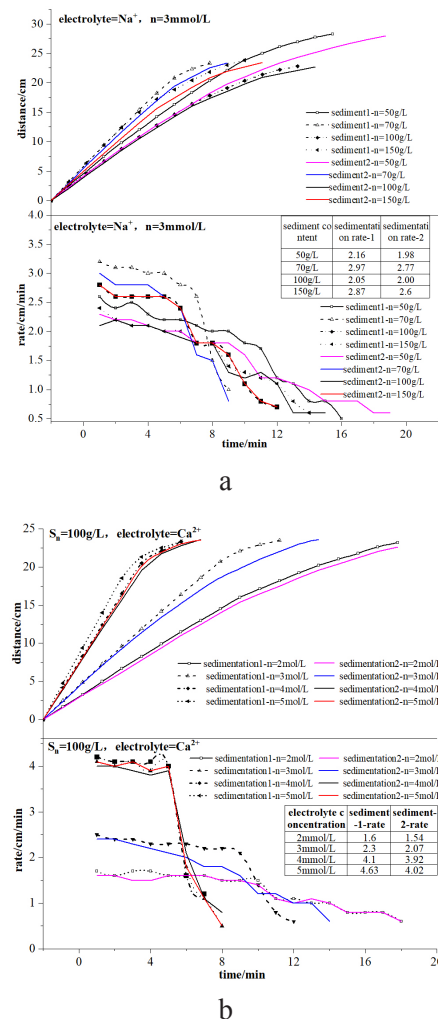


Figure 6. The curve of the floc settling process under different sediment particle sizes. (a) Sedimentation curve of the flocs ($n = 3 \text{ mmol/L}$, $z = 1$). (b) Sedimentation curve of the flocs ($S_n = 100 \text{ g/L}$, $z = 2$).

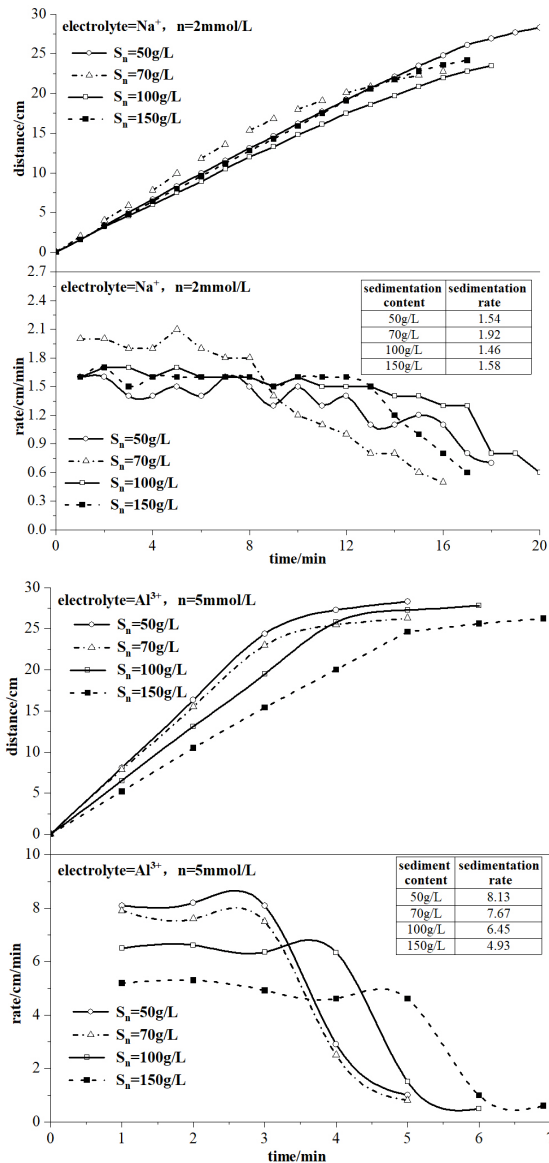


Figure 7. The curve of the floc settling process under different sediment concentrations.

Analysis of the change in floc sedimentation rate under different electrolyte concentrations

Figure 8 shows that when other influencing factors remain unchanged, with the increase in electrolyte concentration, the trends of floc sedimentation are consistent, and the changes in the rapid sedimentation stage almost overlap. When the electrolyte concentration reaches the optimum, sediment particles tend to stick to form flocs during sedimentation, the sedimentation becomes faster, and the flocculation and sedimentation curve tends to deviate from curves of other electrolyte concentrations, with the turning point occurring significantly earlier. Accord-

ing to the DLVO theory and the electric double-layer theory, the preliminary analysis indicates that under the comprehensive cohesive force of the fine-grained sediment particles in the suspension system, when other influencing factors are unchanged, higher cation valence and greater electrolyte strength result in a thinner electric double layer on the surfaces of the sediment particles and thus weaker interparticle repulsion but have almost no effect on the interparticle attraction. Therefore, the increase in the comprehensive force leads to flocculation between the sediment particles, which form relatively dense flocs, thereby increasing the floc sedimentation rate.

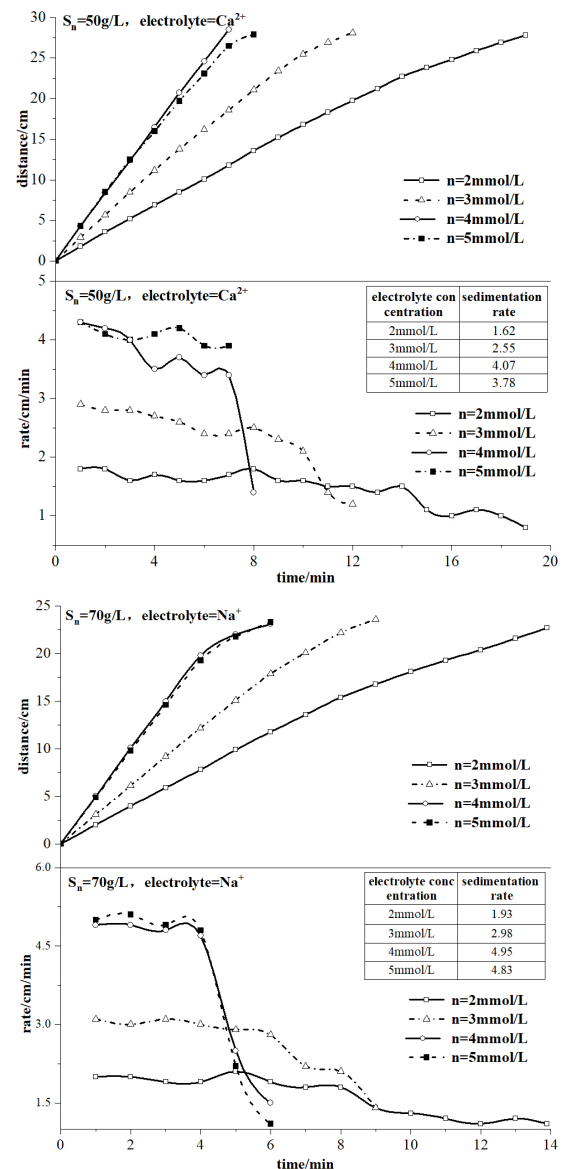


Figure 8. The curve of the floc settling process under different sediment concentrations.

Analysis of the change in the floc sedimentation rate under different cation valences

Figure 9 shows that when the other influencing factors are fixed, with the increase in cation valence, the turning point of the sedimentation at the interface between clear and turbid water becomes increasingly earlier. In the system with the addition of Al^{3+} ions, the floc sedimentation is the fastest, with large fluctuations [20]. Comparing the changes in floc sedimentation rate under different electrolyte strengths reveals that the effect of cationic valence on floc sedimentation is greater.

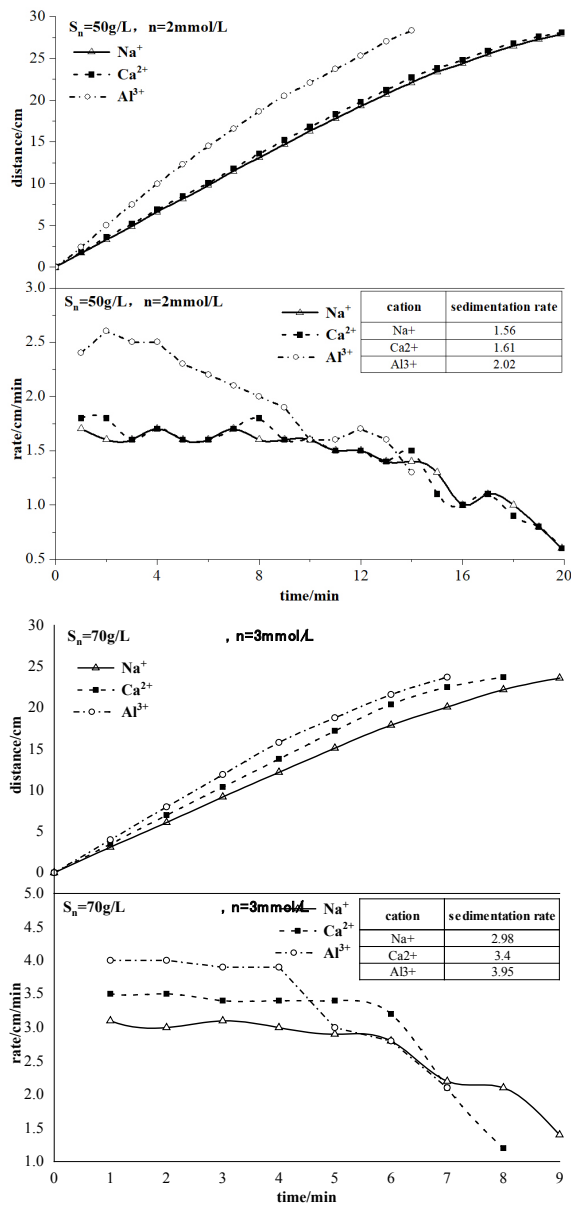


Figure 9. Floc settling process curve under different cationic valence conditions.

3.2 Analysis of the morphological characteristics of flocs

Calculation of floc pore structure parameters

Based on the images of the floc sample observed by microscope scanning, the cross-sectional area S of the floc and the pore area S_a in the floc can be obtained by using IPP image processing software. According to the definition of plane porosity, the porosity of the floc can be calculated.

$$n = \frac{S_a}{S} \times 100\% \quad (1)$$

where n is the porosity of the sediment floc; s is the equivalent area of the polygon corresponding to the floc, μm^2 ; and s_a is the area of the equivalent polygon of pores within the floc, μm^2 .

Figure 10 indicates that when the sediment concentration is constant, the floc porosity decreases with increasing electrolyte strength, and under the same electrolyte strength, the floc porosity decreases with increasing cation valence, which is related to the force between the cohesive sediment particles. According to the DLVO theory, with the increase in the cationic valence, the repulsive force between the sediment particles gradually decreases, which facilitates bonding between particles. As a result, flocs are formed more densely, and thus, the porosity of the flocs is reduced.

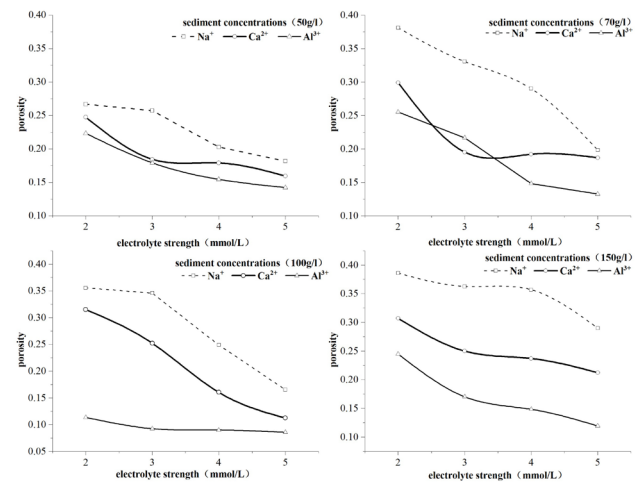


Figure 10. Variation curves of the floc porosities under different conditions.

Fractal dimension of flocs

This paper used MATLAB to find the fractal di-

mension of flocs. Using the box-counting method, a program was written to perform grid division and statistical analysis of the black-and-white binary image ^[19], and a series of data pairs of “grid size” and “number of covered grid cells” were obtained, that is, the data pairs of submatrix order and the number of submatrices containing image points (pixel is 0). Then, the data points were drawn in double logarithmic coordinates, and linear regression analysis was performed; the negative value of the slope of the line is the box-counting dimension of the image (the slope of the line is the absolute floc fractal dimension), and the results are shown in **Figure 11**. The changing pattern of the fractal dimension of flocs under different sediment contents and electrolyte conditions is shown in **Figure 12**.

The calculation principle of the box-counting dimension is to cover the fractal set with small boxes of side length ε ; the total number of small boxes is $N(\varepsilon)$, and the following relationship is obtained:

$$N(\varepsilon) \propto \varepsilon^k \quad (2)$$

Fitting $\log N(\varepsilon)$ vs. $\log \varepsilon$ (in double logarithmic coordinates) by least squares yields the following relationship between the box-counting dimension D and the slope of the line K :

$$D = -K \quad (3)$$

In **Figure 12**, the changing pattern of three different types of cations is similar to that of the fractal dimension of their flocs; i.e., the fractal dimension of the flocs tends to decrease with increasing cation concentration, mainly because after the addition of different types of cations, flocs are formed mainly by electrical neutralization and adsorption-induced bridging between particles. When the electrolyte strength is low, although there are cations in the aqueous solution, which can neutralize some negative charges on the surface of the particles and reduce the interparticle repulsion, the flocculation effect between the particles is weak, the shape of the flocs is irregular, and the fractal dimension of flocs is too large. With a further increase in the electrolyte strength, the optimal salinity for flocculation is reached, and the floc density is the largest; conse-

quently, the fractal dimension gradually decreases. Continuing to increase the flocculant concentration further increases the cation concentration in the water, and when the number of cations exceeds negative charges on the surface of the particle (solid phase), the sign of the external charge of the water film with the electric double layer is reversed, and the stability of the floc in the water body is enhanced, which inhibits the further formation of flocs, causing the fractal dimension of flocs to increase slightly.

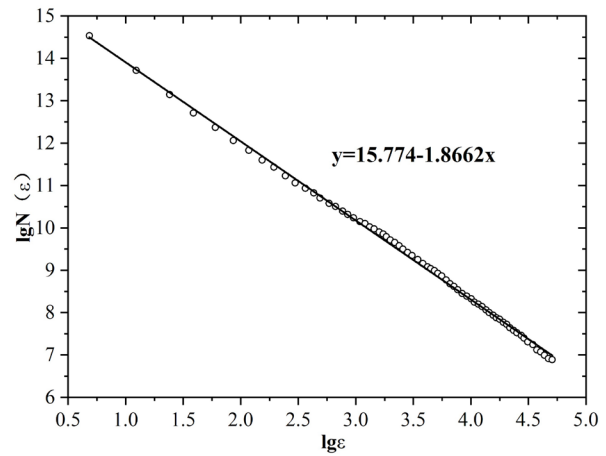


Figure 11. Double logarithmic relationship between the length of sides and number boxes.

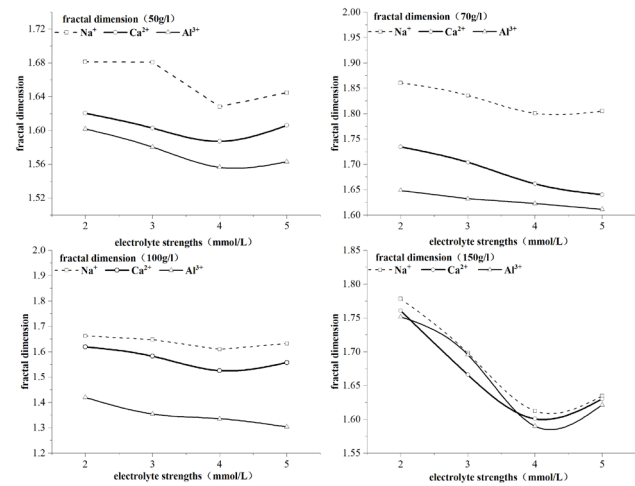


Figure 12. Graph of the fractal dimension change under different conditions.

Modification of the sediment sedimentation rate equation under the influence of different cations

For a single floc, the following relationship is satisfied between the number of sediment particles N_f that make up the floc and the floc diameter d_f :

$$N_f = \left(\frac{d_f}{d_0}\right)^D \quad (4)$$

where d_0 is the median particle size of the analysed sediment sample and D is the fractal dimension of the flocs.

Based on adsorption theory, Wang et al. [21] used the Langmuir adsorption isotherm equation and combined the relationship between the sedimentation rate and particle size to obtain the following:

$$k_\omega = \frac{\omega_f}{\omega_0} = \frac{1}{\lambda_1 C^2 + \lambda_2 C + \lambda_3} \cdot C^2 \quad (5)$$

where k_ω is the flocculation coefficient expressed by the change in sedimentation rate, ω_f is the sedimentation rate of the floc, ω_0 is the sedimentation rate of a single sediment particle, C is the electrolyte concentration, and λ_1 , λ_2 , and λ_3 are the coefficients.

From Equations (2)-(5), the floc sedimentation rate ω_f incorporating the ion concentration-related parameter can be obtained:

$$\omega_f = k_\omega \cdot C^2 \cdot \omega_0 = \frac{1}{\lambda_1 C^2 + \lambda_2 C + \lambda_3} \cdot C^2 \cdot \omega_0 \quad (6)$$

The meaning of the symbols in Equation (6) is the same as above. The coefficients λ_1 , λ_2 , and λ_3 are related to the sediment particle size, surface characteristics, and cation species, respectively, which must be determined experimentally.

Based on the above analysis, the floc porosity ε and fractal dimension D were used to analytically calculate the flocculation coefficient k_ω .

If the volume of a sediment particle satisfies $V_0 = \pi/6 \cdot d_0^3$ and the volume of the floc satisfies $V_f = \pi/6 \cdot d_f^3$, then the floc porosity ε is as follows:

$$\varepsilon = \frac{V_f N_f V_0}{V_f} \quad (7)$$

Substituting Equation (4) into Equation (7), we can obtain Equation (8):

$$\frac{d_f}{d_0} = (1-\varepsilon)^{\frac{1}{D-3}} \quad (8)$$

If the fine sediment and the floc sedimentation are in the stagnation zone and the sediment sedimentation rate in the stagnation zone is proportional to the square of the particle size, then,

$$\frac{\omega_f}{\omega_0} = \left(\frac{d_f}{d_0}\right)^2 \quad (9)$$

According to Equations (5), (8), and (9), we can obtain Equation (10):

$$k_\omega = \frac{\omega_f}{\omega_0} = \left(\frac{d_f}{d_0}\right)^2 = \left((1-\varepsilon)^{\frac{1}{D-3}}\right)^2 = \frac{1}{\lambda_1 C^2 + \lambda_2 C + \lambda_3} \quad (10)$$

Substituting the calculated fractal dimension D and floc porosity ε into Equation (10), the flocculation coefficient k_ω can be calculated, and the relationship between $1/k_\omega$ and the electrolyte concentration C was plotted, as shown in **Figure 13**, and fitted with a quadratic polynomial.

Equation (10) establishes the relationship between the floc sedimentation rate of cohesive sediments and the ion concentration in the water. It should be noted that some simplifications and assumptions have been made in the derivation of Equation (10) to facilitate the establishment of a relationship between the floc sedimentation rate of cohesive sediments and the ion concentration in the water. The coefficients λ_1 , λ_2 , and λ_3 in Equation (10) are correlated with many factors; that is, the coefficients λ_1 , λ_2 , and λ_3 change when conditions change, such as the surface properties of the sediment, the cation type, and the particle size of the sediment; therefore, coefficients λ_1 , λ_2 , and λ_3 should be calibrated under different conditions.

Many studies have demonstrated that there are different sedimentation resistance behaviours for different motion states. For the sedimentation rate equations proposed by Goncharov et al. [22-25], some coefficients are slightly different in various flow zones, but the structural forms of the sedimentation rate equations in the stagnation zone are essentially the same. This paper introduced the ion concentration-related parameter into an existing sedimentation rate equation and obtained the sedimentation rate equation incorporating the ion concentration-related parameter:

$$\omega_f = \frac{1}{\lambda_1 C^2 + \lambda_2 C + \lambda_3} \cdot C^2 \left(\frac{1}{24} \cdot \frac{\gamma_s - \gamma}{\gamma} \cdot g \cdot \frac{d^2}{\nu} \right) \quad (11)$$

where γ_s is the specific gravity of sediment, γ is the specific gravity of water, g is the gravity, ν is the coefficient of hydrodynamic viscosity, and d is the particle size of sediments. Other symbols have the same

meanings as above.

The obtained experimental data are used to test the validity of Equation (11).

The error rate for individual tests is calculated using Equation (12):

$$\text{Error rate} = \frac{(\text{Calculated value} - \text{Experimental value})}{\text{Experimental value}} \quad (12)$$

After substituting the relationship between cation concentration C and flocculation coefficient k_{f0} into Equation (11), the corrected sediment sedimentation rate can be calculated. Compared with the experimental results as shown in **Figure 14**, the average relative error is 16% (**Figure 15**), which essentially meets the computational accuracy requirements. Therefore, in this paper, based on the calculated fractal dimension and porosity of flocs, the obtained flocculation coefficient and sedimentation rate equation incorporating the ion concentration-related parameter for flocs formed by sediments with different particle sizes are essentially reasonable.

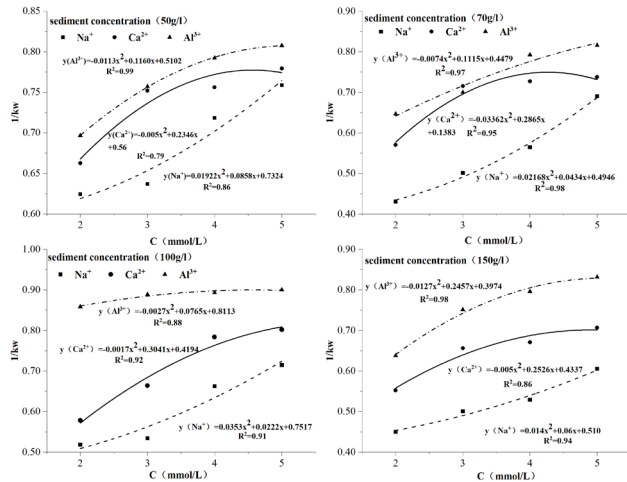


Figure 13. Relationship curves between the different cation concentrations C and $1/kw$.

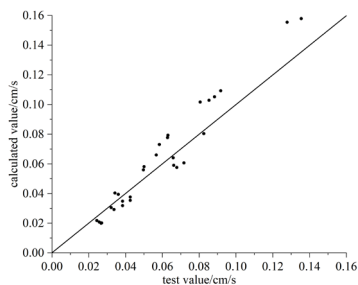


Figure 14. Comparison of the test value and the calculated value of the floc settling rate in Equation.

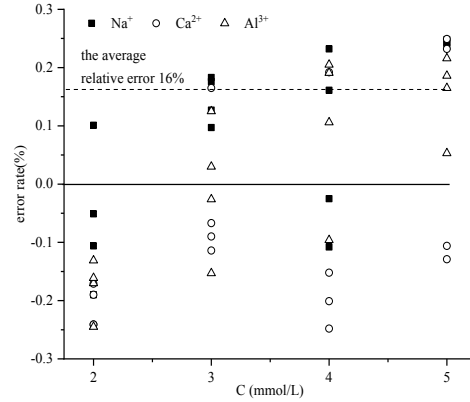


Figure 15. The error rate of settling velocity is calculated by Equation (11).

4. Discussion

(1) IPP image processing software is a relatively complete image analysis software with advanced functional modules for image processing and is widely used in fluorescence imaging, material imaging, medical research, and industrial production. In this paper, IPP image processing software was used to extract the morphological parameters of flocs, and the relationships between the porosity (a structural parameter) of flocs and the sediment and cation concentrations was analysed. The results indicated that the changing pattern of the floc structure characteristics analysed in this paper is consistent with that of Chai [17] and Chen [26], i.e., under the same electrolyte strength, the porosity of flocs decreases with increasing cation valence. The main reason for this finding is that the addition of cations in the water neutralizes some negative charges on the surface of the sediment particles, which reduces the interparticle electrostatic repulsion and increases the interparticle interaction; thus, flocculation can occur between the particles that were not prone to flocculation originally, and the interparticle bonding is enhanced such that the interparticle pores are smaller [17].

The results demonstrate that it is feasible to apply IPP software to analyse scanning electron microscope (SEM) images of flocs. However, IPP is only suitable for 2D observation. To gain a more comprehensive understanding of the complex internal structure of flocs, it is necessary to develop new software

or improve observation techniques.

(2) In natural water bodies, the sedimentation rate of cohesive sediment changes due to the presence of cations. The main reason for this change is the flocculation of cohesive sediments under the action of ions. According to the existing research results, the main cations in the Yellow River are Ca^{2+} , Na^+ , and K^+ [27]. Therefore, this study selected the silt in the Haibowan Reservoir and mainly discusses the flocculation and sedimentation of cohesive sediments under the action of three different cations (Na^+ , Ca^{2+} , and Al^{3+}). The results indicated that under the same sediment and cation concentrations, when the cation valence increases from +1 to +3, the floc sedimentation rate increases, which is essentially consistent with the findings of Wang [4] and Jiang [28]. The main reason for this finding is that according to the DLVO theory and the electric double-layer theory, the surface of the cohesive sediment particles is generally negatively charged; therefore, adding cations can reduce the thickness of the electric double layer on the surface of the sediment particles and the charge repulsion between the sediment particles, increase the chance of sediment particle bonding after collision, increase the formation rate of flocs by sediments, and promote flocculation and sedimentation of cohesive sediments [29]. However, the flocculation and sedimentation of fine-grained cohesive sediment are complex, and under different influencing factors, the sedimentary process and sedimentation rate of formed flocs are different. In actual water bodies, many factors act together; therefore, further research must comprehensively consider the influence of various factors to draw conclusions that are more in line with the actual situation.

5. Conclusions

(1) Under the same initial sediment concentration, the porosity and fractal dimension of flocs decrease with increasing cation concentration. After the cation concentration exceeds the optimal cation concentration for flocculation, the floc porosity and fractal dimension start to decrease more slowly or increase slightly.

(2) Cations with different valences have different effects on sediment sedimentation rates. When other influencing factors are fixed, higher-valence cations in the water have a stronger effect on sediment flocculation, and cation valence has a greater impact on the floc sedimentation rate compared with the sediment and cation concentrations. Therefore, high-valence ions are the main indicators for assessing the effect of ion concentration in water on sediment sedimentation rate.

(3) In natural water bodies, the sedimentation rate of cohesive sediment changes due to the presence of cations. The main reason for this change is the flocculation of cohesive sediments under the action of ions. In this paper, the ion concentration-related parameter was introduced into the existing sedimentation rate equation (stagnation zone) based on the changing patterns of the floc fractal dimension (D) and porosity (ϵ) under different influencing factors and the adsorption isotherm equation. The modified sedimentation rate equation was verified since the calculated values were essentially consistent with the measured values.

Author Contributions

L.X.M conceived and designed the manuscript; Y.Y.T processed and analysed the data and performed the proposed methods; L.X.M interpreted and discussed the results; Y.Y.T edited the manuscript; L.X.M and W.R revised the manuscript; W.W.J and L.Q handled the submission steps. All authors have read and agreed to the published version of the manuscript.

Conflict of Interest

Declaration of conflict of interest.

Funding

This research was funded by The Nature Foundation of Inner Mongolia Autonomous Region 2021MS05042. The National Natural Science Foundation of China project 51969021, 52169016. The

Major Science and Technology Projects of Inner Mongolia Autonomous Region 2021ZD0008.

References

- [1] Li, X.K., Niu, W.Q., Zhang, W.Q., et al., 2019. Liu suan jia fei dui jing zhi huang he shui ni sha xu ning chen jing de ying xiang (Chinese) [Effect of potassium sulfate fertilizer on flocculation and sedimentation of static Yellow River water]. *Shui Tu Bao Chi Xue Bao*. 33(4), 140-146.
- [2] Wang, X.J., Wang, Y.N., Zhao, J., 2022. Recent progress of the effect of suspended sediment movement on the transport of microplastics in rivers. *China Environmental Science*. 42(2), 863-877.
- [3] Liu, J.X., Ji, Z.W., Wang, D.W., 2019. Nian xing xi ke li ni sha xu ning shi yan yan jiu zong shu (Chinese) [Review on the flocculation test of cohesive sediment]. *Ni Sha Yan Jiu*. 44(2), 63-68. DOI: <https://doi.org/10.16239/j.cnki.0468-155x.2019.02.009>
- [4] Wang, J.Sh., Chen, L., Liu, L., et al., 2005. Yang li zi nong du dui ni sha chen su ying xiang shi yan yan jiu (Chinese) [Experimental study on effect of positively charged ion in river on the velocity of sediment particles]. *Shui Ke Xue Jin Zhan*. 16(2), 169-173.
- [5] Chen, H.S., Shao, M.A., 2002. NaCl dui xi ke li ni sha jing shui xu ning chen jiang dong li xue mo shi de ying xiang (Chinese) [Effect of NaCl concentration on dynamic model of fine sediment flocculation and settling in still water]. *Shui Li Xue Bao*. 33(8), 63-68.
- [6] Liu, Q.Zh., Li, J.F., Xu, C.H., et al., 2008. Yan du he fu zhi suan gong tong zuo yong xia de chang jiang kou ni sha xu ning guo cheng yan jiu (Chinese) [Flocculation process of fine-grained sediments by the combining effect of salinity and humus in the Changjiang Estuary in China]. *Hai Yang Xue Bao*. 30(3), 140-147.
- [7] Liu, L., Chen, L., Wang, J.Sh., et al., 2007. Bu tong li zi nong du xia ni sha nong du dui xu ning chen jiang de ying xiang (Chinese) [Effect on the flocculation sedimentation velocity in different conditions of cation concentration by concentration of sediments particles]. *Wu Han Da Xue Xue Bao (Gong Xue Ban)*. (1), 29-32.
- [8] Yao, P., Sun, W., Guo, Q.Q., 2022. Ji pei he han yan du dui shi ying zhi fen sha de jing shui chen jiang ying xiang shi yan yan jiu (Chinese) [Experimental study on the effect of sediment composition and water salinity on settling processes of quartz silt in still water]. *Ni Sha Yan Jiu*. 47(5), 15-22. DOI: <https://doi.org/10.16239/j.cnki.0468-155x.2022.05.003>
- [9] Li, W., Yu, C., Yang, S., et al., 2020. Measurements of the sediment flocculation characteristics in the Three Gorges Reservoir, Yangtze River. *River Research and Applications*. 36(7), 1202-1212. DOI: <https://doi.org/10.1002/rra.3614>
- [10] Guo, L., He, Q., 2011. Freshwater flocculation of suspended sediments in the Yangtze River, China. *Ocean Dynamics*. 61, 371-386.
- [11] Mikeš, D., Manning, A.J., 2010. Assessment of flocculation kinetics of cohesive sediments from the Seine and Gironde estuaries, France, through laboratory and field studies. *Journal of Waterway, Port, Coastal, and Ocean Engineering*. 136(6), 306-318. DOI: [https://doi.org/10.1061/\(ASCE\)WW.1943-5460.0000053](https://doi.org/10.1061/(ASCE)WW.1943-5460.0000053)
- [12] Qiao, G.Q., Zhang, Q.H., Zhang, J.F., et al., 2013. Ji yu XDLVO li lun de nian xing ni sha xu ning mo ni ge zi bo er zi man mo xing (Chinese) [Lattice Boltzmann model of cohesive sediment flocculation simulation based on the XDLVO Theory]. *Tian Jin Da Xue Xue Bao (Zi Ran Ke Xue Yu Gong Cheng Ji Shu Ban)*. 46(3), 232-238.
- [13] Zhang, J.F., Zhang, Q.H., Qiao, G.Q., 2015.

- Nian xing xi ke li ni sha xu ning fa yu shi kong guo cheng de shu zhi mo ni (Chinese) [Temporal and spatial variations of the flocculation process of fine cohesive sediments: A numerical simulation]. *Shui Li Xue Bao*. 46(11), 1305-1311.
- [14] Lee, B.J., Toorman, E., Fettweis, M., 2014. Multimodal particle size distributions of fine-grained sediments: Mathematical modeling and field investigation. *Ocean Dynamics*. 64, 429-441.
DOI: <https://doi.org/10.1007/s10236-014-0692-y>
- [15] Guo, Ch., He, Q., 2021. Nian xing ni sha xu ning yan jiu zong shu yu zhan wang (Chinese) [Review of the research on cohesive sediment flocculation]. *Ni Sha Yan Jiu*. 46(2), 66-73.
DOI: <https://doi.org/10.16239/j.cnki.0468-155x.2021.02.011>
- [16] Chai, Zh.H., Yang, G.L., Chen, M., 2012. Ji yu SEM tu xiang de xi ke li ni sha xu ti 3 wei fen xing yan jiu ji qi ying yong (Chinese) [3-D fractal study of fine sediment floc using SEM image and its application]. *Gong Cheng Ke Xue Yu Ji Shu*. 44(1), 88-92.
- [17] Chai, Zh.H., Yang, G.L., Chen, M., 2011. Tu xiang fen xi nian xing xi ke li ni sha xu ti kong xi chu tan (Chinese) [Study of floc pores of viscous fine sediment by image analysis]. *Ni Sha Yan Jiu*. 55(5), 24-29.
DOI: <https://doi.org/10.16239/j.cnki.0468-155x.2011.05.003>
- [18] Wang, D.W., Yang, G.L., Yu, M.H., 2009. Jing shui zhong nian xing xi ke li ni sha xu ning lin jie li jing de que ding ji qi ying xiang yin su fen xi (Chinese) [Method to determine the maximal diameter of fine sediment aggregation and influence factors analysis]. *Ni Sha Yan Jiu*. (1), 74-80.
DOI: <https://doi.org/10.16239/j.cnki.0468-155x.2009.01.012>
- [19] Liu, Y., Reng, T.W., Wang, P., 2010. Ji yu Matlab li yong fen xing li lun kao cha bian po an quan zhuang tai fang fa yan jiu (Chinese) [Study on inspection of slope safety with fractal theory based on Matlab]. *Shui Li Shui Dian Ji Shu*. 41(7), 17-19+23.
DOI: <https://doi.org/10.13928/j.cnki.wrahe.2010.07.017>
- [20] Varkouhi, S., Tosca, N.J., Cartwright, J.A., 2020. Pore-water chemistry: A proxy for tracking the signature of ongoing silica diagenesis. *Journal of Sedimentary Research*. 90(9), 1037-1067.
DOI: <https://doi.org/10.2110/jsr.2020.56>
- [21] Wang, J.Sh., Chen, L., Wang, Zh.G., et al., 2006. Han li zi nong du can shu de nian xing ni sha chen su gong shi yan jiu (Chinese) [Study on the fine sediment settling velocity formula with the parameter of Ca^{2+} concentration]. *Shui Ke Xue Jin Zhan*. 17(1), 1-6.
- [22] Zhang, R.J., 1998. He liu ni sha dong li xue (Chinese) [River sediment dynamics]. China Water & Power Press: Beijing.
- [23] Dou, G.R., 1963. Ni sha yun dong li lun (Chinese) [Theory of sediment movement]. Nanjing Hydraulic Research Institute: Nanjing.
- [24] Sha, Y.Q., 1965. Ni sha yun dong xue yi lun (Chinese) [Kinematics of sediment]. China Industry Press: Beijing.
- [25] Zhang, R.J., 1961. He liu dong li xue (Chinese) [Dynamics of rivers]. China Industry Press: Beijing.
- [26] Chen, Y.P., Luo, W., Xu, Ch.Y., et al., 2020. Gao nong du nian xing ni sha xu tuan wei guan jie gou ji qi dui chen jiang te xing de ying xiang (Chinese) [Microstructure of cohesive sediment flocs with high concentration and its influence on the deposition characteristics]. *Ni Sha Yan Jiu*. 45(6), 8-14.
DOI: <https://doi.org/10.16239/j.cnki.0468-155x.2020.06.002>
- [27] Chen, J.Sh., Li, H.B., Xia, X.H., et al., 2000. Jin 30 nian lai huang he shui zhi bian hua qu shi ji yuan yin fen xi (Chinese) [A study on water-quality trend in the Yellow River System

- from 1960 to 1990]. *Huan Jing Hua Xue*. (2), 97-102.
- [28] Jiang, G.J., Yao, Y.M., Tang, Z.W., 2002. Changjiang kou xi ke li ni sha xu ning chen jiang ying xiang yin su fen xi (Chinese) [The analysis for influencing factors of fine sediment flocculation in the Changjiang Estuary]. *Hai Yang Xue Bao*. 24(4), 51-57.
- [29] Chai, Ch.H., Fang, H.W., Wang, X., et al., 2017. Shui liu he dian jie zhi dui nian xing ni sha xu ning chen jiang ying xiang shi yan (Chinese) [Effect of flow and electrolyte on the flocculation-settling of cohesive sediment]. *Shui Ke Xue Jin Zhan*. 28(2), 285-292.
DOI: <https://doi.org/10.14042/j.cnki.32.1309.2017.02.014>

ARTICLE

The Relationship between Water Resources Use Efficiency and Scientific and Technological Innovation Level: Case Study of Yangtze River Basin in China

Guangming Yang^{1,2} , Qingqing Gui^{1,2*}, Junyue Liu¹, Fengtai Zhang^{1,2}, Siyi Cheng^{1,2}

¹ School of Management, Chongqing University of Technology, Chongqing, 400054, China

² Rural Revitalization and Regional High-quality Development Research Center, Chongqing University of Technology, Chongqing, 400054, China

ABSTRACT

The Yangtze River Basin's water resource utilization efficiency (WUE) and scientific and technological innovation level (STI) are closely connected, and the comprehension of these relationships will help to improve WUE and promote local economic growth and conservation of water. This study uses 19 provinces and regions along the Yangtze River's mainstream from 2009 to 2019 as its research objects and uses a Vector Auto Regression (VAR) model to quantitatively evaluate the spatiotemporal evolution of the coupling coordination degree (CCD) between the two subsystems of WUE and STI. The findings show that: (1) Both the WUE and STI in the Yangtze River Basin showed an upward trend during the study period, but the STI effectively lagged behind the WUE; (2) The CCD of the two subsystems generally showed an upward trend, and the CCD of each province was improved to varying degrees, but the majority of regions did not develop a high-quality coordination stage; (3) The CCD of the two systems displayed apparent positive spatial autocorrelation in the spatial correlation pattern, and there were only two types: high-high (H-H) urbanization areas and low-low (L-L) urbanization areas; (4) The STI showed no obvious response to the impact of the WUE, while the WUE responded greatly to the STI, and both of them were highly dependent on themselves. Optimizing their interaction mechanisms should be the primary focus of high-quality development in the basin of the Yangtze River in the future. These results give the government an empirical basis to enhance the WUE and promote regional sustainable development.

Keywords: Water resource utilization efficiency (WUE); Scientific and technological innovation level (STI); Coupling coordination; Interactive response; Yangtze River Basin

*CORRESPONDING AUTHOR:

Qingqing Gui, School of Management, Chongqing University of Technology, Chongqing, 400054, China; Rural Revitalization and Regional High-quality Development Research Center, Chongqing University of Technology, Chongqing, 400054, China; Email: guiqingqing@stu.cqut.edu.cn

ARTICLE INFO

Received: 28 May 2023 | Revised: 2 September 2023 | Accepted: 5 September 2023 | Published Online: 14 September 2023

DOI: <https://doi.org/10.30564/jees.v5i2.5745>

CITATION

Yang, G.M., Gui, Q.Q., Liu, J.Y., et al., 2023. The Relationship between Water Resources Use Efficiency and Scientific and Technological Innovation Level: Case Study of Yangtze River Basin in China. *Journal of Environmental & Earth Sciences*. 5(2): 15-35. DOI: <https://doi.org/10.30564/jees.v5i2.5745>

COPYRIGHT

Copyright © 2023 by the author(s). Published by Bilingual Publishing Group. This is an open access article under the Creative Commons Attribution-NonCommercial 4.0 International (CC BY-NC 4.0) License. (<https://creativecommons.org/licenses/by-nc/4.0/>).

1. Introduction

Water, as established by UN-Water (2021), serves as the fundamental element for all developmental processes ^[1]. It holds significance as both a fundamental natural resource and a strategic economic asset, playing a vital function in human life, society development, and the sustainable advancement of the ecological environment ^[2]. However, the progression of social and economic development has resulted in a growing universal demand for water resources at an approximate rate of 1% per year ^[3]. Furthermore, alongside the vulnerable natural ecological environment and the utilization of unsound development approaches, the issue of water scarcity is becoming increasingly evident. Despite China's position as the sixth-largest global holder of water resources, its per capita allocation is merely 25% of the global average level. As a result, China is among the countries confronting severe water shortages ^[4]. It is expected that with further expansion of urbanization and economic growth, water scarcity will become even more severe. This may ultimately hinder the sustainable development of regional areas, but the total usable water resources cannot be expanded due to economic and technical constraints ^[5]. In this case, improving water resource utilization efficiency (WUE) and reducing pollutant discharge are considered two methods to alleviate the current water resource crisis ^[6]. Therefore, scientific evaluation of WUE based on consideration of water pollution is of considerable significance for improving WUE and optimizing water resource allocation ^[7].

Enhancing WUE stands as a reliable and assured approach for China to attain green and sustainable development. Therefore, the Chinese government has started several reform measures. For instance, in 2011, the Chinese government issued a document specifically aimed at expediting water conservation reforms within the country. This document unambiguously emphasized the imperative of strengthening water resource management and enhancing comprehensive WUE ^[8]. In the year 2012, the Chinese authorities declared their stance on enforcing a rigorous system for managing water resources. They also set

up three primary goals known as “three red lines”. These objectives are controlling water resource development and usage, managing water efficiency, and reducing pollution in water function areas ^[9]. China has also piloted innovative economic measures, including water rights and emissions trading. For the purpose of prompting sustainable development and alleviating the shortage of water resources, future development must adhere to these reforms, effectively utilize resources, and strictly protect the ecological environment. Technological innovation has changed the input–output proportion of productive factors and is the core power in improving the WUE ^[10]. Consequently, it becomes imperative to coordinate the Scientific and Technological Innovation (STI) and the water resource capacity. Such integration will ultimately lead to the harmonious convergence of STI and water resource management, culminating in the desired outcomes.

The Yangtze River Basin covers a large portion of China and is home to over 40% of the country's population, making its economic growth crucial. Despite abundant water resources, the basin's intensive production activities have led to water shortages and pollution. This paper focuses on the harmonious relationship between WUE and STI in the Yangtze River Basin through a coupling coordination model and panel VAR model, aimed at offering recommendations for resolving water resource problems and advancing economic development. The paper's structure consists of a literature review of current research, a case study introduction, the methodology of this paper, results, conclusions, and policy recommendations.

2. Literature review

WUE serves as a significant metric for assessing sustainable development at a regional level. At its essence, WUE aims to achieve maximum economic and social benefits while minimizing water loss and environmental pollution. This topic has garnered considerable attention among scholars in recent years. Scientific evaluation of WUE constitutes the initial step towards exploring strategies for balanced

development and water resource utilization, and currently stands as a focal point of research.

Evaluation methods for WUE can generally be categorized into two approaches: single-factor evaluation and total-factor evaluation. Among them, single-factor evaluation methods primarily include the index system method^[11] and the ratio analysis method^[12]. For example, Gregg et al. take the ratio of agricultural water resources input to agricultural output as an index to measure the WUE^[13]. The total-factor evaluation methods generally include Stochastic Frontier Analysis (SFA)^[14,15] and Data Envelopment Analysis (DEA)^[16,17]. In the research on the utilization of total-factor water resources, Carvalho and Marques explore the scale economy and scope economy of the Portuguese water industry by using Bayesian SFA^[18]. Hong and Yabe applied SFA to determine irrigation water efficiency and its effect on small tea plantations in Vietnam and found that there is a large amount of water resource waste under the condition of diminishing rebound to scale^[19]. Zhang et al. use DEA based on the relaxation model to calculate the utilization ratio of interprovincial agricultural water resources capacity in China^[20]. Gautam et al. use the smooth heterogeneous bootstrap program in the DEA method to evaluate irrigation water usage efficiency in crop productive efficiency in Louisiana, USA^[21].

The majority of studies concerning WUE have focused on agriculture and industry, focusing on the evaluation of WUE as their primary research object. This scholarly attention has spurred research investigating the driving factors and mechanisms that influence WUE. For instance, Segovia-Cardozo et al. employed satellite images to estimate crop coefficients and evaluated the WUE of major crops in four irrigated areas in Spain^[22]. Geng et al. utilized DEA to assess the water usage efficiency in agriculture across 31 provinces in China from 2003 to 2013, revealing a noteworthy improvement post-2008^[23]. Chen et al. assessed the industrial WUE in China from 2005 to 2015, exploring provincial variations and spatial spill-over effects through bootstrap DEA analysis^[24]. Oulmane et al. calculated the WUE of

a small horticultural farm in Algeria and employed a Tobit model to identify determinants of WUE, encompassing factors such as total crop and water source count, greenhouse gas emissions percentage, level of educational and technical support, and credit opportunities for farmers^[25]. Wang argued that factors such as age, gender, education level, and farmers' awareness of water scarcity impact the irrigation efficiency of water resources^[26].

The STI serves as a crucial metric for assessing a country's high-quality development. Advancements in STI facilitate the development of environmental protection technologies, which profoundly influence the utilization efficiency of biological resources^[27]. In recent years, scholars have made notable strides in researching the relationship between WUE and STI. Kang et al. posit that enhancing water-saving irrigation technology contributes to improved WUE^[28]. Through empirical research, Miao et al. employ the random frontier analysis method and demonstrate that technological innovation exhibits a vital positive effect on the energy usage efficiency of industries between 2000 and 2015, exhibiting a consistent upward trend^[29]. Wang and Wang, utilizing the generalized method of moments system regression analysis, discover that technological development had a substantial and positive influence on national-level total-factor energy efficiency from 2001 to 2013^[30]. However, they also found that technological innovation in central China impeded the advancement of total-factor energy efficiency.

Recently, the coupling coordination model has gained widespread recognition as an effective tool for evaluating the overall development of research areas^[31]. Prior studies by Xu et al. and Zhang et al. have used this method to study the relationship between WUE and economic development, as well as economic development and the water environment^[32,33]. However, there is little research that has utilized this method to study the mutual relationship between WUE and STI. Most existing research primarily focuses on the one-way impact of STI on WUE, with less attention given to the factors that impede the coordinated development of these two

systems. To facilitate their harmonized development, it is crucial to conduct a systematic evaluation of their spatial and temporal characteristics and identify the factors influencing their development.

This paper aims to utilize the coupling coordination model to assess the relationship between WUE and STI in the Yangtze River Basin. By establishing an overall evaluation index system and measuring both WUE and STI, we will analyze the temporal and spatial characteristics of their coordinated development using a panel VAR model. This empirical analysis will provide valuable insights into the positive interaction between the two systems, ultimately supporting the promotion of their coordinated development.

3. Methodology and data

3.1 Study area

This study focuses on the research conducted in the Yangtze River Basin, which includes its tributaries. The basin boasts a well-developed water system, encompassing a water supply and drainage area of 1.8 million square kilometers, approximately one-fifth of the total area^[34]. Geographically, it spans the eastern, central, and western economic zones of China, covering 19 provinces, autonomous regions, and centrally-administered municipalities. However, the

region grapples with significant resource imbalances, environmental challenges, economic disparities, and unbalanced distribution of water resources, which hinder the development of the Yangtze River Basin. The Yangtze River is categorized into three parts: the upper, middle, and lower reaches, with 19 provinces allocated to each section accordingly (**Figure 1**). Hubei and Jiangxi provinces are designated as part of the middle reaches, based on both geographical and economic regional divisions.

3.2 Methodology

Calculation of ash water footprint

According to the literature^[35-37], the gray water footprint (TWF_{grey}) includes agricultural grey water footprint (AWF_{grey}), industrial grey water footprint (IWF_{grey}), and domestic grey water footprint (DWF_{grey}). As there are many kinds of water pollutants and the concentration difference is large, only the most important pollutants are considered when calculating the grey water footprint. The specific calculation formula can be represented as follows:

$$TWF_{grey} = AWF_{grey} + IWF_{grey} + DWF_{grey} \quad (1)$$

Agricultural grey water footprint (AWF_{grey}) includes planting grey water footprint (AWF_{pla}) and aquaculture grey water footprint (AWF_{bre}). Nitrogen in the fertilization is the largest origin of aquatic pollution in the farming industry. The chemical oxygen de-

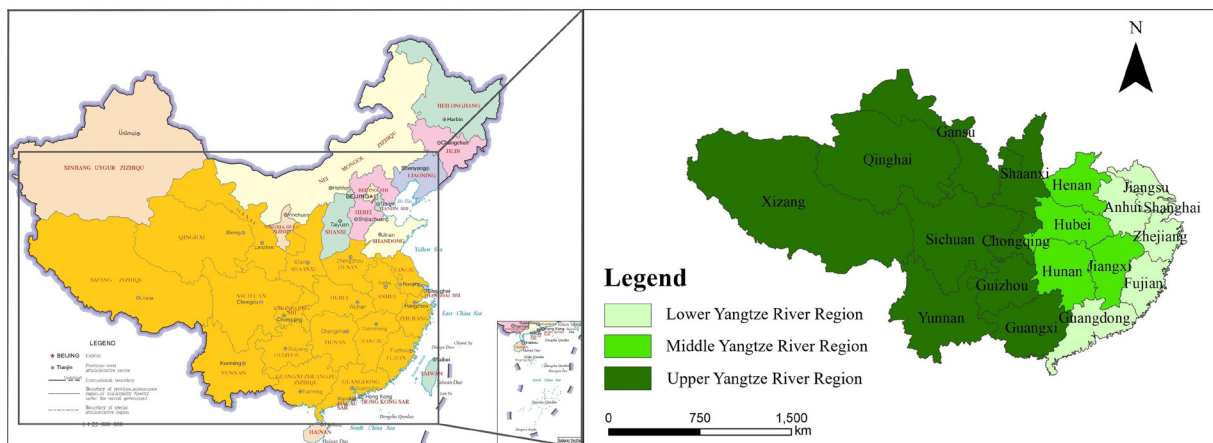


Figure 1. Study area.

mand (*COD*) and total nitrogen in the feces of cattle, sheep, pigs, and poultry are the main source factors of water deterioration in the breeding industry^[37,38]. For calculating grey water footprint, the grey water footprints originating from the same categories of pollutants are summed up, and the grey water footprints originating from different categories of pollutants take the maximum value. The calculation formula is as follows:

$$AWF_{grey} = \max[AWF_{bre(COD)}, (AWF_{pla(TN)} + AWF_{bre(TN)})] \quad (2)$$

$$AWF_{pla} = \frac{\alpha N_{Appl}}{C_{TN, max} - C_{TN, nat}} \quad (3)$$

$$AWF_{bre} = \max(AWF_{bre(COD)}, AWF_{bre(TN)}) \quad (4)$$

$$AWF_{bre(i)} = \frac{L_{bre(i)}}{C_{i, max} - C_{i, nat}}, L_{bre(i)} = \sum_{h=1}^4 N_h D_h (f_h p_{hf} \beta_{hf} + u_h p_{hu} \beta_{hu}) \quad (5)$$

In the above formula: α is the leaching rate of nitrogen fertilizer; N_{appl} is the total amount of nitrogen application; $C_{TN, max}$ is the standard concentration of total nitrogen concerning water quality; $C_{TN, nat}$ is the natural local concentration of total nitrogen; $AWF_{bre(i)}$ is the grey water footprint of the aquaculture industry of category i pollutants; $L_{bre(i)}$ is the emission of class i pollutants; i is total nitrogen or *COD*; h refers to cattle, sheep, pigs, and poultry; N_h , D_h , f_h , u_h , p_{hf} , β_{hf} , β_{hu} , are the quantity of h , feeding cycle, daily urine output, pollutant content per unit of urine, pollutant content per unit of faeces, pollutant flow loss rate per unit of faeces, and pollutant flow loss rate per unit of urine, respectively.

COD and ammonia nitrogen emissions ($NH_3 - N$) are the main pollutants in industrial wastewater^[39,40], and the calculation formula of IWF_{grey} is as follows:

$$IWF_{grey} = \max(IWF_{grey(COD)}, IWF_{grey(NH_3 - N)}) \quad (6)$$

$$IWF_{grey(k)} = \frac{L_{ind(k)}}{C_{k, max} - C_{k, nat}} \quad (7)$$

In the formula: $IWF_{grey(k)}$ is the industrial grey water footprint of class k pollutants; $L_{ind(k)}$ is the

discharge amount of class k pollutants in industrial wastewater; k is the pollutant *COD* or $NH_3 - N$.

Domestic and industrial sewage belong to point source pollution, and the main pollutants are *COD* and $NH_3 - N$ ^[20,41]. The calculation formula of $NH_3 - N$ is as follows:

$$DWF_{grey} = \max(DWF_{grey(COD)}, DWF_{grey(NH_3 - N)}) \quad (8)$$

$$DWF_{grey(k)} = \frac{L_{dom(k)}}{C_{k, max} - C_{k, nat}} \quad (9)$$

Method for estimating WUE

In order to ensure objectivity and minimize deviation in efficiency measurement, this paper employs DEA, a nonparametric frontier approach. DEA is used as the evaluation method for assessing WUE in this study. Unlike traditional DEA models that do not account for input or output relaxation, the calculation model^[42], addresses this limitation and offers a solution to overcome this issue.

$$\begin{aligned} \min_{\rho, \lambda_j^-, s_j^-, s_j^g, s_j^b} \rho &= \frac{1 - (1/m) \sum_{j=1}^m (s_j^- / x_{j0})}{1 + (1/(n_1 + n_2)) \left(\sum_{j=1}^{n_1} (s_j^g / y_{j0}^g) + \sum_{j=1}^{n_2} (s_j^b / y_{j0}^b) \right)} \\ \text{s.t. } x_{j0} &= \sum_{j=1}^m \lambda_j x_j + s_j^-, y_{j0}^g = \sum_{j=1}^{n_1} \lambda_j y_j^g - s_j^g, y_{j0}^b = \sum_{j=1}^{n_2} \lambda_j y_j^b + s_j^b, \lambda_j \geq 0, s_j^- \geq 0, s_j^g \geq 0, s_j^b \geq 0 \end{aligned} \quad (10)$$

where $\rho, s_j^-, s_j^g, s_j^b$ represent efficiency value, input redundancy, undesirable output redundancy, and desirable output deficiency, respectively. When $\rho = 1$ (equivalently, $s_j^- = s_j^g = s_j^b = 0$), DMU_0 is efficient.

Model (2) is generally converted to the following linear programming model:

$$\begin{aligned} \min_{\tau, t, \gamma_j, S_j^-, S_j^g, S_j^b} \tau &= t - \frac{1}{m} \sum_{j=1}^m \frac{S_j^-}{x_{j0}} \\ \text{s.t. } 1 &= t + \frac{1}{n_1 + n_2} \left(\sum_{j=1}^{n_1} \frac{S_j^g}{y_{j0}^g} + \sum_{j=1}^{n_2} \frac{S_j^b}{y_{j0}^b} \right) \\ \text{s.t. } x_{j0} &= \sum_{j=1}^m \gamma_j x_j + S_j^-, ty_{j0}^g = \sum_{j=1}^{n_1} \gamma_j y_j^g - S_j^g, ty_{j0}^b = \sum_{j=1}^{n_2} \gamma_j y_j^b + S_j^b, \gamma_j \geq 0, S_j^- \geq 0, S_j^g \geq 0, S_j^b \geq 0 \end{aligned} \quad (11)$$

where τ is the efficiency value (equal to ρ), $\gamma_j = t\lambda_j$, $S_j^- = ts_j^-$, $S_j^g = ts_j^g$, $S_j^b = ts_j^b$.

Evaluation model for the comprehensive development level

First, the indicators are dimensionless to eliminate the dimensional difference of the indicator system, specifically:

$$X'_{ij} = (X_{ij} - \min X_j) / (\max X_j - \min X_j) \quad (12)$$

$$X'_{ij} = (\max X_j - X_{ij}) / (\max X_j - \min X_j) \quad (13)$$

where Equation (12) is a positive indicator normalization process, and Equation (13) is a negative indicator normalization process.

To mitigate potential measurement biases stemming from subjective weighting, this paper utilizes the entropy weight method. This method is selected due to its strong objectivity, practicality, and widespread applicability in determining the weights of different indicators. By employing this method, the study aims to enhance the objectivity and reliability of the weight allocation process for various indicators^[43].

$$\begin{cases} w_j = d_j / \sum_j d_j, & d_j = 1 - e_j \\ e_j = -k \sum_{i=1}^n P_i \times \ln(P_i), & k = 1 / \ln(n) \\ P_i = X'_i / \sum_{i=1}^n X'_i \end{cases} \quad (14)$$

w_j represents the weight of the j -th index; P_i represents the weight of sample indicators; e_j represents the information entropy of the j -th index; d_j indicates the utility value of the j -th index; n represents the number of samples.

Finally, according to the weights of the different indicators, the comprehensive evaluation indexes of the STI are further calculated:

$$STI = \sum_{j=1}^m w_j \times x'_{ij} \quad (15)$$

CCD model

The CCD model comprises two distinct components, namely the coupling degree model and the coordination degree model. While the former is responsible for delineating the extent of system inter-

action, it falls short of capturing the comprehensive potency and collaborative impact thereof^[44]. Thus, the coordination degree model has been introduced to encompass both the level of inter-system interaction and the degree of coordinated development. The formula for calculating the coupling degree is:

$$C = 2 \left[\frac{WUE \times STI}{(WUE + STI)} \right]^{\frac{1}{2}} \quad (16)$$

C is the coupling degree, in which the value is $[0, 1]$. When C gets smaller, the correlation and coupling relationship between the two subsystems gets smaller. Otherwise correlation and coupling relationship between the two subsystems gets larger. The calculation formula for the degree of coordination is as follows:

$$\begin{cases} D = \sqrt{C \times T} \\ T = \alpha WUE + \beta STI \end{cases} \quad (17)$$

where D is the CCD, and the value is $(0, 1)$; T is the overall coordination index of WUE and the STI, and the value is $(0, 1)$; α and β are undetermined parameters, indicating the weight of the two subsystems to the overall system. In this paper, both α and β are considered equally important, so $\alpha = \beta = 0.5$.

There is no unified standard for the division of coupled cooperative scheduling in the academic community. According to the existing research and the actual coupling coordination value calculated in this paper, the CCD of the two systems is divided into five levels^[45], as shown in **Table 1**.

Table 1. Coupling coordination level.

D	Level
0.0-0.20	Low coordination
0.20-0.40	Basic coordination
0.40-0.50	Moderate coordination
0.50-0.80	Highly coordinated
0.80-1.00	Excellent coordination

Spatial autocorrelation

Spatial autocorrelation is a valuable approach capable of examining the spatial relationships within data. It helps elucidate the interrelationship patterns and spatial clustering characteristics of spatial attribute data^[44]. Moran's I is a commonly utilized

measure for such analysis, and it encompasses both global Moran's I and local Moran's I. Global spatial autocorrelation is employed to describe the overall degree of spatial correlation among attribute values within the study area. The specific formula is as follows:

$$I = \frac{n \times \sum_{i=1}^n \sum_{j \neq 1}^n W_{ij} (x_i - \bar{x})(x_j - \bar{x})}{(\sum_{i=1}^n \sum_{j=1}^n W_{ij}) \times \sum_{i=1}^n (x_i - \bar{x})^2} \quad (18)$$

The above formula I represents Moran's I, n represents the number of provinces and cities, x_i and x_j represent the CCD at the i and j locations of provinces and cities, respectively, and \bar{x} represents the average value of the CCD; W_{ij} represents the neighborhood relationship between i and j . When i and j are adjacent, $W_{ij} = 1$; otherwise, it is 0. The value of global Moran's I is in the interval of $[-1, 1]$. If it is greater than 0, it indicates a positive spatial correlation. The larger value means an evident spatial correlation. Less than 0 indicates a negative spatial correlation, and a smaller value means greater spatial difference. The space equal to 0 presents randomness.

Local spatial autocorrelation can be a useful method to further measure the specific location of the coupling coordination between WUE and STI in local space and then analyze the imbalance in local space and find the spatial heterogeneity of the coupling coordination. The calculation formula of local Moran's I is as follows:

$$I_i = \frac{(x_i - \bar{x})}{m_0} \sum_j W_{ij} (x_j - \bar{x}) \quad (19)$$

The above formula x_i represents the CCD value of province and city i , \bar{x} represents the average value of CCD of all provinces and cities, $I_i > 0$ represents the spatial clustering (high-high [H-H] or low-low [L-L]) of observation values similar to the CCD value of a province and city, and $I_i < 0$ represents the spatial clustering (L-H or H-L) of observation values not similar to the CCD value of a province.

VAR model

The intricate mechanisms of interaction and causality between WUE and STI call for the adoption of a panel VAR (Vector Autoregression) model. By

combining panel data and modeling techniques, the panel VAR model leverages the strengths of both approaches, enabling the prediction of the influence of random disturbances on the variables of interest. Thus, the panel VAR model proves to be a suitable analytical tool for examining the interactive responses between WUE and STI within the context of the Yangtze River Basin.

3.3 Indicator selection and data sources

Indicator selection

Based on the connotation and characteristics of WUE and STI, with reference to existing research results, and following the fundamentals of scientificity, comparability, and representativeness of index selection, select indicators can reflect WUE and STI to a large extent and build an overall evaluation index system. This is shown in **Table 2**. When constructing the evaluation index model of WUE, this paper builds the input and output required by WUE based on the neoclassical growth theory and previous studies^[5,36]. As for the input indicators, the number of employees, fixed assets, and total regional water consumption are selected to reflect this indicator. In terms of output indicators, regional GDP (based on 2009) and gray water footprint are selected to represent both the expected and unexpected output, respectively.

The STI evaluation index system comprises two standard levels, namely STI input and STI output, each consisting of seven indexes. This study has opted for three input indicators, namely the full-time equivalent of research and development (R & D) personnel, the internal expenditure of R & D funds, and the number of R & D institutions. As for output indicators, four have been chosen, comprising the number of patent authorizations, the number of R & D projects, the sales profit of new commodities in high-tech industries, and the number of advanced development projects in high-tech industries.

Based on the above indicators and methods, the framework of this research is established in **Figure 2**.

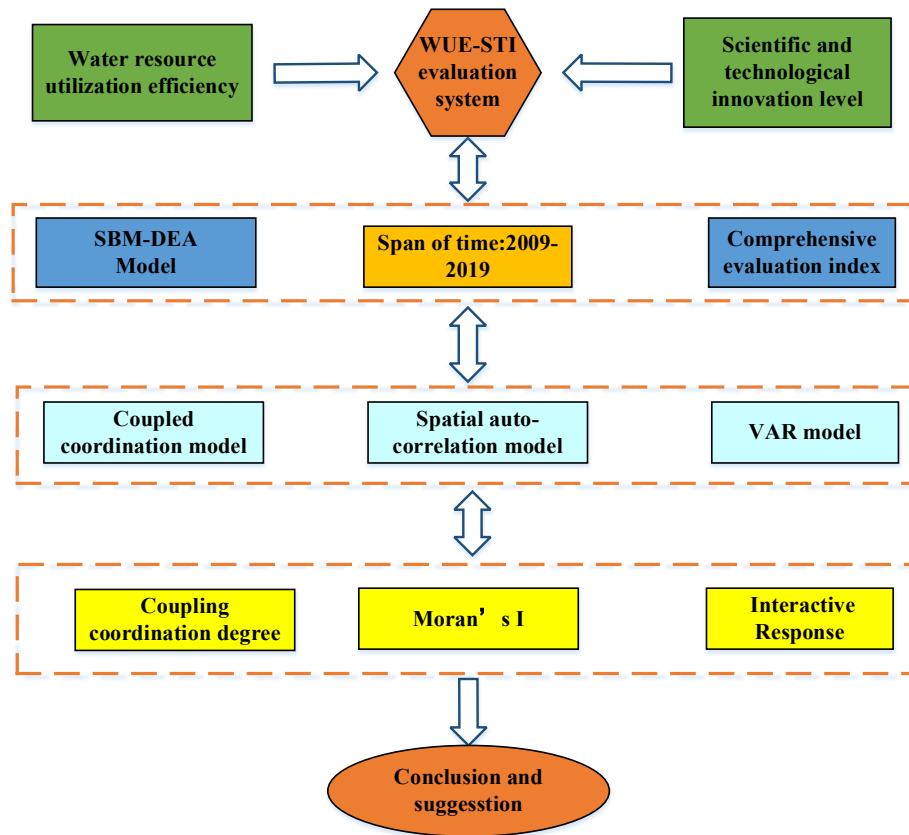


Figure 2. Research framework.

Table 2. Evaluation index system of WUE and STI.

Target level	Criterion level	Indicator level	Unit
WUE	Input indicators	Number of employees	Ten thousand people
		Fixed assets	RMB100 mil
		Total regional water consumption	100 million m ³
	Desirable output indicators	GDP	RMB100 mil
	Undesirable output indicators	Gray water footprint	10,000 t
STI	Investment in scientific and technological innovation	Number of R & D institutions	Individual
		R & D personnel full-time equivalent	Man year
		Internal expenditure of R & D funds	CNY10 thousand
	Scientific and technological innovation output	Number of patent authorizations	Piece
		Number of R & D projects (subjects)	Term
		Sales revenue of new products of high-tech industry	CNY10 thousand
		Number of new product development projects in high-tech industry	Term

Data source

All the information and data utilized in this academic article have been sourced exclusively from

reliable and authoritative references. These include the China Statistical Yearbook, various provincial and city Statistical Yearbooks, China Science and

Technology Statistical Yearbook (covering the period from 2009 to 2019), Science and Technology Statistical Yearbook, Education Statistical Yearbook, Water Conservancy Statistical Yearbook, Water Resources Bulletin, and National Economic and Social Development Statistical Bulletin.

In cases where specific data points were unavailable, they have been estimated employing the average growth rate over the successive three-year period. This approach ensures a consistent and reliable analysis throughout the study. It is important to note that the scope of this analysis encompasses the 19 provinces located within the Yangtze River Basin, providing a comprehensive understanding of the region's dynamics and trends.

4. Result analysis

4.1 Spatial and temporal evolution characteristics of WUE and STI

Using the aforementioned methodologies, we have calculated the WUE index and STI index for the nineteen provinces located within the Yangtze River Basin from 2009 to 2019. Additionally, we have summarized the average values of each year for both indices and examined the CCD of the two systems. Upon careful analysis of **Figure 3**, it becomes evident that there is a consistent upward trend in the average values of WUE and STI within the Yangtze River Basin from 2009 to 2019. Furthermore, the time characteristics of the two indices exhibit a clear positive correlation. This correlation suggests a mutually reinforcing relationship between WUE and STI within the region.

Spatial and temporal distribution of WUE

(1) Temporal characteristics. In terms of temporal analysis, the average rate of the WUE index for the 19 provinces (autonomous regions) within the Yangtze River Basin exhibited a positive trend from 2009 to 2019. The average WUE index rose from 0.3041 in 2009 to 0.3800 in 2019, indicating a stable overall development and a favorable growth trajectory (**Figure 3**). These findings highlight the achievements made in water pollution prevention, energy conser-

vation, emission cutback, and ecological control within the Yangtze River Basin in recent decades. The positive trend in WUE demonstrates the region's progress in the sustainable utilization of water resources.

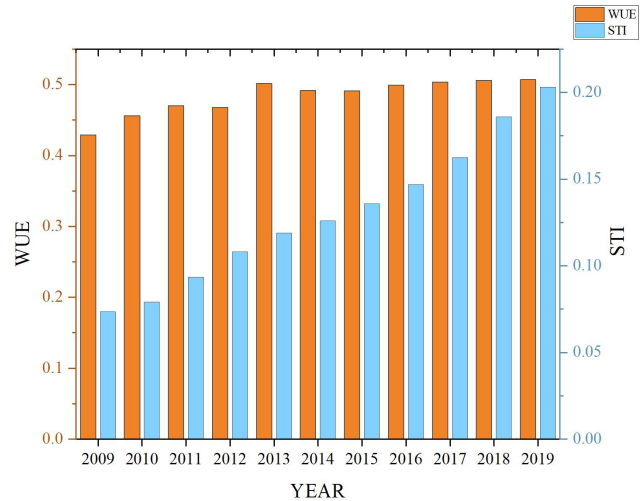


Figure 3. Time series change of WUE and STI in the Yangtze River Basin.

(2) This study employs the DEA model to compute the WUE of 19 provinces and regions located in the Yangtze River Basin from 2009 to 2019, and utilizes the initial, final, and middle years of the research period to investigate the findings within the study area. To better illustrate the dissimilarities in the spatial distribution of WUE in the Yangtze River Basin, ArcGIS10.2 software is employed to visualize the same in 2009, 2013, 2016, and 2019 (**Figure 4**), and subsequently assess the disparity in WUE among different regions. Based on the obtained results, the efficiency index is classified into five ranges using the natural breakpoint method (Jenks), whereby the higher the efficiency value, the darker the shade.

On the whole, the WUE of the Yangtze River Basin changes significantly from 2009 to 2019, and the efficiency value shows an upward trend. From a regional perspective, from 2009 to 2019, the WUE showed an overall development trend higher in the lower reaches and lower in the middle and upper reaches. The efficiency value of the upstream region changes obviously. Excluding that the efficiency value of Tibet remains at the low level of 0.2235, the efficiency value of other upstream provinces and

regions fluctuates to varying degrees, and the spatial pattern changes obviously. In the middle reaches, the efficiency values of Jiangxi and Hubei increased to varying degrees in the four periods, while the efficiency values of Hebei and Hunan both decreased in 2016 after experiencing increases in 2009 and 2013; they increased again in 2019. There is no obvious fluctuation in the WUE in the downstream areas, showing a stable trend. Excluding that the WUE of Anhui remains at the low efficiency level of 0.2 to 0.3, the WUE of Guangdong, Fujian, Zhejiang, Shanghai, and Jiangsu is generally at a high efficiency level of 0.5 to 1.

Spatial and temporal distribution of STI

(1) Temporal characteristics. The temporal analysis reveals that the average value of the STI index for the 19 provinces and regions demonstrates a consistent upward trend, as depicted in **Figure 3**. This trend signifies that the STI of each province and region within the Yangtze River Basin is in a positive state

and is progressing in a favorable direction. Over the period from 2009 to 2019, the overall evaluation index of STI in the Yangtze River Basin experienced a gradual increase, rising from 0.0735 in 2009 to 0.2030 in 2019. Notably, between 2013 and 2019, the comprehensive evaluation index of STI ranged between 0.1 and 0.2, indicating a moderate level of overall technological advancement within the region.

(2) Spatial features. To analyze the spatial distribution of STI, the comprehensive evaluation index value of STI is calculated by employing the overall entropy weight method. Additionally, ArcGIS 10.2 software is employed to visualize the STI in the years 2009, 2013, 2016, and 2019 (**Figure 5**). At the regional level, a consistent pattern of “downstream > midstream > upstream” is observed in the STI of the Yangtze River Basin across the four periods. The spatial pattern of the STI system remains relatively stable. At the provincial level, the STI of the provinces and regions within the Yangtze River Basin

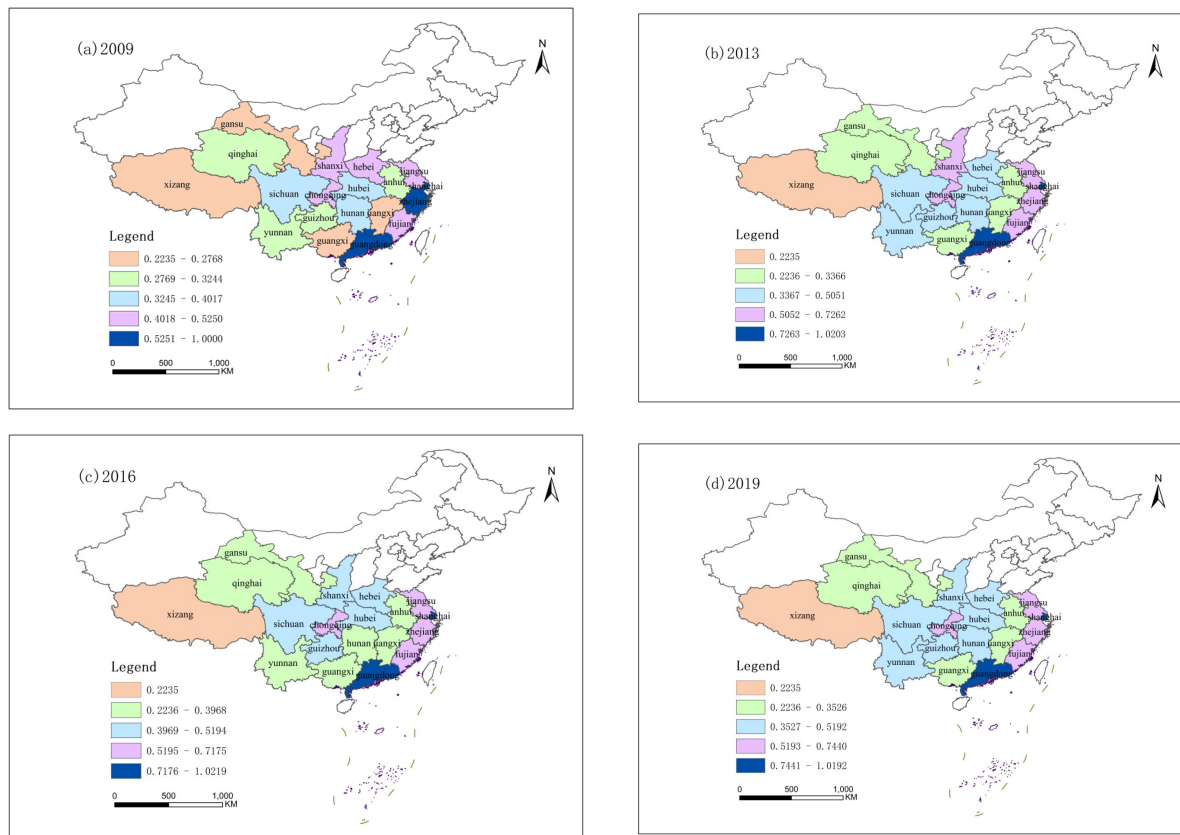


Figure 4. Spatial distribution of WUE of each province in the Yangtze River Basin.

exhibits varying degrees of improvement. There is a notable gap between the upper and middle reaches. On the contrary, the gap between the lower reaches is relatively small. Guangdong and Jiangsu consistently exhibit high STI indices across the four periods, consistently ranking in the top three and representing regions with a high level of STI. Conversely, Tibet and Qinghai consistently demonstrate lower STI indices, consistently ranking in the last three, indicating lower STI levels compared to other provinces and regions during the same period. These findings highlight the close relationship between STI and regional economic development. Provinces and regions with high economic development exhibit stronger human resource capabilities and other factors that contribute to the enhancement of regional STI.

4.2 Spatial and temporal distribution characteristics of CCD

Time characteristics

From the time series changes, the mean value of CCD of the two subsystems showed an increasing trend from 2009 to 2019 (**Figure 6a**). This trend suggests that there was an enhancement in the interaction between WUE and STI. Specifically, the coupling coordination level between WUE and STI during the study duration was within the basic coordination stage from 2009 to 2011, and progressed to the moderate coordination stage from 2012 to 2019. It is noteworthy that the stable improvement of the coupling coordination level throughout the research period was due to the common progress of both subsystems. Improvement in STI provided impetus for WUE, while the progress in WUE in turn facilitated STI improvement, leading to a joint promotion of the coupling coordination level from the basic coordination stage to the intermediate coordination stage. Overall, the coupling coordination level between WUE and STI in the Yangtze River Basin exhibited a positive trend; however, there is still room for further advancement in the overall coordination level.

From the perspective of basin division (**Figure 6b**), the mean CCD of the lower reaches of the

Yangtze River Basin is higher than that of the upper reaches. There are significant differences among different river basins. The average value of the upper reaches of the Yangtze River Basin is between 0.2-0.4, which belongs to the basic coordination stage; the average value of the middle reaches is between 0.4-0.5, which belongs to the moderate coordination stage; while the average value of the lower reaches is between 0.4-0.7, which is mostly in the highly coordinated stage. Mainly due to the influence of geographical factors and regional economic conditions among regions, the eastern coastal areas are relatively developed economically and have higher investment in scientific and technological innovation, so the CCD of STI and WUE is better.

Spatial distribution characteristics

To evaluate the spatial distribution characteristics of the CCD of the two subsystems, the provinces and regions are taken as the basic units, and 2009, 2013, 2016, and 2019 are selected as the representative years. The CCD is visualized using ArcGIS10.2 software, and the spatial distribution map of the CCD is drawn. The results are shown in **Figure 7**.

During the study period, the CCD of all provinces is generally not high, and most provinces and regions are in the basic coordination stage in the early stage. Thanks to the continuous progress of WUE and STI, the CCD of all provinces and regions shows an upward trend. From the regional aspect, the CCD of the two systems in the lower reaches is significantly higher than that in the upper and middle reaches of the Yangtze River Basin. Specifically, in 2009, the two regions of Guangdong and Jiangsu were highly coordinated, the two regions of Tibet and Qinghai were loosely coordinated, and the other regions were in moderate coordination. In 2016, highly coordinated provinces and cities began to appear in Guangdong, and then in 2019, highly coordinated provinces and cities were added in Jiangsu. The CCD of the two subsystems in Anhui, Fujian, and Hebei provinces, in the lower reaches of the Yangtze River, changed from basic coordination in 2009 to high coordination in 2019 after experiencing moderate coordination in 2013 and 2016. The CCD

of Shanghai, Hubei, and Sichuan subsystems experienced three periods of moderate coordination, after that is then rose to high coordination in 2019. In the three periods of 2009, 2013, and 2016, the CCD of the two subsystems in Jiangxi, Chongqing, and Shaanxi had been in the basic coordination stage, but in 2019, they entered the medium coordination stage. Between 2009 and 2019, there was a decrease in the number of provinces and regions that of basic coordination, while the number of highly coordinat-

ed provinces and regions showed an increase. This trend indicates an enhanced coordination between WUE and STI during the coupling process. Notably, the CCD of the two subsystems remains the most stable in Guangxi, Guizhou, Yunnan, Tibet, Gansu, and Qinghai, which are adjacent to the lower reaches of the Yangtze River Basin. However, these regions have predominantly remained in the basic coordination or low-level coordination stage, and the rate of improvement has been relatively slow.

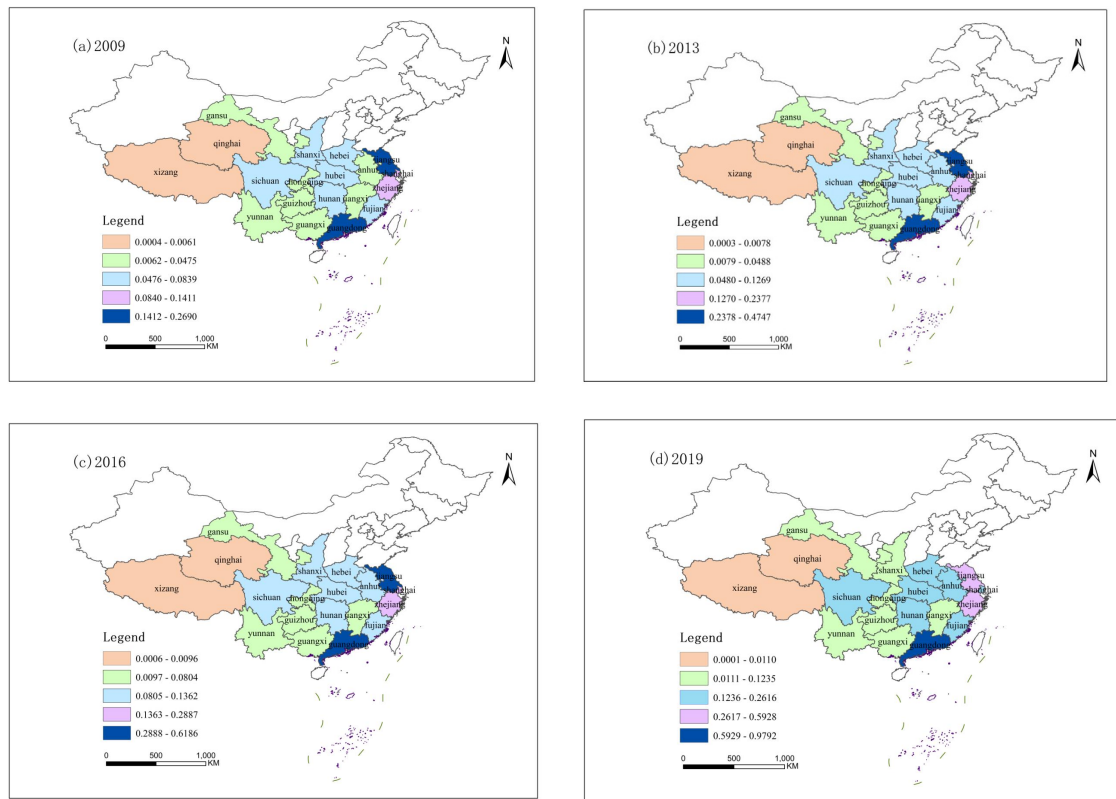


Figure 5. Spatial distribution of STI of each province in the Yangtze River Basin.

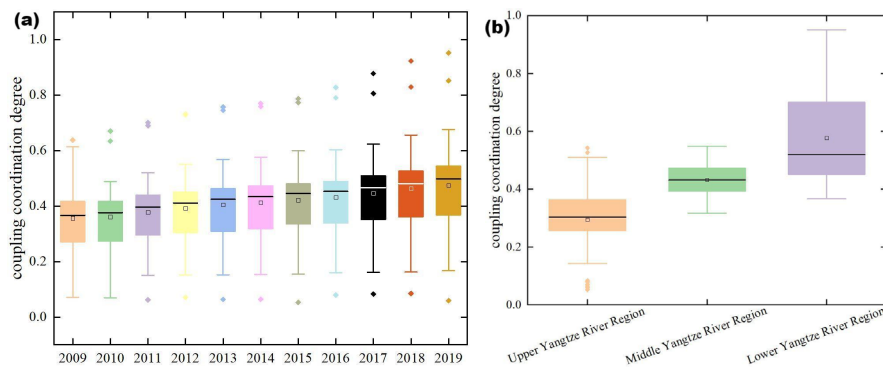


Figure 6. CCD mean time series change.

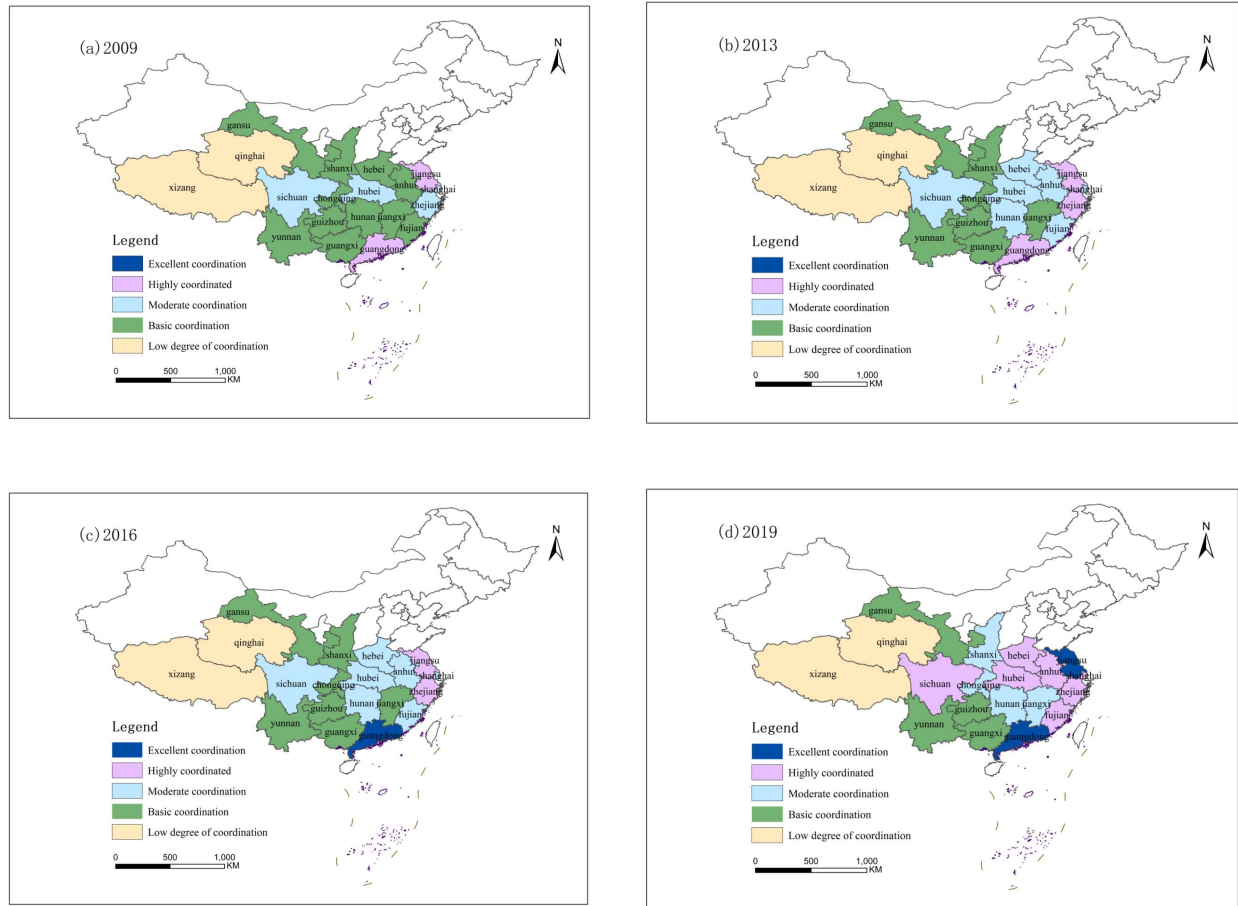


Figure 7. Spatial distribution of CCD between WUE and STI in the Yangtze River Basin.

4.3 Spatial correlation pattern analysis of CCD

The geographical spatial relationship among the 19 provinces in the Yangtze River Basin was taken into account by using distance spatial weight. GeoDa software was utilized to calculate the global Moran's I value. The results of this analysis are summarized in **Table 3**. The findings reveal a significant positive spatial correlation between the coupling coordination level of WUE and STI during the investigation period. This conclusion is supported by statistical indicators such as Moran's I, Z, and P values, which indicate a clear positive spatial autocorrelation.

Table 3. Global Moran's I of CCD.

Year	Moran's I	Z value	P value
2009-2013	0.2873	2.7935	0.0052
2013-2016	0.2915	2.8605	0.0042
2016-2019	0.3080	2.9154	0.0036

The precise location of the provincial spatial cluster and the intensity of regional correlation were determined using the local spatial autocorrelation index. This analysis also characterized the local spatial agglomeration features of the CCD in WUE and STI for the years 2009, 2013, 2016, and 2019. ArcGIS 10.2 software was employed to perform analytical processing on the spatial clustering results, resulting in the generation of a LISA clustering map for the CCD (**Figure 8**). This map provides a visually striking representation of the spatial heterogeneity of the CCD in the Yangtze River Basin. The local spatial correlation characteristics can be classified into two categories: High-High (H-H) concentration and Low-Low (L-L) concentration, observed in both subsystems of the Yangtze River Basin.

The H-H concentration area refers to provinces or cities with a high CCD between WUE and STI. In 2013 and 2016, Jiangsu was the only province in this

category, and its spatial pattern remained unchanged. However, in 2019, influenced by the surrounding provinces and cities, Jiangsu withdrew from the H-H cluster, resulting in zero provinces in this category. Provinces and cities in the H-H concentration area play a crucial role in regional coordinated development and are considered the weak points in provincial development. It is challenging for these regions to improve WUE and STI solely based on their own resources. Therefore, it is crucial for them to enhance connections with surrounding provinces and formulate targeted development strategies to make breakthroughs and promote WUE and STI.

L-L concentration area. In the four periods of

2009, 2013, 2016, and 2019, Tibet and Qinghai remained in the L-L concentration area, with no evident difference in their spatial distribution. The CCD of WUE and STI in this region is consistently low, indicating a need for improvement in regional coordinated development. The L-L agglomeration areas should be prioritized as the main focus for enhancing the level of coupling and coordination. To improve the coupling and coordination development in these provinces, it is important to strengthen exchanges and cooperation with surrounding provinces and cities, and formulate a development path that aligns with the specific circumstances of the region.

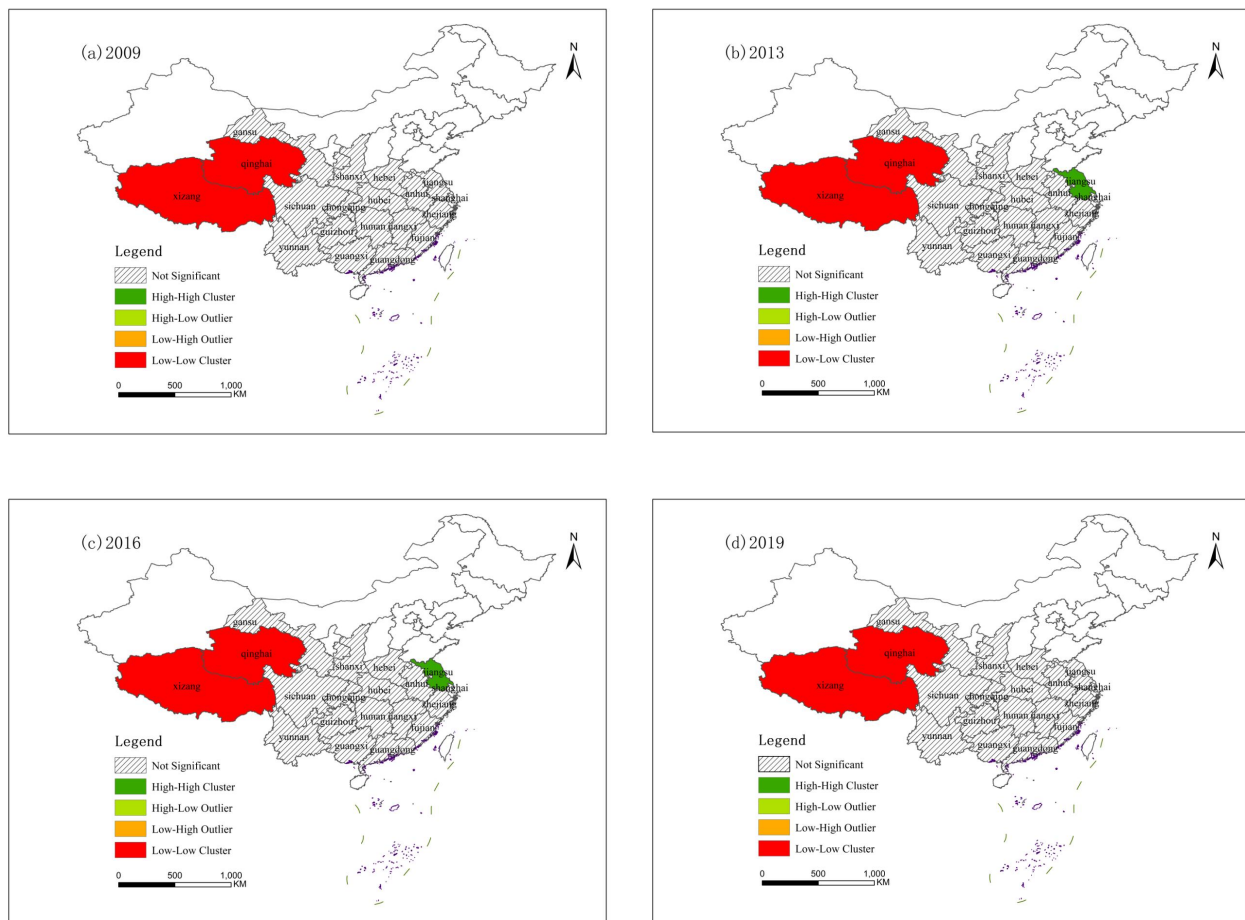


Figure 8. LISA concentration diagram of CCD.

4.4 Interactive response relationship between WUE and STI

Unit root inspection

The premise of the proposed VAR model is that the variables follow a single-order unit process. In this paper, ADF unit root test is performed on the level of each variable by using Eviews10.0 software (Table 4). There are three auxiliary equations for ADF test and three auxiliary equations for DF test:

(1) No intercept term and no trend term:

$$\Delta y_t = \rho y_{t-1} + \sum_{i=1}^k \gamma_i \Delta y_{t-i} + u_t \quad (20)$$

(2) Contains only intercept term:

$$\Delta y_t = c + \rho y_{t-1} + \sum_{i=1}^k \gamma_i \Delta y_{t-i} + u_t \quad (21)$$

(3) Contains intercept term and time trend term:

$$\Delta y_t = c + \alpha t + \rho y_{t-1} + \sum_{i=1}^k \gamma_i \Delta y_{t-i} + u_t \quad (22)$$

where the symbol Δ represents the first-order difference operator, c is the intercept term, αt is the trend term, $\sum_{i=1}^k \gamma_i \Delta y_{t-i}$ is n-distributed lag terms, u_t is the stationary random error term, and k is the maximum lag for determining u_t to satisfy the white noise. According to the calculation results of the three equations and the comparison of Akaike, the variables of WUE and STI are stable, with intercept term and time trend term.

According to the lag order information criterion, the optimal lag order is 8. Based on the criterion, the Granger causality test is performed on the above data. The results show that the P value of STI on WUE is 0.0000 (< 0.05), and the P value of WUE on STI is 0.0000 (< 0.05), which indicates that there is a two-way causal relationship between WUE and STI in each district and county, that is, WUE and STI are mutually endogenous variables.

Impulse response analysis based on panel VAR

In the Yangtze River Basin, it has been observed that the WUE and STI exhibit a notable positive response to the self-generated impulse in the first period, which gradually weakens until it is no longer significant. The study findings indicate that the self-enhancement mechanism of WUE persisted up to the fifth stage (Figure 9a), while that of STI

continued up to the second stage (Figure 9d). These outcomes suggest that the different provinces and regions have varying degrees of self-enhancement and path dependence for STI and WUE. Therefore, in addition to harnessing the self-enhancement mechanism, proactive measures must be implemented to avert any possible weakening of this mechanism.

Table 4. Inspection results of unit root.

	Level	T statistic	P value
WUE		-12.0080	0.0000
	1%	-4.0061	
	5%	-3.4332	
	10%	-3.1404	
STI		-10.5488	0.0000
	1%	-4.0060	
	5%	-3.4332	
	10%	-3.1404	

With regard to the driving effect of STI on WUE (Figure 9c), it is evident that while the former has an effect on the latter, the impacts are not very strong. A crucial factor responsible for this limited effect is the presence of a technical support system that impedes technological innovation in WUE, given the high level of uncertainty involved. Furthermore, the spatial accumulation effect of each district and county is not readily discernible, making it challengingly to pinpoint an overall effect. In response to WUE, the STI does not show an obvious impact, that is, the WUE has no significant encouraging effect on the STI (Figure 9b).

Prediction variance decomposition

The variance decomposition analysis provides insights into the cumulative contribution of one variable to another variable over time. Table 5 presents the results of the variance decomposition, revealing important trends. The impact of WUE on itself shows a declining trend, decreasing from 100% in the first phase to 85.62% in the tenth phase. Conversely, the contribution of WUE to STI shows an increasing trend, starting from 0% in the first phase and reaching 14.38% in the twentieth phase. These findings indicate that WUE has a practical significance in promoting STI, as it plays a role in positively influencing STI over time.

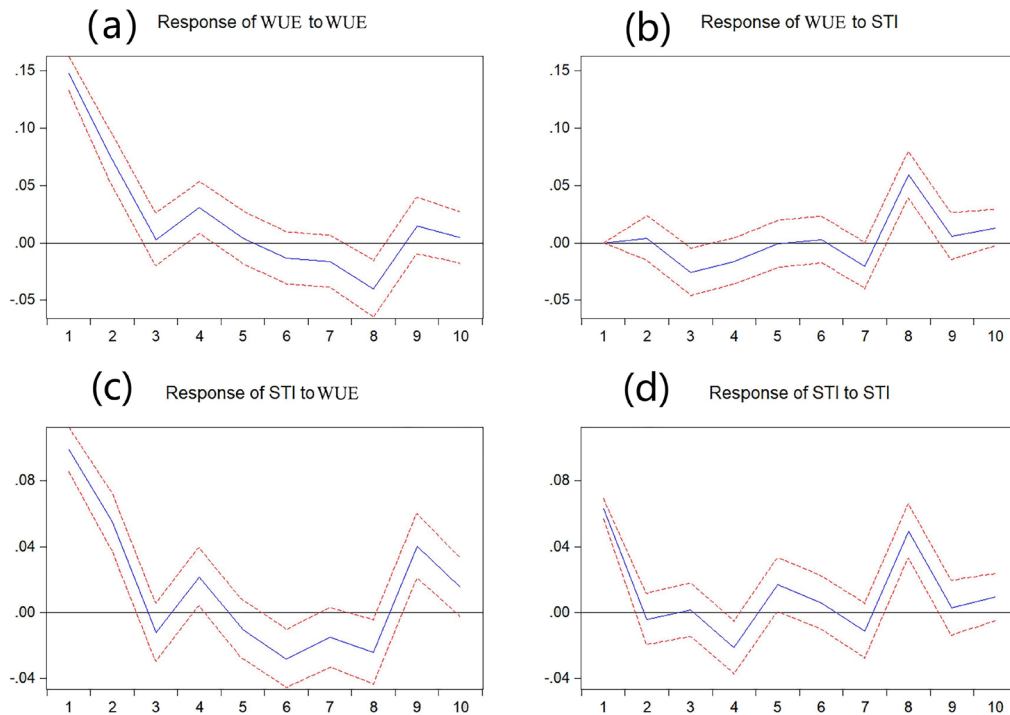


Figure 9. Impulse response of WUE and STI.

The impact of STI on its own decreased first and then increased, but the overall increase, from 28.85% in the first stage to 30.40%, reflects the self-improvement of STI. This suggests that STI has been experiencing self-improvement and growth. However, the impact of STI on WUE exhibits a declining trend, decreasing from 71.15% in the first phase to 69.60% in the tenth phase, albeit at a slow rate. This indicates that STI has a strong and sustainable role in promoting WUE.

Table 5. Variance decomposition results estimated based on panel VAR model.

Number of periods/period	WUE		STI	
	WUE	STI	WUE	STI
1	100.00	0.00	71.15	28.85
2	99.94	0.06	76.33	23.67
3	97.56	2.44	76.52	23.48
4	96.75	3.25	75.19	24.81
5	96.75	3.25	74.16	25.84
6	96.75	3.25	75.10	24.90
7	95.43	4.56	74.90	25.10
8	86.03	13.97	67.37	32.63
9	86.03	13.97	69.55	30.44
10	85.62	14.38	69.60	30.40

5. Conclusions and suggestions

5.1 Conclusions

The Yangtze River Basin plays a significant function in the economic development of China in the present era. Efficient utilization of water resources is vital for promoting sustainable development of the economy and society in this area, given its crucial ecological value. Enhancing WUE is essential for achieving ecological protection and fostering sustainable development in this region. STI is recognized as a key driver to overcome the challenges associated with low water resource efficiency. To delve deeper into this matter, the present study utilizes relevant data from 19 provinces and regions within the Yangtze River Basin spanning the years 2009 to 2019. Through the application of a coupling and coordination model, an indicator system is established to assess the coupling and coordination relationship between WUE and STI. Furthermore, a VAR model is employed to examine the relationship between WUE and STI, shedding light on their interdependence and mutual influence.

(1) A comprehensive analysis of the two systems reveals their overall growth, but also highlights the disparity in their development. The progress of WUE outpaces that of STI. For the spatial distribution, WUE shows a pattern of higher values in the lower reaches, followed by the higher middle reaches and lower upper reaches of the Yangtze River Basin. Similarly, the distribution of STI across different provinces and regions also exhibits a division into lower, middle, and upper reaches, with the lower reaches displaying higher values compared to the middle and upper reaches.

(2) Over time, the CCD values of both the WUE and STI subsystems in the Yangtze River Basin regions have shown varying degrees of improvement. Notably, provinces such as Guangdong, Zhejiang, Shanghai, and Jiangsu have demonstrated significant advancements, with their CCD values consistently leading across all stages. In particular, Guangdong and Jiangsu have achieved high-quality coordination between WUE and STI. However, it is essential to note that the other areas in the region have yet to reach this stage of high-quality coordination and further progress is required in these regions.

(3) The spatial distribution of the CCD in the Yangtze River Basin reveals two distinct patterns: H-H agglomeration areas and L-L agglomeration areas. There are no regions exhibiting L-H or H-L agglomeration. Furthermore, the degree of CCD agglomeration in most provinces is not pronounced. The L-L concentration areas are primarily observed in Tibet and Qinghai, situated in the upper reaches of the Yangtze River. On the other hand, the H-H concentration area is solely located in Guangdong in the lower reaches. The polarization of agglomeration in the basin indicates an imbalance and inadequacy in the coupling coordination of WUE and STI. Consequently, it is crucial for all regions within the basin to prioritize enhancing the mutual development of both subsystems to achieve better coordination and balance.

(4) Moreover, it is observed that the STI does not exhibit a substantial response to the influence of WUE, while WUE demonstrates a noticeable re-

sponse to STI. Both systems display diverse levels of self-enhancement and path dependence. Hence, the optimization of the interaction between these subsystems should be prioritized in order to achieve sustainable development in the Yangtze River Basin.

5.2 Suggestions

To facilitate the coordinated development of WUE and STI in the Yangtze River Basin, the current study offers several recommendations derived from the aforementioned research findings and the prevailing conditions within the basin.

(1) Efforts should be made to enhance WUE in the Yangtze River Basin region. It is imperative to ensure the strict implementation and continuous improvement of regulations pertaining to water resources management, taking into account the current developmental context. Stringent control measures should be imposed on total water consumption, with the refinement of consumption indicators at various levels and effective monitoring of compliance by provincial entities. Rational allocation of water resources is crucial, necessitating the implementation of robust planning and allocation strategies. The intensity of water resource development within the basin should be carefully controlled to maintain a sustainable balance. Coordinated management of water demand for different purposes is essential, while ensuring that ecological water replenishment is not compromised.

(2) Efforts should be directed towards enhancing the STI and achieving sustainable and environmentally friendly development in this regard. Provinces and autonomous regions within the Yangtze River Basin should prioritize optimizing their industrial structures by promoting the growth of low-energy consumption, eco-friendly, and high-tech industries, as well as emphasizing environmental protection and ecological industries. This approach will facilitate the realization of green development within the STI domain. Moreover, it is essential to allocate increased investments towards research and development (R & D) funds and advanced equipment to support scientific research and foster innovation activities.

Furthermore, there should be a focus on nurturing a pool of skilled scientific researchers, expanding the team of innovative talents, and facilitating the successful transformation of STI achievements.

(3) The coordinated development of WUE and STI should be attended to. The achievements of STI will be applied to the management and protection of water resources in the Yangtze River Basin. Through STI, the WUE will be promoted, and the pressure on water environments will be reduced. All provinces and regions should take into account the strengthening of the capacity of STI and the improvement of WUE, establish and improve the linkage between the two, achieve the two-pronged approach, and ensure coordinated development.

Author Contributions

Guangming Yang: Supervision, Funding acquisition. **Fengtai Zhang:** Conceptualization, Supervision. **Junyue Liu:** Formal analysis. **Qingqing Gui:** Data curation, Writing—original draft. **Siyi Cheng:** Visualization, Methodology.

Conflict of Interest

The authors declare that they have no known competing financial interests or personal relationships that could have appeared to influence the work reported in this paper.

Data Availability

The authors do not have permission to share data.

Acknowledgement

This research was funded by the Humanities and Social Science Research Project of Chongqing Education Commission (23SKJD111); Science and Technology Research Project of Chongqing Education Commission (KJQN202101122 and KJQN201904002); Project of Chongqing Higher Education Association (CQGJ21B057); Chongqing Graduate Education Teaching Reform Research Project (yjg223121); Chongqing Higher Education

Teaching Reform Research Project (233337); Higher Education Research Project, Chongqing University of Technology (2022ZD01); Annual project of the “14th Five-Year Plan” for National Business Education in 2022 (SKKT-22015); Party Building and Ideological and Political Project, Chongqing University of Technology (2022DJ307); Chongqing University of Technology Undergraduate Education and Teaching Reform Research Project (2021YB21). We want to thank the editor and anonymous reviewers for their valuable comments and suggestions for this paper.

References

- [1] UN World Water Development Report 2021 [Internet]. UN-Water [cited 2022 Dec 10]. Available from: <https://www.unwater.org/publications/un-world-water-development-report-2021>
- [2] Chang, Y.J., Zhu, D., 2021. Water utilization and treatment efficiency of China’s provinces and decoupling analysis based on policy implementation. *Resources, Conservation and Recycling*. 168, 105270. DOI: <https://doi.org/10.1016/j.resconrec.2020.105270>
- [3] Yang, G., Gong, G., Gui, Q., 2022. Exploring the spatial network structure of agricultural water use efficiency in China: A social network perspective. *Sustainability*. 14(5), 2668. DOI: <https://doi.org/10.3390/su14052668>
- [4] Wang, Q., Wang, X., 2020. Moving to economic growth without water demand growth—a decomposition analysis of decoupling from economic growth and water use in 31 provinces of China. *Science of the Total Environment*. 726, 138362. DOI: <https://doi.org/10.1016/j.scitotenv.2020.138362>
- [5] Song, M., Wang, R., Zeng, X., 2018. Water resources utilization efficiency and influence factors under environmental restrictions. *Journal of Cleaner Production*. 184, 611-621. DOI: <https://doi.org/10.1016/j.jclepro.2018.02.259>
- [6] Wang, Y., Bian, Y., Xu, H., 2015. Water use efficiency and related pollutants’ abatement costs of regional industrial systems in China: A slacks-


- based measure approach. *Journal of Cleaner Production*. 101, 301-310.
DOI: <https://doi.org/10.1016/j.jclepro.2015.03.092>
- [7] Zhao, L., Sun, C., Liu, F., 2017. Interprovincial two-stage water resource utilization efficiency under environmental constraint and spatial spill-over effects in China. *Journal of Cleaner Production*. 164, 715-725.
DOI: <https://doi.org/10.1016/j.jclepro.2017.06.252>
- [8] Bao, C., Fang, C.L., 2007. Water resources constraint force on urbanization in water deficient regions: A case study of the Hexi Corridor, arid area of NW China. *Ecological Economics*. 62(3-4), 508-517.
DOI: <https://doi.org/10.1016/j.ecolecon.2006.07.013>
- [9] Deng, G., Li, L., Song, Y., 2016. Provincial water use efficiency measurement and factor analysis in China: Based on SBM-DEA model. *Ecological Indicators*. 69, 12-18.
DOI: <https://doi.org/10.1016/j.ecolind.2016.03.052>
- [10] Liu, Y., Dong, F., 2021. How technological innovation impacts urban green economy efficiency in emerging economies: A case study of 278 Chinese cities. *Resources, Conservation and Recycling*. 169, 105534.
DOI: <https://doi.org/10.1016/j.resconrec.2021.105534>
- [11] Bouman, B.A.M., 2007. A conceptual framework for the improvement of crop water productivity at different spatial scales. *Agricultural Systems*. 93(1-3), 43-60.
DOI: <https://doi.org/10.1016/j.agsy.2006.04.004>
- [12] Statyukha, G., Kvitka, O., Shakhnovsky, A., et al., 2009. Water-efficiency as indicator for industrial plant sustainability assessment. *Computer Aided Chemical Engineering*. 26, 1227-1232.
DOI: [https://doi.org/10.1016/S1570-7946\(09\)70204-4](https://doi.org/10.1016/S1570-7946(09)70204-4)
- [13] Gregg, T.T., Strub, D., Gross, E., 2007. Water efficiency in Austin, Texas, 1983-2005: An historical perspective. *Journal-American Water Works Association*. 99(2), 76-86.
DOI: <https://doi.org/10.1002/j.1551-8833.2007.tb07870.x>
- [14] Benedetti, I., Branca, G., Zucaro, R., 2019. Evaluating input use efficiency in agriculture through a stochastic frontier production: An application on a case study in Apulia (Italy). *Journal of Cleaner Production*. 236, 117609.
DOI: <https://doi.org/10.1016/j.jclepro.2019.117609>
- [15] Wang, F., Yu, C., Xiong, L., et al., 2019. How can agricultural water use efficiency be promoted in China? A spatial-temporal analysis. *Resources, Conservation and Recycling*. 145, 411-418.
DOI: <https://doi.org/10.1016/j.resconrec.2019.03.017>
- [16] Bian, Y., Yan, S., Xu, H., 2014. Efficiency evaluation for regional urban water use and wastewater decontamination systems in China: A DEA approach. *Resources, Conservation and Recycling*. 83, 15-23.
DOI: <https://doi.org/10.1016/j.resconrec.2013.11.010>
- [17] Lombardi, G.V., Stefani, G., Paci, A., et al., 2019. The sustainability of the Italian water sector: An empirical analysis by DEA. *Journal of Cleaner Production*. 227, 1035-1043.
DOI: <https://doi.org/10.1016/j.jclepro.2019.04.283>
- [18] Carvalho, P., Marques, R.C., 2016. Estimating size and scope economies in the Portuguese water sector using the Bayesian stochastic frontier analysis. *Science of the Total Environment*. 544, 574-586.
DOI: <https://doi.org/10.1016/j.scitotenv.2015.11.169>
- [19] Hong, N.B., Yabe, M., 2017. Improvement in irrigation water use efficiency: A strategy for climate change adaptation and sustainable development of Vietnamese tea production. *Environment, Development and Sustainability*. 19, 1247-1263.
DOI: <https://doi.org/10.1007/s10668-016-9793-8>
- [20] Zhang, F., Xiao, Y., Gao, L., et al., 2022. How agricultural water use efficiency varies in China—A spatial-temporal analysis considering unexpected outputs. *Agricultural Water Management*. 260, 107297.
DOI: <https://doi.org/10.1016/j.agwat.2021.107297>
- [21] Gautam, T.K., Paudel, K.P., Guidry, K.M., 2020. An evaluation of irrigation water use efficiency in crop production using a data envelopment

- analysis approach: A case of Louisiana, USA. *Water*. 12(11), 3193.
DOI: <https://doi.org/10.3390/w12113193>
- [22] Segovia-Cardozo, D.A., Rodríguez-Sinobas, L., Zubelzu, S., 2019. Water use efficiency of corn among the irrigation districts across the Duero river basin (Spain): Estimation of local crop coefficients by satellite images. *Agricultural Water Management*. 212, 241-251.
DOI: <https://doi.org/10.1016/j.agwat.2018.08.042>
- [23] Geng, Q., Ren, Q., Nolan, R.H., et al., 2019. Assessing China's agricultural water use efficiency in a green-blue water perspective: A study based on data envelopment analysis. *Ecological Indicators*. 96, 329-335.
DOI: <https://doi.org/10.1016/j.ecolind.2018.09.011>
- [24] Chen, Y., Yin, G., Liu, K., 2021. Regional differences in the industrial water use efficiency of China: The spatial spillover effect and relevant factors. *Resources, Conservation and Recycling*. 167, 105239.
DOI: <https://doi.org/10.1016/j.resconrec.2020.105239>
- [25] Oulmane, A., Ali, C., Fria, A., 2019. The water use efficiency and its determinants in small horticultural farms in Algeria. *SN Applied Sciences*. 1(10), 1236.
DOI: <https://doi.org/10.1007/s42452-019-1238-1>
- [26] Wang, X.Y., 2010. Irrigation water use efficiency of farmers and its determinants: Evidence from a survey in northwestern China. *Agricultural Sciences in China*. 9(9), 1326-1337.
DOI: [https://doi.org/10.1016/S1671-2927\(09\)60223-6](https://doi.org/10.1016/S1671-2927(09)60223-6)
- [27] Jin, W., Zhang, H.Q., Liu, S.S., et al., 2019. Technological innovation, environmental regulation, and green total factor efficiency of industrial water resources. *Journal of Cleaner Production*. 211, 61-69.
DOI: <https://doi.org/10.1016/j.jclepro.2018.11.172>
- [28] Kang, S., Hao, X., Du, T., et al., 2017. Improving agricultural water productivity to ensure food security in China under changing environment: From research to practice. *Agricultural Water Management*. 179, 5-17.
DOI: <https://doi.org/10.1016/j.agwat.2016.05.007>
- [29] Miao, C., Fang, D., Sun, L., et al., 2018. Driving effect of technology innovation on energy utilization efficiency in strategic emerging industries. *Journal of Cleaner Production*. 170, 1177-1184.
DOI: <https://doi.org/10.1016/j.jclepro.2017.09.225>
- [30] Wang, H., Wang, M., 2020. Effects of technological innovation on energy efficiency in China: Evidence from dynamic panel of 284 cities. *Science of the Total Environment*. 709, 136172.
DOI: <https://doi.org/10.1016/j.scitotenv.2019.136172>
- [31] Yang, G., Gui, Q., Supanyo, P., et al., 2023. Temporal and spatial changes and influencing factors of low-carbon economy efficiency in China. *Environmental Monitoring and Assessment*. 195(1), 55.
DOI: <https://doi.org/10.1007/s10661-022-10599-3>
- [32] Xu, W., Zhang, X., Xu, Q., et al., 2020. Study on the coupling coordination relationship between water-use efficiency and economic development. *Sustainability*. 12(3), 1246.
DOI: <https://doi.org/10.3390/su12031246>
- [33] Zhang, Q., Shen, J., Sun, F., 2021. Spatiotemporal differentiation of coupling coordination degree between economic development and water environment and its influencing factors using GWR in China's province. *Ecological Modelling*. 462, 109794.
DOI: <https://doi.org/10.1016/j.ecolmodel.2021.109794>
- [34] Tang, C., Fan, J., Sun, W., 2015. Distribution characteristics and policy implications of territorial development suitability of the Yangtze River Basin. *Journal of Geographical Sciences*. 25, 1377-1392.
DOI: <https://doi.org/10.1007/s11442-015-1240-5>
- [35] Pellicer-Martínez, F., Martínez-Paz, J.M., 2016. Grey water footprint assessment at the river basin level: Accounting method and case study in the Segura River Basin, Spain. *Ecological Indicators*. 60, 1173-1183.
DOI: <https://doi.org/10.1016/j.ecolind.2015.08.032>
- [36] Sun, C., Zhao, L., Zou, W., et al., 2014. Water resource utilization efficiency and spatial spillover effects in China. *Journal of Geographical*

- Sciences. 24, 771-788.
DOI: <https://doi.org/10.1007/s11442-014-1119-x>
- [37] Zhang, F., Sun, C., An, Y., et al., 2021. Coupling coordination and obstacle factors between tourism and the ecological environment in Chongqing, China: A multi-model comparison. *Asia Pacific Journal of Tourism Research*. 26(7), 811-828.
DOI: <https://doi.org/10.1080/10941665.2021.1925715>
- [38] Hu, Y., Huang, Y., Tang, J., et al., 2018. Evaluating agricultural grey water footprint with modeled nitrogen emission data. *Resources, Conservation and Recycling*. 138, 64-73.
DOI: <https://doi.org/10.1016/j.resconrec.2018.04.020>
- [39] Cui, S., Dong, H., Wilson, J., 2020. Grey water footprint evaluation and driving force analysis of eight economic regions in China. *Environmental Science and Pollution Research*. 27, 20380-20391.
DOI: <https://doi.org/10.1007/s11356-020-08450-8>
- [40] Wu, B., Zeng, W., Chen, H., et al., 2016. Grey water footprint combined with ecological network analysis for assessing regional water quality metabolism. *Journal of Cleaner Production*. 112, 3138-3151.
DOI: <https://doi.org/10.1016/j.jclepro.2015.11.009>
- [41] Zhang, L., Dong, H., Geng, Y., et al., 2019. China's provincial grey water footprint characteristic and driving forces. *Science of the Total Environment*. 677, 427-435.
DOI: <https://doi.org/10.1016/j.scitotenv.2019.04.318>
- [42] Tone, K., 2001. A slacks-based measure of efficiency in data envelopment analysis. *European Journal of Operational Research*. 130(3), 498-509.
DOI: [https://doi.org/10.1016/S0377-2217\(99\)00407-5](https://doi.org/10.1016/S0377-2217(99)00407-5)
- [43] Yang, G., Gong, G., Luo, Y., et al., 2022. Spatiotemporal characteristics and influencing factors of tourism-urbanization-technology-ecological environment on the Yunnan-Guizhou-Sichuan Region: An uncoordinated coupling perspective. *International Journal of Environmental Research and Public Health*. 19(14), 8885.
DOI: <https://doi.org/10.3390/ijerph19148885>
- [44] Yang, G., Zhang, F., Zhang, F., et al., 2021. Spatiotemporal changes in efficiency and influencing factors of China's industrial carbon emissions. *Environmental Science and Pollution Research*. 28, 36288-36302.
DOI: <https://doi.org/10.1007/s11356-021-13003-8>
- [45] Guangming, Y., Qingqing, G., Fengtai, Z., et al., 2022. The temporal and spatial characteristics and influencing factors of low-carbon economy efficiency and science and technology development level in China's provinces from the perspective of uncoordinated coupling. *Frontiers in Environmental Science*. 10, 886886.
DOI: <https://doi.org/10.3389/fenvs.2022.886886>

ARTICLE

Sustainability Evaluation of Mangrove Forest Management System of Tagbanua Tribe in Bgy. Manalo, Puerto Princesa City, Palawan, Philippines

Mark Joseph J. Buncag^{1,3*} , Jaybie S. Arzaga², Liezl F. Tangonan², Jeffrey H. de Castro², Mary Claire M. Villanueva², Lilia Margallo², Imelda R. Lactuan², Sheryl G. Docto², Angelo V. Garcia², Princes Eunice C. Denosta², Sweet Angelikate L. Villaruel²

¹ Environmental Science and Graduate Department, College of Forestry and Environmental Studies, Mindanao State University Main Campus, 9700, Philippines

² College of Sciences, Palawan State University Main Campus, Palawan, 5300, Philippines

³ Social Sciences Division, National Research Council of the Philippines (NRCP), 1631, Philippines

ABSTRACT

Community-based forest management agreement in the country is a needed instrument in attaining sustainability of mangrove management. Sadly, there is no assurance that the system implemented in the mangrove forest management is sustainable. So, evaluating the mangrove management sustainability of the local tribe is a viable avenue for the appropriate management. In this study, the sustainability of the mangrove management system of the Tagbanua tribe in Bgy. Manalo, Puerto Princesa City, Palawan was evaluated. The study utilized various criteria with relevant indicators of sustainable mangrove forest management in assessing the mangrove forest management system. Focused group discussions were conducted to identify the relevant sustainable mangrove forest management C & I and verifiers. Each indicator was rated using the formulated verifiers in the form of the rating scale. Through household interviews, FGD, KII, mangrove assessment, and secondary data analysis, this study also used a mathematical model on the Sustainability Index for Individual Criteria (SIIC) to evaluate the scores for individual criteria and the Overall Sustainability Index (OSI) of the community. As a result, there are a total of seven relevant criteria, and 35 relevant indicators for Mangrove Management in Barangay Manalo. Based on the individual rating of seven criteria, the overall rating of the sustainable mangrove management system is 1.80, which implies a fairly sustainable mangrove management system. Also, the computed overall sustainability index is 0.26, which is fairly or moderately sustainable. Each criterion has strengths and weaknesses and needs to be improved to have a highly sustainable mangrove management system.

Keywords: Mangrove management system; Relevant criteria and indicators; Mangrove sustainability index

*CORRESPONDING AUTHOR:

Mark Joseph J. Buncag, Environmental Science and Graduate Department, College of Forestry and Environmental Studies, Mindanao State University Main Campus, 9700, Philippines; Social Sciences Division, National Research Council of the Philippines (NRCP), 1631, Philippines; Email: markjoseph.buncag@msumain.edu.ph

ARTICLE INFO

Received: 19 June 2023 | Revised: 15 September 2023 | Accepted: 21 September 2023 | Published Online: 28 September 2023

DOI: <https://doi.org/10.30564/jees.v5i2.5756>

CITATION

Buncag, M.J.J., Arzaga, J.S., Tangonan, L.F., et al., 2023. Sustainability Evaluation of Mangrove Forest Management System of Tagbanua Tribe in Bgy. Manalo, Puerto Princesa City, Palawan, Philippines. *Journal of Environmental & Earth Sciences*. 5(2): 36-49. DOI: <https://doi.org/10.30564/jees.v5i2.5756>

COPYRIGHT

Copyright © 2023 by the author(s). Published by Bilingual Publishing Group. This is an open access article under the Creative Commons Attribution-NonCommercial 4.0 International (CC BY-NC 4.0) License. (<https://creativecommons.org/licenses/by-nc/4.0/>).

1. Introduction

Mangrove forests are coastal ecosystems that offer numerous benefits to humans. They play a crucial role in stabilizing coastlines, safeguarding coastal communities against severe weather events, providing essential habitats for numerous animal species, and sequestering substantial amounts of carbon ^[1]. They are home to a diverse range of life forms, including terrestrial and marine animals, as well as humans ^[2]. Mangroves have been used as a source of building materials and charcoal in some areas ^[3]. In addition to their direct benefits, mangrove forests also provide important indirect benefits. For example, they can offer protective services by absorbing wave energy and serving as natural buffers against storms ^[4]. Mangroves have the ability to filter water by trapping sediments and pollutants with their roots, which prevents these materials from being disposed to the sea ^[5]. They serve as a habitat for a diverse range of bird and marine species and can serve as important nurseries and spawning grounds for aquatic life, such as shrimp and milkfish. Furthermore, the detritus food chain which is supported by the organic matter produced by mangroves provides a source of food for many marine animals ^[4].

Effective ecosystem management, such as the mangrove ecosystem, is essential for achieving sustainability and guaranteeing sustainable health and productivity of these ecosystems. One approach to achieving this is through co-management and community-based mangrove forest management, which involves collaboration between local communities and government agencies to develop and implement sustainable management practices ^[6,7]. While co-management between local government and community and sole management of mangrove forests by the community can be effective in promoting sustainability, it is important to recognize that not every management system is sustainable ^[8,9]. In this case, sustainability evaluation of the management system of the mangrove ecosystem is a practical approach to ensure the proper management of natural resources ^[7].

In Palawan, there are ongoing Mangrove Forest Management Systems, including the sole mangrove

management of the community in Barangay Manalo, City of Puerto Princesa, Palawan. The management of this 40-hectare mangrove forest is being overseen by the Manalo Tribal Organization, an Indigenous Cultural Community (ICC), as well as the local government of Bgy. Manalo and Puerto Princesa City Government. However, the management of the forest faces several challenges, including illegal cutting of mangrove trees, land title disputes, inadequate monitoring and law enforcement, and unsustainable aquaculture practices. Therefore, it is essential to assess the sustainability status of various mangrove management approaches to ensure proper management of these valuable resources. This study aims to assess the perception and awareness of the respondents towards criteria and indicators of sustainable mangrove management and to assess the sustainability of the mangrove forest management system of the Tagbanua tribe in Bgy. Manalo, Puerto Princesa City, Palawan, considering these challenges and opportunities for improvement.

2. Materials and methods

2.1 Research locale

The research was carried out in Barangay Manalo, Puerto Princesa City, Palawan, which is located at 9°58'30"N and 118°48'30"E, approximately 40 km from Puerto Princesa City proper as shown in **Figure 1**. The study focused on a 40-hectare mangrove forest within this area.



Figure 1. Map of Barangay Manalo.

2.2 Research design and instruments

The adopted research design is a mixed method which is a combination of both qualitative and quantitative research methods. The qualitative part of the study includes the identification of the relevant C & I existing management style. Meanwhile, the quantitative part of the method includes the assessment of the sustainability status of the existing management approach.

There are seven criteria and 57 indicators of forest management sustainability set by the Forest Management Bureau (FMB) to assess the sustainability status of the existing management approach. Note that the set C & I originate from the International Tropical Timber Organization (ITTO) ^[10]. To determine the applicable Sustainable Mangrove Forest Management Criteria and Indicators, this study utilized a Focus Group Discussion (FGD) approach. The FGDs were conducted with 12-15 participants and were guided by a set of questions, a recorder, and visual aids. In total, three FGDs were conducted as part of the study, including a validation process to ensure the relevance and applicability of the identified criteria and indicators ^[7,11,12].

Once the applicable criteria and indicators were identified, the study proceeded to verify the verifiers for each criterion and indicator. The verifiers were established in collaboration with the community and researchers, using a rating scale of 1 (poor), 2 (fair), and 3 (good) for individual indicators identified. The verifiers were established through a process of FGDs and KII, which involved a diverse group of stakeholders ^[12]. Three FGDs of at least 15 participants were conducted to formulate and validate the verifiers for each indicator that is applicable. The researchers performed validation and consultation on the developed rating scale. The participants for the FGD were multi-sectoral, which included community leaders, fishers, tour guides, leaders, members of Indigenous People (IP), farmers, women, the elderly, and community members ^[11,12].

Each indicator was rated using the formulated verifiers (rating scale) through household interviews (HHI), FGD, KII, mangrove assessment, and

analysis of existing and available secondary data. Also, the local community's awareness of applicable criteria and indicators is rated on a scale of 1 to 5. One signifies a very low awareness (below 20% awareness). Meanwhile, a value of two is rated for low awareness (with 21%-40% awareness), three for moderate awareness (with 41%-60% awareness), four for high awareness (with 61%-80% awareness), and five for very high awareness (81%-100% awareness) ^[12]. The local community's perception of the importance of applicable criteria and indicators was evaluated using a rating scale of 1 to 5. One is very insignificant, two (insignificant), three (no opinion), four (significant), and five (very significant).

The study implemented 50-meter transect lines with 10 m × 10 m quadrats along each transect to assess present mangrove species composition, population density, and DBH.

2.3 Research sample

The study used Robert Slovin's formula to decide the sample size for the HHI, based on 0.05 marginal error and a 95% confidence level. The computed sample size was 40 which was computed from the total number of households (n = 48) of the Manalo Tribal Organization. Included in the HHI are the members and officers of the said organization. For the Focus Group Discussions (FGDs), community leaders and members were selected as participants in each area. The sampling frame used in selecting the samples was the household list in each area, and random sampling was conducted using the Microsoft Excel random generator. Through these methods, the study was able to collect representative data from a sample of households and community members in the study area.

2.4 Data analysis

Descriptive statistics was used to analyze the socioeconomic characteristics of the respondents and the biophysical conditions. Furthermore, an FGD was implemented, and the resulting transcriptions were analyzed to determine the appropriate C & I for

forest management sustainability^[11]. To assess the management sustainability of the mangrove forest, other criteria were developed by the community, utilizing a rating scale. This scale was applied to each indicator. The data collected included ordinal data from the rating scale, as well as nominal and ratio data from socioeconomic characteristics such as household income, educational attainment, gender, age, and length of residence in the area. Spearman correlation test and Point-Biserial correlation analysis, conducted through SPSS software, were used to determine the relationship between the socioeconomic characteristics of the households and their perceptions^[13,14].

In this study, a mathematical model known as the SIIC was employed to assess the scores of individual criteria, as well as the OSI^[7]. This was used to compare the level of sustainability for each criterion and overall.

$$SIIC = \frac{\text{Sum of Weighted scores of indicators}}{\text{number of indicators in the respective criteria}}$$

$$OSI = \frac{\text{Sum of SIIC}}{\text{Number of Criteria}}$$

Source: Pokharel et al.^[7].

3. Results and discussions

3.1 Mangrove species composition in Bgy. Manalo, Puerto Princesa City

The mangrove species composition in Barangay Manalo, Puerto Princesa City, is shown in **Figure 2**. The most abundant species is *Rhizophora apiculata*, which comprises 34% of mangroves identified. Next is *Rhizophora mucronata* (29%) and *Xylocarpus granatum* (25%). Other mangroves species present are *Sonneratia alba*, *Rhizophora stylosa*, *Bruguiera cylindrica*, *Bruguiera gymnorrhiza*, *Avicennia alba*, *Ceriops tagal*, and *Lumnitzera granatum*.

3.2 Awareness and perception levels of respondents to applicable criteria and indicators

There are seven criteria, and 35 indicators are ap-

plicable to Mangrove Management in Bgy. Manalo. **Table 1** shows the awareness and perception of the respondents on the enabling condition of SFM. Except for item 1.5, it can be seen that the respondents have a high level of awareness of all the other items with weighted means of 3.825, 3.825, 3.525, 3.8, 4.025, and 3.85, respectively. Item 1.5 gained a mean of 3.275 which means that the respondents have moderate awareness of the procedures for for planning sustainable forest management. Similarly, the respondents were moderately aware of the process of regular monitoring, monitoring, evaluation, and progress feedback. The average of all the means is 3.73, which can be interpreted that the respondents have a high level of awareness of the enabling condition of SFM.

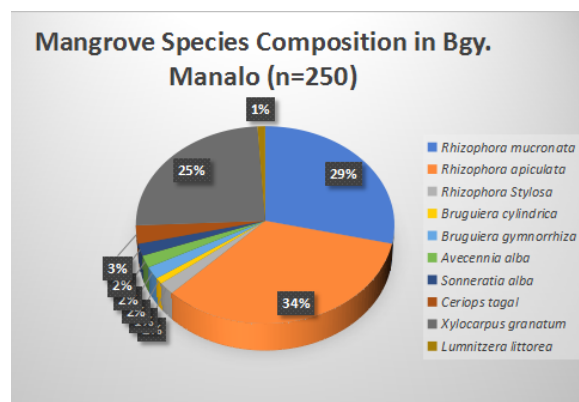


Figure 2. Mangrove species composition in Brgy. Manalo, Puerto Princesa City.

Regarding the perception of the respondents to the enabling condition of SMF, the table shows that they perceived that all the items are significant with averages of 4.175, 4.125, 3.85, 4.05, 4.05, 4.025, and 3.925, respectively. The overall mean of 4.02 reveals that the respondents perceived that the enabling condition of SFM is significant.

Table 2 presents the awareness and perception of the respondents on the extent and condition of the forest. It is indicated that the respondents have a high awareness of (a) the area and proportion of land area under the CLUP, (b) the area of forest allotted to production and protection, (c) the area and proportion of total land area under each forest type, and the (d) changes in a forested area with means of

4.025, 3.675, 3.925, and 4.125, respectively. Meanwhile, the respondents have moderate awareness of the forest condition, as interpreted from the mean of

3.4. The overall average is 3.83, which signifies that the respondents have a high awareness of the forest's extent and condition.

Table 1. Awareness and perception of the respondents on the enabling condition of SFM.

	<i>Indicator</i>	<i>Awareness</i>	<i>Interpretation</i>	<i>Perception</i>	<i>Interpretation</i>
<i>1. Enabling situation of SFM</i>	1.1 Presence of structure for laws, policies, and regulations.	3.825	High	4.175	Significant
	1.2 Forest Tenurial Instrument	3.825	High	4.125	Significant
	1.3 Amount of investment and reinvestment in forest management, administration, research, and human resource development	3.525	High	3.85	Significant
	1.4 Existence of, and ability to apply, appropriate technology to practice SFM and the efficient utilization and marketing of products.	3.8	High	4.05	Significant
	1.5 Capacity and mechanisms for planning SFM and for periodic monitoring, evaluation, and feedback on progress	3.275	Moderate	4.05	Significant
	1.6 Public participation in forest management planning, decision-making, data collection, monitoring, and assessment.	4.025	High	4.025	Significant
	1.7 Existence of Forest management plans	3.85	High	3.925	Significant
	Average	3.73	High	4.03	Significant
<i>Legend:</i> 4.51-5.00 <i>Very high*</i> <i>Very significant**</i> 3.51-4.50 <i>High*</i> <i>Significant**</i> 2.51-3.50 <i>Moderate*</i> <i>No opinion**</i> 1.51-2.50 <i>Low*</i> <i>Insignificant**</i> 1.00-1.50 <i>Very low*</i> <i>Very insignificant**</i>					

Table 2. Awareness and perception of the respondents on the extent and condition of forest.

	<i>Indicator</i>	<i>Awareness</i>	<i>Interpretation</i>	<i>Perception</i>	<i>Interpretation</i>
<i>2. Area and situation of forest</i>	2.1 Area and Proportion of land area under the comprehensive land-use plan (CLUP)	4.025	High	4.625	Very significant
	2.2 Area of forest allotted to production and protection.	3.675	High	4.025	Significant
	2.3 Area and proportion of total land area under each forest type	3.925	High	4.175	Significant
	2.4 Changes in the forested area	4.125	High	4.475	Significant
	2.5 Forest Condition	3.4	Moderate	3.525	Significant
	Average	3.83	High	4.165	Significant
<i>Legend:</i> 4.51-5.00 <i>Very high*</i> <i>Very significant**</i> 3.51-4.50 <i>High*</i> <i>Significant**</i> 2.51-3.50 <i>Moderate*</i> <i>No opinion**</i> 1.51-2.50 <i>Low*</i> <i>Insignificant**</i> 1.00-1.50 <i>Very low*</i> <i>Very insignificant**</i>					

Moreover, the respondents perceived that the land area covered in the comprehensive land-use plan (CLUP) is very significant, based on the mean of 4.625. Furthermore, they perceived that the (a) forest area intended for production and protection, (b) areal extent of each forest type, (c) variation in the area covered by forest, and (d) forest condition are significant with 4.025, 4.175, 4.475, and 3.525, respectively. The overall mean for perceptions is 4.165, which means that the respondents perceived that the extent and condition of the forest are significant.

Table 3 shows the awareness and perception of the respondents on forest ecosystem health. Respondents generally have a high level of awareness for both indicators of Criterion 3, with means of 3.9 and 4.375, respectively. The average of the means is 4.14, which states that the respondents have a high

awareness of forest ecosystem health.

The respondents perceived that the extent and nature of forest encroachment, degradation, and disturbance due to human interventions are significant. At the same time, they do not agree on the area and nature of forest depletion and disturbance caused by natural means, according to the calculated means of 3.9 and 3.5, respectively. The overall average of 3.7 signifies that the respondents perceived that the forest ecosystem health is significant.

Table 4 presents the awareness and perception of the respondents on forest production. The respondents have a high level of awareness of indicator 4.1 (mean = 3.925) and indicator 4.3 (mean = 4.1). However, they have a moderate awareness indicator 4.2. Despite that, the overall average is still 3.71, which states that the respondents have a high awareness of forest production.

Table 3. Awareness and perception of the respondents on forest ecosystem health.

	<i>Indicator</i>	<i>Awareness</i>	<i>Interpretation</i>	<i>Perception</i>	<i>Interpretation</i>
3. Health of forest	3.1 The area and nature of forest encroachment and disturbance affected by human	3.9	High	3.9	Significant
	3.2 The area and nature of forest depletion and disturbance caused by natural causes.	4.375	High	3.5	No opinion
	Average	4.14	High	3.7	Significant
<i>Legend:</i>					
	4.51-5.00	Very high*	Very significant**		
	3.51-4.50	High*	Significant**		
	2.51-3.50	Moderate*	No opinion**		
	1.51-2.50	Low*	Insignificant**		
	1.00-1.50	Very low*	Very insignificant**		

Table 4. Awareness and perception of the respondents on forest production.

	<i>Indicator</i>	<i>Awareness</i>	<i>Interpretation</i>	<i>Perception</i>	<i>Interpretation</i>
4. Forest production	4.1 Area and proportion of forest which inventory and survey measures have been applied to assess the quantity of the primary forest products.	3.925	High	4.025	Significant
	4.2 Actual yield of wood and non-wood forest products	3.1	Moderate	3.275	No opinion
	4.3 Harvest Composition	4.1	High	3.375	Significant
	Average	3.71	High	3.56	Significant
<i>Legend:</i>					
	4.51-5.00	Very high*	Very significant**		
	3.51-4.50	High*	Significant**		
	2.51-3.50	Moderate*	No opinion**		
	1.51-2.50	Low*	Insignificant**		
	1.00-1.50	Very low*	Very insignificant**		

In terms of the respondent's perception, the area and proportion of forest for which inventory and survey measures have been applied to assess the quantity of the forest products and composition of harvest are perceived to be significant, as revealed from their means of 4.025, and 3.275, respectively. Nonetheless, the participants in the study have no opinion about wood and non-wood forest products (mean = 3.275). The overall mean of 3.56 reveals that they perceived that forest production is significant.

Table 5 portrays the awareness and perception of the respondents on biological diversity. They have a high level of awareness for indicator 5.1. The respondents are also highly aware of the quantity of endangered and threatened forest-reliant plants and animals, measures of in situ, and ex-situ of the genetic variation within the commercial, endangered, rare, and threatened species of forest plants and animals, and the presence and enactment of procedures for safety and monitoring of plants and animals species

in the production zone of forests, with means of 3.9, 3.975, 3.875, and 4.2, respectively. The overall mean of 3.99 suggests that the respondents have a high level of awareness of biological diversity.

Regarding their perception of biological diversity, they perceived that the presence and enactment of procedures to classify and guard endangered and threatened species of forest plants and animals, the number of endangered, rare, and threatened forest-dependent species. The measures of in situ and ex-situ of the genetic variation within the commercial, endangered, rare, and threatened species of forest flora and fauna are all significant with means 4.225, 4.025, and 4.1, respectively. Furthermore, they perceived that the presence and enactment of procedures for safeguarding and checking biodiversity in the production zone of forest area is very significant, having an average of 4.7. The whole mean of 4.26 indicates that their perception of biological diversity is significant.

Table 5. Awareness and perception of the respondents on biological diversity.

	<i>Indicator</i>	<i>Awareness</i>	<i>Interpretation</i>	<i>Perception</i>	<i>Interpretation</i>
5. Biodiversity	5.1 Presence and enactment of procedures to identify and safeguard endangered and threatened species of forest plants and animals.	3.9	High	4.225	Significant
	5.2 Quantity of endangered and threatened forest-dependent species	3.975	High	4.025	Significant
	5.3 Measures of in situ and ex-situ of the genetic variation within the commercial, endangered, rare, and threatened species of forest flora and fauna	3.875	High	4.1	Significant
	5.4 Presence and implementation of procedures for protection and monitoring of biodiversity in production forests	4.2	High	4.7	Very significant
	Average	3.99	High	4.26	Significant
<i>Legend:</i> <div> <div>4.51-5.00</div> <div>3.51-4.50</div> <div>2.51-3.50</div> <div>1.51-2.50</div> <div>1.00-1.50</div> </div> <div> <div>Very high*</div> <div>High*</div> <div>Moderate*</div> <div>Low*</div> <div>Very low*</div> </div> <div> <div>Very significant**</div> <div>Significant**</div> <div>No opinion**</div> <div>Insignificant**</div> <div>Very insignificant**</div> </div>					

Table 6 presents the awareness and perception of the respondents on soil and water protection. The respondents have a high level of awareness of the procedures to guard downriver catchment and measures to maintain the productivity of soil and the capability of the soil to hold water inside a production zone of forests, as implied by means 4.225 and 4.4, respectively. However, there is a moderate level of awareness of the procedures for forest engineering based on the mean of 3.375. The combined means resulted in an average of 4, which translates to high awareness for soil and water protection.

The respondents perceived that the processes in safeguarding downstream catchment values, productivity of soil and water holding capacity, forest industry and engineering are all significant, having an average of 4.2, 4.25, and 3.85, respectively. They perceived that soil and water protection is significant from the overall average of 4.1.

Table 7 shows the awareness and perception of the respondents on the economic, social, and cultural aspects. It can be interpreted from the table that the participants of the study have a very high level of awareness for the participation of the indigenous cultural community, local people, and other forest inhabitants, in forest management capacity building, discussion, decision-making, and implementation (mean = 4.65). Moreover, the respondents have a high level of awareness of (a) the forest products industry organization and effectiveness (mean = 3.6), (b) the presence and enactment of conflict resolution

procedures for solving disagreements between interested parties (mean = 3.775), (c) the number of community members depending on forests for their occupation (mean = 3.825), (d) the area of forests use for traditional and customary lifestyles (3.825), (e) the area of forest sites allotted and accessible for research and instruction, and recreational activity (mean = 3.9), (f) the quantity of significant cultural, and spiritual sites discovered and safeguarded (mean = 3.9), (g) the level to which user rights of the indigenous cultural community over publicly owned forests are acknowledged and practised (mean = 3.85), and (h) the indigenous knowledge is utilized in forest management planning and implementation (mean = 3.725). In addition, they have a moderate level of awareness for (a) the worth of produced wood, and non-wood forest products in the market (mean = 3.375), and (b) the coaching, capacity building, and workforce development programs for forest workforce (mean = 3.325). The overall mean of 3.84 signifies that the respondents have a high awareness of the economic, social, and cultural aspects.

On the other hand, the overall mean of 4.06 for the perception suggests that the study's respondents perceived the economic, social, and cultural aspects as significant. Specifically, they perceived that the worth of produced wood, non-wood forest products in the market (mean = 3.525), the forest products industry organization and effectiveness is significant, the presence and enactment of conflict resolution procedures for solving disagreements between interested party

Table 6. Awareness and perception of the respondents on soil and water protection.

		<i>Awareness</i>	<i>Interpretation</i>	<i>Perception</i>	<i>Interpretation</i>
<i>6. Protection of soil and water</i>	6.1. Processes to assure protection of downstream catchment values	4.225	High	4.2	Significant
	6.2 Processes to safeguard soil productivity and water retention capacity within production zone of forest area	4.4	High	4.25	Significant
	6.3 Processes for forest engineering	3.375	Moderate	3.85	Significant
	Average	4	High	4.1	Significant
<i>Legend:</i>	4.51-5.00	Very high*	Very significant**		
	3.51-4.50	High*	Significant**		
	2.51-3.50	Moderate*	No opinion**		
	1.51-2.50	Low*	Insignificant**		
	1.00-1.50	Very low*	Very insignificant**		

(mean = 4.1), the quantity of community members depending on forests for their occupation (mean = 3.875), the coaching, capacity building, and workforce development programs for forest workforce (mean = 3.925), the area of forests use for traditional and customary lifestyles (mean = 4.05), the area of forest sites allotted and accessible for research and instruction, and tourism activity (mean = 3.975), the quantity of significant cultural, and spiritual sites discovered and safeguarded (mean = 4.175), the level to which user rights of

indigenous cultural community over publicly owned forests are acknowledged and practiced (mean = 4.45), and the indigenous knowledge is utilized in forest management planning and implementation (4.0) are all significant. Besides, they have perceived that the participation of indigenous cultural community, local people, and other forest inhabitants, in forest management capacity building, discussion, decision-making, and implementation is very significant, having a mean of 4.80.

Table 7. Awareness and perception of the respondents on the economic, social, and cultural aspects.

		<i>Awareness</i>	<i>Interpretation</i>	<i>Perception</i>	<i>Interpretation</i>
<i>7. Economic, social, and cultural</i>	7.1 Worth of produced wood, non-wood forest products in the market	3.375	Moderate	3.525	Significant
	7.2 Forest products industry organization and effectiveness	3.6	High	4.1	Significant
	7.3 Presence and enactment of conflict resolution procedures for solving disagreements between interested party.	3.775	High	3.875	Significant
	7.4 Quantity of community members depending on forests for their occupation	3.825	High	3.925	Significant
	7.5 Coaching, capacity building, and workforce development programs for forest workforce.	3.325	Moderate	3.825	Significant
	7.6 Area of forests use for traditional and customary lifestyles.	3.825	High	4.05	Significant
	7.7 Area of forest sites allotted and accessible for research and instruction, and tourism activity.	3.9	High	3.975	Significant
	7.8 Quantity of significant cultural, and spiritual sites discovered and safeguarded.	3.85	High	4.175	Significant
	7.9 Level to which user rights of indigenous cultural community over publicly owned forests are acknowledged and practiced.	4.425	High	4.45	Significant
	7.10 Indigenous knowledge is utilized in forest management planning and implementation.	3.725	High	4	Significant
	7.11 Participation of indigenous cultural community, local people, and other forest inhabitants, in forest management capacity building, discussion, decision-making, and implementation	4.65	Very high	4.8	Very significant
	Average	3.84	High	4.06	Significant
<i>Legend:</i> <div> <div>4.51-5.00</div> <div>3.51-4.50</div> <div>2.51-3.50</div> <div>1.51-2.50</div> <div>1.00-1.50</div> </div> <div> <div>Very high*</div> <div>High*</div> <div>Moderate*</div> <div>Low*</div> <div>Very low*</div> </div> <div> <div>Very significant**</div> <div>Significant**</div> <div>No opinion**</div> <div>Insignificant**</div> <div>Very insignificant**</div> </div>					

3.3 Relationship between socioeconomic characteristics and awareness of applicable criteria and indicators (C & I) of the community in Bgy. Manalo, Puerto Princesa City

The relationship between socioeconomic characteristics and awareness level on the suitable C & I in Bgy. Manalo was analyzed using the non-parametric Spearman correlation test, except for gender, where the point-biserial correlation was applied. **Table 8** shows that livelihood has a p-value of 0.030 and a positive coefficient. The p-value is less than 0.05 alpha level ($0.030 < 0.05$). Therefore, the livelihood and awareness level on the relevant C & I significantly correlates (positive correlation). Also, income has a p-value of 0.000 and a negative coefficient. The p-value is less than 0.01 and 0.05 alpha level ($0.049 < 0.01 < 0.05$). Therefore, the income and awareness level on the suitable C & I significantly correlates (negative correlation).

Table 8. Socioeconomic characteristics and awareness level on the suitable C & I in Bgy. Manalo.

Level of awareness	Coefficient	P-value
Age	-0.306	0.055
Gender	0.273	0.088
Civil status	-0.060	0.713
Educational Attainment	-0.115	0.478
Livelihood	0.343*	0.030
Income	-0.528**	0.000
No. of years living in the community	0.112	0.493
**Significant correlation at the 0.01		
*.Significant correlation at the 0.05		

3.4 Relationship between socioeconomic characteristics and perception of the importance of applicable criteria and indicators (C&I) of the community in Bgy. Manalo

Similarly, statistical treatments were applied to determine the relationship between socioeconomic characteristics and perception of the importance of the suitable C & I in Bgy. Manalo. **Table 9** shows that age obtained a p-value of 0.021 and a positive

coefficient. Therefore, the age and perception of the importance of the relevant C & I have a significant correlation (positive correlation). Gender, livelihood, civil status, educational attainment, livelihood, and income have a weak negative correlation, while the number of years living in the community has a trivial positive correlation.

Table 9. Socioeconomic characteristics and perception on the importance of relevant C & I in Manalo.

Perception to importance of applicable C & I	Coefficient	P-value
Age	0.363*	0.021
Gender	-0.233	0.147
Civil status	-0.155	0.339
Educational Attainment	-0.163	0.316
Livelihood	-0.175	0.280
Income	-0.032	0.844
No. of years living in the community	0.116	0.475
*. Correlation is significant at the 0.05 level (2-tailed).		

3.6 Evaluation of sustainability

The evaluation of the mangrove management sustainability is mainly based on the mean scores of each criterion ^[15], presented in **Table 10**. Verifiers through a Likert scale of 1-3 (1 = Poor, 2 = Fair, 3 = Good) were used to quantify each indicator for each criterion. The meaning of 1.29 on Criterion 1 translates to poor condition. Reasons such as lack of policy implementation for mangrove management, no awarded tenurial instrument to the community, no available funding for mangrove forest management and protection, no existing adopted technology for the management, and low capacity of the community in mangrove management planning may be associated to the result of the assessment. Meanwhile, Criterion 2 has a mean score of 2.20 or fair condition. Note that there have been neither significant good nor bad changes in the mangrove area for the last five years. Only 70% of the mangrove area is in good condition. The mangrove management system garnered a mean of 2.50 (Fair Condition) on Criterion 3.

An estimated 10% of the total area was degraded and disturbed caused by human activities. Also, an estimated 2% of the total area was damaged or affected by natural calamities. Criterion 4 has a mean score of 1.67 or fair condition. During the focus group discussion, it was found that there is no existing inventory system of harvested products (wood and non-wood) from the mangrove area.

Criterion 5 has a mean score of 1.25, which is considered poor condition. There are no implemented procedures to protect the wildlife in the area. Also, Criterion 6 has a rating of 1.67 (fair condition). The management has procedures to protect water, soil productivity, and water retention capacity within the production forest but has not implemented them. In terms of forest engineering, there is no existing plan or implemented plan provided. Lastly, Criterion 7 has a mean score of 2.00, under poor conditions. Their existing management has no structure for forest product industry efficiency and no available forest site for recreation, research, and educational use. The community has an existing conflict resolution mechanism but has not implemented it. In addition, there is a high level of involvement of the indigenous cultural community in the management. The traditional practices of Tagbanua were adopted in their management system. In the case of Tagpait, Aborlan mangrove, indigenous people use traditional practices in implementing ecotourism to protect mangroves and generate income^[16]. Sustainable forest management practices provide welfare impact like in the case scenario presented in Sabah, Malaysia where the reduction of harvested area or control of harvest of natural resources and increase in market access may provide higher social benefits^[17].

Based on the individual rating of seven criteria, the overall rating of the sustainable mangrove management system of Bgy. Manalo is 1.80, which implies a fairly sustainable mangrove management system.

In addition, the Sustainable Index for Individual Criteria (SIIC) and the Overall Sustainability Index (OSI) were applied to the mean scores of each criterion further to assess the status sustainability of the

management approach. These are mathematically expressed as:

Table 10. Mean of scores for each criterion.

Criteria	Score
C1 enabling situation of SFM	1.29
C2 area and situation of forest	2.20
C3 forest health	2.50
C4 forest production	1.67
C5 biodiversity	1.25
C6 protection of soil and water	1.67
C7 economic, social, and cultural	2.00
Grand mean	1.80
Note: If > 2.5 (Good); > 1.5 ≤ 2.5 (Fair); ≤ 1.5 (Poor)	

$$SIIC = \frac{\text{Sum of Weighted scores of indicators}}{\text{number of indicators in the respective criteria}}$$

$$OSI = \frac{\text{Sum of SIIC}}{\text{Number of Criteria}}$$

Source: Based on Pokharel et al., 2015.

The sum of scores for each indicator is presented in **Table 11**. Criterion weight and a number of criteria and indicators were utilized in the calculation. 14.28% is the criterion weight which is evenly divided into seven criteria. It is highly sustainable if the computed value of SIIC and OSI is ≥ 0.40 and ≥ 0.25 if moderately sustainable. Also, if the value is < 0.25 , it is poor or low sustainable.

Table 11. The sum of scores for each indicator of the criteria for Sustainable Mangrove Forest Management.

Criterion	Sum of scores
Criterion 1	9
Criterion 2	11
Criterion 3	5
Criterion 4	5
Criterion 5	5
Criterion 6	5
Criterion 7	22

Table 12 presents the sustainability index for individual criteria of the mangrove management system of Bgy. Manalo, Puerto Princesa City. Each criterion should be improved in order to have a highly sustainable mangrove management system—the computed overall sustainability index of Bgy. Manalo mangrove management system is 0.26, which is

considered moderately sustainable.

The evaluation of the sustainability of the mangrove forest management system is a useful mechanism for sustainable mangrove forest management. In Indonesia, the evaluation of the sustainability of mangrove management was adopted as their planning and management tool for its sustainability. In the mangrove forest in Damas Beach, Trenggalek, Indonesia, the status of management is unsustainable because the ecological dimensions fall under fairly sustainable. Also, the economic, social, legal and institutional category falls under the less sustainable category due to the conversion of mangroves into coconut plantations ^[18]. In the case of North Sumatra, Indonesia, mangroves ecotourism was adopted as a mechanism for sustainable management of mangrove, particularly in improving ecological, social, and economic dimensions, including the local community from upland ^[19]. Their management, the upland ecosystem and upland communities are directly part of their sustainable mangrove management. In the case of the Matang mangrove reserve in Malaysia, the local community is aware that the mangrove provides charcoals and timber but is not knowledgeable about other services like carbon sequestration, which serves as a barrier to sustainability ^[20].

Table 12. SIIC and OSI values.

Criteria	SIIC
Criterion 1	0.18
Criterion 2	0.31
Criterion 3	0.36
Criterion 4	0.24
Criterion 5	0.18
Criterion 6	0.24
Criterion 7	0.29
(OSI)	0.26
Note: Highly sustainable if ≥ 0.40 ; moderately sustainable if ≥ 0.25 but < 0.40 ; poorly sustainable if < 0.25 .	

4. Conclusions and recommendations

4.1 Conclusions

The sustainability of a mangrove management

system is inseparable from continuous monitoring and improvement of the weak points. No monitoring tool is “one size fits all”; hence, there is a need to formulate one such that it encompasses the monitoring indicators that are appropriate to the context. After a series of data gathering, 35 indicators under the seven criteria were identified as applicable to managing mangroves in Brgy. Manalo, Puerto Princesa City. The result of the initial application of the monitoring tool concludes that there is moderate sustainability in the current mangrove management system. The management was even rated with low sustainability on four criteria. These problems, when not addressed, could jeopardize the availability of the mangroves’ ecosystem services to the nearby community. Information in this study would be a call to both leaders of the organizations and the community residents to create actions that could strengthen the weak management points and reinforce the strong ones.

4.2 Recommendations

The authors of this study have created a monitoring tool that applies to the current mangrove management system in Brgy. Manalo, Puerto Princesa City. The tool is crafted to be appropriate, convenient, easy to use, and requires less technical knowledge. It is highly recommended that the governing organization adopt this tool when conducting a regular assessment of the sustainability status. This tool is also helpful in determining both the strong and weak points of the management. Leaders could now create action plans focusing on these identified points to enhance the overall sustainability status of the management approach. The academe is willing to provide technical support to the community leaders in addressing the issues related to mangrove management.

With a few modifications, the monitoring tool can be applied to other mangrove communities in the city. Using this tool would capacitate the leaders in improving the sustainability of the mangrove management so that the residents would maximize the benefits from the mangroves. It is suggested that

more research and extension activities be conducted in other mangrove areas.

Author Contributions

The first author served as the team leader, who was directly involved in proposal making, instrument development and validation, data gathering, data analyses and report writing and revisions. The second to fourth authors were directly involved in instrument development and validation, data gathering, data analyses and report writing. The rest of the authors including the last author were directly involved in instrument development and validation and data gathering, report improvement. Also, the last author was directly involved in writing and paper revision.

Conflict of Interest

There is no conflict of interest.

Data Availability Statement

Data stated in this paper can be publicly available. The use of data can be for reading and citation only. The publicly available data are only those stated in the manuscript and some data that are not allowed to be disclosed are not stated.

References

- [1] Mangroves [Internet]. United Nations University-Institute for Water, Environment, and Health; 2016. Available from: <https://inweh.unu.edu/mangroves/>
- [2] Carter, H.N., Schmidt, S.W., Hirons, A.C., 2015. An international assessment of mangrove management: incorporation in integrated coastal zone management. *Diversity*. 7(2), 74-104.
- [3] Gonzales, B.J., Sario, R.S., Montaño, B.S., 2017. Social benefits and impacts of mangrove resource utilization in Rio Tuba, Bataraza, Palawan, Philippines. *Advances in Environmental Sciences*. 9(2), 135-147.
- [4] Daupan, S.M.M.A.V., 2016. Community participation in mangrove forest management in the Philippines: management strategies, influences to participation, and socioeconomic and environmental impacts [Ph.D. thesis]. Ann Arbor: University of Michigan.
- [5] Hema, M., Indira Devi, P., 2014. Factors of mangrove destruction and management of mangrove ecosystem of Kerala, India. *Journal of Aquatic Biology and Fisheries*. 2, 184-196.
- [6] Datta, D., Chattopadhyay, R.N., Guha, P., 2012. Community based mangrove management: A review on status and sustainability. *Journal of Environmental Management*. 107, 84-95.
- [7] Pokharel, R.K., Neupane, P.R., Tiwari, K.R., et al., 2015. Assessing the sustainability in community based forestry: A case from Nepal. *Forest Policy and Economics*. 58, 75-84.
- [8] Garcia, C.A., Lescuyer, G., 2008. Monitoring, indicators and community based forest management in the tropics: Pretexts or red herrings? *Biodiversity and Conservation*. 17, 1303-1317.
- [9] Prabhu, R., Colfer, C., Shepherd G., 1998. Criteria and indicators for sustainable forest management: New findings from CIFOR's forest management unit level research. *Rural Development Forestry Network*. 23, 1-15.
- [10] Development of Criteria and Indicators for Sustainable Forest Management in the Philippines [Internet]. International Tropical Timber Organization. Available from: [https://www.itto.int/files/itto_project_db_input/2744/Project/PPD%2029-01%20rev%201%20\(F\)%20e.pdf](https://www.itto.int/files/itto_project_db_input/2744/Project/PPD%2029-01%20rev%201%20(F)%20e.pdf)
- [11] Deguit, E., Smith, R., Jatulan, W., et al., 2004. Participatory coastal resource assessment training guide. Coastal resource management project of the department of environment and natural resources. Coastal Resource Management Project. pp. 5-35.
- [12] Buncag, M.J.J., 2022. Community-based mangrove forest management sustainability analysis in Tagpait, Aborlan and Bacungan, Puerto Princesa City, Palawan, Philippines. *Environment and Ecology Research*. 10(3), 325-333. DOI: <https://doi.org/10.13189/eer.2022.100301>
- [13] Gile, K.J., 2013. Statistical Analysis of Social

- Networks [Internet]. Available from: <https://people.math.umass.edu/~gile/kgileSAMSUndergrad2013.pdf>
- [14] Kendal, B., Costello, C., 2006. Data Analysis for Environmental Science and Management [Internet]. Available from: <https://citeseerx.ist.psu.edu/document?repid=rep1&type=pdf&doi=c-d0e20098e967a29d43f4ac425e75bbc77f4834a>
- [15] Buncag, M.J.J., 2020. Developing applicable criteria and indicators and verifiers for sustainability evaluation of mangrove forest management in Tagpait, Aborlan and Bacungan, Puerto Princesa City, Palawan, Philippines. *International Journal of Science and Management Studies (IJSMS)*. 3, 8-20.
- [16] Peña, H.D., Flores, C.A.M., Buncag, M.J., et al., 2013. Ecotourism in a community-based mangrove afforestation in Tagpait, Aborlan, Palawan. *BIMP-EAGA Journal for Sustainable Tourism Development*. 2(2), 47-50.
- [17] Rahim, A.A., Shahwahid, H.M., Nasir, S.M., et al., 2012. Market and welfare economic impacts of sustainable forest management practices—An empirical analysis of timber market in Sabah, Malaysia. *Journal of Tropical Forest Science*. 24(4), 440-454.
- [18] Pudji, P., Erlinda, I., Mochammad, F., 2018. The analysis of mangrove forest management sustainability in Damas Beach, Trenggalek. *Russian Journal of Agricultural and Socio-Economic Sciences*. 84(12), 252-259. DOI: <https://doi.org/10.18551/rjoas.2018-12.32>
- [19] Basyuni, M., Bimantara, Y., Siagian, M., et al., 2018. Developing community-based mangrove management through eco-tourism in North Sumatra, Indonesia. *IOP Conference Series: Earth and Environmental Science*. 126(1), 012109.
- [20] Martínez-Espinosa, C., Wolfs, P., Velde, K.V., et al., 2020. Call for a collaborative management at Matang Mangrove Forest Reserve, Malaysia: An assessment from local stakeholders' view point. *Forest Ecology and Management*. 458, 117741. DOI: <https://doi.org/10.1016/j.foreco.2019.117741>

ARTICLE

Energy Emissions Profile and Floating Solar Mitigation Potential for a Malaysia's State

Suraya Nabilah Zaini¹, Azlin Mohd Azmi^{1,2*}, Annie Syazrin Ismail³

¹ School of Mechanical Engineering, College of Engineering, Universiti Teknologi Mara (UiTM), Shah Alam Selangor, 40450, Malaysia

² Solar Research Institute (SRI), Universiti Teknologi MARA (UiTM), Shah Alam, Selangor, 40450, Malaysia

³ Jabatan Perancangan, Majlis Bandaraya Shah Alam, Wisma MBSA, Persiaran Perbandaran, Shah Alam, Selangor, 40000, Malaysia

ABSTRACT

The establishment of the National Low Carbon City Master Plan (NLCCM) by Malaysia's government presents a significant opportunity to minimize carbon emissions at the subnational or local scales, while simultaneously fostering remarkable economic potential. However, the lack of data management and understanding of emissions at the subnational level are hindering effective climate policies and planning to achieve the nationally determined contribution and carbon neutrality goal. There is an urgent need for a subnational emission inventory to understand and manage subnational emissions, particularly that of the energy sector which contribute the biggest to Malaysia's emission. This research aims to estimate carbon emissions for Selangor state in accordance with the Global Protocol for Community-Scale Greenhouse Gas Emission Inventories (GPC), for stationary energy activities. The study also evaluates the mitigation potential of Floating Solar Photovoltaic (FSPV) proposed for Selangor. It was found that the total stationary energy emission for Selangor for the year 2019 was 18,070.16 ktCO₂e, contributed the most by the Manufacturing sub-sector (40%), followed by the Commercial and Institutional sub-sector; with 82% contribution coming from the Scope 2 emission. The highest sub-sector of Scope 1 emissions was contributed by Manufacturing while Scope 2 emissions from the Commercial and Institutional. Additionally, the highest fuel consumed was natural gas, which amounted to 1404.32 ktCO₂e (44%) of total emissions. The FSPV assessment showed the potential generation of 2.213 TWh per year, by only utilizing 10% of the identified available ponds and dams in Selangor, equivalent to an emission reduction of 1726.02 ktCO₂e, offsetting 11.6% Scope 2 electricity emission. The results from the study can be used to better evaluate existing policies at the sub-national level, discover mitigation opportunities, and guide the creation of future policies.

Keywords: Greenhouse gas emission; Floating solar; GPC protocol; Stationary energy; Low carbon state

*CORRESPONDING AUTHOR:

Azlin Mohd Azmi, School of Mechanical Engineering, College of Engineering, Universiti Teknologi Mara (UiTM), Shah Alam Selangor, 40450, Malaysia; Solar Research Institute (SRI), Universiti Teknologi MARA (UiTM), Shah Alam, Selangor, 40450, Malaysia; Email: azlinazmi@uitm.edu.my

ARTICLE INFO

Received: 25 August 2023 | Revised: 24 September 2023 | Accepted: 26 September 2023 | Published Online: 7 October 2023

DOI: <https://doi.org/10.30564/jees.v5i2.5923>

CITATION

Zaini, S.N., Azmi, A.M., Ismail, A.S., 2023. Energy Emissions Profile and Floating Solar Mitigation Potential for a Malaysia's State. *Journal of Environmental & Earth Sciences*. 5(2): 50-60. DOI: <https://doi.org/10.30564/jees.v5i2.5923>

COPYRIGHT

Copyright © 2023 by the author(s). Published by Bilingual Publishing Group. This is an open access article under the Creative Commons Attribution-NonCommercial 4.0 International (CC BY-NC 4.0) License. (<https://creativecommons.org/licenses/by-nc/4.0/>).

1. Introduction

Over time, rapid urbanization, industrialization, and relatively high carbon intensity dependence on fossil fuels make cities and their populations more at risk of the effect of climate change that led to extreme weather conditions such as flash floods, droughts, and heat waves. The Intergovernmental Panel on Climate Change (IPCC) reported in February 2022 that the result of climate change is putting our planet and those within it at grave risk and how our actions shall influence the adaptation to increasing climate risk. According to experts, the rising greenhouse gas emissions are threatening the existence of our civilization ^[1,2]. The absolute amount of greenhouse gases that have been released into the atmosphere has increased significantly during the last decade. If the efforts to reduce these emissions are not made soon, the chances of achieving low-term emissions become more difficult. According to the IPCC special report on the impacts of global warming, the world must limit its temperature increase from 1.5 °C to 2 °C (degrees Celsius) to avoid dangerous climate change ^[3,4]. The reduction of greenhouse gas emissions should be dramatically implemented to avoid dangerous climate change. This can only be achieved through the establishment of a zero-emission economy which assumes that the decline in emissions begins immediately and progresses gradually to 2050. Even slightly exceeding the warming level temporarily will result in a severe impact of which some will be irreversible, especially in the low-lying coastal settlement ^[5].

Malaysia pledges to contribute to the implementation and achievement of the goals of the Paris Agreement through its Nationally Determined Contributions, NDCs in reducing as much as 45% of carbon intensity by 2030 across the economy (based on the Gross Domestic Product) and aspire to achieve Net-Zero GHG emission by 2050 in which the National Low Carbon Cities Master Plan (NLCCM) will be one of its urban strategies ^[3,4]. Taking urgent action to combat climate change and its devastating impacts is therefore an imperative to save lives and livelihood. Previously, Malaysian government introduced

the Low Carbon City Framework as an opportunity to reduce carbon emissions while offering incredible economic opportunities that align with Sustainable Development Goals 2030 (SDG2030) of its 17 Goals and New Urban Agenda Blueprint ^[6].

Monitoring and reporting are crucial in tracking the progress and path towards the goals and targets set for low carbon emissions. Malaysia has recently submitted its greenhouse gas (GHG) inventory through the fourth Biennial Update Report (BUR3) as part of Malaysia's obligations as a Party to the United Nations Framework Convention on Climate Change (UNFCCC). At the local level, cities in Malaysia are using the Low Carbon City Framework and Assessment System (LCCF) formulated by the government in 2011. However, NLCCM reported that the LCCF was not inclusive and did not consider the inclusion of forest and agriculture. It is also not aligned with the GPC standard. Thus, NLCCM explicitly stipulated that cities adopt Global Protocol for Community-Scale Greenhouse Gas Emission Inventories (GPC) in their GHG inventory ^[7]. The GPC standard is an internationally accepted framework for reporting emissions at the community scale which is also applicable at the subnational level. It was established through the partnership of the World Resources Institute, C40 Cities Climate Leadership Group and Local Governments for Sustainability (ICLEI). In 2011, a group of professionals with the aim of making Iskandar City Malaysia's first low-carbon city developed a blueprint consisting of GHG emissions analysis and GHG reduction targets for 2025, which also included action plans to achieve these targets. The study also highlighted the effectiveness of the city's mitigation measures due to the lack of understanding of the city's emissions profile and addressed this by conducting a GHG inventory based on GPC ^[8,9].

Although the government has established the LCCF reporting framework for Malaysian cities, there is no reporting framework requirement at the state level. Currently, there is no GHG emissions inventory and reporting framework for Malaysia's state due to the lack of data availability and limited

resources to conduct a bottom-up approach inventory analysis. An estimation of GHG Inventory through scaling down of the national data using appropriate scaling factors, would be a great starting point for the establishment of a state inventory. This is crucial in identifying the sources of emissions and their trends, for the identification and implementation of effective subnational climate mitigation measures to reduce greenhouse gas (GHG) emissions.

At the present time, although the specific GHG emissions from renewable energy sources are extremely low, a large portion of energy sources are still utilising the conventional energy system. Within the context of solar photovoltaic (PV) technologies, traditionally, they have been regarded as the most expensive choice for generating electricity^[10]. A recent finding reported that with increased investment in research and development as well as advances in technology and materials, FSPV technology is likely to become more accessible at a lower cost in the future^[11]. A report by PV Insights, a leading international solar PV research business informed of the most recent significant drop in PV pricing from 2.36 USD/watt peak (Wp) in 2010 to 0.35 USD/Wp in 2020 and predicted to decrease much more by half by 2030^[12]. Over the past few decades, installed photovoltaic (PV) capacity has increased significantly as PV has improved its competitiveness against other renewables and conventional power systems.

This study proposes a floating solar or floating photovoltaics (FSPV) system placed on top of a body of water as a mitigation measure as it is yet to be explored widely in Malaysia. Malaysia possesses a strategic advantage in the deployment of FSPV, attributed to its favourable geographical location and abundant water bodies. The Southeast Asia region enjoys constant exposure to the sun, and solar power has been identified as one of the most promising forms of renewable energy in this region^[13]. Malaysia lies in the equatorial region, with an average monthly solar radiation of 4000-5000 Wh/m₂ that receives abundant sunshine of about 2200 h in a year^[14]. Thus, it has the potential to establish large-scale solar power installations in the country. The study

will estimate the prospective electricity output, using local irradiance data and utilising 1%, 5% and 10% of the total water body surface area for emission reduction calculation potential.

The importance of this study lies in its attempt to compile and analyse a subnational GHG emission inventory for Malaysia's state using the Global Protocol for Community-Scale Greenhouse Gas Emission Inventories (GPC) with Selangor as the first case study, providing a standardized and replicable framework for data gathering, calculation, and reporting. Another significant contribution is the investigation into floating solar potential as a mitigation measure. This research would help in resolving data limitation issues, promoting uniform reporting, and providing novel energy alternatives, in fostering Malaysia's sustainable development.

2. Methodology

The methodology used in the study was structured according to the two objectives, shown in the research process flow in **Figure 1**.

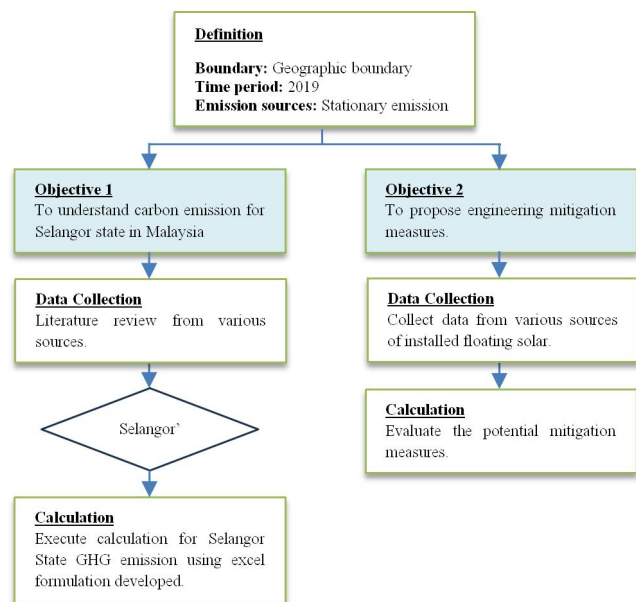


Figure 1. Research process flow.

There were three scopes of emissions sources that accounted for GPC Basic reporting^[15]. However, due to data limitations, this study estimated GHG inventory limited to Scope 1 (fugitive emissions and

energy industries were not included) and Scope 2 as shown in **Figure 2**.

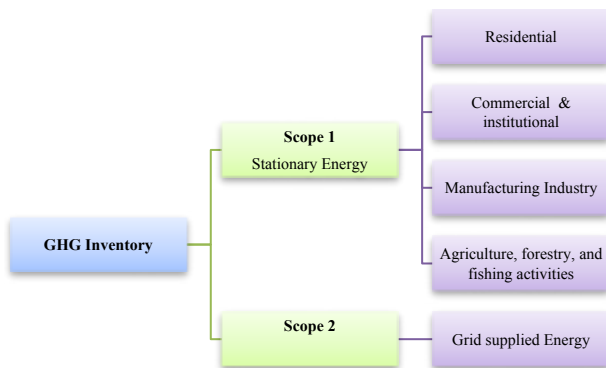


Figure 2. GHG inventory coverage.

In the GPC, the city-induced reporting framework sought to account for emissions because of activities in the city or subnationally ^[15]. The scope framework referred to stationary energy emissions from sources within the geographic boundary of the Selangor state in Malaysia. The research scope was to employ GPC standards and benchmark carbon emission limited to Stationary Energy emissions that were accounted for carbon emissions from **Figure 3**.

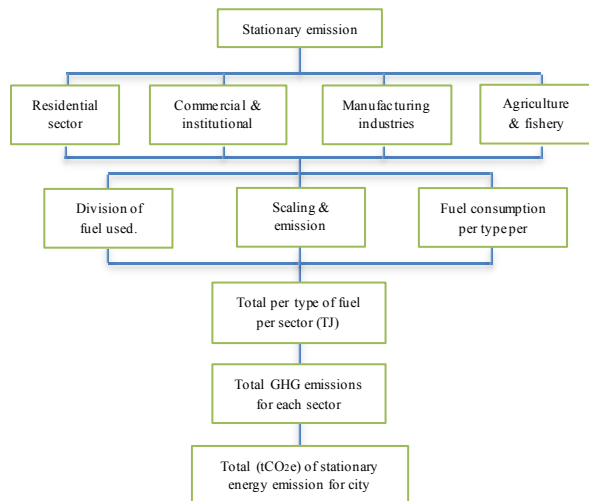


Figure 3. Breakdown of the emission inventory.

The first objective incorporated the details of data collection and GHG estimation calculation. The approach used was based on the Global Protocol for Community-Scale Greenhouse Gas Emission Inventories (GPC).

Secondary data collection

The present study conducted a comprehensive analysis of quantifiable data by conducting a sys-

tematic literature review, which included city-scale greenhouse gas (GHG) inventory methodologies presented in scholarly journal articles, Malaysian government policies, official publications, census data, and various reports ^[16,17].

The secondary data for electricity consumption and energy consumption were collected respectively from the Energy Commission (ST), using the latest National Energy Balance (NEB) 2019. The data was scaled down either using population or industrial GDP (depending on sectors) to estimate Selangor's consumption. Apart from that, relevant data was collected and referred from various sources of reports such as GHG Protocol Policy and Action Standard, Population and GDP, National Policy on Climate Change, Biennial reports, census for city, NLCCM, GPC & etc.

Activity data were identified from data provided in the National Energy Balance of the year 2019 for electricity and various fuel consumption such as natural gas, petrol, diesel, fuel oil, LPG, kerosene, ATF & AV gas, coal & coke, and biodiesel ^[18,19]. These data were then tabulated into GPC reporting format and converted from Kilo Tonnes of oil equivalent (ktoe) value to terajoules (TJ) using the conversion factor of 1 ktoe = 41.868 TJ.

Identification of scaling factor

The scaling factor needed to be highly correlated, as it indicated the ratio between the available data and the required inventory data. In the absence of large technical and behavioural changes, the population is a significant source of GHG emissions, particularly in the residential sector. On the other hand, data on economic activities were better suited for using other scaling factors such as gross domestic product or industrial yield or turnover. For this study scaling factor was either the population of the state or Gross domestic product (GDP) by state and type of economic activity, for the year 2019 at constant 2015 prices - RM Million. This information was obtained from the Malaysia census. Suitable scaling factors and scale data to state boundaries were identified ^[20-23].

Identification of emission factor

The relevant emission factors were sourced from

the 2006 Intergovernmental Panel on Climate Change (IPCC) Guidelines and data provided in the Third Biennial Update Report submitted to UNFCCC [18]. Emission factors quantified the quantity of greenhouse gas (GHG) emissions released for each unit of fuel combusted. The consumed fuel scaling factors were selected from either population or Gross domestic product (GDP) retrieved from Key Summary Statistics for Local Authority Areas in Malaysia for the selected period.

The emission factor for electricity was obtained from the Grid Emission Factor (GEF) from the Malaysia Energy Commission, where GEF measures the weighted average emissions of greenhouse gases (GHGs) per unit of net electricity generated by all power plants that provided electricity for the grid, as shown in **Table 1** [24].

Table 1. Grid emission factor [24].

Grid emission factor (Gg CO ₂ e/GWh)			
	2017	2018	2019
Peninsular Malaysia	0.776	0.807	0.780
Sabah	0.513	0.520	0.527
Sarawak	0.213	0.193	0.222

Estimation of GHG emissions

GHG emissions of the Selangor state were estimated by multiplying activity data by an emission factor associated with the activity being measured. The degree of activity leading to greenhouse gas emissions within a specified time was quantified by the data on activities.

$$GHG \text{ emissions} = \text{Activity data} \times \text{Emission factor} \quad (1)$$

Floating solar potential

Upon completion of the GHG estimation, the second objective followed, which was to propose a mitigation measure of floating solar photovoltaic (FSPV), by estimating the FSPV sizing and potential energy generation.

Identification of water bodies

The available water bodies in Selangor including ponds, lakes, former mines, and dams were identified and retrieved from the Selangor Water Management Authority (LUAS) website [25]. The selected water bodies for potential PV estimate had a minimum

depth of not less than 3 m.

Estimation of PV sizing

Several stages and factors were considered when determining the optimal size of photovoltaic (PV) systems and the potential power generation from water bodies in Selangor. The sizing and PV generation estimation for Selangor's water bodies were done with 1%, 5%, and 10% of the area used, with an average of peak sun hours (PSH) of 4.823 kWh/m² per day as shown in **Figure 4** [26,27]. The calculation included a derate factor of (0.77) which encompassed all the environmental and system losses [28].

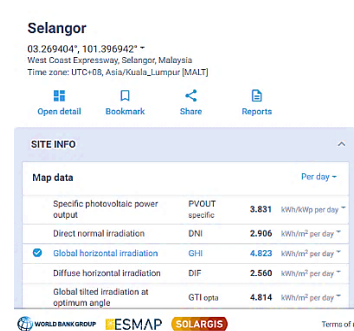


Figure 4. Selangor global horizontal irradiation.

The estimation varied depending on the specification of the selected module. For this purpose, Jinko Solar panel was selected, and details of its specification as shown in **Table 2**. With the selected PV, the required number of PV modules for installation could be determined according to the intended surface area of the water bodies.

Table 2. PV module specification [29].

Brand	Jinko Solar
Type	Mono-Facial Module (P-Type)
Model	Tiger Pro 72HC (530-550 Watt)
Watt/Panel (W)	550
Surface area (m ²)	2.578716

3. Results and analysis

3.1 Analysis of GHG emissions

The total GHG emissions for Selangor for the year 2019 were summarized and shown in **Figure 5**. The total emissions contributed by both consumption of fuels and electricity is 18,070.16 ktCO₂e, where

80% of the GHG emissions are contributed by Scope 2 source (electricity). Logically, reducing emissions from electricity use will significantly reduce the overall GHG emissions in Selangor.

Figure 6 shows both Scope 1 and Scope 2 emission contributions by each sub-sector. The total GHG emissions from residential, commercial and institutional, manufacturing and agriculture, and forestry and fishing activities are 5,261.56 ktCO₂e, 5,492.72 ktCO₂e, 7,395.84 ktCO₂e and 10.03 ktCO₂e respectively. The manufacturing sector contributes mostly (around 40%) to the total emissions in Selangor, followed by the commercial (30%) and residential (29%) sectors. This is attributed to Selangor being the industrialised state in Malaysia, with little agriculture, forestry, and fishery activities. In comparing the various fuel types for Scope 1 emission, natural gas is the highest emission source, consumed the most by the manufacturing industries sector of 1404.32 ktCO₂e (44%), followed by diesel coal and coke, as shown in **Figure 7**. LPG was also used widely by residential, contributing quite considerably to Selangor's total emissions. Selangor's population in 2019 was around 6.51 million, signifying substantial contribution from the residential sector in addition to the other sectors in Selangor.

Breaking down the emissions by scope from different sub-sectors, it is noteworthy that Manufacturing is the highest emission contributor for Scope 1 as shown in **Figure 8**, while Commercial and Institutional is the highest contributor for Scope 2 as shown in **Figure 9**. Interestingly, the amount of emission contributions by the Manufacturing, Commercial and Residential is around 30% each.

In order to attain a carbon balance, it is necessary that strategies aimed at emission reduction prioritise the high-emitting sectors. These encompass sustainable industrial practices, a transition towards renewable energy sources, and the implementation of energy efficiency measures. Furthermore, promoting the use of sustainable energy sources such as floating solar photovoltaics (FSPV) has the potential to significantly reduce emissions and facilitate the transition towards carbon neutrality.

Figure 10 shows the breakdown of gas emissions, with carbon dioxide (CO₂) contributing the most at 18,060.83 ktCO₂e, representing more than 99% of emissions. Methane and nitrous oxide contribute comparatively lesser quantities, with emissions of 4.56 ktCO₂e and 4.77 ktCO₂e, respectively. The high CO₂ emission is largely attributed to Scope 2 electricity emissions. Understanding this breakdown of emissions by specific gas types and sources yields useful insights that can influence targeted strategies for abatement. For example, mitigating carbon dioxide emissions from specific sectors has the potential to achieve significant reductions, considering its large contributions to the total emissions in Selangor.

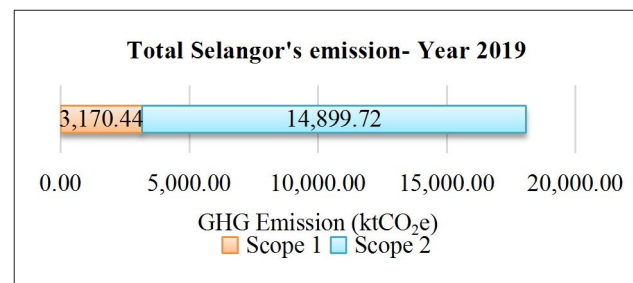


Figure 5. Total Selangor's emissions for the year 2019.

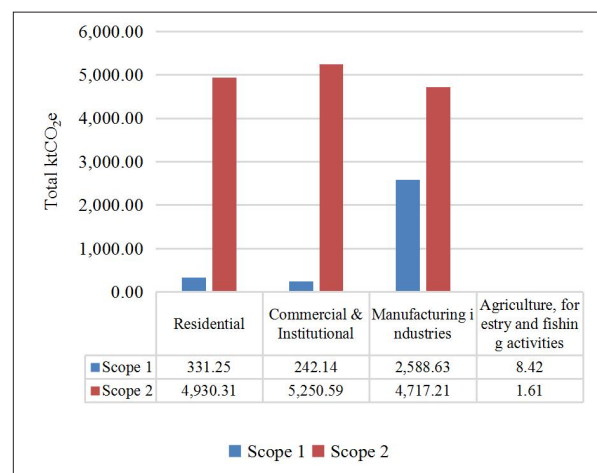


Figure 6. Sectoral distributions of Scope 1 and Scope 2 (electricity) emissions.

3.2 Estimation of FSPV potential

In this study, 27 waterbodies including ponds (lake and former mines) and dams in Selangor were found to be suitable for floating PV installations as shown in **Tables 3 and 4**. The study proved that

floating PV installations in Selangor have great potential for generating electricity with only just 1%, 5% and 10% utilization of the water body surface area. With 10% surface coverage, the system would be capable of generating nearly 2.213 TWh for Selangor in a year, offsetting around 11.6% (1726.02 ktCO₂e) of the Scope 2 emissions.

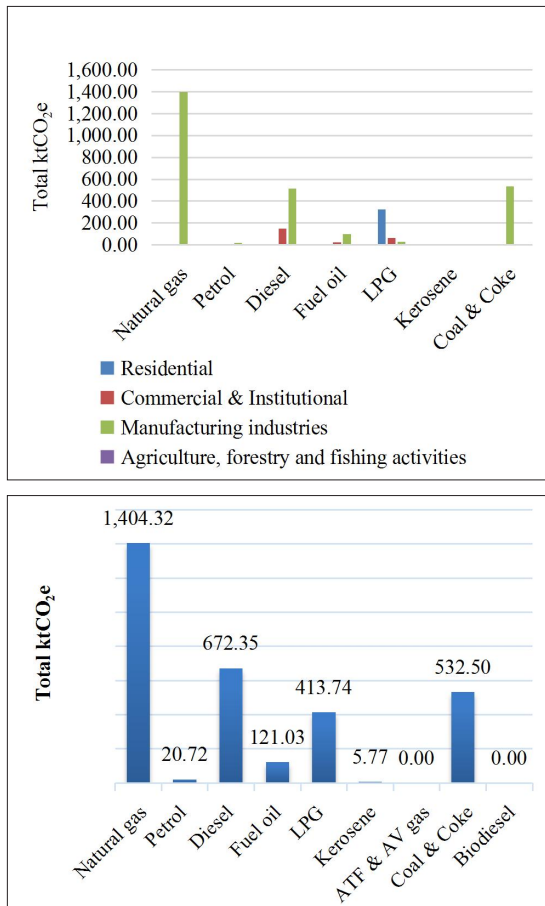


Figure 7. Sub-sector breakdown and source of Scope 1 emission.

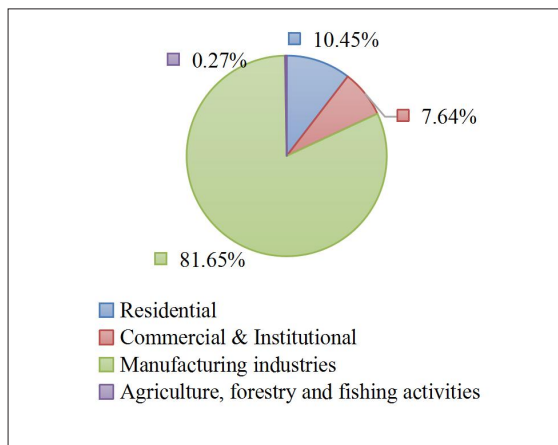


Figure 8. Scope 1 contribution by sectors.

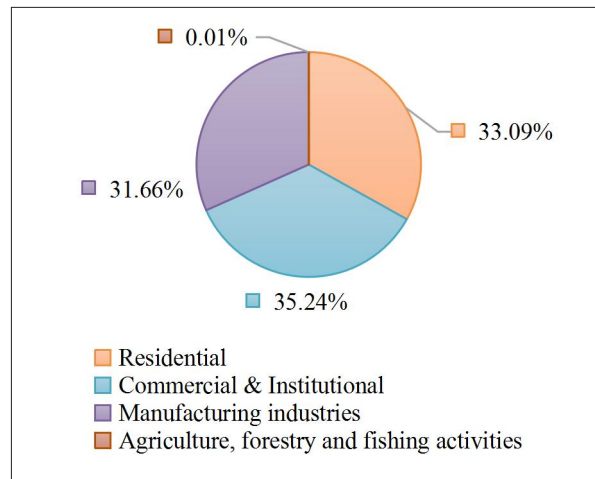


Figure 9. Scope 2 contribution by sectors.

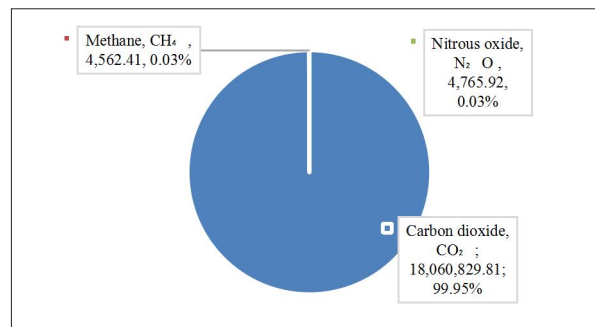


Figure 10. Gasses profile for Selangor's emission in 2019.

3.3 Policy implications

The findings of this study highlight the urgency of mitigating GHG emissions in Selangor and throughout Malaysia. This research is an effort to estimate emissions from available secondary primary data and better understand emissions in the stationary energy sector, which is crucial not just for Selangor's GHG inventory but also for demonstrating progress towards emission reduction targets considering Malaysia's commitments to Sustainable Development Goals 2030 and the Paris Agreement. For this purpose, numerous important policy implications and suggestions might be drawn:

Improvements in data management and availability

To achieve uniform reporting across states and regions, a standardised reporting structure should be created, one that is in line with international standards like the Global Protocol for Community-Scale Greenhouse Gas Emission Inventories (GPC). In

Table 3. PV Sizing and energy generation for the available pond in Selangor.

Pond name	Area (Ha)	Area used (m ²)			No of module for % area used (nos)			Possible annual energy generation (GWh/year)		
		1%	5%	10%	1%	5%	10%	1%	5%	10%
P1	114.32	11,432	57,160	114,320	4,433	22,166	44,332	3.30	16.53	33.05
P2	99.63	9,963	49,815	99,630	3,864	19,318	38,636	2.88	14.40	28.80
P3	479.64	47,964	239,820	479,640	18,600	93,000	186,000	13.87	69.33	138.67
P4	31.27	3,127	15,633	31,266	1,212	6,062	12,125	0.90	4.52	9.04
P5	11.23	1,123	5,615	11,230	435	2,177	4,355	0.32	1.62	3.25
P6	25.50	2,550	12,750	25,500	989	4,944	9,889	0.74	3.69	7.37
P7	5.60	560	2,800	5,600	217	1,086	2,172	0.16	0.81	1.62
P8	11.80	1,180	5,900	11,800	458	2,288	4,576	0.34	1.71	3.41
P9	3.90	390	1,950	3,900	151	756	1,512	0.11	0.56	1.13
P10	106.41	10,641	53,205	106,410	4,126	20,632	41,265	3.08	15.38	30.76
P11	63.41	6,341	31,705	63,410	2,459	12,295	24,590	1.83	9.17	18.33
P12	132.60	13,260	66,300	132,600	5,142	25,710	51,421	3.83	19.17	38.34
P13	176.40	17,640	88,200	176,400	6,841	34,203	68,406	5.10	25.50	51.00
P14	65.20	6,520	32,600	65,200	2,528	12,642	25,284	1.88	9.42	18.85
P15	21.10	2,110	10,550	21,100	818	4,091	8,182	0.61	3.05	6.10
P16	182.80	18,280	91,400	182,800	7,089	35,444	70,888	5.29	26.42	52.85
P17	3,349.79	334,979	1,674,895	3,349,790	129,901	649,507	1,299,015	96.84	484.23	968.45
P18	10.00	1,000	5,000	10,000	388	1,939	3,878	0.29	1.45	2.89
P19	405.64	40,564	202,820	405,640	15,730	78,652	157,303	11.73	58.64	117.27
P20	2.83	283	1,415	2,830	110	549	1,097	0.08	0.41	0.82

Table 4. PV Sizing and energy generation for available dams in Selangor.

Dam name	Area (km ²)	Area used (m ²)			No of module for % area used (nos)			Possible annual energy generation (GWh/year)		
		1%	5%	10%	1%	5%	10%	1%	5%	10%
D1	5.09	50,900	254,500	509,000	19,739	98,693	197,385	14.72	73.58	147.16
D2	8.05	80,500	402,500	805,000	31,217	156,085	312,171	23.27	116.37	232.73
D3	2.03	20,300	101,500	203,000	7,872	39,361	78,721	5.87	29.34	58.69
D4	2.55	25,500	127,500	255,000	9,889	49,443	98,886	7.37	36.86	73.72
D5	0.81	8,100	40,500	81,000	3,141	15,705	31,411	2.34	11.71	23.42
D6	2.01	20,100	100,500	201,000	7,795	38,973	77,946	5.81	29.06	58.11
D7	3.01	30,100	150,500	301,000	11,672	58,362	116,725	8.70	43.51	87.02

the absence of local data, an inventory development using national data can be first established, to kick off the inventory activities before proper local data management can be set up.

Understanding local emissions profiles

This case study of Selangor demonstrates how important it is to have detailed subnational emission inventories for identifying emissions hot spots, conducting thorough risk assessments, creating effective

mitigation strategies, and assessing the effectiveness of policies. Emissions trends and patterns can be better understood if this analysis is expanded to include additional Malaysian states and extended time periods.

Reduction through Scope 2 emissions

Given that electricity consumption (Scope 2 emissions) accounted for a sizeable portion of Selangor's carbon footprint, reducing this source of emissions

requires coordinated efforts to shift to renewable energy sources and improve energy efficiency in the industry, residential and commercial sectors.

FSPV as a mitigation measure

The study demonstrates the significant potential of FSPV technology in Selangor, providing an opportunity for emission reduction. More research is needed on policies and incentives that could speed up the adoption of FSPV systems on waterways.

4. Conclusions

In conclusion, Malaysia's commitment to the Sustainable Development Goals 2030 and Paris Agreement shows that the country is serious about reducing carbon emissions while fostering long-term economic prosperity. However, effective climate policies and planning are hindered, due to issues in data management and availability, uniform reporting framework and understanding of subnational emission profiles. This study addressed those issues by estimating carbon emissions using GPC framework and assessed the emission reduction potential via FSPV (Floating Solar PV) systems, utilising available ponds and dams in Selangor. Furthermore, the study stressed the need for detailed subnational emission inventories for proper risk assessment, mitigation strategy development, and policy evaluation.

The recommendation that can be made to this study is to extend the data period, covering the remaining Malaysia states for an in-depth analysis of state inventory, to provide a more comprehensive and robust knowledge of emissions trends and patterns. Longer time periods, for instance, a decade or more, allow for a more accurate assessment of how economic fluctuations, policy moves, technology developments, and changes in energy consumption patterns affect emissions. Additional research is required to explore viable approaches in order to effectively mitigate emissions and attain carbon neutrality.

Author Contributions

A.M.A. designed the study and outlined the structure of manuscript; interpreted and discussed the

result; and edited and revised the manuscript. S.N.Z processed and analysed the data and performed the proposed methods; drafted the manuscripts, interpreted, and discussed the results; and handled the submission steps. A.S.I. provided the data and documents for relevant analysis. All authors have read and agreed to the published version of the manuscript.

Conflict of Interest

The authors declare that there is no conflict of interest.

References

- [1] Climate Change: A Threat to Human Wellbeing and Health of the Planet. Taking Action Now Can Secure Our Future [Internet]. IPCC; 2022 [cited 2022 Dec 25]. Available from: <https://www.ipcc.ch/2022/02/28/pr-wgii-ar6/>
- [2] Understanding Global Warming Potentials [Internet]. EPA; 2022 [cited 2023 Jan 2]. Available from: <https://www.epa.gov/ghgemissions/understanding-global-warming-potentials>
- [3] Intergovernmental Panel on Climate Change (IPCC), 2022. Summary for policymakers. Global warming of 1.5 °C: IPCC special report on impacts of global warming of 1.5 °C above pre-industrial levels in context of strengthening response to climate change, sustainable development, and efforts to eradicate poverty. Cambridge University Press: Cambridge. pp. 1-24. DOI: <https://doi.org/10.1017/9781009157940.001>
- [4] Rogelj, J., Shindell, D., Jiang, K., et al., 2018. Mitigation Pathways Compatible with 1.5°C in the Context of Sustainable Development [Internet] [cited 2022 Dec 2]. Available from: https://www.ipcc.ch/site/assets/uploads/sites/2/2019/02/SR15_Chapter2_Low_Res.pdf
- [5] Solar PV Global Supply Chains [Internet]. IEA; 2022. Available from: <https://www.iea.org/reports/solar-pv-global-supply-chains>
- [6] Green Technology Master Plan Malaysia 2017-2030 [Internet]. Ministry of Energy, Green

- Technology and Water Malaysia (KeTTHA); 2017 [cited 2022 Dec 2]. Available from: <https://www.pmo.gov.my/wp-content/uploads/2019/07/Green-Technology-Master-Plan-Malaysia-2017-2030.pdf>
- [7] National Low Carbon Cities Masterplan [Internet]. Ministry of Environment and Water (KASA); 2021 [cited 2022 Dec 2]. Available from: <https://www.nrecc.gov.my/ms-my/teras/alamsekitar/Documents/NLCCM.pdf>
- [8] Abdul-Azeez, I.A., 2020. Low carbon development through measuring and monitoring carbon emission in Johor Bahru, Malaysia. *Journal of Environmental Treatment Techniques*. 9(1), 242-252.
- [9] Rahman, H.A., 2020. Malaysia commitment towards low carbon cities. *International Journal of Academic Research in Business and Social Sciences*. 10(15), 253-266.
DOI: <https://doi.org/10.6007/ijarbss/v10-i15/8247>
- [10] Breyer, C., Koskinen, O., Blechinger, P., 2015. Profitable climate change mitigation: The case of greenhouse gas emission reduction benefits enabled by solar photovoltaic systems. *Renewable and Sustainable Energy Reviews*. 49, 610-628.
DOI: <https://doi.org/10.1016/j.rser.2015.04.061>
- [11] Gorjian, S., Sharon, H., Ebadi, H., et al., 2021. Recent technical advancements, economics and environmental impacts of floating photovoltaic solar energy conversion systems. *Journal of Cleaner Production*. 278, 124285.
DOI: <https://doi.org/10.1016/j.jclepro.2020.124285>
- [12] Dehghanimadvar, M., Egan, R., Chang, N.L., 2022. Economic assessment of local solar module assembly in a global market. *Cell Reports Physical Science*. 3(2).
DOI: <https://doi.org/10.1016/j.xcrp.2022.100747>
- [13] Jamalludin, M.A.S., Muhammad-Sukki, F., Abu-Bakar, S.H., et al., 2019. Potential of floating solar technology in Malaysia. *International Journal of Power Electronics and Drive Systems (IJPEDS)*. 10(3), 1638-1644.
DOI: <https://doi.org/10.11591/ijped.v10.i3.pp1638-1644>
- [14] Mohammad, S.T., Al-Kayiem, H.H., Aurybi, M.A., et al., 2020. Measurement of global and direct normal solar energy radiation in Seri Iskandar and comparison with other cities of Malaysia. *Case Studies in Thermal Engineering*. 18, 100591.
DOI: <https://doi.org/10.1016/j.csite.2020.100591>
- [15] GHG Protocol for Cities [Internet]. GPC; 2014 [cited 2022 Nov 2]. Available from: <https://ghg-protocol.org/greenhouse-gas-protocol-accounting-reporting-standard-cities>
- [16] Dahal, K., Niemelä, J., 2017. Cities' greenhouse gas accounting methods: A study of Helsinki, Stockholm, and Copenhagen. *Climate*. 5(2), 31.
DOI: <https://doi.org/10.3390/cli5020031>
- [17] Dodman, D., 2009. Blaming cities for climate change? An analysis of urban greenhouse gas emissions inventories. *Environment and Urbanization*. 21(1), 185-201.
DOI: <https://doi.org/10.1177/0956247809103016>
- [18] Malaysia Third Biennial Update Report to the UNFCCC [Internet]. Unfccc.int; 2020 [cited 2022 Dec 23]. Available from: https://unfccc.int/sites/default/files/resource/MALAYSIA_BUR3-UNFCCC_Submission.pdf
- [19] Malaysia's Update of Its First Nationally Determined Contribution [Internet] [cited 2022 Dec 2]. Available from: <https://unfccc.int/NDCREG>
- [20] Ministry of Economy Department of Statistics Malaysia Official Portal [Internet]. Available from: https://www.dosm.gov.my/v1/index.php?r=column/cthemByCat&cat=491&bul_id=L3NnMU44VnA0YjRjVXhuYUpZTmVnZz09&menu_id=TE5CRUZCblh4ZTZMODZlbnk2aWRRQT09
- [21] Population and Housing Census of Malaysia 2020 [Internet]. Department of Statistic Malaysia; 2020. Available from: https://www.selangor.gov.my/sabakbernam/resources/PEN-ERBITAN_PENEMUAN_UTAMA_BANCI_PENDUDUK_DAN_PERUMAHAN_MALAYSIA_2020.pdf
- [22] Current Population Estimates, Malaysia [Inter-

- net]. eStatistic; 2019. Available from: <https://newss.statistics.gov.my/newss-portalx/ep/epProductFreeDownloadSearch.seam>
- [23] National Energy Balance 2019 [Internet]. Suruhanjaya Tenaga (Energy Commission); 2019 [cited 2023 Mar 1]. Available from: <https://meih.st.gov.my/documents/10620/19759/National+Energy+Balance+2019>
- [24] Grid Emission Factor (GEF) in Malaysia [Internet]. Energy Commissioner; 2019 [cited 2023 Jan 2]. Available from: <https://meih.st.gov.my/publications>
- [25] Alternative Water Source Profile [Internet]. LUAS Selangor [cited 2022 Dec 5]. Available from: <https://www.luas.gov.my/en/water-resource-info/alternative-water-source-profile>
- [26] Solar Resource Maps of Malaysia [Internet]. Solargis; 2022 [cited 2023 Jan 2]. Available from: <https://solargis.com/maps-and-gis-data/download/malaysia>
- [27] Global Horizontal Irradiation. Global Solar Atlas [Internet]. Solargis; 2023 [cited 2023 Jan 5]. Available from: <https://www.globalsolaratlas.info/map?c=2.836403%2C101.496506%2C11&s=2.836562%2C101.496182&m=site>
- [28] Abu Samad, I.A., 2020. 3 Easy Steps to Estimate Solar Size [Internet]. TNBX [cited 2023 Jan 5]. Available from: <https://www.tnbx.com.my/post/3-easy-steps-to-estimate-solar-size>
- [29] Tiger Pro 72HC 530-550-Watt Mono-Facial Module Catalogue [Internet]. Jinko Solar; 2020. Available from: [https://www.jinkosolar.com/uploads/5ff587a0/JKM530-550M-72HL4-\(V\)-F1-EN.pdf](https://www.jinkosolar.com/uploads/5ff587a0/JKM530-550M-72HL4-(V)-F1-EN.pdf)

REVIEW

Maximizing Oil Palm Yield: Innovative Replanting Strategies for Sustainable Productivity

Ahmed Abubakar¹, Susilawati Kasim^{2}, Mohd Yusoff Ishak¹, Md Kamal Uddin²*

¹ Faculty of Forestry and Environment, Universiti Putra Malaysia, Serdang, Selangor, 43400, Malaysia

² Faculty of Agriculture University Putra Malaysia, Serdang, Selangor, 43400, Malaysia

ABSTRACT

This paper examines the significance of innovative replanting strategies in maximizing oil palm yield while ensuring sustainable productivity. Through a comprehensive review of literature and analysis of current practices, the major findings of this research highlighted the importance of advanced breeding and clonal selection in developing high-yielding and disease-resistant oil palm varieties. Precision agriculture technologies, including IoT devices, drones, and sensors, were identified as critical tools for data-driven decision making, optimizing resource efficiency, and reducing environmental impact. Sustainable land use planning and agroforestry integration emerged as key strategies to balance productivity with environmental conservation. The broader impacts of this work extend to other agricultural sectors and land use planning, offering valuable insights for policymakers and stakeholders to promote responsible and resilient agricultural practices. By embracing innovative replanting strategies, the oil palm industry can contribute to a more sustainable and prosperous future, balancing economic growth with environmental stewardship. Continued research and collaboration are essential to achieve these goals and foster a harmonious coexistence between productivity and sustainability, integrating precision agriculture technologies for resource optimization and reduced environmental impact, promoting sustainable land use planning and agroforestry integration to enhance biodiversity and ecosystem services. Strengthening collaborations between governments, industry players, and research institutions for innovation and knowledge exchange is essential.

Keyword: Replanting strategies; Oil palm yield; Sustainable productivity; Precision agriculture; Agroforestry integration

*CORRESPONDING AUTHOR:

Susilawati Kasim, Faculty of Agriculture University Putra Malaysia, Serdang, Selangor, 43400, Malaysia; Email: susilawati@upm.edu.my

ARTICLE INFO

Received: 17 August 2023 | Revised: 19 September 2023 | Accepted: 27 September 2023 | Published Online: 8 October 2023

DOI: <https://doi.org/10.30564/jees.v5i2.5904>

CITATION

Abubakar, A., Kasim, S., Ishak, M.Y., et al., 2023. Maximizing Oil Palm Yield: Innovative Replanting Strategies for Sustainable Productivity. *Journal of Environmental & Earth Sciences*. 5(2): 61-75. DOI: <https://doi.org/10.30564/jees.v5i2.5904>

COPYRIGHT

Copyright © 2023 by the author(s). Published by Bilingual Publishing Group. This is an open access article under the Creative Commons Attribution-NonCommercial 4.0 International (CC BY-NC 4.0) License. (<https://creativecommons.org/licenses/by-nc/4.0/>).

1. Introduction

The oil palm (*Elaeis guineensis*) is an essential crop that plays a significant role in meeting the ever-growing global demand for edible oils, industrial applications, and biofuels^[1-3]. Renowned for its high oil content and efficient land use, the oil palm has become a crucial contributor to the economies of various tropical regions^[4-6]. To ensure the long-term viability of this industry and meet the escalating demand, it is imperative to focus on enhancing oil palm yields through innovative replanting practices^[7,8].

Replanting, the process of replacing old and unproductive oil palm trees with high-yielding varieties, is a pivotal step in the journey towards sustainable productivity^[9-11]. In this pursuit, traditional approaches have often led to challenges related to environmental impact, resource inefficiency, and disease susceptibility. To address these concerns, the implementation of innovative replanting practices has emerged as a crucial solution to boost yields while simultaneously minimizing.

Previous studies have examined various aspects related to oil palm replanting and its consequences on the ecosystem^[8,12]. These studies encompass a range of topics, including the potential decline in regional oil palm productivity due to the age-distribution structure within existing plantations^[13], the challenges faced by smallholders during the replanting process^[14], the impact of smallholder palm oil replanting programs^[15], the income of growers during replanting^[16], and the income from independent oil palm farming after replanting^[17]. Additionally, research has explored the influence of oil palm replanting, age, and management zones on soil carbon^[18], both internal and external factors affecting oil palm replanting^[17], priority patterns for replanting among independent smallholders^[19], and predictions regarding the contribution of smallholders' income to household living expenses during the replanting period^[20]. Other studies have focused on assessing the effects of oil palm replanting on arthropod biodiversity^[20], determining the incidence of Ganoderma disease among smallholder farmers participating in oil palm replanting incentives^[21], developing an es-

timation method for oil palm replanting potential^[22], and identifying an optimal replanting rate for the oil palm industry in Malaysia^[23]. Despite several previous studies examining various aspects of oil palm replanting, none have comprehensively addressed the significance of innovative replanting strategies in maximizing oil palm yield while ensuring sustainable productivity. The study conducted by Ardana et al.^[24] underscores the urgent need for innovation in Indonesian palm oil production. This necessity arises from the challenges posed by ageing plants and the presence of illicit seeds.

In this article, we explore a range of forward-thinking techniques and methodologies that aim to revolutionize oil palm replanting practices. By embracing cutting-edge technologies, environmentally friendly approaches, and data-driven decision-making, the oil palm industry can significantly optimize productivity, ensuring the supply of high-quality palm oil to meet the needs of a growing global population^[24].

Through careful consideration of factors such as palm variety selection, nutrient management, pest control, water usage, and climate-smart agriculture^[25], we delve into the various facets that contribute to elevating oil palm yields. By adopting these innovative approaches, oil palm plantations can not only achieve enhanced yields but also promote sustainable practices that protect the environment and support the livelihoods of local communities^[26].

As we embark on this exploration of innovative replanting practices, it becomes evident that the future of the oil palm industry lies in the hands of those who embrace progressive and eco-conscious methodologies^[27], that offer an opportunity for additional income for farmers, presenting a profitable and sustainable business model^[28-30]. The objective of this review is to explore innovative replanting practices for oil palm plantations, aiming to maximize oil palm yield while promoting sustainability and environmental responsibility. This research seeks to identify and evaluate a range of modern techniques and methodologies that can be implemented during the replanting process to optimize productivity, resource efficiency, and disease control. By focusing

on innovative practices, this research aims to offer practical insights and recommendations for the oil palm industry to enhance its yields and ensure the long-term viability of the sector.

This research contributes innovative replanting practices, sustainable approaches, and data-driven decision-making insights to enhance oil palm cultivation. It aims to optimize yields, minimize environmental impact, and meet the increasing global demand for palm oil, promoting responsible and sustainable production in the industry. The beneficiaries of this research include oil palm growers and plantation managers, palm oil industry stakeholders, environmental conservation organizations, consumers, and the academic community. These stakeholders are expected to gain valuable insights and recommendations to adopt innovative and sustainable practices,

ensuring increased yields, improved profitability, and responsible palm oil production that protects the environment and meets global demand.

2. Understanding the oil palm lifecycle and replanting necessity

Oil palm is a versatile and widely cultivated crop primarily grown for its fruit, which produces both palm oil and palm kernel oil. Oil palm plantations are significant contributors to the global vegetable oil supply, with palm oil being used in various food products, cosmetics, biofuels, and industrial applications ^[31,32]. Understanding the oil palm lifecycle and the necessity for replanting is crucial for sustainable cultivation and maintaining productivity. The data presented in **Table 1** can serve as an illustrative example of this phenomenon.

Table 1. Summary of studies related to oil palm replanting.

Author and year	Title of the article	Research objectives	Significant findings	Comments
[13]	"Replanting and yield increase strategies for alleviating the potential decline in palm oil production in Indonesia".	"To assess the potential decline of regional oil palm productivity given the landscape-level age-distribution structure on existing oil palm plantation land and evaluated strategies to alleviate this potential decline".	Replanting oil palm at 4% annually with yield improvements stabilizes production by around 45 million metric tons. Combining both counters declining trends.	This study highlights the crucial role of replanting and yield improvement strategies in stabilizing palm oil production in Riau. Collaboration among stakeholders is imperative.
[14]	"Replanting challenges among Indonesian oil palm smallholders: a narrative review".	"To highlight the challenges that smallholders face during replanting".	Smallholder oil palm replanting is critical; delayed or poorly executed replanting worsens socio-economic and environmental issues, requiring targeted support.	Overaged smallholder oil palm plantations demand replanting for enhanced productivity and livelihoods. Overcoming barriers like input access and knowledge is crucial.
[15]	"Technical formulation for estimating the economic loss impact of the smallholder oil palm replanting program in Indonesia".	"To determine the impact of the smallholder palm oil replanting program (SPR Program) in stages as a material for consideration in formulating more anticipatory and responsive policies so that they are right on target".	Increasing the productivity of smallholder oil palm plantations in Indonesia (42% of the national area) is crucial for the sustainable palm oil industry. Replanting old trees is vital but challenging for smallholders.	Increasing smallholder oil palm productivity is crucial for Indonesia's sustainable palm oil industry. Replanting old trees, addressing income loss, and informing policies are essential.
[16]	"Analysis of oil palm smallholder income during replanting in Siak Regency, Riau".	"To identify the types of food crops and to know the analysis of farming as well as the income contribution of oil palm and food crop farmers in Siak Regency".	This study highlights the income impact of oil palm replanting on farmers, emphasizing the significance of diversifying income through food crops in Siak Regency. Food crops contribute 71.89% to total income, emphasizing their economic importance.	This study in Siak Regency highlights the income loss in oil palm replanting and the importance of diversifying income sources with food crops.

Table 1 continued

Author and year	Title of the article	Research objectives	Significant findings	Comments
[17]	"Identification of internal and external factors in replanting oil palm".	"To identify internal and external factor in replanting oil palm".	Indonesia's leading role in crude palm oil production since 2006 emphasizes oil palm's vital role in national economic sustainability, demanding strategic replanting initiatives considering internal and external factors.	Oil palm plantations are vital for national growth; Indonesia a leading CPO producer since 2006. Sustainability is crucial. for the economy; replanting program assessed.
[18]	"Influence of Oil Palm Replanting, Age and Management Zones on Soil Carbon".	"To assess whether there is a build-up of soil carbon throughout the growth of oil palm and will those amassed carbon (if any) be lost during replanting".	This study finds that oil palm cultivation doesn't significantly impact soil carbon levels, with no losses during replanting, but variations in sections warrant consideration.	Oil palm cultivation doesn't significantly affect soil carbon; replanting doesn't cause losses. Soil carbon varies in plantation sections.
[19]	"The impact of replanting oil palm plantations on the farming income of the Sungai Bahar community in Muaro Jambi Regency".	"To know the description of oil palm farming income in replanting to underplanting and conventional method".	The findings indicated variations in the plant counts between the two replanting scenarios, which subsequently influenced both production levels and income.	This research explores oil palm farming income in replanting vs. underplanting and conventional methods, highlighting income disparities.
[20]	"Assessing the effects of oil palm replanting on arthropod biodiversity".	"To assess the impacts of replanting over 8 years period on arthropods in the ground, understorey and canopy microhabitats".	Palm oil, a globally traded vegetable oil, shows resilience in arthropod abundance after replanting but alters community composition and spider biodiversity.	Palm oil trade thrives in Southeast Asia, impacting biodiversity. Replanting affects arthropod and spider communities, requiring further ecological assessment.
[21]	"Surveillance of Ganoderma disease in oil palm planted by participants of the smallholders replanting incentive scheme in Malaysia".	"To determine the status of incidence and distribution of Ganoderma disease of smallholders (SH) particularly participating in replanting incentive scheme in Malaysia".	Basal stem rot disease (BSR) caused by Ganoderma sp. affects 9.2% of Malaysian oil palm plantations, with high incidence in Johor, Sabah, and Perak states.	The Malaysian Palm Oil Board conducted a survey to assess Ganoderma disease in oil palm, finding a 9.2% incidence, with the highest in Johor, Sabah, and Perak. Important data for disease management.

2.1 Oil palm lifecycle in stages

1) Nursery Phase: The oil palm lifecycle begins in the nursery, where seeds are germinated to produce seedlings. These seedlings are carefully nurtured until they are ready for transplantation into the field ^[33].

2) Field Planting: Once the seedlings have developed sufficiently, they are transplanted into the plantation field. The planting distance and arrangement are planned to optimize land use and facilitate efficient management ^[33].

3) Immature Phase: During the first three years after planting, the oil palm trees are in the immature phase. They grow and establish their root systems, trunk, and fronds.

4) Juvenile Phase: After the immature phase, the oil palms enter the juvenile phase, which lasts from the fourth to the seventh year. During this stage, the trees continue to grow taller and produce more leaves, but they do not yet bear fruit.

5) Pre-Pruning Phase: Around the seventh year, the pre-pruning phase begins. The lower fronds are

removed to improve access and visibility within the plantation, making it easier for workers to carry out essential tasks.

6) Prime Phase: The prime phase typically begins in the eighth year and can last up to around 25-30 years. During this phase, the oil palm trees reach maturity and start producing fruit bunches. This is the most productive phase of the oil palm's lifecycle.

7) Senescence Phase: After several decades of productive life, oil palm trees enter the senescence phase, where their productivity declines. The rate of fruit production decreases, and the trees become less economically viable ^[34-36].

2.2 Replanting necessity

The necessity for replanting oil palm plantations arises due to several reasons:

1) Declining Productivity: As oil palm trees enter the senescence phase, their productivity declines significantly. The yield per hectare decreases, making it economically unviable to keep the old trees.

2) Disease and Pest Management: Older oil palm trees may become more susceptible to diseases and pest infestations, which can further reduce yields and increase production costs.

3) Sustainability: Replanting allows for the adoption of more sustainable practices, such as using improved palm varieties with better disease resistance and higher oil yields, and implementing more efficient agricultural methods.

4) Land Optimization: Replanting allows for the proper management of land resources. By removing old, less productive trees, farmers can allocate land to new, high-yielding oil palm seedlings.

5) Legislation and Certification: In some regions, there are legal requirements or industry certifications that necessitate replanting to ensure compliance with sustainability standards.

6) Improved Technology: Replanting provides an opportunity to incorporate advancements in agricultural technology, irrigation systems, and precision farming, leading to improved overall efficiency.

3. Factors influencing the decline in productivity of ageing oil palm plantations

The decline in productivity of ageing oil palm plantations can be attributed to several factors ^[37]. As oil palm trees enter the senescence phase and reach the end of their productive life, they become more vulnerable to various challenges that affect their growth and fruit production. Firstly, as oil palm trees age, their oil yield per hectare decreases due to reduced fruit bunch production and a decline in the oil content of the fruit ^[37]. Secondly, older oil palm trees are more susceptible to various diseases and pest attacks, such as basal stem rot and Fusarium wilt, as well as pests like the red palm weevil and bagworm, which can significantly impact the health and productivity of the ageing palms ^[38]. Thirdly, over time, oil palm plantations may experience nutrient depletion in the soil, leading to deficiencies in essential elements like potassium, magnesium, and boron, which adversely affect tree growth and fruit production ^[39]. Moreover, ageing oil palm trees may face increased water stress, especially in regions with water scarcity or irregular rainfall patterns, leading to stunted growth and reduced fruit development ^[37]. Additionally, the root systems of ageing oil palm trees may become less efficient at absorbing water and nutrients from the soil, exacerbating nutrient deficiencies and water stress. Neglecting proper pruning and maintenance practices in ageing plantations can result in overcrowded canopies, reduced light penetration, and hindered fruit bunch development. Some older oil palm trees may also suffer from genetic degeneration, leading to weaker offspring with lower productivity and poorer disease resistance. Extreme weather events like storms, droughts, and floods can further negatively impact ageing oil palm plantations, disrupting growth and fruit production ^[25]. Lastly, as oil palm trees age and their productivity declines, the cost of maintenance and harvesting relative to the yield may become less economically viable for the plantation owner.

4. Growers replanting challenges

Oil palm growers face numerous challenges when it comes to replanting their plantations. In this review, we explored the multifaceted challenges that confront oil palm growers during the replanting process and emphasized the importance of addressing these issues for the industry's long-term sustainability and responsible agricultural practices. Petri et al.^[14] identified that gaining access to inputs, and managing finances were pivotal challenges that could significantly impact the decisions of smallholders regarding the timing, methods, and choices involved in replanting. Other barriers to successful smallholder replanting include a lack of knowledge about replanting and inadequate training, unequal access to high-quality seedlings, and varying eligibility for public replanting funds^[14]. Fauzia et al.^[17] argued that capital is a crucial factor in farming, and in the context of replanting oil palm, access to capital is not readily available to farmers. On average, farmers often lack the financial capacity to undertake oil palm replanting using their own resources. Replanting is associated with elevated expenses and intricate management procedures. Consequently, effective pest control and precise fertilization practices become even more vital^[8,14].

5. Challenges in traditional replanting approaches

The traditional replanting approaches in oil palm cultivation face several challenges that can hinder their effectiveness and sustainability. The primary obstacles include the significant time and cost involved in uprooting old palm trees and replacing them with new seedlings, especially for large-scale plantations, leading to economic challenges for smallholder farmers and potential delays in rejuvenating the plantation^[8,40]. Land preparation demands considerable effort and resources, involving labor-intensive activities and, at times, the use of heavy machinery, contributing to overall cost and time investment^[41]. Access to high-quality oil palm seedlings can be challenging in some regions, where

obtaining disease-resistant and genetically improved seedlings is crucial for successful replanting efforts, as inconsistent seedling quality can compromise the overall productivity and health of newly established palm trees^[14].

Moreover, traditional replanting methods can have detrimental environmental impacts, including air pollution and greenhouse gas emissions from burning old palm trees and deforestation leading to habitat loss and biodiversity decline^[14,42]. Soil erosion and nutrient loss, particularly on steep terrains, can adversely affect soil fertility and long-term plantation productivity^[43]. Additionally, replanting causes temporary disruptions in palm oil production, affecting revenue and supply chains, while also creating risks of disease spread to healthy trees^[44].

Limited technology adoption in traditional approaches hinders optimization and may lead to sub-optimal outcomes, necessitating the incorporation of modern agricultural technologies and best practices. Furthermore, the lack of knowledge on replanting and proper training can hinder the successful implementation of innovative strategies, with growers facing challenges in adopting advanced techniques and understanding the benefits of sustainable practices^[14].

Replanting initiatives may bring social challenges, particularly job displacement for laborers during the transition period, affecting affected communities economically and socially. Addressing these challenges requires developing sustainable and efficient replanting strategies that consider environmental, economic, and social aspects to ensure the long-term viability of oil palm cultivation. Collaborative efforts between stakeholders are essential in overcoming these limitations and promoting responsible and sustainable practices in the oil palm industry.

6. Innovative replanting strategies for maximizing yield and sustainability

Innovative replanting strategies for oil palm that aim to maximize yield and sustainability involve a combination of advanced agricultural techniques, technology adoption, and sustainable practices. Here are strategies that can help achieve both high yields

and sustainability.

Advanced Breeding: Advanced breeding techniques involve the systematic selection and cross-breeding of oil palm varieties with desirable genetic traits. This includes traits such as high oil yield, disease resistance, improved fruit quality, and tolerance to environmental stresses. By carefully selecting parent palms with these advantageous traits and using advanced genetic analysis, breeders can develop superior oil palm varieties that outperform conventional ones ^[45].

Clonal Selection: Clonal selection involves identifying and propagating superior oil palm individuals through vegetative propagation, such as tissue culture or bud grafting. This ensures that genetically identical, high-performing individuals are reproduced, maintaining the desired traits in the next generation ^[46].

Selecting High-Yielding Palm Varieties: Choose improved oil palm varieties that have been bred for high oil yield, disease resistance, and adaptability to specific growing conditions ^[47]. These varieties can significantly impact the overall productivity of the plantation.

Precision Agriculture and Technology Integration: Embracing precision agriculture practices and integrating cutting-edge technology, including IoT devices, drones, and sensors, revolutionizes data-driven decision making in oil palm cultivation ^[48]. Real-time monitoring of soil conditions, weather patterns, and plant health allows for targeted resource management ^[48]. This precision application of inputs optimizes irrigation, fertilization, and pest control, resulting in heightened efficiency, reduced waste, and responsible resource conservation ^[49,50].

Sustainable Land Use Planning: Responsible land use planning is paramount in maximizing oil palm yield sustainably ^[51]. Identifying suitable areas for replanting, preserving high conservation value areas, and adhering to best practices ensure that land is used efficiently and responsibly, safeguarding biodiversity and environmental integrity.

Agroforestry Integration: Integrating oil palm plantations with agroforestry systems fosters envi-

ronmental resilience and productivity ^[52]. By inter-planting oil palms with compatible crops and native trees, agroforestry promotes biodiversity, soil health, and ecosystem services, contributing to sustainable and balanced cultivation practices ^[52,53].

Soil Health Management: Prioritizing soil health through practices like cover cropping, mulching, and organic matter incorporation enhances nutrient availability and soil structure ^[3,54]. Improved root development and nutrient uptake lead to higher oil palm yields, promoting long-term sustainability.

Integrated Pest and Disease Management: Implementing integrated pest and disease management techniques reduces reliance on chemical pesticides ^[55]. Employing biological controls, beneficial insects, and pest-resistant varieties effectively manages pests while preserving the natural balance of ecosystems ^[56-58].

Efficient Water Management: Employing efficient water management practices, such as drip irrigation and water recycling, optimizes water usage and ensures equitable distribution, particularly in regions facing water scarcity. This responsible approach contributes to water conservation, sustainable cultivation and an increase in yield ^[59].

Continuous Research and Innovation: Fostering ongoing research and innovation in oil palm cultivation is essential for continuous improvement ^[60]. Advancements in techniques, technologies, and best practices enable growers to optimize their replanting strategies, fostering productivity and sustainability in the industry ^[61-63]. Collaborative efforts between stakeholders, including researchers, governments, and industry players, drive progress and promote a resilient and thriving oil palm sector ^[25].

Intercropping and Multilayer Farming: Introduce intercropping and multilayer farming practices to make efficient use of available land and resources ^[64,26]. For example, planting leguminous crops or covering crops between the oil palm rows can improve soil fertility and moisture retention.

Tissue Culture Propagation: Use tissue culture propagation techniques to produce high-quality, disease-free planting materials ^[60,62]. Tissue culture ensures uniformity in the new palm population and

minimizes the risk of introducing diseases from the old plantation.

Regular Pruning and Thinning: Pruning and thinning the oil palm canopy helps improve light penetration and air circulation within the plantation, leading to better fruit development and lower disease incidence ^[25,26,65].

Enhancing Pollination: It is imperative to actively encourage pollinators to visit the oil palm plantation. By doing so, we foster improved pollination, which directly translates into better fruit sets and ultimately higher oil yields ^[66]. Employing eco-friendly practices and preserving natural habitats around the plantation can further enhance pollinator populations, benefiting the entire ecosystem.

Climate-Smart Agriculture: Adapt to changing climatic conditions by implementing climate-smart agriculture practices. This might include adjusting planting schedules, using drought-resistant varieties, or employing shade management techniques ^[25,26].

Data-Driven Decision Making: Utilize data and analytics to monitor and optimize various aspects of plantation management, from pest and disease monitoring to yield forecasting. Data-driven decisions can lead to more efficient resource allocation and increased productivity.

7. Overcoming barriers to adoption

7.1 Addressing economic, regulatory, and technical challenges

Economic Incentives: Overcoming economic barriers to adoption requires providing incentives to farmers and plantation owners to invest in innovative practices. This may include offering financial support, tax incentives, or subsidies for adopting advanced breeding, precision agriculture technologies, and other sustainable replanting strategies ^[8,67].

Access to Finance: Access to affordable financing is crucial for smallholder farmers and plantation owners to adopt innovative practices. Establishing accessible credit and financing schemes tailored to the specific needs of oil palm growers can facilitate the transition to more sustainable and productive re-

planting methods ^[8,67].

Capacity Building and Training: Addressing technical challenges involves providing training and capacity-building programs for farmers and workers to effectively implement sustainable innovative practices ^[68]. Embracing certification and enhancing technical knowledge and skills empowers growers to confidently adopt new technologies and approaches ^[69].

Regulatory Support: Governments can play a vital role in overcoming regulatory barriers by creating a supportive policy environment. Streamlining approval processes, providing clear guidelines, and promoting sustainable practices through regulations can encourage the widespread adoption of innovative replanting strategies ^[25].

Research and Development Investment: Investing in research and development (Research and Development) is essential for addressing technical challenges and fostering innovation. Governments, private sectors, and research institutions can collaborate to develop and disseminate knowledge on effective replanting techniques and technologies ^[1].

7.2 Strategies for encouraging widespread adoption of innovative practices

Demonstration Plots and Farmer Field Schools: Establishing demonstration plots and farmer field schools allows farmers to witness the benefits of innovative practices firsthand. Hands-on learning experiences and knowledge sharing through these platforms can build confidence and encourage wider adoption ^[70].

Knowledge Exchange and Extension Services: Facilitating knowledge exchange between successful adopters of innovative practices and other farmers can inspire and motivate broader implementation. Utilizing extension services to disseminate information, provide technical support, and facilitate learning networks can promote adoption at the community level ^[10,25,71].

Public-Private Partnerships: Collaborations between governments, private companies, NGOs, and research institutions can accelerate the adoption

of innovative replanting strategies. Public-private partnerships can leverage resources and expertise to drive the development and dissemination of sustainable practices.

Certification and Market Incentives: Certification schemes that recognize sustainable replanting practices can create market incentives for growers. Sustainable palm oil certifications, such as RSPO (Roundtable on Sustainable Palm Oil), provide market access and premium prices for certified products, encouraging wider adoption of sustainability practices^[72].

Awareness and Advocacy: Raising awareness about the benefits of innovative replanting strategies and their positive impacts on the environment, society, and economic outcomes can garner support and advocacy from various stakeholders, fostering broader adoption of these practices.

Voluntary Agreements and Commitments: Encouraging voluntary agreements and commitments from industry players to adopt sustainable replanting practices can drive change across the sector^[8]. Engaging key stakeholders in setting and meeting sustainability targets reinforces a collective effort towards widespread adoption.

8. Implications of replanting

Oil palm replanting constitutes a multifaceted endeavour with far-reaching implications encompassing economic, environmental, social, and sustainability dimensions. It offers smallholder farmers a pivotal opportunity to bolster the productivity of their plantations, thus narrowing the yield gaps that often exist when compared to plantations managed by larger companies. This surge in productivity holds the potential to translate into augmented incomes for smallholder households, a significant socio-economic benefit^[14,73,74]. Moreover, oil palm replanting can serve as a platform for plantation redesign, thereby introducing more efficient layouts and practices. Despite the controversial reputation of oil palm cultivation, it has demonstrated its capacity to contribute to poverty reduction in certain contexts^[2,14]. This economic aspect emphasizes the importance of strategic replanting initiatives. Environmental concerns

also loom large in the realm of oil palm replanting. The expansion of oil palm plantations can impact biodiversity, contribute to deforestation, influence soil quality, and affect water quality. These consequences necessitate careful consideration and sustainable practices to mitigate negative ecological effects. Socially, the process of oil palm replanting can bring about various changes. It may influence employment patterns, potentially leading to shifts in labor demand. Additionally, it can result in community displacement and raise issues related to land tenure and ownership. Within the ambit of sustainability, oil palm replanting opens doors for the adoption of eco-friendly agricultural practices and the pursuit of certifications that validate sustainable production methods. This avenue offers a potential pathway for harmonizing economic development with environmental and social responsibilities, aligning with the broader goal of sustainable palm oil production.

9. Conclusions

This review has shed light on the importance of innovative replanting strategies in maximizing oil palm yield sustainably. The main findings indicate that advanced breeding and clonal selection play a pivotal role in developing high-yielding and disease-resistant oil palm varieties, leading to increased productivity and reduced environmental impact. Integrating precision agriculture technologies enables data-driven decision making, optimizing resource management, and minimizing waste. Sustainable land use planning and agroforestry integration emerged as key strategies to balance productivity with environmental conservation. Despite the valuable insights gained, this work has certain limitations. The scope of the study focused on replanting strategies, and additional research may be needed to investigate other aspects of oil palm cultivation, such as post-harvest practices and market dynamics. Furthermore, the applicability of the findings may vary across different geographical regions and farming systems, necessitating further studies to account for regional variations. Future research in this field should continue to explore the potential of advanced breeding techniques and preci-

sion agriculture technologies in maximizing oil palm yield. Investigating the long-term impacts of sustainable land use planning and agroforestry integration on biodiversity and ecosystem services is crucial for comprehensive sustainability assessments. Additionally, examining the socio-economic implications of adopting these innovative strategies can contribute to a more holistic understanding of their feasibility and potential benefits. The broader impacts of this work extend beyond the oil palm industry. Other sectors of agriculture and land use can draw valuable insights from the successful adoption of advanced breeding and precision agriculture practices. The knowledge gained from sustainable land use planning and agroforestry integration can be applied to other crops and contribute to landscape-level conservation efforts. Policymakers and agricultural stakeholders can leverage the findings of this research to develop policies and initiatives that promote environmentally responsible and economically viable agricultural practices.

Author Contributions

Ahmed Abubakar: Conceptualization, data collection and analysis, writing the original draft. Susilawati Kasim: Supervision, methodology design, critical review and editing. Mohd Yusoff Ishak: Data interpretation, manuscript revision, and validation. Md Kamal Uddin: Research design, literature review, and manuscript refinement.

Conflict of Interest

The authors declare no conflicts of interest related to this research work.

Data Availability Statement

The data and materials presented in this manuscript are available upon reasonable request from the corresponding author

Acknowledgement

The authors express their gratitude to Universiti Putra Malaysia, Selangor Darul Ehsan, Malaysia, for

providing the research facilities. This paper received support from the Universiti Putra Malaysia Fundamental Research Grant Scheme (FRGS 1/2020/WAB04/Vote no 5540305) and D'Khairan Farm Sdn Bhd (Vote no 6300349).

References

- [1] Abubakar, A., Mohd, Y.I., Makmom, A.A., 2021. Oil palm in the face of climate change: A review of recommendations. IOP Conference Series: Earth and Environmental Science. 646(1), 1-10.
DOI: <https://doi.org/10.1088/1755-1315/646/1/012065>
- [2] Abubakar, A., Ishak, M.Y., 2022. An overview of the role of smallholders in oil palm production systems in changing climate. *Nature Environment & Pollution Technology*. 21(Suppl.), 2055-2071.
- [3] Abubakar, A., Ishak, M.Y., Bakar, A.A., et al., 2023. Geospatial simulation and mapping of climate suitability for oil palm (*Elaeis guineensis*) production in Peninsular Malaysia using GIS/remote sensing techniques and analytic hierarchy process. *Modeling Earth Systems and Environment*. 9(1), 73-96.
DOI: <https://doi.org/10.1007/s40808-022-01465-9>
- [4] Susila, W.R., 2004. Contribution of oil palm industry to economic growth and poverty alleviation in Indonesia. *Jurnal Penelitian dan Pengembangan Pertanian*. 23(3), 107-113.
- [5] Fleiss, S., Hill, J.K., Mcclean, C., et al., 2017. Potential Impacts of Climate Change on Oil Palm Cultivation [Internet]. Available from: <http://www.sensorproject.net/wp-content/uploads/2018/01/Climate-change-report-FINAL.pdf>
- [6] Qaim, M., Sibhatu, K.T., Siregar, H., et al., 2020. Environmental, economic, and social consequences of the oil palm boom. *Annual Review of Resource Economics*. 12, 321-344.
DOI: <https://doi.org/10.1146/annurev-resource-110119-024922>
- [7] Syahza, A., Bakce, D., Asmit, B., 2018. Increasing the awareness of palm oil plantation replanting through farmers training. *Riau Journal of*

- Empowerment. 1(1), 1-9.
DOI: <https://doi.org/10.31258/raje.1.1.1>
- [8] Nurfatriani, F., Ramawati, Sari, G.K., Komarudin, H., 2019. Optimization of crude palm oil fund to support smallholder oil palm replanting in reducing deforestation in Indonesia. *Sustainability*. 11(18), 4914.
DOI: <https://doi.org/10.3390/su11184914>
- [9] Ismail, A., Mamat, M.N., 2002. The optimal age of oil palm replanting. *Oil Palm Industry Economic Journal*. 2(1), 11-18.
- [10] Ishak, S.M., Aman, Z., Taib, H.M., 2020. An evaluation on outcome of oil palm replanting scheme (TSSPK) and new planting scheme (TBSPK). *International Journal of Modern Trends in Social Sciences*. 3(14), 129-114.
DOI: <https://doi.org/10.35631/ijmtss.3140011>
- [11] Sembiring, N., Napitupulu, H.L., Sembiring, M.T., et al., 2021. The role of model simulation for replanting activities: A review. *IOP Conference Series: Materials Science and Engineering*. 1122(1), 012055.
DOI: <https://doi.org/10.1088/1757-899x/1122/1/012055>
- [12] Hideki, H., 2018. The replanting problems of plasma estates in the Indonesian state-owned oil palm estate: A case in Sanggau Regency, West Kalimantan Province. *Japanese Journal of Southeast Asian Studies*. 55(2), 292-319.
DOI: <https://doi.org/10.20495/tak.55.2>
- [13] Zhao, J., Elmore, A.J., Lee, J.S.H., et al., 2023. Replanting and yield increase strategies for alleviating the potential decline in palm oil production in Indonesia. *Agricultural Systems*. 210, 103714.
DOI: <https://doi.org/10.1016/j.agry.2023.103714>
- [14] Petri, H., Hendrawan, D., Bähr, T., et al., 2023. Replanting challenges among Indonesian oil palm smallholders: A narrative review. *Environment, Development and Sustainability*. 1-17.
DOI: <https://doi.org/10.1007/s10668-023-03527-z>
- [15] Novra, A., Fatati, Novianti, S., Andayani, J., et al., 2023. Technical formulation for estimating the economic loss impact of the smallholder oil palm replanting program in Indonesia. *African Journal of Food, Agriculture, Nutrition and Development*. 23(5), 23389-23405.
- [16] Siswati, L., Insusanty, E., Susi, N., et al., 2023. Analysis of oil palm smallholder income during replanting in Siak Regency, Riau. *IOP Conference Series: Earth and Environmental Science*. 1160(1), 1-8.
DOI: <https://doi.org/10.1088/1755-1315/1160/1/012067>
- [17] Fauzia, G., Alamsyah, Z., Yanita, M., et al., 2021. Identification of internal and external factors in replanting oil palm. *IOP Conference Series: Earth and Environmental Science*. 782(3), 32063.
DOI: <https://doi.org/10.1088/1755-1315/782/3/032063>
- [18] Fadzilah, S., Adibah, M., Sim, C., et al., 2022. Influence of oil palm replanting, age and management zones on soil carbon. *Malaysian Journal of Soil Science*. 26, 73-79.
- [19] Ernawati, H.D., Suandi, S., Yanita, M., et al., 2019. The impact of replanting oil palm plantations on the farming income of the Sungai Bahar community in Muaro Jambi Regency. *IOP Conference Series: Earth and Environmental Science*. 336(1).
DOI: <https://doi.org/10.1088/1755-1315/336/1/012003>
- [20] Pashkevich, M.D., Aryawan, A.A.K., Luke, S.H., et al., 2021. Assessing the effects of oil palm replanting on arthropod biodiversity. *Journal of Applied Ecology*. 58(1), 27-43.
DOI: <https://doi.org/10.1111/1365-2664.13749>
- [21] Ibrahim, M.S., Seman, I.A., Rusli, M.H., et al., 2020. Surveillance of Ganoderma disease in oil palm planted by participants of the smallholders replanting incentive scheme in Malaysia. *Journal of Oil Palm Research*. 32(2), 237-244.
DOI: <https://doi.org/10.21894/jopr.2020.0024>
- [22] Hati, D.P., Mulyani, A., Nugroho, E.S., 2021. An estimation method for oil palm replanting potential in Kampar Regency, Province of Riau. *IOP Conference Series: Earth and Environmental Science*. 757(1), 012034.
DOI: <https://doi.org/10.1088/1755-1315/757/1/012034>
- [23] Faeid, M.Z.M., Abidin, N.Z., Applanaidu, S.D., 2020. Determining optimal replanting rate in

- palm oil industry, Malaysia: A system dynamics approach optimal policy search in oil palm plantation feedback loops using system dynamics optimisation. *International Journal of Information and Decision Sciences*. 12(2), 136-153.
DOI: <https://doi.org/10.1504/IJIDS.2020.106728>
- [24] Ardana, I.K., Wulandari, S., Hartati, R.S., 2022. Urgency to accelerate replanting of Indonesian oil palm: A review of the role of seed institutions. *IOP Conference Series: Earth and Environmental Science*. 974(1), 12104.
DOI: <https://doi.org/10.1088/1755-1315/974/1/012104>
- [25] Abubakar, A., Ishak, M.Y., Makmom, A.A., 2021. Impacts of and adaptation to climate change on the oil palm in Malaysia: A systematic review. *Environmental Science and Pollution Research*. 28(39), 54339-54361.
DOI: <https://doi.org/https://doi.org/10.1007/s11356-021-15890-3>
- [26] Abubakar, A., Ishak, M.Y., Makmom, A.A., 2022. Nexus between climate change and oil palm production in Malaysia: A review. *Environmental Monitoring and Assessment*. 194(4), 262.
DOI: <https://doi.org/10.1007/s10661-022-09915-8>
- [27] Ooi, L.H., Heriansyah, H., 2005. Palm pulverisation in sustainable oil palm replanting. *Plant Production Science*, 8(3), 345-348.
DOI: <https://doi.org/10.1626/pps.8.345>
- [28] Siswati, L., Insusanty, E., Susi, N., et al., 2022. Oil palm trunk replanting as brown sugar raw materials. *IOP Conference Series: Earth and Environmental Science*. 1041(1), 12054.
DOI: <https://doi.org/10.1088/1755-1315/1041/1/012054>
- [29] Ernawati, H.D., Saputra, A., Alamsyah, Z., et al., 2021. Analysis of independent oil palm farming income after replanting in Muaro Jambi District. *IOP Conference Series: Earth and Environmental Science*. 782(3), 32055.
DOI: <https://doi.org/10.1088/1755-1315/782/3/032055>
- [30] Yanita, M., Napitupulu, D., Alamsyah, Z., et al., 2021. What is the priority pattern for replanting the independent smallholders oil palm in Jambi Province? *IOP Conference Series: Earth and Environmental Science*. 782(3), 32059.
DOI: <https://doi.org/10.1088/1755-1315/782/3/032059>
- [31] Corley, R.H.V., 2009. How much palm oil do we need? *Environmental Science & Policy*. 12(2), 134-139.
DOI: <https://doi.org/10.1016/j.envsci.2008.10.011>
- [32] Kurnia, J.C., Jangam, S.V., Akhtar, S., et al., 2016. Advances in biofuel production from oil palm and palm oil processing wastes: A review. *Biofuel Research Journal*. 3(1), 332-346.
DOI: <https://doi.org/10.18331/BRJ2016.3.1.3>
- [33] Verheye, W., 2010. Growth and production of oil palm. *Land use, land cover and soil sciences. Encyclopedia of Life Support Systems (EOLSS), UNESCO-EOLSS Publishers: Oxford, UK*.
- [34] Forero, D.C., Hormaza, P., Romero, H.M., 2012. Phenological growth stages of African oil palm (*Elaeis guineensis*). *Annals of Applied Biology*. 160(1), 56-65.
DOI: <https://doi.org/10.1111/j.1744-7348.2011.00520.x>
- [35] Hormaza, P., Fuquen, E.M., Romero, H.M., 2012. Phenology of the oil palm interspecific hybrid *Elaeis oleifera* × *Elaeis guineensis*. *Scientia Agricola*. 69, 275-280.
DOI: <https://doi.org/10.1590/S0103-90162012000400007>
- [36] Khor, J.F., Ling, L., Yusop, Z., et al., 2021. Impact of El Niño on oil palm yield in Malaysia. *Agronomy*. 11(11), 2189.
DOI: <https://doi.org/10.3390/agronomy11112189>
- [37] Khor, J.F., Ling, L., Yusop, Z., et al., 2023. Impact comparison of El Niño and ageing crops on Malaysian oil palm yield. *Plants*. 12(3), 424.
DOI: <https://doi.org/10.3390/plants12030424>
- [38] Santoso, H., Gunawan, T., Jatmiko, R.H., et al., 2011. Mapping and identifying basal stem rot disease in oil palms in North Sumatra with QuickBird imagery. *Precision Agriculture*. 12, 233-248.
DOI: <https://doi.org/10.1007/s11119-010-9172-7>
- [39] Kindohoundé, N.S., Nodichao, L., Aholoukpè, N.S.H., et al., 2021. Mapping of soil nutrient de-

- iciency in oil palm plantations of Southern Benin. *African Crop Science Journal*. 29(1), 141-156.
DOI: <https://doi.org/10.4314/acsj.v29i1.10>
- [40] Abazue, C.M., Er, A.C., Ferdous Alam, A.S.A., et al., 2015. Oil palm smallholders and its sustainability practices in Malaysia. *Mediterranean Journal of Social Sciences*. 6(S4), 482-488.
DOI: <https://doi.org/10.5901/mjss.2015.v6n6s4p482>
- [41] Ukwuteno, S.O., Eboh, E.C., Ocheja, J.O., 2018. Determination of costs and returns of oil palm production in Kogi State, Nigeria. *International Journal of Research in Agriculture and Forestry*. 5(1), 27-33.
- [42] Ashton-Butt, A., Willcock, S., Purnomo, D., et al., 2019. Replanting of first-cycle oil palm results in a second wave of biodiversity loss. *Ecology and Evolution*. 9(11), 6433-6443.
DOI: <https://doi.org/10.1002/ece3.5218>
- [43] Satriawan, H., Fuady, Z., Mayani, N., 2016. Soil conservation by vegetative systems in oil palm cultivation. *Polish Journal of Soil Science*. 49(2).
- [44] Abubakar, A., Ishak, M.Y., Bakar, A.A., et al., 2022. *Ganoderma boninense* basal stem rot induced by climate change and its effect on oil palm. *Environmental Sustainability*. 5(3), 289-303.
DOI: <https://doi.org/10.1007/s42398-022-00244-7>
- [45] Murphy, D.J., 2007. Future prospects for oil palm in the 21st century: Biological and related challenges. *European Journal of Lipid Science and Technology*. 109(4), 296-306.
DOI: <https://doi.org/10.1002/ejlt.200600229>
- [46] Nyouma, A., Bell, J.M., Jacob, F., et al., 2020. Genomic predictions improve clonal selection in oil palm (*Elaeis guineensis* Jacq.) hybrids. *Plant Science*. 299, 110547.
DOI: <https://doi.org/10.1016/j.plantsci.2020.110547>
- [47] Nabara, I.S., Norsida, M., 2018. The role of extension in activity-based adaptation strategies towards climate impact among oil palm smallholders in Malaysia : A systematic review. *Journal of Agriculture and Veterinary Science*. 11(8), 37-44.
- [48] Ruslan, A.A., Salleh, S.M., Hatta, S.F.W.M., et al., 2021. IoT soil monitoring based on LoRa module for oil palm plantation. *International Journal of Advanced Computer Science and Applications*. 12(5), 215-220.
DOI: <https://doi.org/10.14569/IJACSA.2021.0120527>
- [49] Culman, M.A., Gomez, J.A., Talavera, J., et al. (editors), 2017. A novel application for identification of nutrient deficiencies in oil palm using the Internet of Things. 2017 5th IEEE International Conference on Mobile Cloud Computing, Services, and Engineering (MobileCloud); 2017 Apr 6-8; San Francisco, CA, USA. New York: IEEE. p. 169-172.
DOI: <https://doi.org/10.1109/MobileCloud.2017.32>
- [50] Adib, N.M., Daliman, S., 2021. Conceptual framework of smart fertilization management for oil palm tree based on IOT and deep learning. *IOP Conference Series: Earth and Environmental Science*. 842(1), 012072.
DOI: <https://doi.org/10.1088/1755-1315/842/1/012072>
- [51] Van der Laan, C., Wicke, B., Verweij, P.A., et al., 2017. Mitigation of unwanted direct and indirect land-use change—an integrated approach illustrated for palm oil, pulpwood, rubber and rice production in North and East Kalimantan, Indonesia. *Gcb Bioenergy*. 9(2), 429-444.
DOI: <https://doi.org/10.1111/gcbb.12353>
- [52] Khasanah, N., van Noordwijk, M., Slingerland, M., et al., 2020. Oil palm agroforestry can achieve economic and environmental gains as indicated by multifunctional land equivalent ratios. *Frontiers in Sustainable Food Systems*. 3, 122.
DOI: <https://doi.org/10.3389/fsufs.2019.00122>
- [53] Ahirwal, J., Sahoo, U.K., Thangjam, U., et al., 2022. Oil palm agroforestry enhances crop yield and ecosystem carbon stock in northeast India: Implications for the United Nations sustainable development goals. *Sustainable Production and Consumption*. 30, 478-487.
DOI: <https://doi.org/10.1016/j.spc.2021.12.022>

- [54] Sundram, S., Angel, L.P.L., Sirajuddin, S.A., 2019. Integrated balanced fertiliser management in soil health rejuvenation for a sustainable oil palm cultivation: A review. *Journal of Oil Palm Research*. 31(3), 348-363.
DOI: <https://doi.org/10.21894/jopr.2019.0045>
- [55] Egonyu, J.P., Baguma, J., Martínez, L.C., et al., 2022. Global advances on insect pest management research in oil palm. *Sustainability*. 14(23), 16288.
DOI: <https://doi.org/10.3390/su142316288>
- [56] Susanto, A., Sudharto, P.S., Purba, R.Y., 2005. Enhancing biological control of basal stem rot disease (*Ganoderma boninense*) in oil palm plantations. *Mycopathologia*. 159(1), 153-157.
DOI: <https://doi.org/10.1007/s11046-004-4438-0>
- [57] Shafawati, S.N., Siddiquee, S., 2013. Composting of oil palm fibres and *Trichoderma* spp. as the biological control agent: A review. *International Biodeterioration & Biodegradation*. 85, 243-253.
DOI: <https://doi.org/10.1016/j.ibiod.2013.08.005>
- [58] Nurdiansyah, F., Denmead, L.H., Clough, Y., et al., 2016. Biological control in Indonesian oil palm potentially enhanced by landscape context. *Agriculture, Ecosystems & Environment*. 232, 141-149.
DOI: <https://doi.org/10.1016/j.agee.2016.08.006>
- [59] Rhebergen, T., Fairhurst, T., Giller, K.E., et al., 2019. The influence of water and nutrient management on oil palm yield trends on a large-scale plantation in Ghana. *Agricultural Water Management*. 221, 377-387.
DOI: <https://doi.org/10.1016/j.agwat.2019.05.003>
- [60] Soh, A.C., Wong, G., Tan, C.C., et al., 2011. Commercial-scale propagation and planting of elite oil palm clones: Research and development towards realization. *Journal of Oil Palm Research*. 23, 935-952.
- [61] Oberthür, T., Cock, J., Donough, C.R., et al. (editors), 2012. Best management practices (BMP) in oil palm fertilization for sustainable intensification. *Proceedings of the 17th International Oil Palm Conference*; Cartagena, Colombia. p. 1-28.
- [62] Subhi, S.M., Tahir, N.I., Abd Rasid, O., et al., 2017. Post-genomic technologies for the advancement of oil palm research. *Journal of Oil Palm Research*. 29(4), 469-486.
DOI: <https://doi.org/10.21894/jopr.2017.00013>
- [63] Rhebergen, T., Zingore, S., Giller, K.E., et al., 2020. Closing yield gaps in oil palm production systems in Ghana through Best Management Practices. *European Journal of Agronomy*. 115, 126011.
DOI: <https://doi.org/10.1016/j.eja.2020.126011>
- [64] Nchanji, Y.K., Nkongho, R.N., Mala, W.A., et al., 2016. Efficacy of oil palm intercropping by smallholders. Case study in South-West Cameroon. *Agroforestry Systems*. 90(3), 509-519.
DOI: <https://doi.org/10.1007/s10457-015-9873-z>
- [65] Murtalaksono, K., Darmosarkoro, W., Sutarta, E.S., et al., 2011. Feasibility of soil and water conservation techniques on oil palm plantation. *AGRIVITA, Journal of Agricultural Science*. 33(1), 63-69.
- [66] Li, K., Tschardtke, T., Saintes, B., et al., 2019. Critical factors limiting pollination success in oil palm: A systematic review. *Agriculture, Ecosystems & Environment*. 280, 152-160.
DOI: <https://doi.org/10.1016/j.agee.2019.05.001>
- [67] Johnston, D., Smit, H.H., Bronkhorst, E., et al., 2018. Innovative Replanting Financing Model for Oil Palm Smallholder Farmers in Indonesia: Potential for Upscaling, Improving Livelihoods and Supporting Deforestation-Free Supply Chains [Internet]. Available from: <https://www.tropicalforestalliance.org/assets/Uploads/TFA2020-Innovative-Replanting-Models-2018-online.pdf>
- [68] Senawi, R., Rahman, N.K., Mansor, N., et al., 2019. Transformation of oil palm independent smallholders through Malaysian sustainable palm oil. *Journal of Oil Palm Research*. 31(3), 496-507.
DOI: <https://doi.org/10.21894/jopr.2019.0038>
- [69] Nagiah, C., Azmi, R., 2013. A review of smallholder oil palm production: Challenges and

- opportunities for enhancing sustainability—a Malaysian perspective. *Journal of Oil Palm, Environment and Health (JOPEH)*. 3, 114-120.
DOI: <https://doi.org/10.5366/jope.2012.12>
- [70] Waddington, H., White, H., 2014. Farmer Field Schools: From Agricultural Extension to Adult Education, 3ie Systematic Review Summary 1 [Internet]. Available from: <https://www.3ieimpact.org/evidence-hub/publications/systematic-review-summaries/farmer-field-schools-agricultural-extension>
- [71] Aker, J.C., 2011. Dial “A” for agriculture: A review of information and communication technologies for agricultural extension in developing countries. *Agricultural Economics*. 42(6), 631-647.
DOI: <https://doi.org/10.1111/j.1574-0862.2011.00545.x>
- [72] Tey, Y.S., Brindal, M., Darham, S., et al., 2020. Early mover advantage in roundtable on sustainable palm oil certification: A panel evidence of plantation companies. *Journal of Cleaner Production*. 252, 119775.
DOI: <https://doi.org/10.1016/j.jclepro.2019.119775>
- [73] Lee, J.S.H., Ghazoul, J., Obidzinski, K., et al., 2014. Oil palm smallholder yields and incomes constrained by harvesting practices and type of smallholder management in Indonesia. *Agronomy for Sustainable Development*. 34, 501-513.
DOI: <https://doi.org/10.1007/s13593-013-0159-4>
- [74] Woittiez, L.S., Van Wijk, M.T., Slingerland, M., et al., 2017. Yield gaps in oil palm: A quantitative review of contributing factors. *European Journal of Agronomy*. 83, 57-77.
DOI: <https://doi.org/10.1016/j.eja.2016.11.002>

ARTICLE

Hyperspectral Inversion and Analysis of Zinc Concentration in Urban Soil in the Urumqi City of China

Qing Zhong¹, Mamattursun Eziz^{1,2}, Mireguli Ainiwaer^{1,2}, Rukeya Sawut^{1,2}*

¹ College of Geographical Science and Tourism, Xinjiang Normal University, Urumqi, Xinjiang, 830054, China

² Laboratory of Arid Zone Lake Environment and Resources, Xinjiang Normal University, Urumqi, Xinjiang, 830054, China

ABSTRACT

Excessive accumulation of zinc (Zn) in urban soil can lead to environmental pollution and pose a potential threat to human health and the ecosystem. How to quickly and accurately monitor the urban soil zinc content on a large scale in real time and dynamically is crucial. Hyperspectral remote sensing technology provides a new method for rapid and nondestructive soil property detection. The main goal of this study is to find an optimal combination of spectral transformation and a hyperspectral estimation model to predict the Zn content in urban soil. A total of 88 soil samples were collected to obtain the Zn contents and related hyperspectral data, and perform 18 transformations on the original spectral data. Then, select important wavelengths by Pearson's correlation coefficient analysis (PCC) and CARS. Finally, establish a partial least squares regression model (PLSR) and random forest regression model (RFR) with soil Zn content and important wavelengths. The results indicated that the average Zn content of the collected soil samples is 60.88 mg/kg. Pearson's correlation coefficient analysis (PCC) and CARS for the original and transformed wavelengths can effectively improve the correlations between the spectral data and soil Zn content. The number of important wavelengths selected by CARS is less than the important wavelengths selected by PCC. Partial least squares regression model based on first-order differentiation of the reciprocal by CARS (CARS-RTFD-PLSR) is more stable and has the highest prediction ability ($R^2 = 0.937$, RMSE = 8.914, MAE = 2.735, RPD = 3.985). The CARS-RTFD-PLSR method can be used as a means of prediction of Zn content in soil in oasis cities. The results of the study can provide technical support for the hyperspectral estimation of the soil Zn content.

Keywords: Urban soil; Zinc; Hyperspectral remote sensing; Prediction; PLSR; RFR

*CORRESPONDING AUTHOR:

Mamattursun Eziz, College of Geographical Science and Tourism, Xinjiang Normal University, Urumqi, Xinjiang, 830054, China; Laboratory of Arid Zone Lake Environment and Resources, Xinjiang Normal University, Urumqi, Xinjiang, 830054, China; Email: oasiseco@126.com

ARTICLE INFO

Received: 5 September 2023 | Revised: 28 September 2023 | Accepted: 8 October 2023 | Published Online: 17 October 2023

DOI: <https://doi.org/10.30564/jees.v5i2.5947>

CITATION

Qing, Zh., Eziz, M., Ainiwaer, M., et al., 2023. Hyperspectral Inversion and Analysis of Zinc Concentration in Urban Soil in the Urumqi City of China. *Journal of Environmental & Earth Sciences*. 5(2): 76-87. DOI: <https://doi.org/10.30564/jees.v5i2.5947>

COPYRIGHT

Copyright © 2023 by the author(s). Published by Bilingual Publishing Group. This is an open access article under the Creative Commons Attribution-NonCommercial 4.0 International (CC BY-NC 4.0) License. (<https://creativecommons.org/licenses/by-nc/4.0/>).

1. Introduction

Zinc (Zn) and its compounds are often enriched in soil by substitution reactions and adsorption and immobilization, resulting in environmental pollution^[1]. Through accumulation, migration and transport in the food chain, Zn in soil eventually poses a serious threat to human health^[2]. Therefore, it is vital to protect the safety of the urban soil environment by rapid and accurate monitoring of the Zn content. The traditional methods for determining heavy metal content in soil require field sampling followed by laboratory experimentation, but it is time-consuming, costly and inefficient^[3,4]. Hyperspectral remote sensing technology has been applied to the prediction of heavy metal contents in soil due to the advantages of rapid, accurate, non-destructive, lower cost, and dynamic monitoring over a large area^[5-7].

In recent years, hyperspectral remote sensing technology has shown good results in the prediction of soil Zn content. For example, the BPNN model has good generalization ability ($R^2 = 0.74$, RPIQ = 1.44) to predict the soil Zn content for Dehong Prefecture, southwest Yunnan Province, China^[8], CWT-RF model has a good prediction accuracy ($R^2 = 0.77$, RMSE = 9.54, MAE = 7.39) to estimate the Zn content for Ordos City, Inner Mongolia Autonomous Region, China^[9] and PLSR model can effectively achieve quantitative inversion ($R^2 = 0.796$, RMSE = 2.574) of soil Zn content in mining areas of the city of Zoucheng, Shandong Province, China^[10]. El-Sayed E^[11] found that the PLSR model had the optimal prediction for Bahr El-Baqar region with R^2 of 0.66, RMSE of 20.42, and RPD of 2.05. Yang et al.^[12] pointed out that the PLSR model had the highest stability and accuracy ($R^2 = 0.95$, RMSE = 33.65) in predicting the Zn content in mining areas of the city of Tongling, Anhui Province, China.

With the acceleration of urbanization and the influence of the “Silk Road Economic Belt”, eco-envi-

ronmental problems in oases in the northwestern arid zones garnered more attention^[13,14]. In addition, due to the impact of strong human activities, factories and high traffic volumes, the level of Zn in urban soil is higher than that in farmland and natural soil^[15]. Relevant studies also reported that there is serious trace element contamination exists in soil and surface dust in Urumqi^[16,17]. Therefore, it is very important to analyze the possibility of the hyperspectral inversion of Zn contents in urban soils. The main objective of this study was to find an optimal model to predict the Zn content in soil. Thus, the work of this study was to identify the important wavelengths of Zn in urban soil and evaluate the efficiency of different spectral transformations and soil Zn contents. Then, select an optimum hyperspectral prediction model for Zn content in urban soil based on the partial least squares regression (PLSR) and random forests regression (RFR). The results will solve the existing problems in the current hyperspectral inversion of Zn content in urban soil.

2. Description of the study area

The experimental field (87°28'-87°37' E and 43°48'-44°04' N) is selected in the central parts of the Urumqi, which is situated in the southern edge of the Junggar Basin, the northwest arid regions of China, and is one of the important metropolitan cities in NW China (**Figure 1**). The main soil type of this region is mainly grey desert soil^[15]. The climate is regionally marked by a continental arid climate with an annual average temperature, precipitation, and evaporation of about 6.7 °C, 280 mm, and 2730 mm, respectively. Urumqi has become the capital of Xinjiang and the second-largest city in northwestern China due to its rapid economic development and expanding industrial scale. Toxic elements in the soil are accumulating and are prone to soil pollution.

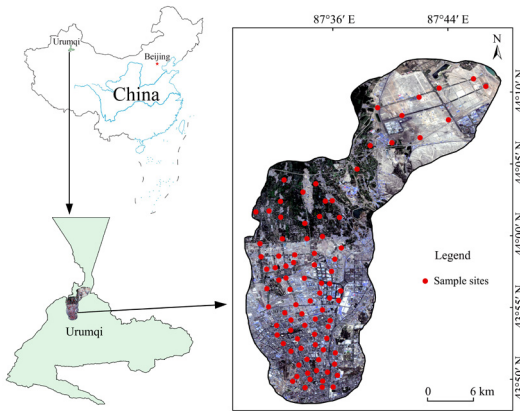


Figure 1. Location of experimental field and sample sites.

3. Materials and methods

3.1 Sample collection and analysis

A total of 88 topsoil samples (0-20 cm) were collected within the study area (**Figure 1**) in April 2021. At each sample site, five sub-samples from the topsoil (0-20 cm) layer were taken within 100 m × 100 m areas and then mixed together to form one composite soil sample, weighing more than 500 g. All the samples were returned to the laboratory and sieved for 20 meshes after naturally air dried. Each sample was divided into two groups, one for the determination of Zn content and another one for the hyperspectral measurement. The Zn content of soil samples was determined as described in “HJ 803-2016”^[18], using an Inductively Coupled Plasma Mass Spectrometer (ICP-MS 7800). The analytical data quality was analyzed by the laboratory quality control methods, including the use of reagent blanks, duplicates and standard reference materials for each batch of soil samples. For the precision of the analytical procedures, a standard solution was used to compare samples to national standards (Chinese national standards samples, GSS-12). All of the soil samples were tested repeatedly, and the determined consistency of the Zn measurements was 96.5%.

3.2 Spectrometric determination and pre-processing

The spectral determination of collected soil sam-

ples was measured using a FieldSpec®3 portable object spectrometer manufactured by Analytical Spectral Devices (ASD), USA. The interval of data acquisition was 1 nm with a spectral measurement range from 350 to 2500 nm. Firstly, the instrument was preheated, and secondly, a 40 cm × 40 cm white board was placed on a 2 m × 2 m black cardboard for calibration to obtain the absolute reflectance before determining the spectral data. Finally, the soil samples were kept in a natural state on the black cardboard with the sensor probe perpendicular to 15 cm above the soil surface, and the sensor probe was optimized with a white board every 5 minutes. A total of 15 replicate measurements were taken on the same soil sample, and 15 spectral curves were collected.

The 15 spectral curves were averaged using ViewSpecPro software, and the arithmetic mean was taken as the original reflectance spectral value of the soil sample. Due to the influence of the surrounding environment and the spectral instrument itself, the spectral bands within 350-399 nm, 1350-1430 nm, 1781-1970 nm and 2401-2500 nm were excluded before constructing the hyperspectral models, which were outputted in a total of 1730 bands. The Savitzky-Golay (S-G) filter algorithm is applied for smoothing and removing noise from spectral curves. **Figure 2** illustrates the spectral reflectance curves of the original spectra and spectra processed by the S-G smoothing.

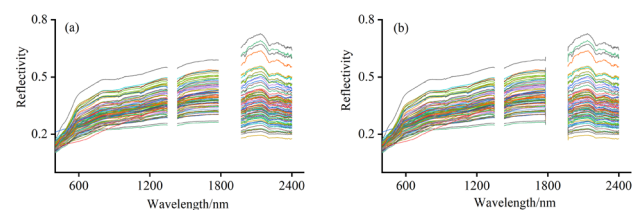


Figure 2. Original (a) and Savitzky-Golay smoothing (b) spectral reflectance curve of soil.

3.3 Spectral transformation and important wavelength selection

In order to enhance the spectral information related to Zn in soil samples, the original spectral reflectance data (R) are subjected to logarithm of the

reciprocal (AT), root mean square (RMS), logarithm (LT), reciprocal of the logarithm (RL), reciprocal (RT), first-order differentiation (FD), second-order differentiation (SD), first-order differentiation of the reciprocal (RTFD), second-order differentiation of the reciprocal (RTSD), first-order differentiation of the logarithm (LTFD), second-order differentiation of the logarithm (LTSD), root mean square first-order differentiation (RMSFD), root mean square second-order differentiation (RMSSD), logarithmic first order differentiation of the reciprocal (ATFD), logarithmic second order differentiation of the reciprocal (ATSD), logarithmic first order differentiation of the reciprocal (RLFD), and logarithmic second order differentiation of the reciprocal (RLSD).

Firstly, Pearson's correlation coefficient analysis (PCC) was performed between soil Zn content and 18 forms of soil spectral data, and the bands with larger correlation coefficients were screened out as important wavelengths for hyperspectral prediction modeling. Secondly, all the original and 17 types of transformed spectral data were intelligently extracted for the important wavelengths by using Competitive Adaptive Re-weighted Sampling (CARS) to exclude further removed wavelengths with low correlation^[19,20]. The CARS method is constructed in Python.

3.4 Modelling of hyperspectral inversion

Soil samples were randomly divided into a modeling data set (70 samples) and a validation data set (18 samples) in order to ensure the rationality of hyperspectral modeling. The modeling data set was used to build hyperspectral prediction models, while the validation data set was used to test the accuracy of prediction models. The partial least squares regression (PLSR) and random forests regression (RFR) were used to select the optimum hyperspectral prediction model. The PLSR algorithm considers both spectral information (x) and the corresponding reference values (y) of samples during modeling and transforms the original spectral data into mutually orthogonal and unrelated new variables via linear transformation, thereby eliminating multicollinearity

between datasets^[21].

The RFR is a relatively new data mining technique that is designed to produce accurate predictions that do not overfit the data. RFR is easy to use as it requires only three input parameters: the number of two 'random_state' and 'n_estimators'. The three input parameters are used to partition the modeling set and validation set, and determine the optimal partitioning of each tree node^[22], respectively. The individual trees in the RFR ensemble are built on a bootstrapped training sample, and only a small group of predictor variables are considered at each split; this ensures that trees are de-correlated with each other. Additionally, studies have shown that the three input parameters provide accurate results^[23].

3.5 Model validation

A robust model has high R^2 and RPD and low RMSE and MAE^[24]. Thus, the determination coefficient (R^2), root mean square error (RMSE), mean absolute error (MAE) and residual prediction deviation (RPD) were chosen to evaluate the prediction accuracy of the hyperspectral prediction models. When $R^2 < 0.5$, the prediction model does not have prediction ability, when $0.5 \leq R^2 < 0.7$, the model has preliminary prediction ability, and when $R^2 \geq 0.7$, the model has good prediction ability^[25]. When $RPD \geq 2.0$, the prediction model has a good prediction ability, when $1.4 \leq RPD < 2.0$, the model has the initial predictive capability, and when $RPD < 1.4$, the model has a poor predictive capability. In general, lower RMSE and MAE indicate better model prediction accuracy^[26].

4. Results and analyses

4.1 Statistical analysis of Zn content in soil

Statistical results of Zn contents for soil samples in the Urumqi are given in **Table 1**. Standard deviation (SD) and coefficient of variation (CV) were used to measure data dispersion, with the CV used as a complement to the SD. **Table 1** shows that the Zn contents of soil samples are distributed in the range

of 34.00-200.00 mg/kg, with an average value of 60.88 mg/kg. The average Zn contents of modeling set and validation set are 60.57 mg/kg and 62.06 mg/kg, respectively. The SD of modeling set and validation set are 21.18 and 35.28 mg/kg, respectively. And, the CV values of modeling set and validation set are 0.35 and 0.57, respectively. It's clear that the average and CV values of Zn contents in the modeling set are essentially the same as those of the validation set. Influenced by two high value sample points, the SD values have a difference. This is because the main factories are located in the northern and northeastern parts of Urumqi and the roads with high traffic volumes stretch across the city center^[16]. So, two high value sample points were split into modelling set and a validation set respectively. Overall, it indicates that the division of soil samples was reasonable and can be used for subsequent model construction.

4.2 Correlation between soil Zn content and reflectance data

The PCC analysis was performed between the Zn content and the spectral data after 17 types of transformations and R, which can identify the correlation between Zn content and spectral data of soil samples. The degree of correlation was expressed by the Pearson coefficient (r), and PCC was examined in the significance test at the $P < 0.01$ level (two-sided).

In **Figure 3**, the spectrum of the R, RMS, and LT showed a highly significant negative correlation with Zn content with 1730 important wavelengths selected. The spectrum of the AT, RL, and RT showed a highly significant positive correlation with Zn content with 1730 important wavelengths selected. The correlation analysis of the Zn content and spectral data processed by first-order and second-order differentiation transformed indicated that both positive and negative correlation coefficients showed extreme values, and the positive and negative correlations of the filtered important wavelengths were more uniformly distributed. Thus, 18 types of spectrum can filter out characteristic bands for data modeling,

and the number of the important wavelengths is descended in the order of: $R(1730) = RMS(1730) = LT(1730) = RL(1730) = RT(1730) = AT(1730) > RLFD(663) > FD(502) > RTFD(436) > RTSD(387) > RMSFD(306) > LTSD(253) = ATSD(253) > LTFD(194) = ATFD(194) > RMSSD(186) > SD(125) > RLSD(82)$.

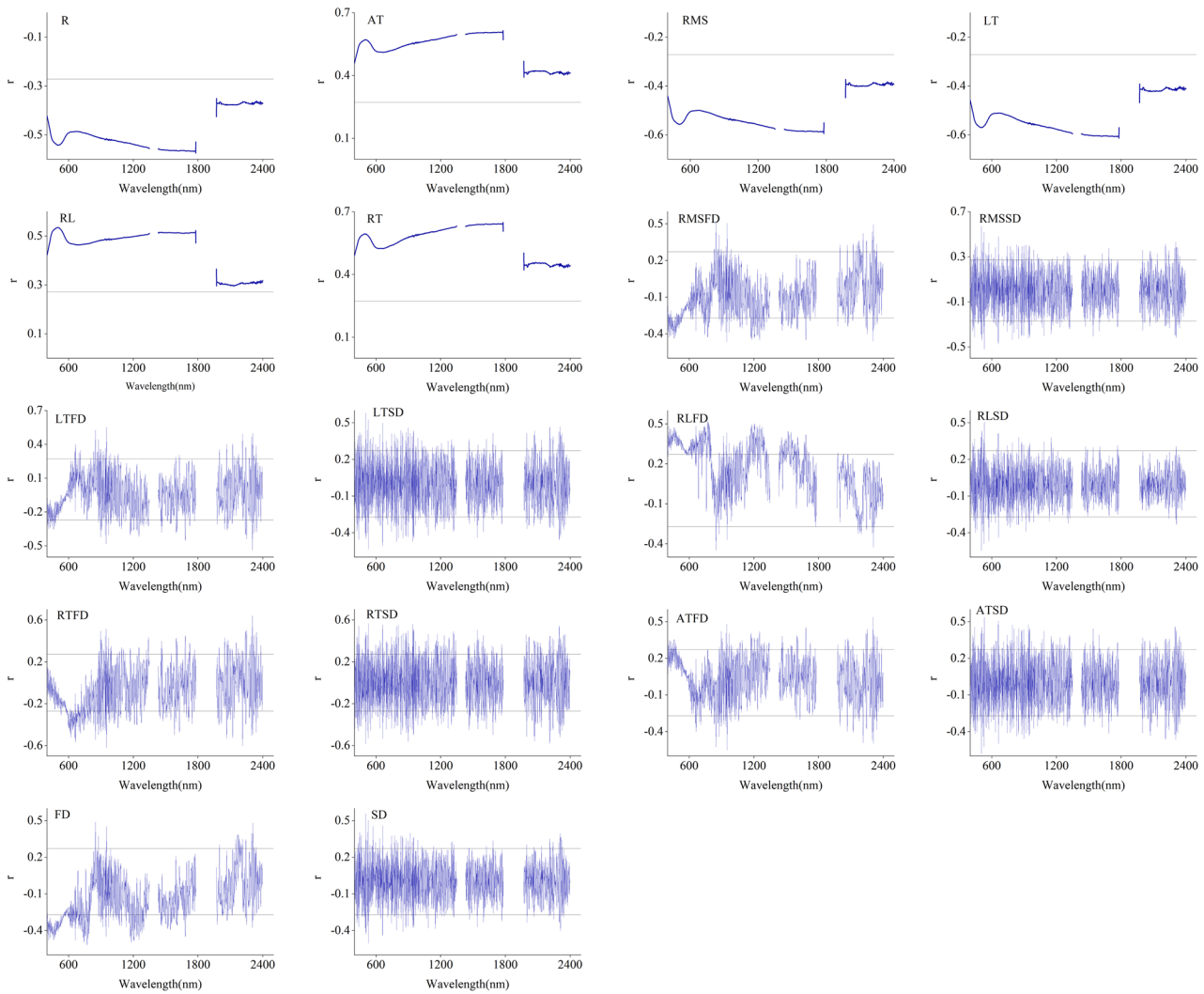
The number of important wavelengths selected by CARS is descended in the order of $RMSSD(25) = RMSFD(25) = RTFD(25) > RLSD(23) > RTSD(22) > ATSD(21) > LTFD(20) = ATFD(20) = FD(20) > SD(19) > R(16) > LTSD(14) > RLFD(13) = AT(13) > RMS(12) > RL(11) > LT(9) = RT(9)$. The number of important wavelengths selected by CARS is less than the important wavelengths selected by PCC.

4.3 The establishment and analysis of the spectral inversion prediction model

Partial least squares regression model (PLSR) and random forest regression model (RFR) were constructed to predict the Zn content of soil in this study. Based on Python, the "random_state" of three models was set as 48. Due to the randomness of the RFR model, the number of parameters ("n_estimators" and another "random_state") will disturb the predictive performance of the model. Under the consideration of model performance, model running time, sample number and other factors, the number of parameters ("n_estimators" and another "random_state") of the RFR model was set in the range from 1 to 99. The modeling set is used to construct the inversion model, whereas the validation set is used to evaluate the performance of the final model. According to the correlation coefficient between the Zn content and the spectrum, wavelengths with absolute values more than 0.272 under the processed spectral reflectance data were taken as important wavelengths. Then, the important wavelengths are selected as the independent variables (x), and the Zn contents of the soil are selected as the dependent variables (y). The hyperspectral inversion model for soil Zn content was established by the partial least squares regression (PLSR) and the random forests regression algorithms, respectively.

Table 1. Statistical values of Zn contents in soil in the Urumqi.

Data set	Samples/n	Minimum	Maximum	Average	SD	CV
Modeling set (mg/kg)	70	37.00	164.00	60.57	21.18	0.35
Validation set (mg/kg)	18	34.00	200.00	62.06	35.52	0.57
Total (mg/kg)	88	34.00	200.00	60.88	24.81	0.41

**Figure 3.** Correlations of PCC between soil Zn content and spectral reflectance data.

The analysis of the PLSR model

The basic statistics related to the stability and accuracy of the PLSR model are given in **Table 2**.

As shown in **Table 2**, the R^2 inverted by the PLSR model based on the important wavelengths selected by PCC range from 0.208 to 0.540, RMSE values range from 24.089 to 31.621, MAE values range from 3.981 to 4.095, and RPD values range from 1.123 to 1.475. For the RTSD-PLSR model ($R^2 = 0.540$, RMSE = 24.089, MAE = 3.981, and RPD =

1.475), the estimation capability of the remaining models is poor and the prediction accuracy is low.

The ranges of R^2 , RMSE, MAE, and RPD values inverted by PLSR based on the important wavelengths selected by CARS are 0.135-0.937, 8.914-33.039, 2.735-4.305, and 3.985-1.075, respectively. The prediction accuracy of CARS-RTFD-PLSR model is highest ($R^2 = 0.937$, RMSE = 8.914, MAE = 2.735, RPD = 3.985). PLSR model based on AT, RMS, RT, RMSFD, LTFD, ATFD, and FD has the better estimation capability.

Table 2. Statistics of accuracy parameters of PLSR model for soil Zn content in Urumqi.

Transformation	PCC				CARS			
	R ²	RMSE	MAE	RPD	R ²	RMSE	MAE	RPD
R	0.376	25.051	4.037	1.418	0.496	24.209	3.919	1.467
AT	0.329	29.095	4.215	1.221	0.550	23.833	3.935	1.490
RMS	0.303	29.650	4.232	1.198	0.532	24.297	4.050	1.462
LT	0.329	29.095	4.215	1.221	0.480	25.624	3.805	1.386
RL	0.271	30.334	4.048	1.171	0.200	31.770	4.651	1.118
RT	0.346	28.735	3.951	1.236	0.506	24.977	3.653	1.422
RMSFD	0.263	30.502	3.894	1.165	0.591	22.722	4.128	1.563
RMSSD	0.389	27.776	4.079	1.279	0.332	29.023	4.307	1.224
LTFD	0.481	25.579	3.752	1.389	0.762	17.323	3.536	2.050
LTSD	0.427	26.899	4.032	1.320	0.135	33.039	4.305	1.075
RLFD	0.208	31.621	4.095	1.123	0.168	32.402	4.294	1.096
RLSD	0.372	28.158	4.066	1.261	0.299	29.732	4.038	1.195
RTFD	0.358	28.451	3.916	1.248	0.937	8.914	2.735	3.985
RTSD	0.540	24.089	3.981	1.475	0.337	28.932	4.045	1.228
ATFD	0.474	25.765	3.926	1.379	0.510	24.856	4.114	1.429
ATSD	0.426	26.905	4.036	1.320	0.333	29.017	4.367	1.224
FD	0.384	27.889	4.036	1.274	0.687	19.833	3.871	1.791
SD	0.367	28.263	4.095	1.257	0.397	27.594	4.062	1.287

R (original spectral reflectance data); AT (logarithm of the reciprocal); RMS (root mean square); LT (logarithm); RL (reciprocal of the logarithm); RT (reciprocal); RMSFD (root mean square first-order differentiation); RMSSD (root mean square second-order differentiation); LTFD (first-order differentiation of the logarithm); LTSD (second-order differentiation of the logarithm); RLFD (logarithmic first order differentiation of the reciprocal); RLSD (logarithmic second order differentiation of the reciprocal); RTFD (first-order differentiation of the reciprocal); RTSD (second-order differentiation of the reciprocal); ATFD (logarithmic first order differentiation of the reciprocal); ATSD (logarithmic second order differentiation of the reciprocal); FD (first-order differentiation), SD (second-order differentiation).

In general, CARS is superior to PCC, and the CARS-RTFD-PLSR model is better than the RTFD-PLSR model. A map of the spatial distribution (**Figure 4**) illustrates the relationship between the predicted contents of Zn and the measured contents of Zn in the study area.

The analysis of the RFR model

In **Table 3**, the ranges of R², RMSE, MAE and RPD values inversed by the RFR model based on the important wavelengths selected by PCC are 0.477-0.799, 1.414-4.714, 12.417-21.481, and 7.535-25.120, respectively. The R² is higher than 0.5 except for the RLSD-RFR model, so the RFR model has good prediction ability. The best inverse prediction model is the FD-RFR model (R² = 0.799, RMSE = 2.711, MAE = 12.417, and RPD = 13.102).

The R² inversed by the RFR model based on the important wavelengths selected by CARS ranges from 0.316 to 0.856, the ranges of RMSE and MAE values are 1.100-7.377 and 10.074-20.343, and the RPD values are 4.815-30.127. The prediction accuracy of CARS-LTFD-RFR model is highest (R² = 0.856, RMSE = 2.514, MAE = 10.074, and RPD = 14.129).

CARS is superior to PCC, and the CARS-LTFD-RFR model is better than the FD-RFR model. However, all the estimation capability of the RFR model is good because the values of RPD are higher than 2.0. A map of the spatial distribution illustrates the relationship between the predicted contents of Zn and the measured contents of Zn in the study area (**Figure 5**).

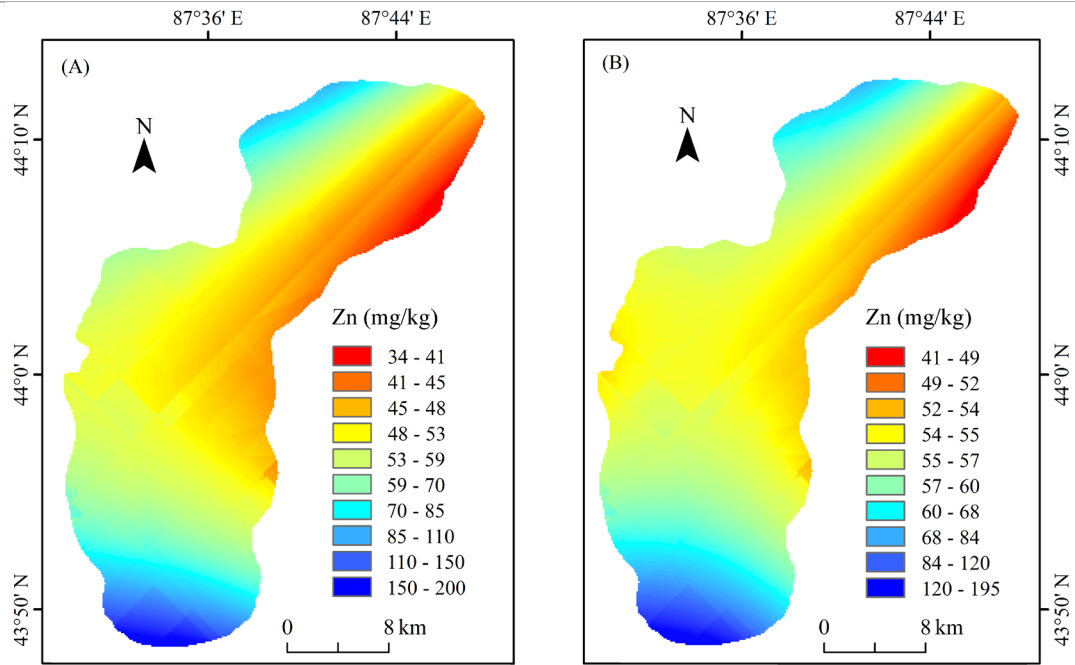


Figure 4. Distribution of Zn content based on measured values (A) and PLSR predicted values (B).

Table 3. Statistics of accuracy parameters of RFR model for Zn content of soils in Urumqi.

Transformation	PCC				CARS			
	R ²	RMSE	MAE	RPD	R ²	RMSE	MAE	RPD
R	0.509	3.012	14.228	11.793	0.437	1.179	14.926	30.127
AT	0.584	2.593	14.722	13.698	0.470	3.477	17.097	10.216
RMS	0.509	3.012	14.228	11.793	0.437	3.693	16.259	9.618
LT	0.508	3.012	14.253	11.793	0.488	2.357	14.426	15.070
RL	0.584	2.593	14.806	13.698	0.457	1.100	14.148	32.291
RT	0.584	2.593	14.722	13.698	0.518	5.215	15.646	6.811
RMSFD	0.578	2.671	21.481	13.298	0.598	3.435	12.992	10.341
RMSSD	0.640	2.027	14.822	17.523	0.316	2.678	18.884	13.264
LTFD	0.524	1.500	14.126	23.680	0.856	2.514	10.074	14.129
LTSD	0.714	2.216	13.622	16.029	0.388	3.359	18.903	10.575
RLFD	0.744	3.614	12.963	9.828	0.463	7.377	15.206	4.815
RLSD	0.477	2.269	15.729	15.654	0.318	2.721	20.343	13.054
RTFD	0.692	3.300	16.944	10.764	0.747	2.095	11.648	16.955
RTSD	0.683	2.711	14.694	13.102	0.536	1.886	13.846	18.834
ATFD	0.628	1.414	17.556	25.120	0.709	2.887	12.352	12.303
ATSD	0.655	2.828	15.556	12.560	0.454	3.435	18.111	10.341
FD	0.799	2.711	12.417	13.102	0.777	1.886	11.778	18.834
SD	0.593	4.714	16.889	7.535	0.465	2.528	15.949	14.051

R (original spectral reflectance data); AT (logarithm of the reciprocal); RMS (root mean square); LT (logarithm); RL (reciprocal of the logarithm); RT (reciprocal); RMSFD (root mean square first-order differentiation); RMSSD (root mean square second-order differentiation); LTFD (first-order differentiation of the logarithm); LTSD (second-order differentiation of the logarithm); RLFD (logarithmic first order differentiation of the reciprocal); RLSD (logarithmic second order differentiation of the reciprocal); RTFD (first-order differentiation of the reciprocal); RTSD (second-order differentiation of the reciprocal); ATFD (logarithmic first order differentiation of the reciprocal); ATSD (logarithmic second order differentiation of the reciprocal); FD (first-order differentiation), SD (second-order differentiation).

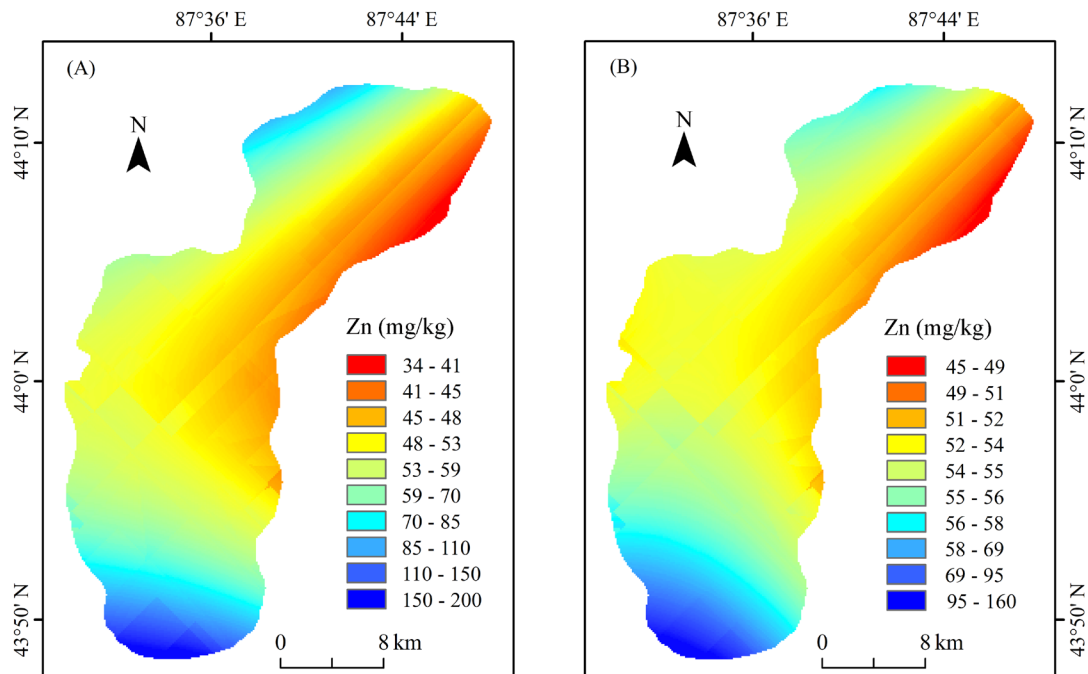


Figure 5. Distribution of Zn content based on field measured values (A) and RFR predicted values (B).

4.4 Discussion of optimal prediction models

On the one hand, estimating Zn content in soils using hyperspectral remote sensing is a cost-efficient method but challenging due to the effects of natural environmental conditions and soil properties [27]. On the other hand, high-data dimensionality is a common problem in hyperspectral data processing, so the inversion accuracy of the constructed model is biased by redundant spectra and noise [23,28].

In this study, the predicted accuracy of the soil Zn content is $R^2_{\text{CARS-RTFD-PLSR}} > R^2_{\text{RLSD-RFR}} > R^2_{\text{CARS-LTFD-RFR}} > R^2_{\text{RTSD-PLSR}}$. Therefore, combined with the performance of the prediction accuracy of soil Zn content, the prediction accuracy of PLSR among the modeling methods is significantly better than that of RFR. As shown in **Tables 2 and 3**, the fitness, stability and accuracy of the prediction model are changed to different degrees after processing methods of the original spectral data. The best predict prediction model is the CARS-RTFD-PLSR (partial least squares regression model based on first-order differentiation of the reciprocal by CARS) model ($R^2 = 0.937$, RMSE = 8.914, MAE = 2.735, and RPD = 3.985),

which has the better ability to invert the soil heavy metal content in the study area. The scatter plot of the measured and predicted values of Zn content modeling by CARS-RTFD-PLSR and R-PLSR model was exhibited in **Figure 6**.

The R^2 calculated by the PLSR model constructed based on CARS-RTFD of the important wavelengths is significantly higher than that modeled from the original spectral data, and both the RMSE and MAE are significantly decreased. From **Figure 6**, it can be intuitively seen that the prediction accuracy of the PLSR model based on original spectral data was not high, and the R^2 between the measured and predicted values was 0.496. The prediction accuracy of the CARS-RTFD was improved significantly, and the predicted and measured values presented a good agreement with each other, with R^2 of 0.937, which was improved by 0.441 compared with the R-PLSR model. Overall, a faster and more convenient method for estimating Zn content in soil is described in this work. This method provides an effective way for predicting soil Zn contents in oasis cities.

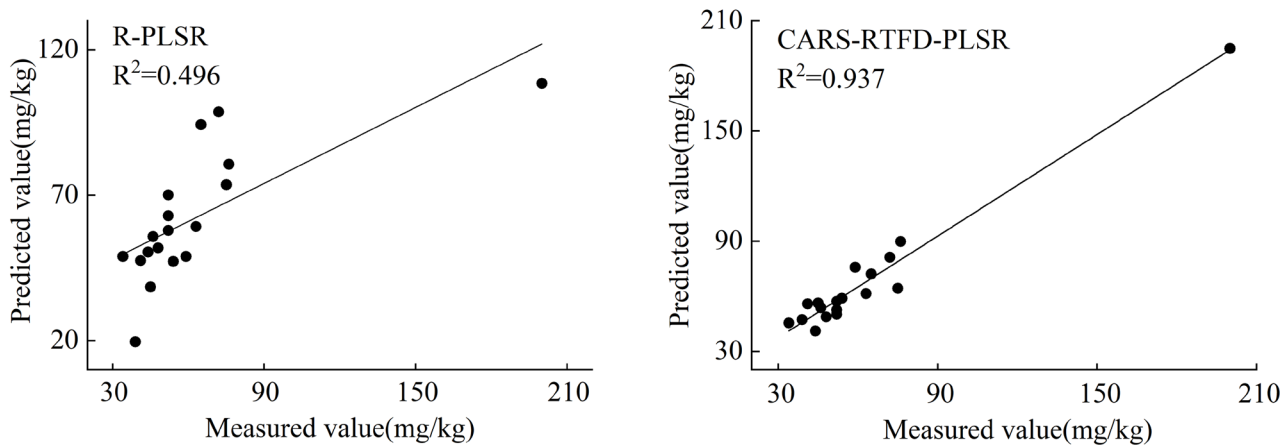


Figure 6. Measured and CARS-RTFD-PLSR predicted values of Zn content in soil.

5. Conclusions

To find an optimal model to predict the soil Zn content for the study area, the PLSR model and the RFR model were constructed based on the important wavelengths and Zn content from soil samples. The results of this study lead to the following conclusions:

1) Transformed spectral data with Pearson's correlation coefficient analysis and CARS can obviously reduce the interference of the environmental background and improve the correlations between soil spectral reflectance data and Zn contents of soil. The first-order differentiation of the reciprocal (RTFD) has the most significant enhancement of spectral features.

2) The results showed that the CARS-RTFD-PLSR model is more stable with the highest prediction ability ($R^2 = 0.937$, RMSE = 8.914, MAE = 2.735, and RPD = 3.985) for soil Zn content in the research region. The CARS-RTFD-PLSR method can provide a reference method and technical support for the prediction of soil Zn content in oasis cities.

Overall, the results of this study demonstrate the possibility of directly applying hyperspectral remote sensing approaches to estimating soil Zn contents in oasis cities. This method can provide technical support for the hyperspectral estimation of the soil Zn content and can require rapid detection of Zn a contamination of soil. However, the limitation of this

study is the lack of combination of hyperspectral and remote sensing imagery, which needs to be further verified in subsequent studies.

Author Contributions

Qing Zhong completed all the experiments to obtain data, processed the data, and wrote the main manuscript text. Mamattursun Eziz provided support and gave guidance for this study. Rukeya Sawut and Mireguli Ainiwaer taught the methods. All authors reviewed the manuscript.

Conflict of Interest

The authors declare no conflicts of interest.

Funding

This research was funded by the National Natural Science Foundation of China (No. U2003301) and the Tianshan Talent Training Project of Xinjiang.

Acknowledgement

The original version of this paper was substantially improved thanks to the constructive comments by anonymous reviewers.

References

- [1] Zhao, R.X., 2004. Huan jing wu ran hua xue

- (Chinese) [Environmental pollution chemistry]. China Industry Press: Beijing.
- [2] Chen, Y.Z., Wang, F., Wang, G., et al., 2012. Research advances on zinc pollution and remediation of soil system. *Fujian Journal of Agricultural Sciences*. 27(8), 901-908.
- [3] Patel, A.K., Ghosh, J.K., Sayyad, S.U., 2022. Fractional abundances study of macronutrients in soil using hyperspectral remote sensing. *Geocarto International*. 37(2), 474-493.
- [4] Yang, Y., Cui, Q.F., Jia, P., et al., 2021. Estimating the heavy metal concentrations in topsoil in the Daxigou mining area, China, using multi-spectral satellite imagery. *Scientific Reports*. 11, 11718.
- [5] Wei, L.F., Pu, H.C., Wang, Z.X., et al., 2020. Estimation of soil arsenic content with hyperspectral remote sensing. *Sensor*. 20, 4056-4071.
- [6] Tan, K., Wang, H.M., Chen, L.H., et al., 2021. Estimating the distribution trend of soil heavy metals in mining area from HyMap airborne hyperspectral imagery based on ensemble learning. *Journal of Hazardous Materials*. 401, 1-17.
- [7] Ye, M., Zhu, L., Li, X.J., et al., 2022. Estimation of the soil arsenic concentration using a geographically weighted XGBoost model based on hyperspectral data. *Science of the Total Environment*. 858, 159798-159798.
- [8] Bian, Z.J., Sun, L.N., Tian, K., et al., 2021. Estimation of heavy metals in Tailings and soils using hyperspectral technology: A case study in a Tin Polymetallic mining area. *Bulletin of Environmental Contamination and Toxicology*. 107, 1022-1031.
- [9] Zhang, B., Guo, B., Zou, B., et al., 2022. Retrieving soil heavy metals concentrations based on GaoFen-5 hyperspectral satellite image at an opencast coal mine, Inner Mongolia, China. *Environmental Pollution*. 300, 118981-118992.
- [10] Hou, L., Li, X.J., Li, F., 2018. Hyperspectral-based inversion of heavy metal content in the soil of coal mining areas. *Journal of Environmental Quality*. 48, 57-63.
- [11] Omran, E.S.E., 2016. Inference model to predict heavy metals of Bahr El Baqar soils, Egypt using spectroscopy and chemometrics technique. *Modeling Earth Systems and Environment*. 2, 1-17.
- [12] Yang, H.F., Xu, H., Zhong, X.N., 2022. Prediction of soil heavy metal concentrations in copper tailings area using hyperspectral reflectance. *Environmental Earth Sciences*. 81, 183-193.
- [13] Wei, B., Jiang, F., Li, X., et al., 2010. Heavy metal induced ecological risk in the city of Urumqi, NW China. *Environmental Monitoring and Assessment*. 160, 33-45.
- [14] Li, J.M., Zhang, Y.T., 2019. Wu lu mu qi bu tong gong neng qu lin dai tu rang zhong jin shu wu ran te zheng fen xi (Chinese) [Characteristics of heavy metal pollution in forest belt soil of different functional zones in Urumqi, Xinjiang]. *Journal of Environmental Sciences*. 28, 1859-1866.
- [15] Sidikjan, N., Eziz, M., Li, X., et al., 2022. Spatial distribution, contamination levels, and health risks of trace elements in topsoil along an urbanization gradient in the City of Urumqi, China. *Sustainability*. 14(19), 12646.
- [16] Hini, G., Eziz, M., Wang, W., et al., 2020. Spatial distribution, contamination levels, sources, and potential health risk assessment of trace elements in street dusts of Urumqi city, NW China. *Human and Ecological Risk Assessment: An International Journal*. 26(8), 2112-2128.
- [17] Yao, X.D., Wang, J., Wang, Y.M., et al., 2022. Wu lu mu qi mou gong ye yuan qu tu rang zhong jin shu qian zai sheng tai feng xian ping jia (Chinese) [Potential ecological risk assessment on heavy metals in the soil of an industrial park in Urumqi, China]. *Transactions of Nonferrous Metals Society of China*. 12, 160-166.
- [18] Soil and Sediment-Determination of Aqua Regia Extracts of 12 Metal Elements-Inductively Coupled Plasma Mass Spectrometry [Internet]. Ministry of Environmental Protection of the People's Republic of China; 2016. Available from: https://english.mee.gov.cn/Resources/standards/Soil/Method_Standard4/201607/t20160704_357088.shtml
- [19] Yuan, Z.R., Wei, L.F., Zhang, Y.X., et al., 2020.

- Hyperspectral inversion and analysis of heavy metal arsenic content in farmland soil based on optimizing CARS combined with PSO-SVM algorithm. *Spectroscopy and Spectral Analysis*. 40(2), 567-573.
- [20] Zhong, X.J., Yang, L., Zhang, D.X., et al., 2022. Effect of different particle sizes on the prediction of soil organic matter content by visible-near infrared spectroscopy. *Spectroscopy and Spectral Analysis*. 42(8), 2542-2550.
- [21] Ma, X.M., Zhou, K.F., Wand, J.L., et al., 2022. Optimal bandwidth selection for retrieving Cu content in rock based on hyperspectral remote sensing. *Journal of Arid Land*. 14(1), 102-114.
- [22] Samuel, N.A., Anna, F.H., Andreas, A., et al., 2021. Advances in soil moisture retrieval from multispectral remote sensing using unoccupied aircraft systems and machine learning techniques. *Hydrology and Earth System Sciences*. 25, 2739-2758.
- [23] Michelle, D., Onesimo, M., Riyad, I., 2011. Examining the utility of random forest and AISA Eagle hyperspectral image data to predict *Pinus patula* age in KwaZulu-Natal, South Africa. *Geocarto International*. 26(4), 275-289.
- [24] Rukeya, S., Nijat, K., Abdugheni, A., et al., 2018. Possibility of optimized indices for the assessment of heavy metal contents in soil around an open pit coal mine area. *International Journal of Applied Earth Observation and Geoinformation*. 73, 14-25.
- [25] Vohland, M., Joachim, B., Joachim, H., et al., 2011. Comparing different multivariate calibration methods for the determination of soil organic carbon pools with visible to near infrared spectroscopy. *Geoderma*. 166, 198-205.
- [26] Wang, Y.Y., Niu, R.Q., Lin, G., et al., 2023. Estimate of soil heavy metal in a mining region using PCC-SVM-RFECV-AdaBoost combined with reflectance spectroscopy. *Environmental Geochemistry and Health*. Ahead of print. DOI: <https://doi.org/10.1007/s10653-023-01488-W>
- [27] Liu, W.W., Li, M.J., Zhang, M.Y., et al., 2020. Hyperspectral inversion of mercury in reed leaves under different levels of soil mercury contamination. *Environmental Science and Pollution Research*. 27, 22935-22945.
- [28] Zhou, M., Zou, B., Tu, Y.L., et al., 2022. Spectral response feature bands extracted from near standard soil samples for estimating soil Pb in a mining area. *Geocarto International*. 37(26), 13248-13267.

ARTICLE

SAR Change Detection Algorithm Combined with FFDNet Spatial Denoising

Yuqing Wu¹, Qing Xu^{*}, Zheng Zhang, Jingzhen Ma, Tianming Zhao, Xinming Zhu

Institute of Geospatial Information, Information Engineering University, Zhengzhou, Henan, 450001, China

ABSTRACT

Objectives: When detecting changes in synthetic aperture radar (SAR) images, the quality of the difference map has an important impact on the detection results, and the speckle noise in the image interferes with the extraction of change information. In order to improve the detection accuracy of SAR image change detection and improve the quality of the difference map, this paper proposes a method that combines the popular deep neural network with the clustering algorithm. **Methods:** Firstly, the SAR image with speckle noise was constructed, and the FFDNet architecture was used to retrain the SAR image, and the network parameters with better effect on speckle noise suppression were obtained. Then the log ratio operator is generated by using the reconstructed image output from the network. Finally, K-means and FCM clustering algorithms are used to analyze the difference images, and the binary map of change detection results is generated. **Results:** The experimental results have high detection accuracy on Bern and Sulzberger's real data, which proves the effectiveness of the method.

Keywords: SAR change detection; Image noise reduction; FFDNet; Difference diagram; Clustering algorithm

1. Introduction

Synthetic aperture radar (SAR) imagery has been widely utilized in various fields^[1]. It can be applied by public institutions for urban planning purposes, while also providing valuable assistance to military

personnel in decision-making processes^[2]. Various surface features have a significant impact on SAR imaging^[3]. Factors such as snow cover, topographic characteristics, and man-made structures need to be taken into account for accurate interpretation and analysis of SAR image data. For fields like environ-

*CORRESPONDING AUTHOR:

Qing Xu, Institute of Geospatial Information, Information Engineering University, Zhengzhou, Henan, 450001, China; Email: xq2021ch@126.com

ARTICLE INFO

Received: 21 September 2023 | Revised: 20 October 2023 | Accepted: 26 October 2023 | Published Online: 10 November 2023

DOI: <https://doi.org/10.30564/jees.v5i2.5980>

CITATION

Wu, Y.Q., Xu, Q., Zhang, Zh., et al., 2023. SAR Change Detection Algorithm Combined with FFDNet Spatial Denoising. Journal of Environmental & Earth Sciences. 5(2): 88-101. DOI: <https://doi.org/10.30564/jees.v5i2.5980>

COPYRIGHT

Copyright © 2023 by the author(s). Published by Bilingual Publishing Group. This is an open access article under the Creative Commons Attribution-NonCommercial 4.0 International (CC BY-NC 4.0) License. (<https://creativecommons.org/licenses/by-nc/4.0/>).

mental monitoring, disaster assessment, and urban planning, SAR technology provides valuable and comprehensive information sources^[4]. However, the multiplicative speckle noise in SAR imaging has caused practical difficulties in the interpretation of the targets shot in the image^[5]. Because the speckle noise in SAR images has an important impact on the generation of change detection results, removing the speckle noise in the image has become an important way to improve the detection accuracy of SAR change detection.

For SAR image change detection, there are two main methods: direct classification and generation of difference image (DI)^[2,6]. The first is to process the original input images respectively; the second is to first comprehensively consider the differences between the two-phase images and generate the difference image, and then use clustering and other methods to generate the binary image of the change detection results. In the method of generating the difference image, many scholars have improved the detection accuracy by improving the quality of the difference image and optimizing the clustering algorithm. Many scholars have made important contributions in removing speckle noise and integrating it into the clustering algorithm. K-means clustering is used to generate the detection binary image^[7]. FCM (Fuzzy C-Means Clustering) is used to classify the different images into three categories, and then a neural network is used for classification^[2]. Gong et al.^[6] employed fusion to combine the mean ratio and logarithmic ratio difference graphs, and then used the improved fuzzy C-means algorithm for change detection, which not only improved the quality of the difference graphs, but also made contributions to improving subsequent clustering methods. Gao et al.^[8] introduced the dual-tree complex wavelet transform into the convolutional neural network to classify changed and unchanged pixels, so as to reduce speckle noise in the image. Qu et al.^[9] used the frequency domain information of the image to reduce speckle noise.

The main goal of change detection in SAR image analysis is to identify and analyze SAR images

captured at different time periods within the same region, particularly dual-phase images^[9]. The primary task involves classifying individual pixels in the image as either altered or unaltered. Clustering algorithms are commonly utilized for this purpose, as they effectively classify sample data to detect changes. Several researchers have improved clustering methods to enhance detection accuracy. Shang et al.^[10] introduced a mean classification technique followed by fuzzy clustering, while Gao et al.^[2] employed the FCM clustering algorithm initially to categorize pixel points into three groups and then used neural networks for generating results. Many scholars have also combined deep learning techniques with clustering algorithms, resulting in significant enhancements in detection accuracy. The above methods have greatly improved the detection accuracy of change detection by combining clustering and deep learning. However, whether feature extraction is performed through difference image fusion or convolutional network, the setting of difference image fusion coefficient weight and robust methods for speckle noise suppression are still worth exploring.

Therefore, before change detection, reducing the speckle noise of the image has become the main content of many scholars' research. Because the clustering algorithm is sensitive to noise^[1,11], literature^[12] first uses the PPB (the probabilistic-patch-based algorithm) filter to weaken noise before difference operator fusion. Tan et al.^[13] proposed a new end-to-end self-supervised SAR denoising model: Enhanced Noise2Noise (EN2N) to solve the problem of detail loss caused by CNN. Zhang et al.^[14] proposed FFDNet network architecture, which has excellent ability in image balance denoising and detail retention.

In order to improve the quality of difference maps, this paper proposes a two-phase SAR image change detection method based on FFDNet, which will use a deep neural network to denoise SAR images for change detection. Our contributions are mainly in two aspects:

(1) use the FFDNet model framework in a deep neural network to denoise difference maps and generate more universal difference images;

(2) combine traditional clustering with deep learning, use the network to minimize speckle noise and classify rapidly through clustering. By combining the advantages of the two methods, the performance of the algorithm is improved.

2. Experimental method

The method proposed in this paper is shown in **Figure 1**, which combines the network with the traditional clustering method, takes the two-phase image as the input of the FFDNet network, calculates the corresponding difference operator of the denoised image, and then makes the change detection result graph through clustering analysis. In this section, the difference operator, FFDNet and clustering method in the experiment are introduced.

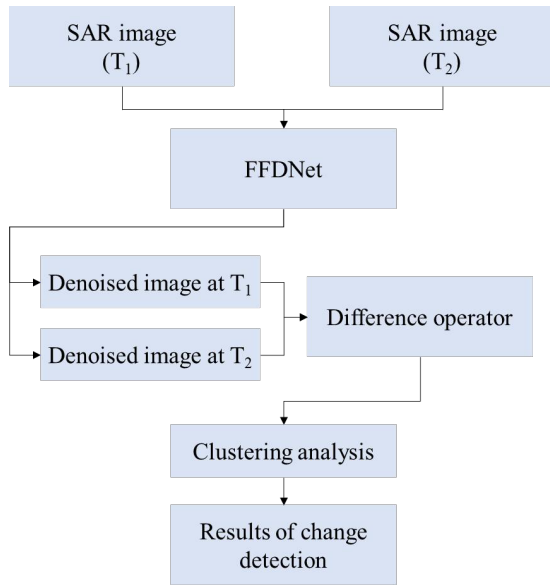


Figure 1. Method flow chart.

2.1 FFDNet denoising model

The main idea of the FFDNet-based image denoising method is to use the network to learn the noise in the original image, and then use the original image and the noise in the network to reduce the noise to achieve image denoising^[15]. The existing CNN denoising tends to Gaussian noise, and has poor generalization ability for real noisy images with more complex noise^[16]. In order to solve the problem of different noise levels, the topic of edge detection on SAR images has been extensively studied in the literature^[17], providing valuable knowledge to improve our understanding and application of Synthetic Aperture Radar (SAR) technology. Kai et al.^[14] used noise level map as input. The research findings^[18] indicate that the use of ratio information is not suitable for edge detection. Nevertheless, incorporating various types of information through fusion techniques has been proven to greatly enhance the precision of detection, thereby enhancing its effectiveness.

FFDNet network uses Gaussian noise to model image noise, and has a weak effect on the removal of speckle noise in SAR images. Therefore, this paper uses speckle noise as a sample to re-train and design a noise model that conforms to SAR images. It is mainly composed of a convolution neural network, which can remove a wider range of noise when processing sampling operators. The experiment uses the speckle noise in the original real SAR image as input, and the network structure is shown in **Figure 2**.

The input Y consists of a reversible downsampling operator, which reshapes the input image into

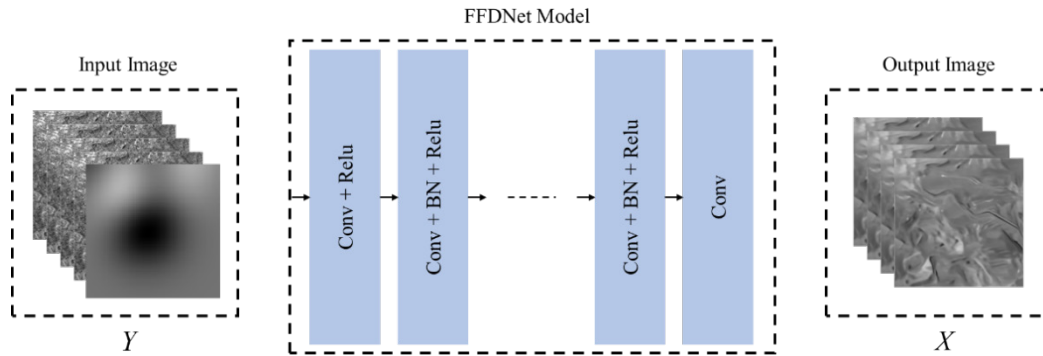


Figure 2. The architecture of the FFDNet for image denoising.

four downsampling images, and together with the noise level image, becomes the input of the convolution. The noise level image specifies a specific noise level for each pixel of the image, which is used to manage the trade-off between noise reduction and detail preservation in the case of spatially varying noise^[16,19,20].

The size of input image Y is defined as $W \times H \times C$, subimage after downsampling is $\frac{W}{2} \times \frac{H}{2} \times 4C$. Y represents the input image object, W denotes the pixel width of the image, and H represents the pixel height of the image. C is the number of channels of the image, and is 1 in the SAR denoising model. Subimage and noise level graphs are connected together as the tensor of $\frac{W}{2} \times \frac{H}{2} \times (4C+1)$, which is used as the data input of CNN.

CNN is composed of a series of 3×3 convolution layers, the first convolution layer is “Conv + ReLU”, the middle 15 layers are “Conv + BN + ReLU”, and the last Conv layer is “CONV”. Fill the feature map with zero to ensure the constant size of the feature map.

The output end is four denoised sub-images, which are restored to the original image after reconstruction. According to the FFDNet^[10] team, when SAR gray image noise reduction is used, the convolutional layer of gray image is set to 15 layers, the feature mapping channel of gray image is set to 64, and the downsampling factor is set to 2.

We normalized the SAR input image without introducing additional errors in the calculation and without changing the information storage of the im-

age itself, and compressed the original image to the range of 0 to 1 by using Equation (1). y_i represents the pixel value of the i -th pixel point corresponding to input image Y . $\max(y)$ and $\min(y)$ are respectively the maximum and minimum pixel values of the corresponding images. The denoising process is shown in **Figure 3**.

$$norm = \frac{y_i - \min(y)}{\max(y) - \min(y)} \quad (1)$$

In forward propagation, FFDNet uses residual learning to train a residual map, as shown in Equation (2):

$$R(y_i; \lambda) \approx y_i - x_i \quad (2)$$

$R(y_i; \lambda)$ is the noise image predicted by the network, λ is the network parameter used for training, y_i is the original noise input image, and x_i is the noise-free label graph. N represents the number of pixels in the image. Δx_i is the substitute quantity used for approximate calculations in the backpropagation, the mean square error is used as the loss function and quantified, as shown in Equation (3), and the adaptive moment estimation (Adam) algorithm is used to minimize the loss function.

$$\partial(\lambda) = \frac{1}{2N} \sum_{i=1}^N \|Vx_i - x_i\|^2 \quad (3)$$

$$Vx_i = y_i - R(y_i - x_i) \quad (4)$$

where N is the number of training samples.

After the network is trained on SAR images with speckle noise, the real dataset is sent to the trained FFDNet, and the new network parameters are used to weaken the noise in the image, and then the four sub-images that generate downsampling are restored to the original image.

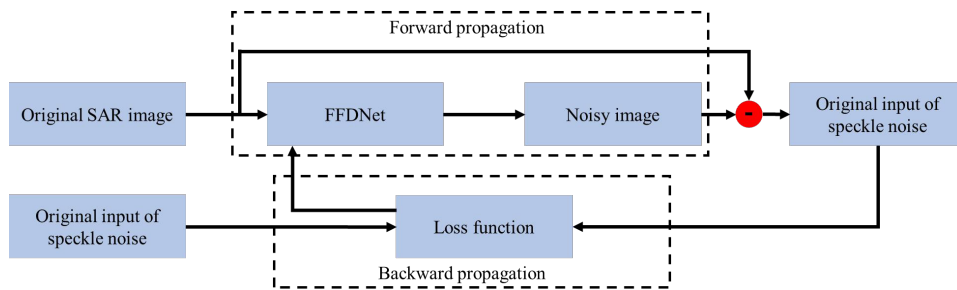


Figure 3. The architecture of the FFDNet for image denoising.

2.2 Logarithmic ratio operator and mean ratio operator

The generation effect of the difference map has a significant impact on the results of change detection. Essentially, the process of generating a difference map involves using specific algorithms to identify discrepancies between two images, initially highlighting areas that have changed in SAR images and providing a basis for subsequent analysis of difference maps to obtain change detection results. The logarithmic ratio operator incorporates logarithmic operations into the ratio method, effectively converting multiplicative noise models into additive noise models^[12]. The logarithmic ratio method is widely employed for acquiring difference maps. However, this approach's drawback lies in its tendency to amplify pixel contraction characteristics through logarithmic operations, potentially resulting in inadequate preservation or even blurring of edge pixel details.

$$X_{LR} = \left| \log \frac{X_2}{X_1} \right| = |\log X_2 - \log X_1| \quad (5)$$

where X_2 and X_1 are input image information, the gray value in SAR image matrix is used in the calculation.

In order to avoid calculation error caused by zero pixel value in image X_{LR} , the calculated pixel value in Equation (5) is added by 1, and the logarithmic ratio operator is obtained by Equation (6).

$$D_L = \left| \log \frac{X_2 + 1}{X_1 + 1} \right| = |\log(X_2 + 1) - \log(X_1 + 1)| \quad (6)$$

$$X_{MR} = 1 - \min\left(\frac{X_2}{X_1}, \frac{X_1}{X_2}\right) \quad (7)$$

By using the neighborhood information of pixels, the mean ratio operator replaces the texture feature value or gray value of the corresponding pixel by averaging the neighborhood pixel, which can suppress the speckle of a single pixel shape. Goodman^[13] has proved that the noise in SAR images is speckle noise. In this paper, a relatively ideal log-ratio and mean-ratio operator is used as the difference operator in the experiment.

2.3 Clustering algorithm

When analyzing the difference map and generating change detection results, there are threshold algorithms^[23] and clustering algorithms^[24]. Because the difference image cannot obtain an obvious boundary^[25], and the clustering algorithm does not need to establish a sample model, it is more flexible than the threshold method and has been widely used. As is widely known in the scientific literature^[20] modeling for the difference image does not need any prior information about the data distribution of the difference image, and creates a feature space, and finally uses K-means clustering to generate detection results. Gong et al.^[6] reconstructed the difference map, and then used the improved fuzzy local information C-means clustering to perform change detection. The following is an explanation of the clustering method used in this experiment. K-means algorithm is an early method used in clustering methods, which can quickly divide the data into multiple categories, and has a good clustering effect and universality. First, k initial clustering centers K_i are randomly selected from the data pixel points, and the sum of the squares of the distances between the pixel points and the selected clustering center points is taken as the objective function.

$$d = \sqrt{\sum_{j=1}^n \sum_{i=1}^m (x_i - K_i)^2} \quad (8)$$

where x_i is the traversal pixel, K_i is the cluster center initially randomly selected, n and m are the number of cluster centers and data dimension respectively. In this algorithm, Euclidean distance is used to calculate the distance from the cluster center, and each sample is classified into the class with the smallest distance. In change detection, each pixel in the SAR image is classified as changed or unchanged under the objective function, that is, the label is designated as one of $\{0,1\}$. Finally, the center of mass of each class is calculated, that is, the average distance between each pixel in the class and the center, and the new center point is adjusted according to this, until the cluster center is no longer changed.

FCM forms the classification of specified data

by optimizing the minimum objective function ^[26], which is an improvement of K-means method and plays an important role in the field of data processing and analysis ^[27]. In change detection, the method calculates the membership degree between each pixel and the cluster center, and makes the objective function obtain the minimum value, so that all pixels can be classified. It is realized in the process of iteratively calculating membership degree u_{ij} and cluster center v_i .

Its objective function is:

$$J = \sum_{i=1}^c \sum_{j=1}^n u_{ij}^m d_{ij}^2 \quad (9)$$

where c is the specified number of categories, $c = 2$ in the change detection experiment, n represents the number of pixels in the image, and u_{ij} represents the membership degree of the j -th pixel in the image belonging to the i cluster center. u_{ij} must satisfy the following two constraints.

$$\begin{cases} \sum_{i=1}^c u_{ij} = 1 \\ 0 \leq u_{ij} \leq 1 \end{cases} \quad (10)$$

m is the fuzzy weight index, and different fuzzy weight indices have an impact on the clustering results and the time complexity of the algorithm. The value of this parameter is usually $[1.5, 2.5]$. Pal et al. considered $m = 2$ to be the best through experimental verification ^[23], and we also adopted this parameter in the experiment. d_{ij} is the distance between the j -th pixel point and the i -th cluster center point, which is consistent with the K-means clustering idea. Euclidean distance, which is simpler to calculate in two-dimensional data, is used for distance calculation.

$$d_{ij}^2 = \|x_j - v_i\|^2 \quad (11)$$

x_j is the vector representation of the j -th sample point in the two-dimensional image, and v_i is the cluster center of the i class.

The iterative calculation formula of membership degree and cluster center is as follows:

$$u_{ij} = \left[\sum_{k=0}^c \frac{d_{kj}^2}{d_{ij}^2} \right]^{-1} \quad (12)$$

$$v_i = \frac{\sum_{j=1}^n u_{ij}^m x_j}{\sum_{j=1}^n u_{ij}^m} \quad (13)$$

$U = [u_{ij}]$ is a matrix of $c \times n$ size composed of membership degree, $V = [v_i]$ is a matrix of $n \times c$ size composed of cluster center, and n is the total number of pixels used for the classification of images. In this paper, cluster classification is carried out for all pixels in well-registered images.

2.4 Evaluation

The quantitative analysis of change detection results is set as follows:

PSNR (Peak Signal-to-Noise Ratio) is used to measure the difference between two images. This method is used to calculate the degree of difference between different difference graphs. The minimum value of PSNR is 0, and the larger the PSNR, the smaller the difference between the two images. The minimum value of SSIM ^[24] (structural similarity index) SSIM is 0 and the maximum value is 1. The larger the SSIM, the more similar the two images are.

FN (False Negatives): The number of changed pixels classified as non-changed pixels; FP (False Positives): Number of pixels that do not change. Total errors OE (Overall errors): Sum of missed FN and false alarms FP; PCC (Percentage Correct Classification): The ratio of the number of correct detections to the total pixels; Kappa coefficient ^[25] takes into account both correctly detected pixels and incorrectly detected pixels.

In the calculation of PCC and Kappa coefficient, two other indicators should be used: True Positive (TP): Change pixels are classified as the number of changed pixels; True Negative (TN): The number of non-changing pixels classified as non-changing pixels.

$$PCC = \frac{Num - OE}{Num} \quad (14)$$

$$\begin{cases} Kappa = \frac{PCC - P}{1 - P} \\ P = \frac{(TP + FN) \times (TP + FP)}{Num} \times \frac{(TN + FP) \times (TN + FN)}{Num} \end{cases} \quad (15)$$

Num can be represented as $Num = TP + FP + FN + TN$, which is the total number of image pixels; The closer the Kappa coefficient is to 1, the better the detection effect is.

In this paper, PSNR and SSIM were used to evaluate the similarity measure of the difference graph, and PCC and Kappa were used to compare the change detection result graph with the reference graph.

3. Experimental results and analysis

3.1 Research data and experimental scheme

The interaction between radar waves and the Earth's surface, as observed through Synthetic Aperture Radar (SAR) imaging technology, is significantly influenced by the moisture content of the soil. The dielectric constant of wet soil is higher compared to dry soil, resulting in increased attenuation of microwave signals emitted by SAR sensors at specific frequencies and subsequently reducing the depth of penetration. At the same time, when SAR sensors are used for observation, the snow-covered surface shows distinct characteristics. The dielectric properties of snow differ from those of other materials found on land, resulting in changes in the levels of backscattering energy detected by SAR systems. Due to the fine-scale roughness of snow, freshly fallen snow typically has increased reflectivity. However, on a larger scale, fresh snow exhibits reduced reflectivity because of volume scattering effects caused by ice crystals within the layer of snow.

tivity because of volume scattering effects caused by ice crystals within the layer of snow.

To validate the practicality of the experiment under the aforementioned circumstances, two distinct sets of actual data were chosen for comparative analysis. The reference figure of the research area and changes is shown in **Figure 4**. The first set of experimental data size 301×301 , SAR images taken by the European Remote Sensing 2 satellite of the Swiss capital Bern city (Bern). **Figures 4a and 4b** show the flood situation near the outskirts of Bern, the capital of Switzerland, taken in April 1999 and May 1999 respectively. **Figure 4c** is the reference map of changes.

The second group of experimental data, 256×256 , was captured by the Envisat satellite. As shown in **Figure 5**, a and b show the process of ice rupture on March 11, 2011 and March 16, 2011, respectively. The changes were mainly caused by the bending and breaking of the ice shelf due to huge sea waves^[8], and **Figure 5c** is the reference diagram of the changes.

In order to prove the effectiveness of the change detection algorithm combined with the FFDNet denoising model, experiments were carried out on the above two real data. Firstly, the FFDNet model is used to pre-process the image denoising, and the globally optimized high-quality difference map is constructed. Secondly, the log-ratio difference operator is constructed, and the performance of the mean-ratio operator in the experimental scheme is compared in the follow-up experiment. Finally, the difference map is classified and the final change detection result map is generated. The experimental

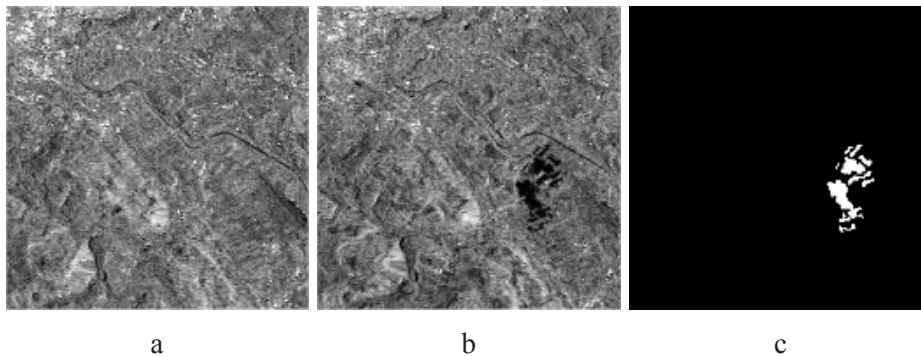


Figure 4. SAR image of Bern area.

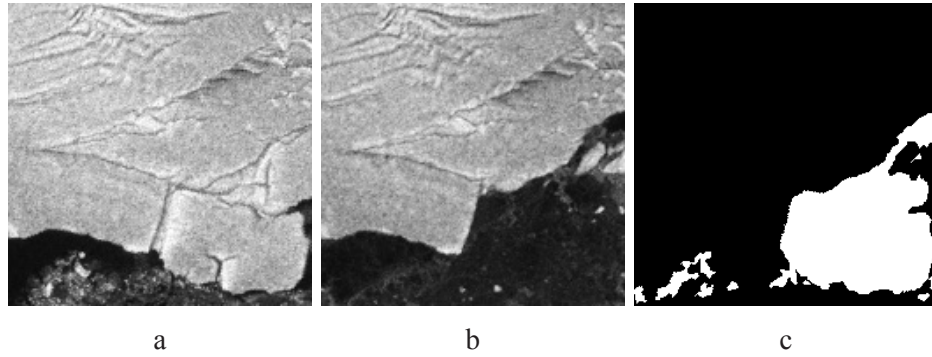


Figure 5. SAR image of Sulzberger area.

environment was Inter Core i7-1160G7, a computer with 16G memory, and the experimental programming language was Python.

3.2 Difference operator denoising results

Figures 6 and 7 are the results of de-noising through the FFDNet network, which inhibits speckle noise and makes the overall image smoother. Areas of change that are not caused by floods are more significant in the Bern dataset, and noise levels in the exposed sea surface in the Sulzberger dataset are reduced.

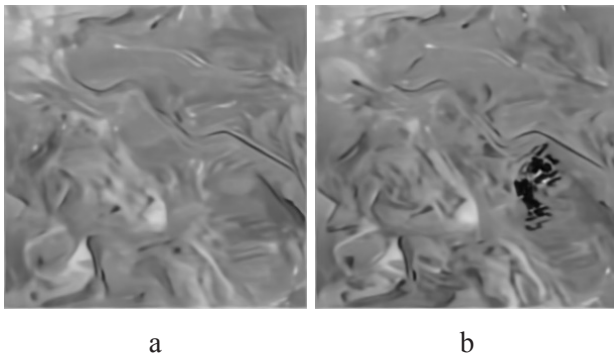


Figure 6. Bern region denoiseurized image.

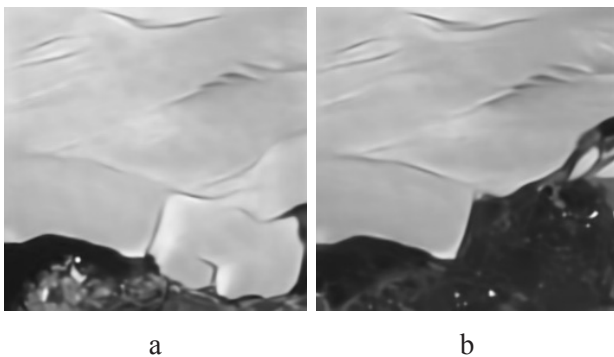


Figure 7. Sulzberger region denoiseurized image.

The difference operator is the earliest method applied to change detection and the simplest one. In this section, to verify the validity of the proposed difference operator, the difference operator is used as the basic operator of the two-phase image, and is compared with the logarithm ratio, the mean value operator and the operator after FFDNet denoising, and the PSNR and SSIM values of the difference operator are calculated. The results are shown in **Figure 8**. The model proposed in this paper takes the average value of the whole image, and some details are lost in the flat region, resulting in a certain degree of blur, but the speckle noise is obviously suppressed.

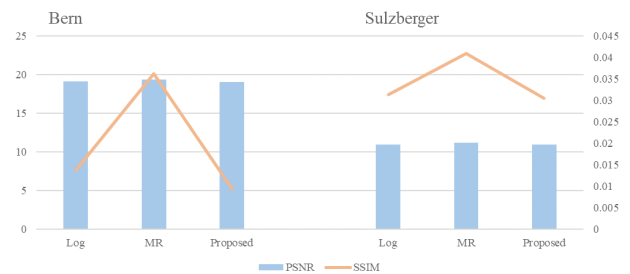


Figure 8. Evaluation index of different difference operators in Bern and Sulzberger region.

3.3 Change detection results and analysis

The experimental results of Bern dataset are shown in **Figure 9** and **Table 1**. Classical K-means clustering^[25] and FCM clustering^[11] algorithms generate more discrete noise points in Bern. As the basic clustering method does not consider other information of the data in the spatial space, it is more

sensitive to image noise. As can be seen from the figure, the original clustering method generates more discrete isolated points, and many missing units are also generated in the flood coverage area. Through feature dimension extraction, PCAKM^[7] algorithm significantly reduces noise points, and makes image edges smoother, edges of changing subjects smoother, and Outlines clearer. PCANet^[2] has an obvious suppression effect on speckle noise after pre-classification, but the main content is also compressed to a certain extent, and part of the change information is lost, so the effect on Kappa index is low.

Sulzberger datasets are shown in **Figure 10** and **Table 2** in several experimental results. The classical K-means clustering and FCM clustering algorithms produced more fissures where the main Sulzberger glacier was melting. The PCAKM^[7] algorithm has improved the crevasses in major places and enhanced the smoothness of the glacier edge. The result of PCANet^[2] still has some deficiencies compared with the reference figure.

Table 1. Metrics of Bern dataset.

Method	FP	FN	OE	PCC	Kappa
K-means	360	326	686	99.24	70.35
FCM	162	554	716	99.21	62.29
PCAKM	179	150	329	99.64	85.75
PCANet	434	31	465	99.49	75.37
FFDNet-K	94	193	287	99.68	86.86
FFDNet-F	83	214	297	99.67	86.20

Table 2. Metrics of Sulzberger dataset.

Method	FP	FN	OE	PCC	Kappa
K-means	1411	610	2021	96.92	90.31
FCM	1376	624	2000	96.95	90.40
PCAKM	1111	768	1879	97.13	90.87
PCANet	473	739	1212	98.15	94.04
FFDNet-K	270	837	1107	98.31	94.47
FFDNet-F	1038	246	1284	98.04	93.84

The Kappa coefficient of PCANet on Bern dataset is 5.02 and 13.08 higher than that of K-means clustering and FCM clustering algorithm, respectively, but the detection accuracy is slightly improved

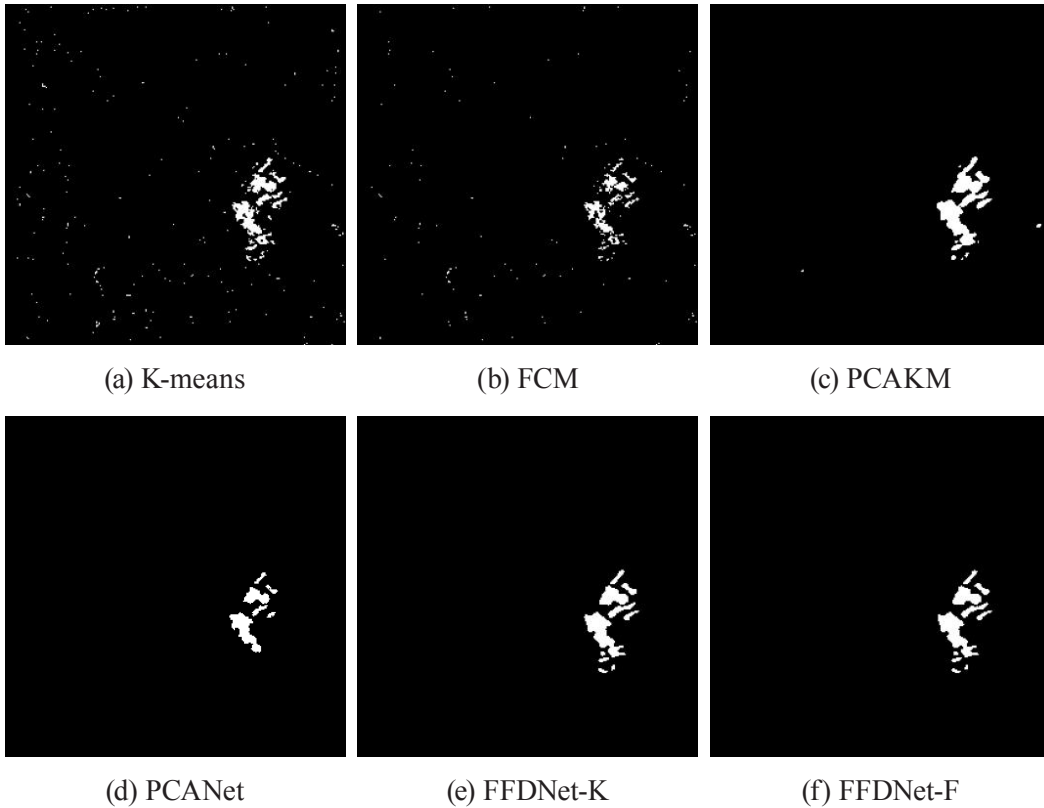


Figure 9. Change detection maps were obtained by using different methods for multi-temporal images in Bern.

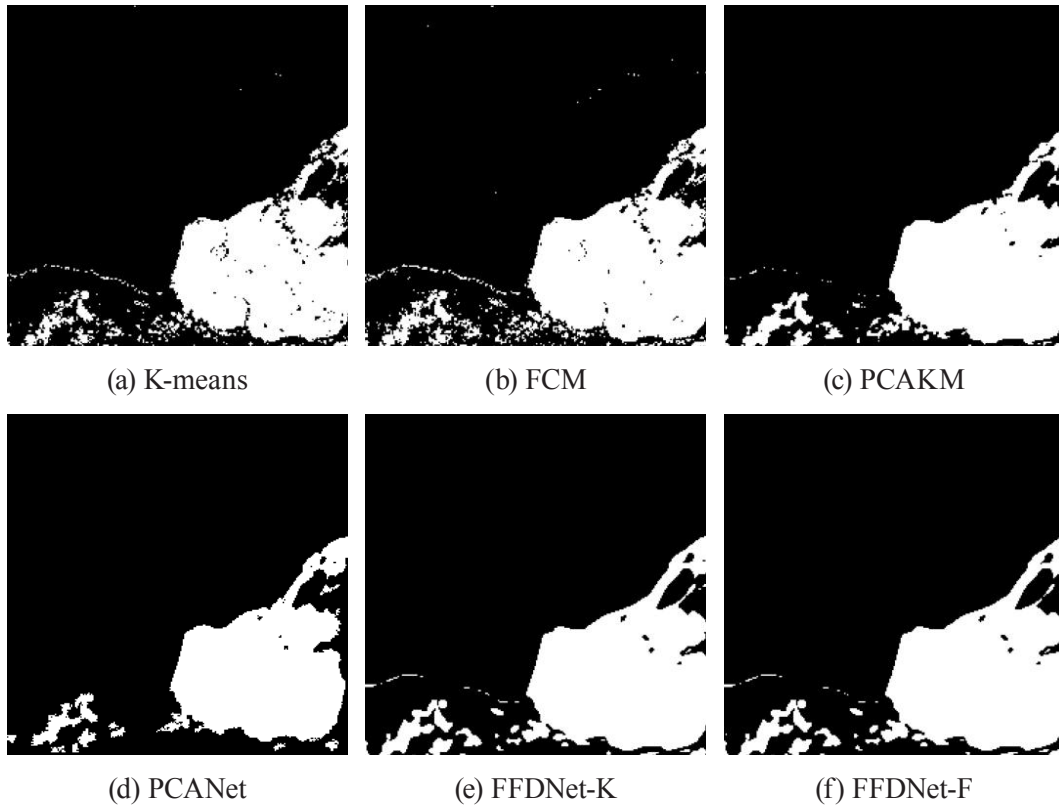


Figure 10. Change detection maps were obtained by using different methods for multi-temporal images in Sulzberger.

compared with the improved K-means clustering, that is, PCAKM algorithm. In Sulzberger dataset, it is 3.73 and 3.64 higher than K-means clustering and FCM clustering algorithm, respectively, and 3.17 higher than PCAKM algorithm. The experimental results show that the robustness to speckle noise can be improved by using PCANet algorithm, but there will be significant differences in different actual situations, and the actual content of the changing subject will be compressed in different degrees. The value of K-means and FCM after combining FFDNet in the OE index decreased significantly, and the content of the change detection results was complete, with good results in denoising and detail retention. Meanwhile, the robustness of the clustering algorithm to the noise in the difference map was improved. The Kappa coefficient of the improved results is significantly increased, indicating that the proposed method is superior to other methods.

3.4 Difference operator and result analysis

Different difference operators have a medium to significant impact on the final change detection results ^[1], and the logarithmic ratio operator is used for subsequent classification in the experiment in Section 3.2. In order to verify the effectiveness of the method in this paper on other difference operators, the logarithmic ratio ^[31] and mean ratio ^[32] operators are compared in the clustering method, and the experimental results are shown in **Tables 3 and 4**. There are certain differences in the experimental results of the datasets using different difference operators. The overall results of the mean ratio operator in the two real datasets are lower than the logarithmic ratio. After the introduction of FFDNet spatial denoising, the Kappa coefficient is improved, and the maximum increase is 35.84 in the K-means method in the Bern dataset; the overall increase is 2.00 in the PCNet network. After the FFDNet is used to preprocess the

input original image in the spatial domain, the method in this paper is helpful in improving the Kappa coefficient in the two classical difference operators.

Table 3. Kappa coefficient of the Bern dataset in the mean-ratio.

Kappa	Non-FFDNet	FFDNet
K-means	23.30	59.14
FCM	5.90	17.58
PCAKM	37.88	58.45
PCANet	2.00	4.00

Table 4. Kappa coefficient of the Sulzberger dataset in the mean-ratio.

Kappa	Non-FFDNet	FFDNet
K-means	83.87	84.03
FCM	82.34	84.30
PCAKM	90.85	91.56
PCANet	8.00	10.00

4. Discussion

The method of SAR change detection allows for the quick identification and analysis of potential pollutants or abnormal conditions in water bodies by comparing image data at different time points. This approach facilitates prompt intervention by relevant authorities to ensure the safety of water sources, while also providing a scientific basis for environmental management and governance. Moreover, this technique can monitor real-time variations in parameters such as liquid level, flooding status, and soil moisture content within aquatic regions like lakes and rivers. Such information is particularly vital for the efficient allocation and administration of water resources, especially during emergency response efforts or disaster relief operations. Hence, we have chosen the widely-utilized Bern dataset as the focus of our research in this study.

The high mountain cryosphere is an extremely vulnerable and sensitive ecosystem on Earth, which has significant implications for global climate change^[33]. To gain a comprehensive understanding and effectively monitor changes in this region, it is

essential to utilize appropriate technological tools. Synthetic Aperture Radar (SAR) technology utilizes electromagnetic wave reflections to provide extensive and continuously updated data of high quality. This technology plays a crucial role in studying the high mountain cryosphere. Additionally, researchers can investigate the impact of climate change on this ecosystem by analyzing long-term trends in snow coverage using historical records of multi-temporal satellite imagery. Therefore, we have chosen representative Sulzberger ice sheet data for our research paper to conduct change detection experiments and validate our analyses.

The present study emphasizes the optimization of two pivotal factors: the construction of disparity images and the clustering methodology. Through meticulous construction of disparity images coupled with the implementation of an efficient clustering technique, it becomes feasible to attain enhanced detection accuracy in change detection, particularly for real synthetic aperture radar (SAR) imagery significantly impacted by speckle noise. In order to evaluate the effectiveness of the suggested methodology, extensive experiments were carried out on two sets of well-known SAR images that are known for their significant interference caused by speckle noise. The results confirm that our approach successfully reduces speckle noise and outperforms existing techniques when assessed using robust metrics like the Kappa coefficient.

The utilization of SAR change detection is a significant approach with substantial benefits. It aids in enhancing our comprehension of intricate and nuanced dynamic procedures within a specific area, while also facilitating early detection and control of natural calamities. Moreover, it offers valuable resources for comprehending worldwide concerns like climate change.

5. Conclusions

To improve detection accuracy and effectively reduce speckle noise, a new method is proposed in this study. It involves the integration of transfer learning by incorporating the gray-level weights suggested

by the FFDNet team. The FFDNet is utilized as a denoising network to alleviate the noise present in the initial input Synthetic Aperture Radar (SAR) images. In order to enhance the model's performance, we integrate SAR graphics containing speckle noise during the retraining phase. This additional training helps fine-tune the model specifically for SAR images impacted by mild speckle noise, thereby improving its ability to handle such complex situations.

In conclusion, significant results have been achieved in processing SAR images with speckle noise by using FFDNet as a denoising network, optimizing the construction of difference images, and employing clustering methods. These research findings can not only be widely applied to change detection tasks in the field of remote sensing but also provide valuable references for other related fields.

Author Contributions

Yuqing Wu: Formulation and evolution of overarching research goals and aims, writing the original draft.

Qing Xu: Writing, review & editing.

Zheng Zhang: Preparation, creation and presentation of the published work, specifically data presentation.

Jingzhen Ma: Formal analysis, verification whether as a part of the activity or separate.

Tianming Zhao: Acquisition of the financial support for the project leading to this publication.

Xinming Zhu: Acquisition of the financial support for the project leading to this publication.

Conflict of Interest

There is no conflict of interest.

References

- [1] Gong, M., Zhao, J., Liu, J., et al., 2015. Change detection in synthetic aperture radar images based on deep neural networks. *IEEE Transactions on Neural Networks and Learning Systems*. 27(1), 125-138.
- [2] Gao, F., Dong, J., Li, B., et al., 2016. Automatic change detection in synthetic aperture radar images based on PCANet. *IEEE Geoscience and Remote Sensing Letters*. 13(12), 1792-1796.
- [3] Touzi, R., 2006. Target scattering decomposition in terms of roll-invariant target parameters. *IEEE Transactions on Geoscience and Remote Sensing*. 45(1), 73-84.
- [4] Muhuri, A., Goita, K., Magagi, R., et al., 2023. Geodesic distance based scattering power decomposition for compact polarimetric SAR data. *IEEE Transactions on Geoscience and Remote Sensing*. 61, 1-12.
- [5] Liu, S., Gao, L., Lei, Y., et al., 2020. SAR speckle removal using hybrid frequency modulations. *IEEE Transactions on Geoscience and Remote Sensing*. 59(5), 3956-3966.
- [6] Gong, M., Zhou, Z., Ma, J., 2011. Change detection in synthetic aperture radar images based on image fusion and fuzzy clustering. *IEEE Transactions on Image Processing*. 21(4), 2141-2151.
- [7] Celik, T., 2009. Unsupervised change detection in satellite images using principal component analysis and k-means clustering. *IEEE Geoscience and Remote Sensing Letters*. 6(4), 772-776.
- [8] Gao, F., Wang, X., Gao, Y., et al., 2019. Sea ice change detection in SAR images based on convolutional-wavelet neural networks. *IEEE Geoscience and Remote Sensing Letters*. 16(8), 1240-1244.
- [9] Qu, X., Gao, F., Dong, J., et al., 2021. Change detection in synthetic aperture radar images using a dual-domain network. *IEEE Geoscience and Remote Sensing Letters*. 19, 1-5.
- [10] Shang, R., Xie, K., Okoth, M.A., et al. (editors), 2019. SAR image change detection based on mean shift pre-classification and fuzzy C-means. *IGARSS 2019-2019 IEEE International Geoscience and Remote Sensing Symposium*; 2019 Jul 28-Aug 2; Yokohama, Japan. New York: IEEE. p. 2358-2361.

- [11] Ghosh, A., Mishra, N.S., Ghosh, S., 2011. Fuzzy clustering algorithms for unsupervised change detection in remote sensing images. *Information Sciences*. 181(4), 699-715.
- [12] Zheng, Y., Zhang, X., Hou, B., et al., 2013. Using combined difference image and k -means clustering for SAR image change detection. *IEEE Geoscience and Remote Sensing Letters*. 11(3), 691-695.
- [13] Tan, S., Zhang, X., Wang, H., et al., 2021. A CNN-based self-supervised synthetic aperture radar image denoising approach. *IEEE Transactions on Geoscience and Remote Sensing*. 60, 1-15.
- [14] Zhang, K., Zuo, W., Zhang, L., 2018. FFDNet: Toward a fast and flexible solution for CNN-based image denoising. *IEEE Transactions on Image Processing*. 27(9), 4608-4622.
- [15] Hao, F., Tang, C., Xu, M., et al., 2019. Batch denoising of ESPI fringe patterns based on convolutional neural network. *Applied Optics*. 58(13), 3338-3346.
- [16] Guo, S., Yan, Z., Zhang, K., et al. (editors), 2019. Toward convolutional blind denoising of real photographs. *Proceedings of the IEEE/CVF Conference on Computer Vision and Pattern Recognition*; 2019 Jun 15-20; Long Beach, CA, USA. New York: IEEE. p. 1712-1722.
- [17] Meester, M.J., Baslamisli, A.S., 2022. SAR image edge detection: Review and benchmark experiments. *International Journal of Remote Sensing*. 43(14), 5372-5438.
- [18] De Borba, A.A., Muhuri, A., Marengoni, M., et al., 2023. Feature Selection for edge detection in PolSAR images. *Remote Sensing*. 15(9), 2479.
- [19] Mildenhall, B., Barron, J.T., Chen, J., et al. (editors), 2018. Burst denoising with kernel prediction networks. *Proceedings of the IEEE Conference on Computer Vision and Pattern Recognition*; 2018 Jun 18-23; Salt Lake City, UT, USA. New York: IEEE. p. 2502-2510.
- [20] Chierchia, G., Cozzolino, D., Poggi, G., et al. (editors), 2017. SAR image despeckling through convolutional neural networks. 2017 IEEE International Geoscience and Remote Sensing Symposium (IGARSS); 2017 Jul 23-28; Fort Worth, Texas. New York: IEEE. p. 5438-5441.
- [21] Bazi, Y., Bruzzone, L., Melgani, F., 2005. An unsupervised approach based on the generalized Gaussian model to automatic change detection in multitemporal SAR images. *IEEE Transactions on Geoscience and Remote Sensing*. 43(4), 874-887.
- [22] Rezaei, H., Karami, A. (editors), 2017. SAR image denoising using homomorphic and shearlet transforms. 2017 3rd International Conference on Pattern Recognition and Image Analysis (IPRIA); 2017 Apr 19-20; Shahrekord, Iran. New York: IEEE. p. 80-83.
- [23] Patra, S., Ghosh, S., Ghosh, A., 2011. Histogram thresholding for unsupervised change detection of remote sensing images. *International Journal of Remote Sensing*. 32(21), 6071-6089.
- [24] Mishra, N.S., Ghosh, S., Ghosh, A., 2012. Fuzzy clustering algorithms incorporating local information for change detection in remotely sensed images. *Applied Soft Computing*. 12(8), 2683-2692.
- [25] Yetgin, Z., 2011. Unsupervised change detection of satellite images using local gradual descent. *IEEE Transactions on Geoscience and Remote Sensing*. 50(5), 1919-1929.
- [26] Ghosh, S., Mishra, N.S., Ghosh, A. (editors), 2009. Unsupervised change detection of remotely sensed images using fuzzy clustering. 2009 Seventh International Conference on Advances in Pattern Recognition; 2009 Feb 4-6; Kolkata, India. New York: IEEE. p. 385-388.
- [27] Gosain, A., Dahiya, S., 2016. Performance analysis of various fuzzy clustering algorithms: A review. *Procedia Computer Science*. 79, 100-111.
- [28] Pal, N.R., Bezdek, J.C., 1995. On cluster validity for the fuzzy c-means model. *IEEE Transactions on Fuzzy Systems*. 3(3), 370-379.
- [29] Wang, Z., Bovik, A.C., Sheikh, H.R., et al., 2004. Image quality assessment: From error vis-

- ibility to structural similarity. *IEEE Transactions on Image Processing*. 13(4), 600-612.
- [30] Rosin, P.L., Ioannidis, E., 2003. Evaluation of global image thresholding for change detection. *Pattern Recognition Letters*. 24(14), 2345-2356.
- [31] Bovolo, F., Bruzzone, L., 2005. A detail-preserving scale-driven approach to change detection in multitemporal SAR images. *IEEE Transactions on Geoscience and Remote Sensing*. 43(12), 2963-2972.
- [32] Inglada, J., Mercier, G., 2007. A new statistical similarity measure for change detection in multitemporal SAR images and its extension to multiscale change analysis. *IEEE Transactions on Geoscience and Remote Sensing*. 45(5), 1432-1445.
- [33] Shugar, D.H., Jacquemart, M., Shean, D., et al., 2021. A massive rock and ice avalanche caused the 2021 disaster at Chamoli, Indian Himalaya. *Science*. 373(6552), 300-306.

ARTICLE

Hydrogeological Investigations of Groundwater and Surface Water Interactions in the Berg River Catchment, Western Cape, South Africa

Seiphi Prudence Mabokela^{1,2}, Ntokozo Malaza^{1*} 

¹ Department of Occupational and Environmental Studies, Faculty of Applied Science, Cape Peninsula University of Technology, Cape Town, 7530, South Africa

² Department of Water and Sanitation, Pretoria, 0001, South Africa

ABSTRACT

The Berg River Catchment based in the Western Cape Province, South Africa services the greater Cape Town area with water, subsequent to supplying the vast agricultural activities that exist in the middle and the lower reaches. This study thus investigates the hydrogeochemical interactions between surface and groundwater in the Berg River Catchment with the aim of establishing trends and transfer of constituents between the surface and groundwater systems, investigates the role that geology plays in water chemistry as well as identifies the geochemical processes controlling surface and groundwater chemistry in the catchment. This study was carried out using three types of research designs namely i) experimental research design; ii) field research design and meta-analysis research design. Furthermore, the study made use of hydrochemical data ranging from 2003 to 2013 obtained from the National Water Monitoring Database owned and maintained by the Department of Water and Sanitation and data that were sampled in 2016 by authors and analyzed using the ICP-MS Technique Ground Water Chart, Arc-GIS and Geosoft (Oasis Montaj) were further employed to model the data. The results indicated that: i) in the Upper Berg there is not much interaction and transfer of constituents between surface and groundwater; ii) the Middle Berg, however, indicated a degree of interaction with the sharing of constituents between the two water systems and iii) the Lower Berg indicated only NaCl water type also noting that the area situated near the river mouth whereby there is the mixing of river and seawater.

Keywords: Hydrogeology; Groundwater; Surface water; Interactions; Berg River Catchment

*CORRESPONDING AUTHOR:

Ntokozo Malaza, Department of Occupational and Environmental Studies, Faculty of Applied Science, Cape Peninsula University of Technology, Cape Town, 7530, South Africa; Email: malazan@cput.ac.za

ARTICLE INFO

Received: 23 August 2023 | Revised: 3 October 2023 Accepted: 7 October 2023 | Published Online: 10 November 2023

DOI: <https://doi.org/10.30564/jees.v5i2.5918>

CITATION

Mabokela, S.P., Malaza, N., 2023. Hydrogeological Investigations of Groundwater and Surface Water Interactions in the Berg River Catchment, Western Cape, South Africa. Journal of Environmental & Earth Sciences. 5(2): 102-117. DOI: <https://doi.org/10.30564/jees.v5i2.5918>

COPYRIGHT

Copyright © 2023 by the author(s). Published by Bilingual Publishing Group. This is an open access article under the Creative Commons Attribution-NonCommercial 4.0 International (CC BY-NC 4.0) License. (<https://creativecommons.org/licenses/by-nc/4.0/>).

1. Introduction

It is well established that the quality of freshwater resources has been and still is deteriorating at an escalated rate globally affecting the chemical, physical and biological composition of water. As a result, fresh water has thus become a rare commodity that is crucial for the survival of any living organism on Earth ^[1]. Fresh water is found in groundwater aquifers and surface water resources such as rivers, streams, lakes and dams however, these resources only comprise 0.3% of fresh water that is available for human consumption out of the 71% of water that constitutes the earth ^[2].

The remaining quantity of water found in oceans and seas requires expensive processes of desalination in order to become potable for human use. According to Khatri, N. et al. ^[2], the deteriorating quality of fresh water is escalating the already existing problem of water scarcity and in the near future the demand will surpass the supply of fresh water.

The surface and groundwater quality is a function of natural setup and processes as well as anthropogenic activities collectively. According to Khatri, N. et al. ^[2], human influences towards the quality of water are a result of economic activities such as the application of fertilizers, irrigation, construction sites, mining operations, sewage and industrial discharge, leaching of contaminants from land fill sites and feedlots of livestock farming amongst many others. On the other hand, groundwater quality is influenced by the leaching of organic matter and nutrients from soil, weathering of bedrock minerals, atmospheric processes involving evapotranspiration, deposition of dust and salts by wind or water. All these processes possess a great potential to introduce contaminants in both surface and groundwater systems ^[2]. Both water systems can further be influenced by physiographical factors such as topography, land cover, climate, stream geomorphology, as well as the positioning of surface water features relative to subsurface water flow paths in catchments ^[3].

As a result, effective water quality management requires a thorough understanding of how and why chemical composition varies across the catchment.

Understanding these many forces playing a role in water quality is thus essential for the development of effective water quality management strategies as per Section 9 of the South African National Water Act, 36 of 1998. According to Lintern, A. ^[1], immense studies linking anthropogenic activities and water quality have been conducted in the Berg River Catchment (referred to as BRC hereto). However, there have been fewer studies on the natural setting particularly geology and soil types influencing the chemistry of water in the BRC. This research thus aims to lessen this gap by discussing the hydrogeochemical interactions between surface and groundwater with respect to geologic settings and soils in the BRC. This study intends to be of good use to water users, catchment managers and researchers to develop water quality management strategies and models.

2. Study area

2.1 Location of study area

The Berg River Catchment is found in the Western Cape Province broadening about 270 km from Jonkershoek and Franschhoek mountains flowing in a north westerly direction where it discharges into the Atlantic Ocean at Laaiplek ^[4,5] (**Figure 1**). From the head waters, the river flows north and joins with the Franschhoek River in the Franschhoek valley where it is further merged by two more tributaries: the Wemmershoek River to the east and the Banhoek River to the west ^[4].

Furthermore, the Berg River flows through Paarl and Wellington where it is joined by the Krom River tributary from the eastern direction ^[6]. In the north of Wellington, the Berg River is connected to several other tributaries namely: Klein Berg River, Kompanjies River and the Twenty Four Rivers ^[4,5]. Further southwards it is joined by the Boontjies River where it begins to flow westwards between the Obiekwa and Voëlvlei mountains into the Berg River Valley and joins the Berg River to the west of Saron ^[6,7]. The Berg River then flows over the Misverstand Weir in which upstream of the weir, the river is joined by the tributaries that drain the areas north of

Porterville and Moorreesburg^[4]. The river then flows in a north-westward direction and drains into the Atlantic Ocean at Velddrift^[4,5,7].

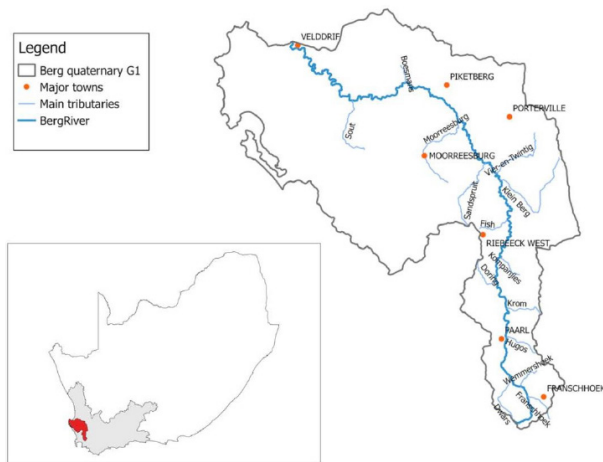


Figure 1. Location of the Berg River Catchment (BRC).

2.2 Land-use activities

The land use in the BRC can be divided into four types namely: i) agriculture which comprises about +60% of the catchment; ii) natural which takes a further +36% of the catchment; iii) urban settlements which take up about +2.5% and iv) forestry which is about, 1%^[8]. Furthermore, the agricultural land is further divided into two sectors namely i) dry land farming activities which comprise about 53% as well as ii) irrigated land which takes up +7%. The catchment, however, has recently experienced high a volume of population increase which results in urbanization in the Paarl, Tulbagh and Wellington areas^[8].

2.3 Topography, rainfall and flow regimes of the catchment

The topography of the BRC varies greatly from the head waters to the mouth of the river, thus resulting in the great variability of the flow. According to Clark, B. et al.^[9], the upper reaches of the Berg River are hydraulically very steep with an average bed slope of 0.67% down to Paarl. From Paarl, the river profile flattens, with an average bed slope to the estuary of 0.045%. According to Madlala T.E.^[3], the topography ranges between minimum, mean, and

maximum elevations of 213 m, 238 m, and 1500 m above sea level respectively. The highest elevation is found at the head waters with mountainous terrain and flattens towards the river mouth into the Atlantic Ocean. It is worth note taking however that the BRC is mostly flat in terrain.

The catchment receives the most rainfall in winter due to its Mediterranean climate, though the precipitation distribution varies greatly in the extent of the catchment^[9]. According to research by Clark, B. et al.^[9], the BRC receives the Mean Annual Precipitation (MAP) that is usually above 1500 mm in the southern parts of the catchment but decreases steadily to less than 500 mm further northwards towards the mouth of the river. The MAP then drops further to below 300 mm at the river mouth in Veldrifi^[10]. There are significant seasonal variations in monthly evaporations which fall typically between 40 mm and 50 mm in winter and 230-250 mm in the summer months^[10]. Furthermore, the Mean Annual Evaporation (MAE) in the southern and western regions of the catchment ranges from 1400 mm to over 1600 mm in the northeast^[4]. The topography of the BRC varies greatly from the head waters to the mouth of the river, thus resulting in the great variability of the flow.

2.4 Geology and soils

The geology of the BRC comprises four groups namely: a) the Table Mountain Group (TMG), b) the Malmesbury Group (MG), c) the Cape Granite Suite (CGS) and d) the Klipheuwel Group (KP). The catchment is however dominated by TMG and MG therefore the CGS and KG form a relatively small component of the total geology of the BRC^[9]. The upper reaches of the BRC consist of a combination of CGS and TMG in areas between Franschhoek and Paarl. According to research by the Council for Geoscience^[11] (Geology Map of South Africa), the lithology includes the medium to fine grained granite and granodiorite with subordinate syenite, gabbro, diorite and quartz porphyry. The TMG nonetheless dominates the uppermost reaches of the catchment. There are two geologic formations making up the

TMG in the BRC namely: a) Nardow Formation and b) Peninsula Formation ^[3]. The Narrow Formation is made up of white coarse-fine-grained, thick-bedded pebbly quartz arenites, thin-bedded feldspathic and ferruginous sandstone, subordinate shale and siltstone.

Furthermore, the Peninsula Formation is made up of pebbly quartz arenites, diamictite, minor conglomerate, mudrock, siltstone and shale. As Madlala, T.E. ^[3] further summarized the abovementioned, the author noted that the two formations comprise primarily of chemically inert granite, quartzitic sandstones, relatively mineralized siltstones, shale, and mudstones. Madlala, T.E. ^[3] further highlighted that the dominant formation in the upper reaches is the Peninsula Formation. A layer of alluvium in the valleys covers these formations and constitutes the primary aquifer material in the catchment ^[3,9].

The MG is the most dominating group of rocks in the middle-lower areas of the catchment such as Darling, Moorreesburg, Piketburg, and Porterville as well as the areas towards the river mouth ^[9]. According to Kisters, A. ^[12], the rocks of the MG are largely marine sediments, shales and greywackes that were deposited in a near-shore to deep-water environment. Structurally, the rocks of the Malmesbury Group are folded and also consist of faults ^[12]. The faults stretch up to numerous kilometer-wide fault zones and are generally thought to disconnect three structurally and lithologically distinct formations comprising the southwestern Tygerberg, central Swartland and northeastern Boland terranes.

The Swartland Formation is the dominant domain compared to Boland Formation within the Malmesbury Group separated by Wellington fault. Therefore, Boland Formation is found east of Swartland in areas such as Piketberg, Porterville and Tulbagh and comprises units such as greenstone, dolomite, chert, quartz-sericite and graphite schist ^[11,12]. Swartland Formation on the other hand is found in areas such as Moorreesburg, Malmesbury, Hopefield and the areas in the lower reaches towards the river mouth and consists of quartz-sericite, chlorite, schist and phyllite ^[11].

There have been numerous claims that groundwater quality in the Berg River Catchment is generally quite poor in the middle-lower reaches of the catchment owing to the geologic setting of the MG ^[8,13]. Clark, B. et al. ^[9] added that groundwater quality is controlled by, amongst other factors, lithology, residence time and rainfall. Aquifers consisting of rocks of the MG generally yield poor quality groundwater with a NaCl character and an EC fluctuating between 100 and 1000 mS/m.

3. Methodology

This study was carried out using three types of research designs namely i) Experimental research design; ii) Field research design and iii) Meta-analysis research design. The primary data were obtained from published scientific journals and books, and governmental institutions. The data were analyzed and incorporated into the literature to explain the geology, hydrology and geohydrology of the area. The surface and groundwater data from 2003 to 2013 were obtained from the National Water Monitoring Database owned by the Department of Water and Sanitation in South Africa (**Figure 2**). The 2016 data was sampled by the authors is depicted in **Figure 3**.

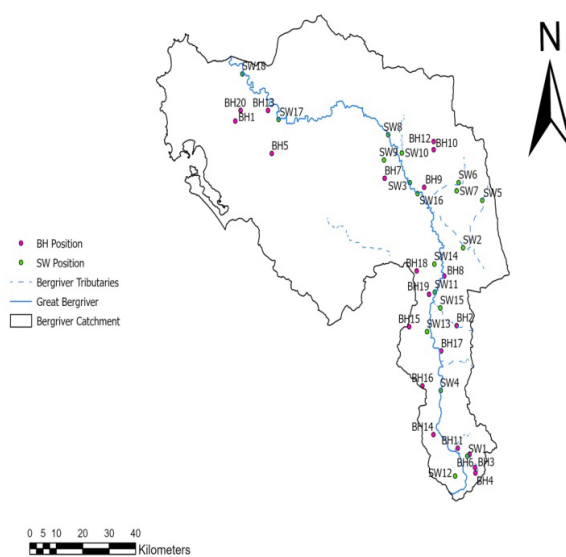


Figure 2. Department of water and sanitation surface and groundwater localities.

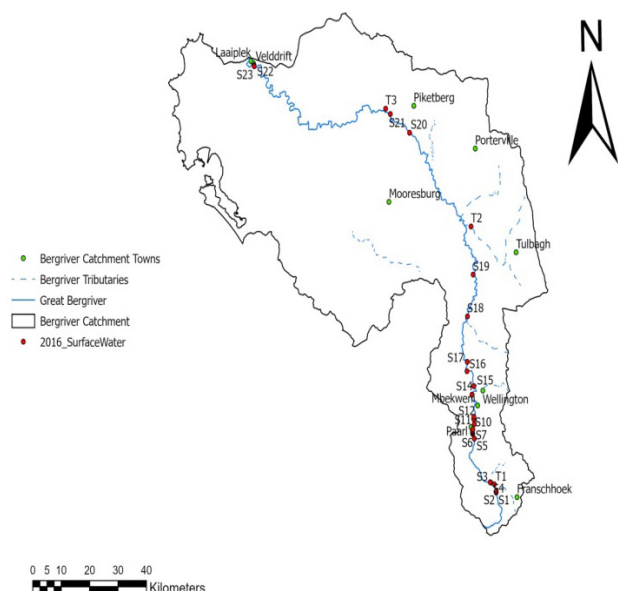


Figure 3. 2016 surface water samples locality collected by authors.

The surface water samples were collected in 2016 during the dry season. The samples were collected from the head waters (Berg River Dam) to the mouth of the river (Laaiplek) by means of grab sample technique. The samples were collected from 23 different locations in the river extent using plastic bottles of 125 mL. Each bottle was labeled by a unique identity (numbers i.e. S1, S2 etc.). To ensure accuracy and avoid cross contamination of the samples, the bucket used to collect water samples was first rinsed with deionized water and secondly rinsed with the water from the river before taking the actual sample. When both the bucket and the bottles were rinsed with deionized water, they were further rinsed again with sample water prior to final sample collection and bottling. This procedure was performed at each sample location to avoid contamination of samples.

Physical parameters (TDS, salinity, pH, EC and temperature) were immediately analyzed in-situ using M99720 Combo Water Meter in order to get the original nature of the sample. The water meter was also rinsed with deionized water prior to taking physical parameter readings from sample water. Thereafter, the samples were stored in cooler boxes whereby the chemical parameters were analyzed in 24-72 hours at the Stellenbosch University (ICP-MS and XRF Laboratory) for the analysis of chemical

parameters (nitrates, calcium, magnesium, sodium, potassium, chloride, sulphates and bicarbonates).

3.1 Analysis method for cations (Ca^{++} , Mg^{++} , Na^{+} , K^{+}) using Perkin Elmer ICP-OES Optima 5300 DV

This method describes multi-elemental determinations by ICP-OES using a simultaneous optical system with axial and radial viewing of the plasma. The instrument measures characteristic emission spectra by optical spectrometry. Samples were nebulized and the resulting aerosol was transported to the plasma torch. Element-specific emission spectra were produced by radio-frequency inductively coupled plasma. The spectra were dispersed by an echelle polychromator, and the intensities of the emission lines were monitored by segmented-array charge-coupled detectors. Simultaneous background correction was performed for each element. The position selected for the background-intensity measurement, on either or both sides of the analytical line, was determined by the complexity of the spectrum adjacent to the analyte line.

3.2 Analysis method for Anions (Cl , SO_4 and HCO_3) using thermo fischer scientific gallery plus discreet analyser

The Gallery Plus Discrete Analyser is designed to selectively analyse chloride, nitrate and sulphate in water samples based on photometric principles where colour-forming complexing reagents were added to a sample to produce a unique coloured solution for each analyte to be determined. Each unique colour was measured at a specific wavelength where colour intensity (absorbance) was directly proportional to the concentration of the analyte.

3.3 Surface water hydrochemical analysis

The samples collected in 2016 were analysed using Waters 717 autosampler, conductivity detector and Waters 2410 pump, controlled with Waters Empower software. An IC Pak A column was used with

a Lithium Borate/Gluconate eluent, conductivity 240 μ S consisting of 20 mL Lithium Borate Gluconate concentrate (34 g Boric acid, 23.5 mL d-Gluconic acid, 8.6 g Lithium hydroxide monohydrate, 250 mL Glycerin, filled up to 1 litre with Milli-Q water), 10 mL n-Butanol, 120 mL Acetonitrile filled up to 1 litre with Milli-Q water. A 5 μ L sample was injected for analysis at a flow rate of 1.2 mL/min.

3.4 Mapping and modeling

Mapping and modelling were done by the use of GW Chart, ArcView and Oasis Montaj (Geosoft) Software packages. GW-Chart is a software program used for creating specialized graphs in groundwater studies. The program can create several types of graphs such as piper diagrams and hydrographs which were created for this study to provide more understanding of the sample results. To create the piper diagrams, raw data from the laboratory which is usually expressed in milligrams per litre “mg/L” units were organized into the Excel spreadsheet and then added onto the GW Chart to create piper plots.

ArcView comprises one of several ArcGIS software that are used for mapping. This software was used in this study for the creation of maps that were used to indicate the direction of water flow, sampling points (location), correlation, trends as well as vulnerable areas that are more prone to contamination. The maps were created using an Excel spreadsheet and base maps by means of shapefiles which were obtained from the Department of Rural Development. The Excel spreadsheet contains the correct sampling location (XY coordinates), sample identity and sample contents (chemical parameters) with concentration. The base maps consist of the following layers: rivers, provincial layers, towns and catchment layers. Oasis Montaj software was used to grid the Nitrates concentrations in both surface and groundwater data to establish the trends and correlations. The color intensity and scale were used to denote the concentration magnitude of the analytes understudied.

4. Results and discussion

4.1 Groundwater and surface water hydrochemical facies correlation

The data from both surface and ground water were grouped according to their geographical locations as explained below (Table 1):

SW1, SW12, BH3, BH4, BH6 and BH11 surface and groundwater hydrochemical correlation

The above sample points are in the G10A+B quaternary catchment in the BRC headwaters where the lithology is mostly dominated by sandstones of the Table Mountain Group. The hydrochemical facies deduce that all the above-mentioned samples are NaCl type. This suggests that the NaCl in the BRC may have originated from the rocks such as siltstone and sandstone which exists in the upper Berg. It can further be observed that surface water samples have both NaCl and Mixed-CaMgCl while groundwater has three additional water types to those of surface including CaHCO_3 , Mixed CaNaHCO_3 and CaCl. It can thus be said there is little to no interaction and transfer of constituents as the water types found in groundwater are not present in surface water. Furthermore, the Mixed-CaMgCl water type in groundwater is only found in BH3, which further suggests that there may be other factors contributing to the presence of this water type in BH3 as it does not occur in other borehole data (Figure 4).

SW4 and BH14 surface and groundwater hydrochemical correlation

SW4 and BH14 are in an area in the G10C quaternary catchment where the underlying geology is predominantly of granitic rocks, most of those belonging to the Cape Granite Suite. Based on the hydrochemical facies, there is very little movement of water from the surface into groundwater, but rather a recharge of surface water by groundwater. The borehole waters in this area recorded only NaCl water type while surface waters reflected both NaCl and Mixed-CaMgCl, meaning, this water type does not originate from groundwater but from other factors.

Table 1. Summary of groundwater and surface hydrochemical facies.

Borehole ID	Hydrochemical facies	Surface point ID	Hydrochemical facie
1. BH1	NaCl	1. SW1	NaCl; Mixed-CaMgCl
2. BH2	NaCl ; Mixed CaMgCl	2. SW2	NaCl
3. BH3	CaHCO ₃ ; NaCl; Mixed CaNaHCO ₃ ; Mixed CaMgCl	3. SW3	NaCl; Mixed-CaMgCl
4. BH4	CaHCO ₃ ; Mixed CaNaHCO ₃ ; NaCl	4. SW4	NaCl; Mixed-CaMgCl
5. BH5	NaCl	5. SW5	NaCl; Mixed-CaMgCl; CaHCO ₃
6. BH6	NaCl; CaHCO ₃ ; Mixed CaNaHCO ₃	6. SW6	NaCl; Mixed-CaMgCl
7. BH7	NaCl	7. SW7	NaCl; Mixed-CaMgCl; CaHCO ₃
8. BH8	NaCl	8. SW8	NaCl
9. BH9	NaCl	9. SW9	NaCl
10. BH10	NaCl	10. SW10	NaCl
11. BH11	NaCl ; CaHCO ₃ ; CaCl	11. SW11	NaCl
12. BH12	NaCl ; CaHCO ₃	12. SW12	NaCl; Mixed-CaMgCl; CaHCO ₃
13. BH13	NaCl	13. SW13	NaCl
14. BH14	NaCl	14. SW14	NaCl; Mixed-CaMgCl
15. BH15	NaCl	15. SW15	NaCl
16. BH16	NaCl; Mixed CaMgCl	16. SW16	NaCl
17. BH17	Mixed CaMgCl; NaCl	17. SW17	NaCl
18. BH18	Mixed CaMgCl; NaCl	18. SW18	NaCl
19. BH19	NaCl		
20. BH20	NaCl		

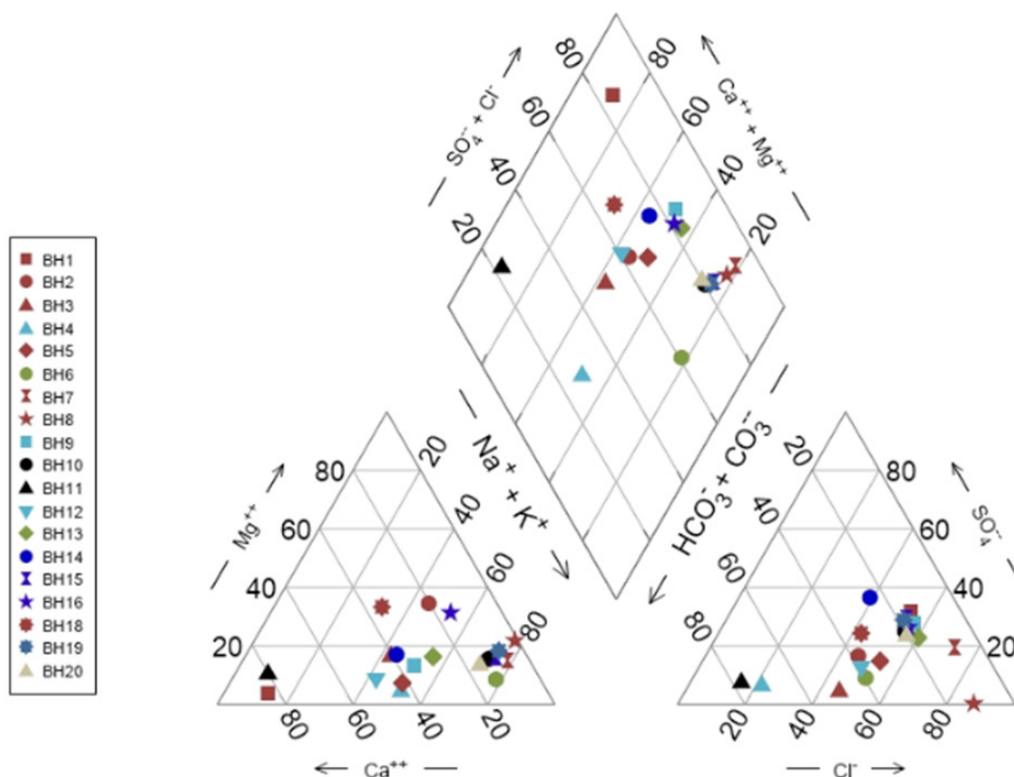


Figure 4. Groundwater chemistry data plot.

SW13, SW15, BH2, BH15 and BH17 surface and groundwater hydrochemical correlation

The correlation of the above-mentioned samples suggested very little interaction of water between the two hydrological components. The groundwater data indicated similarities amongst the boreholes which vary from the surface waters. BH2 and BH17 have both NaCl and Mixed-CaMgCl types; however, BH15, SW13 and SW15 have only NaCl water type (Figure 5).

SW11, SW14, BH8, BH18 and BH19 surface and groundwater hydrochemical correlation

The above samples indicated the presence of NaCl and Mixed-CaMgCl water types, therefore it can be said that there is reasonable interaction between the surface and groundwater in this G10F quaternary catchment.

SW8, BH10 and BH12 surface and groundwater hydrochemical correlation

With reference to the hydrochemical facies, it

can be said there is little interaction and transfer of constituents amongst the above samples. All sample points have NaCl water type. However, BH12 further shows the presence of CaHCO_3 water type.

SW17 and BH5 surface and groundwater hydrochemical correlation

The two sample points above are in the G10L quaternary catchment and both have NaCl water type. It is also worth note-taking that the two sample points are located nearer to the river mouth and therefore, the presence of saline water is inevitable.

SW18, BH1, BH13 and BH20 surface and groundwater hydrochemical correlation

Like those of the G10L quaternary catchment, SW18, BH1, BH13 and BH20 are also located in the G10M quaternary catchment, very close to the river mouth into the Atlantic Ocean and as such the dominant NaCl water type is highly inevitable. All the sample points in the G10M indicated no other water type than NaCl.

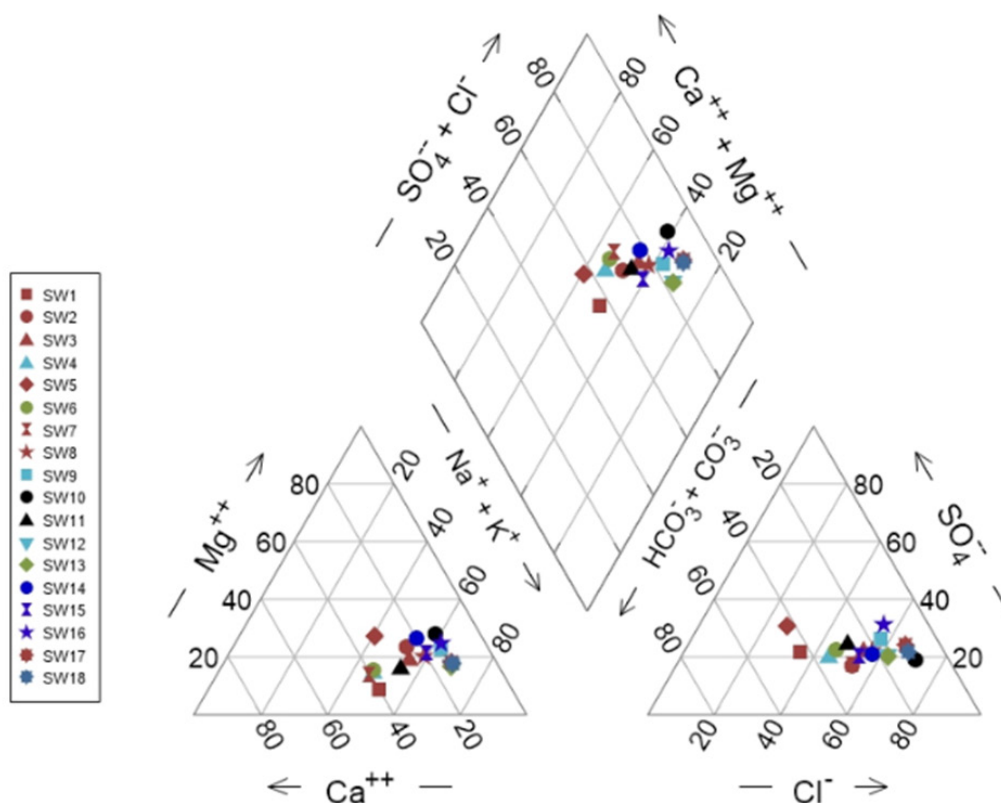


Figure 5. Surface water chemistry data plot.

SW3, SW9, SW10, SW16, BH7 and BH9 surface and groundwater hydrochemical correlation

All the above sample points indicated none other than NaCl water type except for BH3 which reflected both NaCl as well as Mixed-CaMgCl. The presence of Mixed-CaMgCl therefore suggests another factor contributing to its presence as well as no movement of water from surface into groundwater as this water type is not detected in the groundwater.

SW2, SW5, SW6 and SW7 surface and groundwater hydrochemical correlation

These surface water samples could not be correlated with groundwater samples as there were no available groundwater data in the same vicinity (Table 2).

4.2 Surface and groundwater nitrates variations in the Berg River Catchment

The data from both surface and groundwater were grouped according to their geographical locations as explained below:

SW1 surface and groundwater nitrate correlation

The SW1 sample recorded nitrate concentrations that exceeded the permissible drinking water standards as stipulated in the SANS 241-1 2015 for more than half the years involved in this research. In most years, however, the values were just below 1.2 mg/L which is negligible. Only on two occasions were the SW1 sample point recorded just above 2 mg/L and 8.6 mg/L in 2008. This indicates that there may

have been accidental discharges or releases of excess nitrates into the river by either malfunctioning Wastewater Treatment Works (WWTW) or agricultural activities as the area is highly cultivated with various types of grapes and stone fruits. On the other hand, however, the report by Cullis, J.D.S. et al. [8] rules out the possibility of the Franschoek and Wemmershoek areas being the possible sources of nitrates as they are not listed as part of those which are worst performing in the catchment. The report by the DWAF [6] nonetheless indicated that agricultural practices in the area may be the most possible source of excess nitrates by means of fertilizer application and eventually run-off into the river.

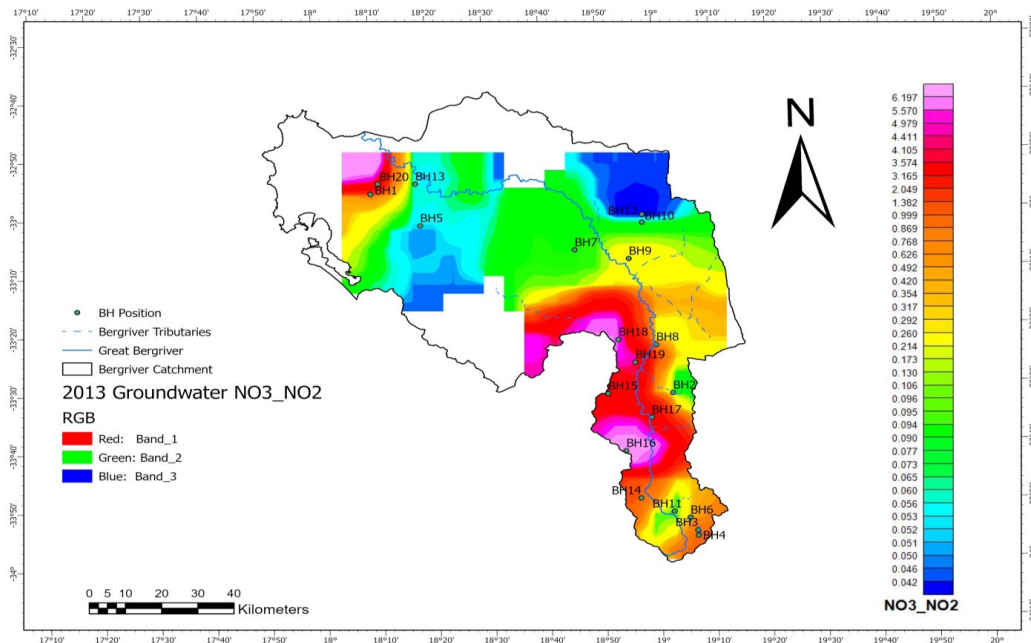
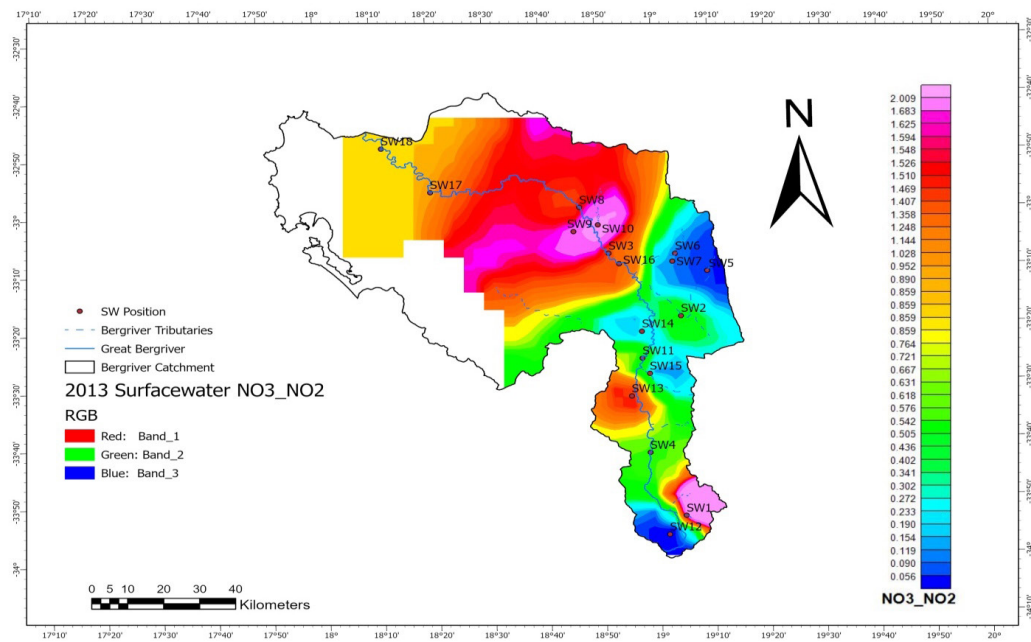
Nonetheless, the boreholes (BH3, BH4, BH6 and BH11) in the same area have not recorded nitrates above 1 mg/L, although the DWAF [6] report indicated the area of Franshoek and Wemmershoek as one of those highly irrigated in the catchment, the boreholes have very low nitrates (Figures 6 and 7). This suggests that the river water used for irrigation may be treated prior to irrigation.

BH14 and BH16 surface and groundwater nitrates correlation

The two boreholes showed more than 80% higher nitrate concentrations with BH16 taking the lead. The boreholes are located in the vicinity of Paarl which is industrialized, cultivated and also consists of residential areas. The Berg River around the area of Paarl has been recorded to have slightly bad quality of water due to many activities taking place as well as non-compliant WWTW which discharge into the Berg River [6]. The possible source of the nitrates however points to agricultural activities by means of

Table 2. Correlation of excessive surface water and groundwater nitrate data.

Quaternary catchment—Location	Surface sample ID	Boreholes ID
G10A—Franschoek	SW1	-
G10C—Paarl	-	BH14 and BH16
G10D—Wellington	SW13 and SW15	-
G10F—Riebeek Kasteel	SW11 and SW14	BH8, BH18 and BH19
G10H—Porterville & Piketberg	SW8	-
G10J—Mooreesburg	SW3, SW9, SW10 and SW16	-
G10M—West Coast	-	BH1 and BH20

Figure 6. Groundwater $\text{NO}_3^- + \text{NO}_2^-$.Figure 7. Surface water $\text{NO}_3^- + \text{NO}_2^-$.

irrigation and not fertilizer application as the surface water sample point only recorded 1.7 mg/L once in 11 years. The SW4 sample has shown nitrates values less than 1 mg/L in 10 out of 11 years involved in this research. Another possible explanation for the high nitrates in the boreholes can be pointed to the broken sewage infrastructure (pipes in particular) which may leak into the groundwater system.

SW13 and SW15 surface and groundwater nitrates correlation

SW15 had shown nitrates above 1mg/L in only one incident out of the 11 years of sampling. This suggests an accidental discharge by means of damaged sewage infrastructure. On the other hand, SW13 indicated high values of concentrations in 7

out of 11 years. This therefore suggests a constant feeder of nitrates into the river such as an ailing sewage system and damaged sewage infrastructure. SW13 is situated adjacent to an area dominated by informal settlements and has an ailing wastewater infrastructure like most informal settlements in the country. The sewage run-off (overflowing manholes) directly into the Berg River as it passes adjacent to the informal settlement. Although SW13 and SW15 are in the same quaternary catchment, recorded highly variable nitrates suggest a significant dilution and or the presence of marine organisms which consume the parameter at hand. Furthermore, the boreholes (BH2, BH15 and BH17) have shown a record of very low nitrate concentrations contrary to surface data. This may be due to the fact that there are no agricultural activities in the vicinity and further there may be significantly low or no interchange of surface and groundwater.

SW11, SW14, BH8, BH18 and BH19 surface and groundwater nitrates correlation

These sample points showed moderately high nitrate concentrations. The area is also highly cultivated and irrigation with river water is highly practiced. The possible source of nitrates in surface water can be pointed to the application of fertilizers which is transported to the Berg River by run-off. It is also worth noting that the farms in this area are adjacent to the Berg River; as a result, fertilizers are easily leached into the river. In addition, the boreholes in the area have also shown significant concentrations of nitrates with BH18 going up to 16.8 mg/L of nitrates. This notion therefore suggests that there is irrigation with the untreated river water and insignificant dilution in groundwater compared to surface water.

SW8 surface and groundwater nitrates correlation

This sample point only recorded on one occasion values exceeding 1 mg/L of nitrates. This may have been due to an accidental discharge of sewage around the area.

SW3, SW9, SW10 and SW16 surface and groundwater nitrates correlation

SW3 recorded values exceeding the permissible limits only in 2 out of 11 years and SW9 in 3 out of 11 years. Such inconsistencies point to accidental discharges such as overflowing manholes. SW10 and SW16 on the other hand have moderately high nitrate concentrations compared to SW3 and SW9. All the surface samples stated above are situated in an area that is highly cultivated. Therefore, the application of fertilizers is the most possible source of excessive nitrates in the river in the vicinity. In addition, the area is dominated by farmhouses and a small informal settlement of the farm workers. Most of the farmhouses use septic tanks whereas areas like other areas use the oxidation ponds as their sewage system and discharge directly into the Berg River. The sewage discharge from the area's oxidation ponds, however, cannot be pointed as the leading source of excessive nitrates in the river as it has not been listed as one of the worst performing ^[8].

There is however no corresponding groundwater data which have recorded abnormal nitrate concentrations in the vicinity. BH7 and BH9 in the area have indicated significantly low nitrates throughout 11 years. This further indicates little or no interchange of surface and groundwater as there is no evidence of an exchange of constituents. In addition, the low nitrates in the borehole data may also suggest that irrigation is practised with treated water.

BH1 and BH20 surface and groundwater nitrates correlation

BH1 and BH20 are located on the West Coast known for the cultivation of stone fruits and winter cereals. These two boreholes recorded the highest nitrate concentrations amongst all other boreholes with BH20 recording high values all throughout the 11 years, with 2008 being the highest with the record of 22.11 mg/L. On the contrary, the surface water samples in the area, SW17 and SW18 have shown incredibly low nitrate concentrations all throughout 11 years.

The data from both the DWS surface and 2016

surface water sampled by the authors were grouped according to their geographical locations as explained below (Figure 8):

SW1, SW12, T1 & S1-S3 surface water hydrochemical correlation

The 2016 surface data indicated that the data located in the G10A+B quaternary catchment had shown much higher nitrate concentrations compared to the DWS surface data throughout the 11 years of sampling. The SW1 and SW12 from the DWS had been fairly compliant with drinking water standards set out in SANS 241-1 wherein the SW12 had only exceeded the set limits on two occasions in 11 years whereas SW1 exceeded in 7 out of 11 years. Their nitrate values were much lower compared to the 2016 data for S1, S2, S3 and T1. Their nitrates values ranged between 55.1 mg/L and 67.8 g/L which far exceed the WHO nitrates limits of 50 mg/L for drinking. Thus far it is unclear as to how these values arose too much in a span of 3 years from 2013 where they were below 10 mg/L to 2016 where they were above 50 mg/L. According to the land-use data it can be deduced that in the entire catchment of BRC the agricultural activities were reduced between 2006 and 2015 however, urban areas development in the catchment has grown significantly. The urban areas development, however, comes with more sewer sys-

tem challenges which may be a possible explanation for such a peculiar rise in nitrates.

SW4, SW13, SW15 and S4-17 surface water hydrochemical correlation

According to the geosoft plots, it can be distinguished that amongst the sample points in G10C & G10D (SW4, SW13 and SW15), the sample SW13 illustrated values exceeding the drinking water standards set out in SANS 241-1 while SW4 and SW15 only exceeded once in 11 years. These values however were still not close to the 2016 samples which were between 60.5 mg/L and 92.1 mg/L. Again, there is no possibility of correlating the two as the values are far apart. It is worth noting however that, SW13 and S17 are very close to each other and are adjacent to the informal settlement which had records of continuous sewer overflows from manholes, dilapidated and damaged sewer infrastructure.

Nevertheless, the increase in urban area development is by far the possible explanation for the abnormal nitrate concentrations. In addition, urban developments for residential habitation resulted in the overloading of municipal sewage systems which were already ailing, pipe bursts, overflowing manholes running off in the streets ending up in the river and further by-passing of sewage treatment processes due to ailing infrastructure. The half-treated efflu-

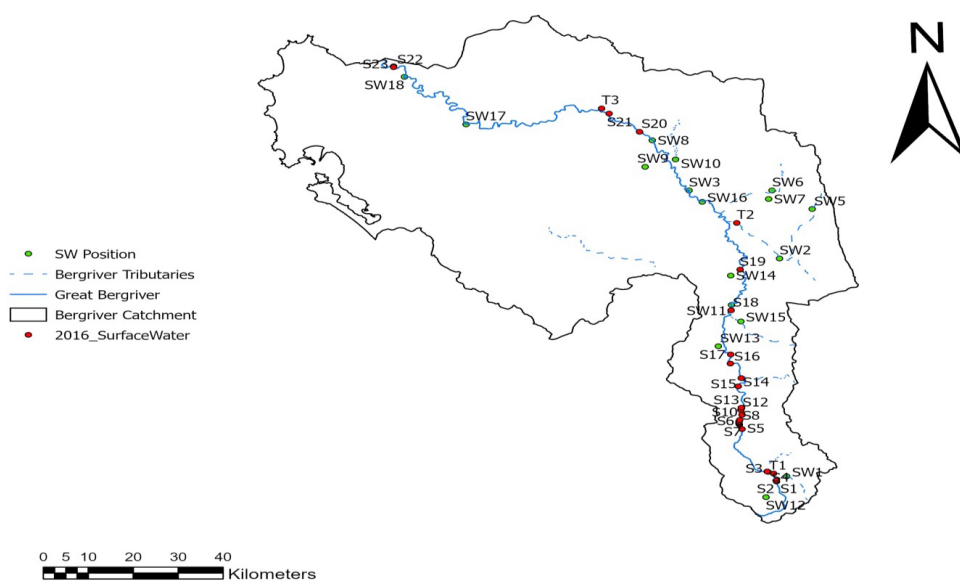


Figure 8. Department of water and sanitation surface sample locations and 2016 sample locations sampled by the authors.

ent is thus discharged into the river.

S18, S19, SW11 and SW14 surface water hydrochemical correlation

The sample points SW14 had moderately high nitrate concentrations. The concentrations however point out to the application of fertilizers since the farms are situated adjacent to the riverbanks and there are no nearby informal settlements. On the other hand, S18 and S19 recorded higher values than other samples from the 2016 surface data wherein S18 had 85.6 mg/L nitrates and S19 had 91.9 mg/L nitrates concentrations. This however, unlike the samples mentioned above are not situated near major towns or informal settlements, as a result, their sources cannot be pointed to anthropogenic influences but rather agriculture through the application of fertilizers. Other parameters were however normal though increasing steadily from S1.

T2, SW3, SW9, SW10 and SW16 surface water hydrochemical correlation

The SW3, SW9, SW10 and SW16 were amongst a group of samples which were among the highest records from the DWS data although they were not any close to the 66.6 mg/L of nitrates recorded in T2. The area where these samples are located is heavily cultivated and there are no nearby major towns and informal settlements with ailing sewer systems. The nitrates are thus the result of fertilizer application which are easily run-off into the river as the farms are adjacent to the riverbanks.

Furthermore, the DWS samples indicated very high NaCl concentrations of more than 3500 mg/L of Cl in some years, with SW9 and SW16 taking the lead. In addition, SW9 and SW16 have also recorded concentrations of Na more than 1000 mg/L in several years wherein the T2 recorded less NaCl with Na⁺ concentration of 103.6 mg/L and Cl with 94.3 mg/L.

S20, S21, T3 and SW8 surface water hydrochemical correlation

Both the DWS surface and the authors' data indicate that there are no linkages in this particular area as with the rest of the samples in terms of nitrate

concentrations. Nonetheless, this area had shown a steep increase in Na and Cl wherein S20 recorded Na 161.6 mg/L and Cl 162.7 mg/L and S21 had a Na concentration of 201.5 mg/L and Cl 219 mg/L. SW8 however had less than 100 mg/L throughout the 11 years studied. T3 however, recorded NaCl concentrations which are low with Na⁺ 61.79 mg/L and Cl 57.8 mg/L.

S22, S23, SW17 and SW18 surface water hydrochemical correlation

S22 and S23 recorded significantly high concentrations in all other parameters excluding nitrates. All these sample points however have similarities in high records of all other parameters except nitrates. Their NaCl is particularly high, and this may be due to the river water mixing with sea water as the sample location is closer to the sea. The nitrates in S22 were undetectable whereas the S23 recorded nitrates just below 30 mg/L which is significantly low compared to other samples from 2016 data. SW17 and SW18 have also significantly low nitrates throughout the 11 years studied except on two occasions the SW17 had nitrates concentrations just above 1 mg/L.

In your results and discussion, you need to include your maps. The maps will help in the understanding of the explanations above. Please work on that.

4.3 Influence of geological features on the water chemistry of the BRC

The Table Mountain Group (TMG) dominates the uppermost reaches of the catchment. The TMG rocks represent a multi-porous medium, consisting of two major components, namely fractures and inter-fracture rock matrix ^[14]. In general, the fractures act as the more permeable conduits for groundwater movement, while the matrix blocks form the main storage unit or reservoir ^[15]. However, the TMG rock matrices are very inert and do not contribute much to the mineral content of the groundwater in the aquifers ^[14]. As a result, the macro-chemical character of the groundwater is determined more by the character of the precipitation than by mineralogy of the rock

through which it percolates ^[16]. Groundwater from the TMG aquifers is generally of the Na-Cl type, reflecting the fact that precipitation generally derives from frontal systems in the Atlantic and Indian Oceans.

The Malmusbury Group (MG) is the most dominating group of rocks in the middle-lower areas of the catchment as well as the areas towards the river mouth ^[9]. The rocks of the MG are largely marine sediments, shales and greywackes that were deposited in a near-shore to deep-water environment. Structurally, rocks of the Malmesbury Group are folded and consist of many faults ^[2]. The indication of a degree of interaction between surface and groundwater, is a result of the heavily structured middle and lower parts of the catchment.

4.4 Influence of anthropogenic activities on the water chemistry of the BRC

The NaCl hydrochemical facies in the headwaters suggest disturbances of groundwater quality by activities such as irrigation with saline water which may have enhanced NaCl concentrations as the area is heavily cultivated. In the upper catchment, the underlying geology resembles very little possibility of weathering of salt bearing rocks ^[9]. As a result, the presence of salt may not be the result of the underlying geology but rather other external factors. Several studies have highlighted that nitrates have for some years become an environmental issue in certain areas of the BRC that have ailing sewage infrastructure. Farmers apply nitrogen-based fertilizers to their crops to enhance plant growth and increase agricultural productivity. When applied excessively or improperly, these nitrates can leach into the soil and, ultimately, groundwater. As a result of the dynamic hydrological system, both surface water and groundwater may be affected by excess nitrates from these activities. Runoff from rainfall or irrigation can wash excess nitrates from agricultural fields into nearby water bodies, such as rivers, lakes, and streams. This runoff contributes to elevated nitrate levels in surface waters of the BRC. Livestock agricultural activities can also contribute to nitrate pollution. Manure

from livestock contains nitrogen, and if not managed properly, it also releases nitrates into the environment through leaching and runoff.

4.5 Policies and management implications

To address these issues, sustainable agricultural practices and effective nutrient management are essential to minimize the impact of agricultural activities on nitrate levels in the environment while ensuring food security and economic viability for farmers.

Efficient irrigation practices like drip irrigation, soil moisture monitoring, and rainwater harvesting are crucial for sustainable agriculture as they help conserve water resources, reduce energy costs, and promote healthier crops. Effective soil management practices like nutrient management, compost and organic matter incorporation, soil testing and analysis, and crop rotation are key to maintaining productive and sustainable agriculture while minimizing adverse environmental impacts. Farmers and land managers must adapt these practices to their specific conditions and crop types to achieve optimal results. Effective fertilizer application practices like split application and fertigation, reduce the environmental impact of agriculture and protect both surface water and groundwater quality while maintaining crop productivity.

It is recommended that authorities at the surrounding wastewater treatment works should improve nutrient removal processes and educate the community about the benefits of these activities. Government authorities should also host regular awareness programs that highlight the impacts of pollution in rivers. In South Africa, the Fertilizers, Farm Feeds, Seeds and Remedies Act 36 of 1947 intends to provide a guide on the manufacturing and use of fertilizers. However, it is recommended that the government needs to enforce such regulations on farmers.

5. Conclusions

Water is a precious and scarce resource that is extremely crucial for life on Earth. In South Afri-

ca, water is crucial not only for the socio-economic development but for other forms of ecosystems at large. As a result, it is therefore important to investigate, monitor, record, and rectify water quality degradation and hold accountable those who degrade the water resources.

Therefore, this study investigated the hydrogeochemical interactions between surface and groundwater in the BRC with the aim of establishing trends and transfer of constituents between surface and groundwater systems. The hydrochemical facies indicated that in the upper Berg River Catchment, there is very minimal interaction between surface and groundwater systems. Other water types that were found in the groundwater other than NaCl were barely found in surface water and vice versa. This may be due to the underlying consolidated hard rock formations (granitic rocks) having less geohydrological properties like fractures and voids.

The Middle Berg, however, indicated a degree of interaction with the sharing of constituents between the two water systems. Most of the water types found in borehole data were also found in the surface water. This can be explained with reference to the structural geology of the area in which a northwest-trending strike-slip faults of the Piketberg-Wellington faults occurred which gave rise to more permeability and movement of water. Moreover, the Lower Berg indicated only NaCl water type. It is worth noting that Lower Berg is situated near the river mouth where there is the mixing of river and sea water. This notion therefore further explains the NaCl being the sole water type in the area. In surface water, this may have further been exacerbated by means of sea spray. With reference to groundwater, Lintern, et al. ^[9] highlighted that there may have been a possibility of seawater intrusion also enhanced by the faulting of rocks originating from the Colenso fault.

With reference to nitrates, the data indicated no interaction and transfer of constituents. The data illustrate that there are 3 boreholes (BH8, BH18 and BH19) which were correlated with the 2 surface samples (SW11 and SW14). The rest of the

surface and groundwater samples did not indicate correspondence. It can therefore be deduced that the nitrates in the boreholes came by because of using nitrate rich water from agricultural activities like irrigation.

Overall, the results obtained in this study indicated that:

- The entire catchment geology consists of rocks containing various minerals with varying chemical make-up however, the NaCl exists in the entire geology even though in some areas it is not dominant.
- The geology and soils do not entirely control the water chemistry of the surface water however, in areas which have been affected by geological faults; there was a correlation of water chemistry between the surface and groundwater systems.
- The surface and groundwater interaction and transfer of constituents occurs mostly in the Middle Berg, and Lower Berg of the catchment.
- Nitrates in groundwaters are believed to be a result of agricultural activities as a result of the application of nitrate rich fertilizers, these nitrates can leach into the soil and, ultimately, groundwater.

Author Contributions

The authors confirm their contribution to the paper as follows:

Study conception and design: N. Malaza

Data collection: N. Malaza and S.P Mabokela

Analysis and interpretation of results: M. Malaza and S.P. Mabokela

Draft manuscript preparation: S.P. Mabokela

All authors reviewed the results and approved the final version of the manuscript.

Conflict of Interest

There is no conflict of interest.

Acknowledgement

The study was made possible by the CPUT University Research Fund (URF) and the South African Department of Water and Sanitation.

References

- [1] Lintern, A., Webb, J.A., Ryu, D., et al., 2018. Key factors influencing differences in stream water quality across space. *Wiley Interdisciplinary Reviews: Water*. 5(1), e1260.
- [2] Khatri, N., Tyagi, S., 2015. Influences of natural and anthropogenic factors on surface and groundwater quality in rural and urban areas. *Frontiers in Life Science*. 8(1), 23-39.
- [3] Madlala, T.E., 2015. Determination of groundwater-surface water interaction, upper Berg River catchment, South Africa [Master's thesis]. Cape Town: University of Western Cape.
- [4] Görgens, A.H.N., Clercq, W.P., 2005. Research on Berg River Management: Summary of Water Quality Information System and Soil Quality Studies [Internet]. Available from: <https://www.wrc.org.za/wp-content/uploads/mdocs/TT%20252.06.pdf>
- [5] Rossouw, N., Malan, S., 2007. The importance of theory in shaping social impact monitoring: Lessons from the Berg River Dam, South Africa. *Impact Assessment and Project Appraisal*. 25(4), 291-299.
- [6] Albhaisi, M., Brendonck, L., Batelaan, O., 2013. Predicted impacts of land use change on groundwater recharge of the upper Berg catchment, South Africa. *Water SA*. 39(2).
- [7] Berg River Improvement Plan 2012 [Internet]. Western Cape Government; 2012. Available from: https://www.westerncape.gov.za/eadp/sites/eadp.westerncape.gov.za/files/atoms/files/BRIP_Final%20Report_abridged.pdf
- [8] Cullis, J.D., Horn, A., Rossouw, N., et al., 2019. Urbanisation, climate change and its impact on water quality and economic risks in a water scarce and rapidly urbanising catchment: Case study of the Berg River Catchment. *H2Open Journal*. 2(1), 146-167.
- [9] DWAF., 2007. Berg River Baseline Monitoring Programme. Final Report—Volume 5: Synthesis. Pretoria, South Africa.
- [10] Midgley, D.C., Pitman, W.V., Middleton, B.J., 1994. Surface water resources of South Africa 1990. Water Research Commission: Pretoria.
- [11] Council for Geoscience, 2019. Geology map of South Africa. Council for Geoscience: Pretoria.
- [12] Kisters, A., 2016. What Lies Beneath Table Mountain or All Models are Wrong, But Some are Useful [Internet]. Available from: <https://www.sun.ac.za/english/Inaugurallectures/Inaugural%20lectures/InauguralLectureProfAlex-Kisters.pdf>
- [13] Nitsche, N., Kamish, W., Gorgens., AHM. 2006. Research on Berg River Water Management Volume 1: Application of Hydrodynamic River Flow and Reservoir Water Quality Models to the Berg River System [Internet]. Available from: <https://www.wrc.org.za/wp-content/uploads/mdocs/951-1-06.pdf>
- [14] Makiwane, N., 2019. Characterisation of the deep aquifers of South Africa-the Karoo Supergroup and Table Mountain Group [Ph.D. thesis]. Bloemfontein: University of the Free State.
- [15] Duah, A.A., 2010. Sustainable utilisation of Table Mountain Group aquifers [Ph.D. thesis]. Cape Town: University of the Western Cape.
- [16] Rosewarne, P., Weaver, J.M.C., 2002. Identification of Targets for Drilling in Table Mountain Group Aquifers. A Synthesis of the Hydrogeology of the Table Mountain Group—Formation of a Research Strategy [Internet]. Available from: <https://www.wrc.org.za/wp-content/uploads/mdocs/TT-158-01.pdf>

ARTICLE

Comparison of Machine Learning Methods for Satellite Image Classification: A Case Study of Casablanca Using Landsat Imagery and Google Earth Engine

Hafsa Ouchra^{1*}, Abdessamad Belangour¹, Allae Erraissi²

¹ Laboratory of Information Technology and Modeling LTIM, Hassan II University, Faculty of Sciences Ben M'sik, Casablanca, 20670, Morocco

² Chouaib Doukkali University, Polydisciplinary Faculty of Sidi Bennour, El Jadida, 24000, Morocco

ABSTRACT

Satellite image classification is crucial in various applications such as urban planning, environmental monitoring, and land use analysis. In this study, the authors present a comparative analysis of different supervised and unsupervised learning methods for satellite image classification, focusing on a case study in Casablanca using Landsat 8 imagery. This research aims to identify the most effective machine-learning approach for accurately classifying land cover in an urban environment. The methodology used consists of the pre-processing of Landsat imagery data from Casablanca city, the authors extract relevant features and partition them into training and test sets, and then use random forest (RF), SVM (support vector machine), classification, and regression tree (CART), gradient tree boost (GTB), decision tree (DT), and minimum distance (MD) algorithms. Through a series of experiments, the authors evaluate the performance of each machine learning method in terms of accuracy, and Kappa coefficient. This work shows that random forest is the best-performing algorithm, with an accuracy of 95.42% and 0.94 Kappa coefficient. The authors discuss the factors of their performance, including data characteristics, accurate selection, and model influencing.

Keywords: Supervised learning; Unsupervised learning; Satellite image classification; Machine learning; Google Earth Engine

*CORRESPONDING AUTHOR:

Hafsa Ouchra, Laboratory of Information Technology and Modeling LTIM, Hassan II University, Faculty of Sciences Ben M'sik, Casablanca, 20670, Morocco; Email: ouchra.hafsa@gmail.com

ARTICLE INFO

Received: 27 August 2023 | Revised: 27 October 2023 | Accepted: 31 October 2023 | Published Online: 14 November 2023

DOI: <https://doi.org/10.30564/jees.v5i2.5928>

CITATION

Ouchra, H., Belangour, A., Erraissi, A., 2023. Comparison of Machine Learning Methods for Satellite Image Classification: A Case Study of Casablanca Using Landsat Imagery and Google Earth Engine. *Journal of Environmental & Earth Sciences*. 5(2): 118-134. DOI: <https://doi.org/10.30564/jees.v5i2.5928>

COPYRIGHT

Copyright © 2023 by the author(s). Published by Bilingual Publishing Group. This is an open access article under the Creative Commons Attribution-NonCommercial 4.0 International (CC BY-NC 4.0) License. (<https://creativecommons.org/licenses/by-nc/4.0/>).

1. Introduction

Accurate classification of satellite images plays an essential role in many fields such as urban management, environmental planning, precision agriculture, and natural resource monitoring ^[1]. With the rapid advance of machine learning, a wide range of methods has emerged to automate this complex and crucial task ^[2].

Casablanca, a dynamic and constantly growing metropolis, faces complex challenges in urban management and sustainable development. Accurate classification of satellite imagery ^[3] in this region is a major challenge to enable informed decisions on planning, land use, and environmental preservation. For these challenges, machine learning methods offer promising prospects by providing tools for extracting meaningful information from large amounts of imagery data.

In this context, this study proposes to compare machine learning methods for satellite image classification ^[4,5], focusing on a case study carried out in Casablanca using Landsat imagery data. This study aims to evaluate and compare the performance of different machine learning methods in the context of satellite image classification, using Landsat 8 OLI data ^[6] from Casablanca. We examine supervised learning methods ^[7] such as support vector machines (SVMs) ^[8] and random forest (RF) ^[9], gradient tree boost (GTB) ^[10], etc., as well as unsupervised learning methods ^[2] such as K-means ^[11] and Lvq ^[12] using the Google Earth Engine platform ^[13]. By evaluating these methods through appropriate performance metrics, we aim to identify the most suitable method for accurate land use classification in a complex urban environment.

The importance of this study lies in its contribution to the scientific literature, offering essential information to practitioners and researchers engaged in satellite image classification. The results of this study could guide the choice of appropriate methods for specific applications in urban areas like Casablanca. In addition, this research could inspire future improvements in the design of hybrid methods or the exploration of deep learning techniques to meet the

increasingly complex challenges of satellite image classification.

In the following sections, we detail the machine learning methods examined, the data used in this study, experimental protocols, and evaluation metrics. Finally, we present and discuss in depth the results obtained, while highlighting the implications and future perspectives arising from this in-depth comparison of machine learning methods for satellite image classification in Casablanca.

2. Related work

Numerous studies in the scientific literature have focused on land cover classification using various machine learning techniques ^[14], including CART ^[15], SVM ^[8], and random forest ^[9] classifiers for supervised learning. **Table 1** provides an overview of other related works.

Yang et al. ^[16] highlighted the advantages of automated monitoring programs based on remote sensing, such as early change detection, informed decision-making, and wide spatial coverage, making them valuable tools for resource management and decision-making.

Wahbi et al. ^[17] highlighted the evolution from simple algebraic methods to artificial intelligence-based techniques ^[18,19], such as machine learning and deep learning ^[20], to generate accurate and useful settlement data. They highlighted the challenge of information extraction and image classification, proposing a system for assigning classes to pixels in the input image.

Phan et al. ^[21] demonstrated that satellite image time series gave higher classification accuracies than single-date images in land cover studies over the last decade. They noted the importance of Google Earth Engine (GEE) in remote sensing applications due to its efficient temporal aggregation methods and cloud-based nature.

Although the literature review ^[14,22-24] indicates extensive research on land cover classification using GEE and various algorithms in European and Asian regions, there is little specific research for Morocco. This review is an opportunity for researchers to ex-

plore land cover classification in Casablanca, Morocco, using supervised and unsupervised algorithms by exploiting the advantages of the GEE platform^[13,25].

For unsupervised learning methods, previous work^[11,26-28] highlights the ability of unsupervised learning to autonomously identify and categorize distinct land-use classes, offering a data-driven approach to land-use analysis.

Land cover mapping in urban environments has received particular attention due to the challenges associated with dynamic and heterogeneous urban settings^[29]. Previous studies have highlighted the complexity of urban land cover analysis, including spectral heterogene-

ity, mixed pixels, and temporal changes^[30]. They also demonstrated the usefulness of Landsat data for urban land use analysis, leading to a better understanding of urban growth and dynamics^[31].

This research makes a valuable contribution to the field by examining six supervised and two unsupervised machine learning algorithms to broaden our understanding of land use dynamics in the region and to promote more comprehensive land use studies specific to the city of Casablanca and to compare in terms of accuracy and Kappa coefficient the effectiveness of each algorithm for the classification of different areas of Casablanca.

Table 1. Overview of related work.

Classification methods	Datasets satellite	Better methods from researcher study	References
<ul style="list-style-type: none"> • Maximum Likelihood • Minimum Distance • Mahalanobis Distance 	Landsat 7 ETM+ data	Maximum likelihood	[32]
<ul style="list-style-type: none"> • ISODATA • Maximum Likelihood • Hybrid Method 	Desert Outlay Datasets	Hybrid method	[33]
<ul style="list-style-type: none"> • Minimum Distance • Maximum Likelihood • K-Nearest Neighbour 	IRIS Plants Dataset	K-Nearest neighbour	[34]
<ul style="list-style-type: none"> • Maximum Likelihood • Minimum Distance • Parallelepiped • Maximum Likelihood 	Landsat 7 ETM+ Images	Maximum likelihood	[35]
<ul style="list-style-type: none"> • Support Vector Machine • Maximum Likelihood • Mahalanobis Distance • Minimum Distance • Spectral Information Divergence • Binary Codes • Parallelepiped 	Landsat 7 ETM+ data	Support vector machine	[36]
<ul style="list-style-type: none"> • Random Forest • Classification and regression tree • Gradient tree boost • Support vector machine • Minimum distance • Decision tree 	Landsat 8 OLI	Minimum distance	[14]

3. Study area and datasets

3.1 Casablanca study area

The study area for this research encompasses the vibrant urban landscape of Casablanca, a prominent

coastal city in Morocco. As the largest city in the country, Casablanca represents a dynamic hub of economic, cultural, and social activities. It is geographical features, urban expansion, and diverse land uses make it an ideal case study for evaluating and comparing machine learning methods for satellite

image classification.

Casablanca's geographical coordinates range from 33.5441° N latitude to 7.5864° W longitude. The city is situated along the northwestern coast of Morocco, overlooking the Atlantic Ocean as shown in **Figure 1**. The study area includes the densely populated urban core, and the surrounding suburban regions, capturing the intricacies of different land cover types and their interactions.

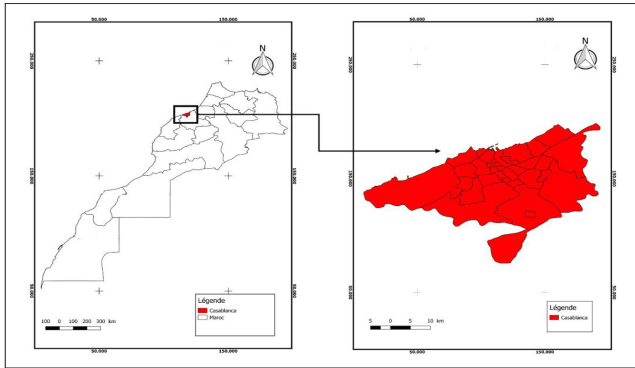


Figure 1. Casablanca study area.

3.2 Landsat 8 OLI dataset

Landsat imagery serves as the primary data source for this study. The Landsat satellites provide multispectral images with different wavelength bands, enabling the extraction of valuable information about land cover, vegetation, water bodies, and urban structures. These images have been collected over specific time frames, allowing the assessment of seasonal variations and changes in land use. This study collects Landsat images from 1-1-2021 to 31-12-2021.

The complex urban environment of Casablanca presents a rich array of land cover classes, including residential areas, industrial zones, commercial districts, green spaces, water bodies, and transportation networks. The diversity of these classes poses a significant challenge for accurate satellite image classification, highlighting the importance of selecting appropriate machine learning methods and techniques.

This study utilized Landsat 8 OLI satellite imagery for land cover mapping in the designated study area. For land cover classification, the study

obtained reflectance data from Landsat 8 OLI image bands spanning from January 1, 2021, to December 31, 2021. These images had a spatial resolution of 30 meters for bands B1 to B7. They were captured every 16 days using the GEE cloud platform, which offered data availability, storage, and advantages.

4. Methodology

Through the utilization of the methodology illustrated in **Figures 2 and 3**, researchers can proficiently employ both supervised and unsupervised machine learning algorithms for the classification of Landsat satellite images within the Google Earth Engine platform, enabling them to gain valuable insights into the dynamics of land use change and make informed decisions about urban planning and environmental management^[37]. Invariably, the first step of data pre-processing is shared between the methodologies of supervised and non-supervised algorithms.

• Data acquisition and preprocessing

We obtained Landsat 8 OLI satellite imagery^[38] for the target region, Casablanca, Morocco, from the Google Earth Engine data catalogue^[13], then pre-processed and filtered the imagery to correct for atmospheric distortions and radiometric calibration, to ensure data quality and consistency. We then selected January 1, 2021, to December 31, 2021, to capture the different land cover conditions and changes over time.

4.1 Workflow of supervised methods

• Data preparation and feature extraction

After the data acquisition stage, we moved on to the data preparation and feature extraction stage, in which we defined five land cover classes (built-up area, cropped area, forest area, barren area, and water body) based on the study objectives and the specific characteristics of our study area, these classes are presented in **Table 2**. Next, we created a representative training dataset by selecting sample pixels from the pre-processed imagery for each land-use class. The samples had to be accurately labeled using ground truth data or existing land cover maps.

Then we extracted from the Landsat 8 OLI imagery the spectral bands and indices that distinguish the different land cover types. The most common visible bands are B2, B3, and B4, the NIR band is B5 and the short-wave infrared bands are B6 and B7 (**Table 3**).

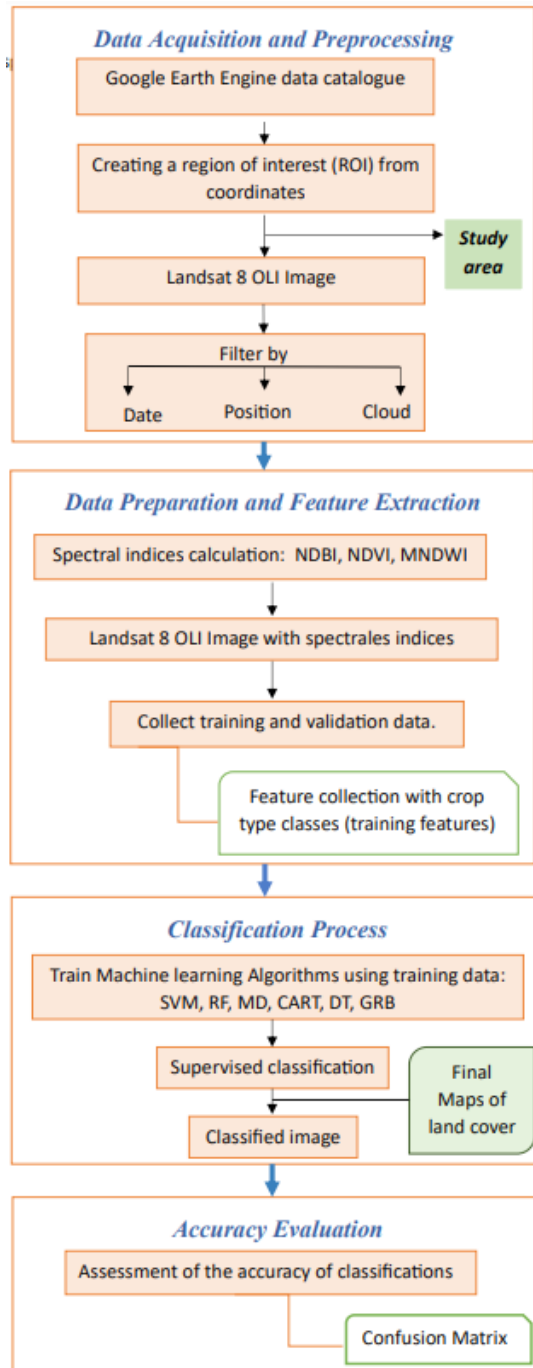


Figure 2. Workflow of the presented method.

• Training the models

In this step, we selected six supervised algorithms

to apply a land cover classification of the six classes (built-up area, cropped area, forest area, barren area, and water body) extracted in the previous step. The supervised machine learning algorithms chosen to classify the Casablanca study area are random forest (RF) ^[9], CART ^[15], support vector machine (SVM) ^[8], decision tree (DT) ^[15], minimum distance (MD) ^[39], and gradient tree boost (GTB) ^[10]. **Table 4** provides an overview of the parameters for each algorithm.

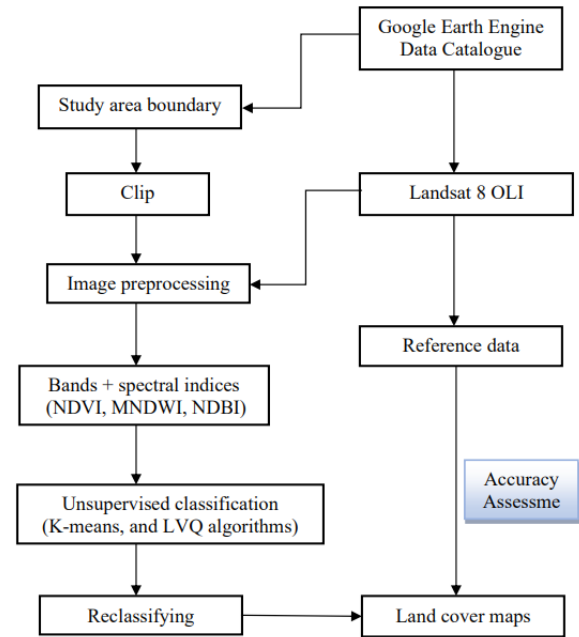


Figure 3. Workflow of methodology implemented in Google Earth Engine (GEE).

These algorithms are implemented in the Google Earth Engine platform using available built-in functions or custom scripts. We trained the supervised algorithms using the prepared training dataset. During training, the algorithms learn to associate the extracted features with the corresponding in these step land-use classes. Note that we have already divided the training data into training (80%) and validation (20%) sets to evaluate model performance during training and avoid over-fitting.

• Model evaluation

We evaluated the performance of the trained models using a validation dataset to measure their accuracy and generalization capabilities. Evaluation measures such as accuracy, producer accuracy, user accuracy, and coefficient Kappa. **Table 5** shows

these metrics.

- Land cover classification

Finally, we generated land-use maps and visualization outputs to evaluate the results and identify classification errors or ambiguities.

A confusion matrix ^[40] analysis was conducted for each method to evaluate the accuracy of the classified land cover maps generated by the supervised machine learning algorithms in GEE. The confusion matrix provided an overview of the accuracy assessment, and the metrics were presented in **Table A1**.

4.2 Workflow of unsupervised methods

The unsupervised learning methodology for mapping the land cover of Casablanca using Google

Earth Engine involves a sequence of steps encompassing data preparation, unsupervised clustering, interpretation, accuracy assessment, and visualization. The integration of Google Earth Engine's capabilities and satellite imagery facilitates efficient and accurate land cover classification within the urban context of Casablanca. The following steps describe the methodology shown in **Figure 3**:

- Region of interest (ROI) selection

Next, we defined the specific area of Casablanca that will be the focus of the classification. The ROI should encompass the land cover types of interest and account for the urban complexity of the city.

- Unsupervised learning algorithm

Subsequently, unsupervised learning algorithms,

Table 2. Land cover classes/references.

Land cover classes	Numbers of points	Description
Water_area	115	A water area refers to a geographical region or surface covered by various types of water bodies, such as oceans, seas, rivers, lakes, ponds, reservoirs, and wetlands.
Forest_area	174	A forest area refers to a large expanse of land characterized by dense vegetation dominated by trees, shrubs, and other woody plants. Forests are vital ecosystems that provide numerous ecological, economic, and social benefits.
Barren_area	150	Barren areas are characterized by minimal or no vegetation cover, and they can be found in various environments
Built-up_area	130	This class represents densely built urban areas with structures, buildings, roads, and other urban infrastructure.
Cropped_area	119	A cropped area, also known as cropland or agricultural land, refers to a specific portion of land that is actively used for cultivating crops and agricultural activities. In such areas, farmers engage in planting, growing, and harvesting various crops to produce food, fiber, and other agricultural products.
Total	688	

Table 3. Bands of Landsat 8 OLI satellite.

Bands			
Name	Spatial resolution (Pixel size) meters	Spectral resolution (µm)	Wavelength
B3	30	0.53-0.59	Green
B4	30	0.64-0.67	Red
B5	30	0.85-0.88	Near infrared (NIR)
B6	30	1.57-1.65	Shortwave infrared (SWIR 1)
B7	30	2.11-2.29	Shortwave infrared (SWIR 2)

Source: ^[38].

specifically k-means clustering^[43], and LVQ^[12] are applied to the pre-processed Landsat imagery.

K-means clustering^[11] is chosen for its capability to autonomously group pixels with similar spectral characteristics into distinct clusters, representing different land cover classes. The algorithm is initialized with a user-defined number of clusters and iteratively assigns pixels to the nearest cluster centroid based on spectral similarity. Google Earth Engine's cloud-based processing capabilities play a pivotal role in

the scalability of the methodology.

LVQ, or learning vector quantization^[12], is a supervised learning algorithm, but it always works with unlabeled data; it can also be said to be an unsupervised learning algorithm. It has been used to compare the differences between unsupervised and supervised learning algorithms. It uses a training data set to classify new data points according to their similarity to labeled examples in the training set. In this paper, we used LVQ as an unsupervised cluster-

Table 4. Parameters for each algorithm.

Machine learning algorithms type	Algorithms	Parameters	Description
Supervised algorithms	MD	metric = Mhalanobis	The distance metric to use.
	RF	numberOfTrees = 15	The number of decision trees to create.
	Cart	maxNodes = 15	The maximum number of leaf nodes in each tree
	SVM	kernel = linear	The kernel type. One of LINEAR ($\mathbf{u}' \times \mathbf{v}$), POLY ($(\gamma \times \mathbf{u}' \times \mathbf{v} + \mathbf{coef}_0)^{\text{degree}}$)
	DT	treeString	The decision tree, specified in the text format
	GTB	numberOfTrees = 15	The number of decision trees to create.
Unsupervised algorithms		nCluster = 5	The number of clusters.
	K-means	distanceFunction = Euclidean	Distance function to use.
	LVQ	numCluster = 5	The number of clusters.

Table 5. Evaluation metric equations for each classification.

Metrics	Equation	Description
(OA) Overall accuracy	$OA = \frac{\text{Number of correctly classified samples}}{\text{Number of samples}}$	It was used to determine the proportion of correctly mapped reference sites among all reference sites, expressed as a percentage. It was calculated by dividing the number of correctly classified samples by the total number of samples ^[40,41] .
(UA) User accuracy	$UA = \frac{\text{Correct imprevious surface pixel}}{\text{Correct} + \text{Misclassified pixel}}$	It represented the frequency with which the actual terrain features were correctly displayed on the classified map or the probability of correctly classifying a certain land cover in a ground area. It was calculated by dividing the number of accurately classified reference sites for a particular class by the total number of reference sites for that class ^[34] .
(PA) Producer accuracy	$PA = \frac{\text{Correct imprevious surface pixel}}{\text{Total imprevious pixels}}$	It indicated the reliability of the class on the map with respect to its presence in the field. It was calculated by dividing the total number of correct classifications for a specific class by the sum of correct and misclassified pixels for that class ^[34] .
Kappa coefficient	$K = \frac{P_{\text{accord}} - P_{\text{Hasard}}}{1 - P_{\text{Hasard}}}$	It provided an overall evaluation of the classification performance compared to random assignment. It ranged from -1 to 1 and was derived from a statistical test to evaluate the classification accuracy, determining if the classification performed better than random ^[42] . <ul style="list-style-type: none"> • The observation of inter-rater agreement is: P_{accord} • The overall probability that graders agree is: P_{Hasard}

ing algorithm to group pixels or data points based on their similarity. The LVQ algorithm in GEE works by iteratively adjusting a set of cluster prototypes to minimize the distance between prototypes and data points. It assigns each data point to the nearest prototype, effectively clustering the data into distinct groups. The platform efficiently computes clustering algorithms across Landsat imagery spatial and temporal coverage of Landsat imagery, enabling rapid analysis of the entire study area.

- Accuracy assessment and validation

Validation and accuracy assessment are integral components of the methodology. A stratified random sampling approach generates reference data points across the study area. These reference points are used to validate the accuracy of the unsupervised classification results. **Table 2** shows the reference data used. Various accuracy metrics, including overall accuracy and kappa coefficient, are calculated to quantify the agreement between the classified land cover map and the reference data.

- Visualization and mapping

The final step of the methodology involves visual interpretation and refinement. The unsupervised classification results are visually compared with high-resolution imagery and existing land cover maps to identify and rectify misclassifications or inconsistencies.

In summary, throughout the methodology, Google Earth Engine's computational capabilities are leveraged for efficient processing, enabling the analysis of large-scale Landsat datasets. The cloud-based nature of the platform facilitates scalability and accelerates data processing to achieve accurate land cover mapping in the urban environment of Casablanca.

5. Results and discussion

5.1 Supervised learning

The study area comprised multiple land cover classes (5 classes), as shown in **Table 2**, which required considerable computational effort in local computation mode.

Various classification methods ^[8-10,15,39] were applied to map the study area in Casablanca, including random forest (RF), classification and regression trees (CART), gradient tree boosting, support vector machine (SVM), minimum distance (MD), and decision trees (DT). The resulting land cover maps for each approach are displayed in **Figure 4**, and you'll find the legend showing the names of each classified class with its very visible color in **Figure 5**.

The performance of each classification method was evaluated using several metrics ^[13]: overall accuracy, user accuracy for each class, producer accuracy for each class, and the Kappa coefficient derived from the confusion matrix. The equations utilized for the computation of these metrics are illustrated in **Table A1**.

We have integrated spectral indices with the extracted features and Landsat image bands to guarantee high accuracy for each algorithm. These spectral indices are combinations of pixel values from multiple spectral bands in a multispectral image. These indices provide valuable information about the relative presence or absence of specific land cover types. One widely recognized index is the Normalized Difference Vegetation Index (NDVI) ^[33]. Besides NDVI, several other indices like the Modified Normalized Difference Water Index (MNDWI), among others, utilize various spectral bands to emphasize different phenomena such as vegetation, water, soil, etc. In this study, we employed three specific spectral indices ^[33]: NDVI for vegetation, soil, MNDWI for water, and Normalized Difference Built-up Index (NDBI) for built-up areas. **Table 6** outlines the formulas for calculating each of these indices.

This research incorporated the four spectral indices into the feature extraction phase and incorporated them integrated the training data creation process. During this step, the indices were computed and appended as additional spectral bands to enhance the classification outcomes for each classifier utilized in this project. By incorporating these indices, the study aimed to improve the classification accuracy and achieve more precise identification of land cover categories.

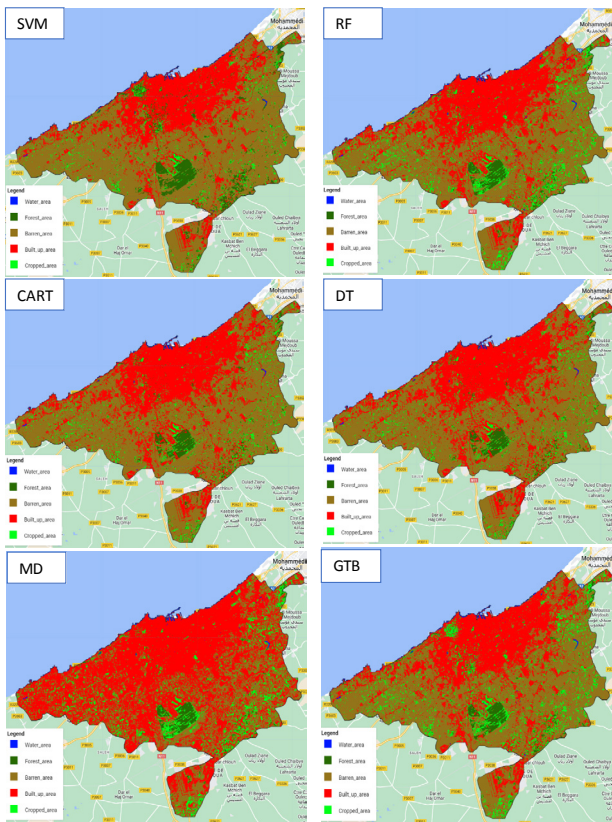


Figure 4. Classification results of Casablanca's land cover map.



Figure 5. Legend of classification results in the land cover mapping of Casablanca.

This study used Landsat 8 OLI datasets and processing tools, including the Google Earth Engine (GEE) platform, to map land cover categories in Casablanca. The study used various classifiers, such as CART, RF, SVM, Gradient Tree Boost, DT, and MD, to delineate the territory into different zones, including Water, Forest, Built-up, Barren, and Cropped areas.

Based on previous studies [9,14,16,19-23,46-52] and our own research, we found that the methodology em-

ployed in our experiment can be adapted to map and evaluate different regions in various countries or cities, as this methodology is not oriented solely toward Casablanca city. The main contribution of this research has been the successful adaptation of the method to map and evaluate land use in other regions or countries. Based on the confusion matrix for each classifier, it was evident that the random forest classifier was the most effective, boasting a Kappa coefficient of 0.94. This value is close to 1, indicating that the classification is significantly superior to random. Moreover, it achieved an accuracy of 95.42%, significantly higher than the accuracy of the other classifiers, which were 94.77%, 91.50%, 91.50%, 83%, and 93.46% for MD, DT, CART, SVM, and GTB, respectively. **Figure 6** shows the overall accuracy of these classifiers. The results for the DT and CART classifiers were very similar. However, the SVM classifier exhibited a considerably lower accuracy of 83% compared to the other classifiers, and its Kappa coefficient was 0.78.

Table 6. Spectral indices used.

Index	Equation	References
Normalized difference vegetation index (NDVI)	$NDVI = \frac{NIR - RED}{NIR + RED}$	[27]
Modified normalized difference water index (MNDWI)	$MNDWI = \frac{Green - SWIR1}{Green + SWIR1}$	[44]
Normalized difference built-up index (NDBI)	$NDBI = \frac{SWIR - NIR}{SWIR + NIR}$	[45]

The user and producer accuracy of random forest for a given class was generally different. For example, the built-up class showed a difference between the producer accuracy (84.61%) and user accuracy (91.66%), indicating that some areas were correctly identified as built-up areas. **Table A1** shows the land cover confusion matrix of each classifier. In the confusion matrix of the SVM classifier, which has high accuracy compared to other classifiers, we found the producer's accuracy for the cropped class was 50%. By comparison, **Table A1** reveals that the user

achieved an accuracy of 86.66%. This signifies that only half of the reference cropped areas were accurately identified as such, while 86.66% of the areas classified as cropped were indeed cropped.

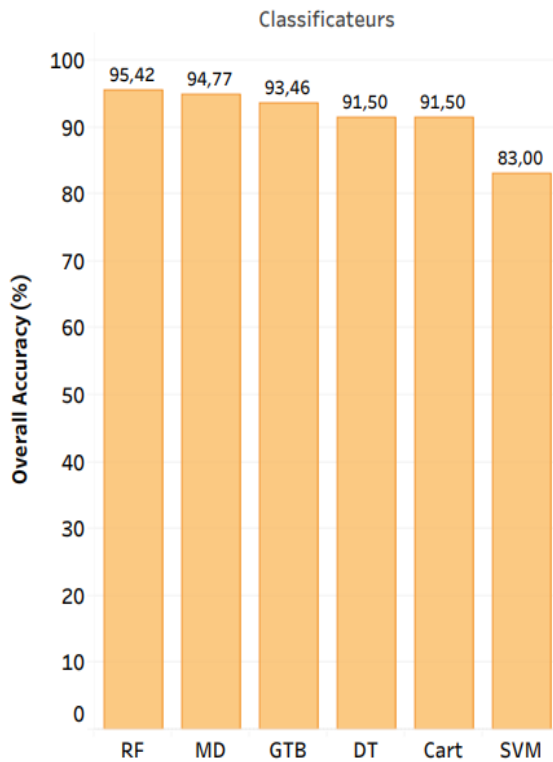


Figure 6. The overall accuracy (OA) of different methods.

The study also incorporated spectral indices, such as NDVI, MNDWI, and NDBI, to enhance land cover classification. These indices were useful in separating different land cover characteristics in Casablanca, including vegetation, water, soil, and built-up areas. Each index had its calculation equation, as detailed in **Table 6**.

Overall, the research demonstrated that some classes achieved high accuracy. In contrast, others had relatively poorer accuracy, indicating the complexity and challenges of land cover classification in diverse regions and environmental conditions.

5.2 Unsupervised learning

This section presents the results and subsequent analysis of the Weka K-means and Lvq algorithm applied in Google Earth Engine (GEE) for land cover mapping of Casablanca using Landsat 8 OLI satellite

data for the specified period 1-1-2021 to 31-12-2021. The image was segmented into five distinct land-use classes: water, forest, cultivated areas, barren land, and built-up areas. Performance metrics, including accuracy and Kappa coefficient, provide insight into the effectiveness of these algorithms. **Table 5** shows the equations for these evaluation metrics.

In the Google Earth Engine platform, clusters are used the same way as classifiers. The training data are feature collection properties, fed into the cluster. Unlike classifiers, there is no input class value for a cluster file. The general clustering workflow we followed in this paper is presented in **Figure 3**: First, we collected features with numerical properties in which we searched for clusters, second, we instantiated our cluster and trained the cluster using the training data, then we applied the cluster to the Landsat satellite image of our study area (Casablanca) and finally we labeled the clusters.

In this study, several underlying factors contribute to the accuracy achieved by the K-means and Lvq algorithm:

- **Spectral discrimination:** The ability of the algorithm to discriminate between land-use classes is highly dependent on the selection of spectral bands and derived indices. Making an informed choice of features with high discriminating power.
- **Number of clusters (K):** Determining the optimum number of clusters (K) is essentially crucial. An inappropriate choice can lead to classes being merged or split, affecting classification accuracy.
- **Spectral similarity:** Spectral similarity between certain land use classes can confuse and reduce classification accuracy.

Based on the results obtained by the algorithms used, it can be concluded that unsupervised methods do not achieve optimum performance in the classification and clustering of satellite images for land cover mapping. Supervised approaches, on the other hand, achieve significantly higher accuracy rates. Nevertheless, in the context of this study, considerable efforts have been made to improve the performance of the K-means and Lvq algorithms. Before the application of techniques to improve data quality,

the results of K-means and Lvq had demonstrated particularly low accuracy, amounting to 31.47% and 19.96%, respectively, with a Kappa coefficient of 0.14 and 0.0009, respectively, as shown in **Table 7**. The land-use maps obtained for each algorithm are shown in **Figure 7**.

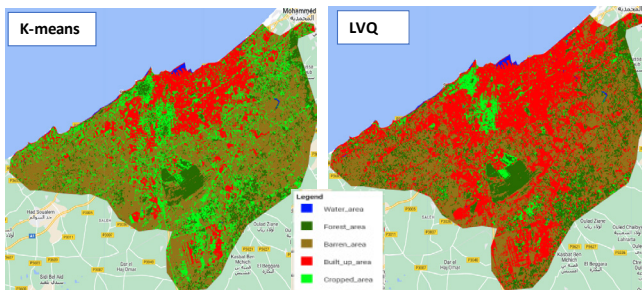


Figure 7. Land cover classification of Casablanca of each algorithm.

To improve these results, a series of improvements were made to the pre-processing stages. Atmospheric correction and cloud removal were applied to enhance source data quality. Next, integrating spectral indices such as NDBI, NDVI, and WNDVI was carried out in conjunction with the image bands. We were incorporating these indices aimed to increase separability between the different classes. **Table 6** shows the equations for these spectral indices.

This approach proved to generate a clear improvement in the accuracy of the K-means algorithm, reaching an accuracy of 38.66% with 0.06 Kappa coefficients, and for the LVQ algorithm, unfortunately, we have a poor accuracy of 26.01% with Kappa coefficients of 0.06. **Figure 8** illustrates these results.

This improvement reflects moderate accuracy but represents significant advances in the initial results. From these results, we can say that the K-means algorithm performs better than the Lvq algorithm, but we concluded that unsupervised learning algorithms do not perform well for land cover mapping. On the other hand, in these previous studies and my previous work ^[14], we demonstrated that supervised learning algorithms perform well for satellite image classification and land cover mapping.

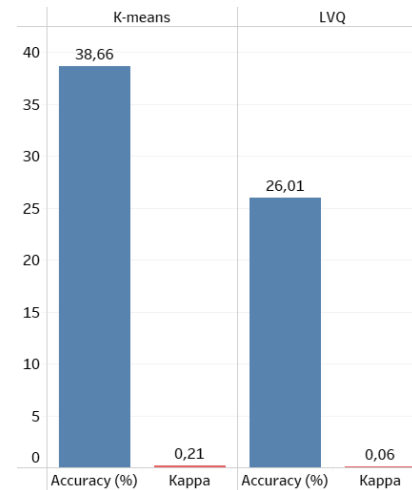


Figure 8. The overall accuracy and Kappa coefficient values of each adopted algorithm.

5.3 Comparison results of supervised and unsupervised methods

According to the results presented in the previous sections, the random forest classifier outperformed the other supervised and unsupervised learning algorithms, achieving an accuracy of 95.42% and a Kappa coefficient of 0.94, indicating its significant superiority over the other classifiers.

The analysis involved comparing the accuracy of each classifier using confusion matrices and various measures such as overall accuracy (OA), user accuracy (UA), producer accuracy (PA), and Kappa coefficient, as shown in **Table 5**. The results showed that the random forest classifier consistently outperformed and outperformed the other algorithms in terms of accuracy and Kappa coefficient, achieving an accuracy of 95.42%, significantly higher than that of the other supervised and unsupervised algorithms, which were 94.77%, 91.50%, 91.50%, 83%, 93.46%, 38.66%, and 26.01% for MD, DT, CART, SVM, GTB, K-means, and Lvq respectively.

As shown in **Table 7**, the SVM classifier showed a significantly lower accuracy of 83% compared to the other supervised algorithms. Its Kappa coefficient was 0.78, while for the non-supervised algorithms, the results indicate that K-means and Lvq showed

particularly low accuracy, amounting to 31.47% and 19.96%, respectively, with Kappa coefficients of 0.14 and 0.0009, respectively.

These results allow us to assert that supervised learning algorithms perform better for land cover mapping

than non-supervised learning algorithms. In this work, we have demonstrated that the supervised random forest algorithm outperforms all other algorithms, and that supervised learning algorithms perform well for satellite image classification and land cover mapping.

Table 7. Overall accuracy and Kappa coefficient of each supervised and unsupervised method.

Evaluation metrics	Supervised methods						Unsupervised methods	
	SVM	Cart	RF	GTB	DT	MD	K-means	LVQ
Overall accuracy %	83	91.50	95.42	93.46	91.50	94.77	38.66	26.01
Kappa coefficient	0.78	0.89	0.94	0.91	0.89	0.93	0.21	0.06

6. Conclusions and prospects

In summary, this study highlights the importance of methodological selection in achieving accurate classification of satellite imagery and underlines the need for context-sensitive assessments. The results of this research have significant implications for improving land use mapping, urban planning, and environmental management in similar areas of Casablanca. This study provides useful information for selecting appropriate machine-learning methods for satellite image classification in urban areas like Casablanca. By highlighting the advantages and disadvantages of each technique, we offer practical advice to practitioners and researchers.

This work carried out an in-depth evaluation of various supervised and unsupervised algorithms for the classification of Landsat satellite images in the Casablanca region of Morocco. The aim was to assess the ability of these algorithms to represent various land cover categories. Based on the results presented in this work, accurately the reliability and versatility of the GEE platform, with its cloud-based architecture, eliminates the need to integrate other external and often commercial software. According to the experimental results, the supervised random forest algorithm achieved high accuracy. This success can be attributed to the supervised learning methodology, which involves the collection of training and validation points in the study area. This approach improves the classification process of

the study area. This study differs from the existing literature in that previous work has mainly focused on specific phenomena in various study areas in Morocco or other cities and countries.

For future work, the study will explore integrating hybrid methods and exploration of more advanced neural networks, which offer increased efficiency in the classification of satellite images to achieve a more accurate classification of land cover and detection of urban areas in the Casablanca study area in Morocco.

Author Contributions

Hafsa Ouchra designed and processed the data, analyzed the proposed methods, and edited the manuscript; Abdessamad Belangour interpreted and discussed the results; Allae Erraissi revised the manuscript.

Conflict of Interest

All authors have read and agreed to the published version of the manuscript.

Funding

This research received no external funding.

References

- [1] Ouchra, H., Belangour, A., Erraissi, A. (editors),

2023. An overview of GeoSpatial Artificial Intelligence technologies for city planning and development. 2023 Fifth International Conference on Electrical, Computer and Communication Technologies (ICECCT); 2023 Feb 22-24; Erode, India. New York: IEEE. p. 1-7.
DOI: <https://doi.org/10.1109/ICECCT56650.2023.10179796>
- [2] Ouchra, H., Belangour, A. (editors), 2021. Satellite image classification methods and techniques: A survey. 2021 IEEE International Conference on Imaging Systems and Techniques (IST); 2021 Aug 24-26; Kaohsiung, Taiwan. New York: IEEE. p. 1-6.
DOI: <https://doi.org/10.1109/IST50367.2021.9651454>
- [3] Ouchra, H., Belangour, A., Erraissi, A., 2022. A comparative study on pixel-based classification and object-oriented classification of satellite image. *International Journal of Engineering Trends and Technology*. 70(8), 206-215.
DOI: <https://doi.org/10.14445/22315381/IJETT-V70I8P221>
- [4] Ouchra, H., Belangour, A., Erraissi, A. (editors), 2022. Satellite data analysis and geographic information system for urban planning: A systematic review. 2022 International Conference on Data Analytics for Business and Industry (ICDABI); 2022 Oct 25-26; Sakhir, Bahrain. New York: IEEE. p. 558-564.
DOI: <https://doi.org/10.1109/ICDABI56818.2022.10041487>
- [5] Ouchra, H., Belangour, A., Erraissi, A. (editors), 2022. Spatial data mining technology for GIS: A review. 2022 International Conference on Data Analytics for Business and Industry (ICDABI); 2022 Oct 25-26; Sakhir, Bahrain. New York: IEEE. p. 655-659.
DOI: <https://doi.org/10.1109/ICDABI56818.2022.10041574>
- [6] Landsat Data Access [Internet]. U.S. Geological Survey [cited 2022 Aug 20]. Available from: https://www.usgs.gov/landsat-missions/landsat-data-access?qt-science_support_page_related_con=0#qt-science_support_page_related_con
- [7] Ouchra, H., Belangour, A., Erraissi, A. (editors), 2022. Machine learning for satellite image classification: A comprehensive review. 2022 International Conference on Data Analytics for Business and Industry (ICDABI); 2022 Oct 25-26; Sakhir, Bahrain. New York: IEEE. p. 1-5.
DOI: <https://doi.org/10.1109/ICDABI56818.2022.10041606>
- [8] Awad, M. (editor), 2021. Google Earth Engine (GEE) cloud computing based crop classification using radar, optical images and Support Vector Machine Algorithm (SVM). 2021 IEEE 3rd International Multidisciplinary Conference on Engineering Technology (IMCET); 2021 Dec 8-10; Beirut, Lebanon. New York: IEEE. p. 71-76.
DOI: <https://doi.org/10.1109/IMCET53404.2021.9665519>
- [9] Magidi, J., Nhamo, L., Mpandeli, S., et al., 2021. Application of the random forest classifier to map irrigated areas using google earth engine. *Remote Sensing*. 13(5), 876.
DOI: <https://doi.org/10.3390/RS13050876>
- [10] Natekin, A., Knoll, A., 2013. Gradient boosting machines, a tutorial. *Frontiers in Neurorobotics*. 7, 21.
DOI: <https://doi.org/10.3389/fnbot.2013.00021>
- [11] Ali, I., Rehman, A.U., Khan, D.M., et al., 2022. Model selection using K-means clustering algorithm for the symmetrical segmentation of remote sensing datasets. *Symmetry*. 14(6), 1149.
DOI: <https://doi.org/10.3390/sym14061149>
- [12] Artelt, A., Hammer, B., 2019. Efficient computation of counterfactual explanations of LVQ models. *arXiv preprint arXiv:1908.00735*.
- [13] Gorelick, N., Hancher, M., Dixon, M., et al., 2017. Google Earth Engine: Planetary-scale geospatial analysis for everyone. *Remote Sensing of Environment*. 202, 18-27.
DOI: <https://doi.org/10.1016/j.rse.2017.06.031>
- [14] Ouchra, H.A.F.S.A., Belangour, A., Erraissi, A.L.L.A.E., 2023. Machine learning algorithms for satellite image classification using Google Earth Engine and Landsat satellite data: Moroc-

- co case study. *IEEE Access*. 11, 71127-71142.
DOI: <https://doi.org/10.1109/ACCESS.2023.3293828>
- [15] Hu, Y., Dong, Y., 2018. An automatic approach for land-change detection and land updates based on integrated NDVI timing analysis and the CVAPS method with GEE support. *ISPRS Journal of Photogrammetry and Remote Sensing*. 146, 347-359.
DOI: <https://doi.org/10.1016/J.ISPRSJPRS.2018.10.008>
- [16] Yang, L., Driscoll, J., Sarigai, S., et al., 2022. Google Earth Engine and artificial intelligence (AI): A comprehensive review. *Remote Sensing*. 14(14), 3253.
DOI: <https://doi.org/10.3390/RS14143253>
- [17] Wahbi, M., El Bakali, I., Ez-zahouani, B., et al., 2023. A deep learning classification approach using high spatial satellite images for detection of built-up areas in rural zones: Case study of Souss-Massa region-Morocco. *Remote Sensing Applications: Society and Environment*. 29, 100898.
DOI: <https://doi.org/10.1016/J.RSASE.2022.100898>
- [18] Taji, K., Ait Abdelouahid, R., Ezzahoui, I., et al. (editors), 2021. Review on architectures of aquaponic systems based on the Internet of Things and artificial intelligence: Comparative study. *Proceedings of the 4th International Conference on Networking, Information Systems & Security*; 2021 Apr 1-2; KENITRA AA Morocco. New York: Association for Computing Machinery. p. 1-9.
DOI: <https://doi.org/10.1145/3454127.3457625>
- [19] Ouchra, H., Belangour, A., 2021. Object detection approaches in images: A survey. *Thirteenth International Conference on Digital Image Processing (ICDIP 2021)*. 11878, 132-141.
DOI: <https://doi.org/10.1117/12.2601452>
- [20] Ouchra, H., Belangour, A., 2021. Object detection approaches in images: A weighted scoring model based comparative study. *International Journal of Advanced Computer Science and Applications(IJACSA)*. 12(8).
- [21] Phan, T.N., Kuch, V., Lehnert, L.W., 2020. Land cover classification using Google Earth Engine and random forest classifier—The role of image composition. *Remote Sensing*. 12(15), 2411.
DOI: <https://doi.org/10.3390/RS12152411>
- [22] Mahyoub, S., Rhinane, H., Fadil, A., et al. (editors), 2020. Using of open access remote sensing data in google earth engine platform for mapping built-up area in Marrakech City, Morocco. 2020 IEEE International Conference of Moroccan Geomatics, MORCEO; 2020 May 11-13; Casablanca, Morocco. New York: IEEE.
DOI: <https://doi.org/10.1109/MORCEO49228.2020.9121912>
- [23] Sellami, E.M., Rhinane, H.A.S.S.A.N., 2023. A new approach for mapping land use/land cover using Google Earth Engine: A comparison of composition images. *The International Archives of the Photogrammetry, Remote Sensing and Spatial Information Sciences*. 48, 343-349.
DOI: <https://doi.org/10.5194/isprs-archives-XLVIII-4-W6-2022-343-2023>
- [24] Chemchaoui, A., Brhadda, N., Alaoui, H.I., et al. 2023. Accuracy assessment and uncertainty of the 2020 10-meter resolution land use land cover maps at local scale. Case: talassemtane national park, Morocco.
DOI: <https://doi.org/10.21203/rs.3.rs-2953599/v2>
- [25] Pérez-Cutillas, P., Pérez-Navarro, A., Conesa-García, C., et al., 2023. What is going on within google earth engine? A systematic review and meta-analysis. *Remote Sensing Applications: Society and Environment*. 29, 100907.
DOI: <https://doi.org/10.1016/j.rsase.2022.100907>
- [26] Jamali, A., 2019. Evaluation and comparison of eight machine learning models in land use/land cover mapping using Landsat 8 OLI: A case study of the northern region of Iran. *SN Applied Sciences*. 1(11), 1448.
DOI: <https://doi.org/10.1007/s42452-019-1527-8>
- [27] Duda, T., Canty, M., 2002. Unsupervised classification of satellite imagery: Choosing a good algorithm. *International Journal of Remote Sensing*. 23(11), 2193-2212.

- DOI: <https://doi.org/10.1080/01431160110078467>
- [28] Celik, T., 2009. Unsupervised change detection in satellite images using principal component analysis and k-means clustering. *IEEE Geoscience and Remote Sensing Letters*. 6(4), 772-776.
DOI: <https://doi.org/10.1109/LGRS.2009.2025059>
- [29] Zurqani, H.A., Post, C.J., Mikhailova, E.A., et al., 2019. Mapping urbanization trends in a forested landscape using Google Earth Engine. *Remote Sensing in Earth Systems Sciences*. 2, 173-182.
DOI: <https://doi.org/10.1007/s41976-019-00020-y>
- [30] Masek, J.G., Huang, C., Wolfe, R., et al., 2008. North American forest disturbance mapped from a decadal Landsat record. *Remote Sensing of Environment*. 112(6), 2914-2926.
DOI: <https://doi.org/10.1016/j.rse.2008.02.010>
- [31] Duro, D.C., Franklin, S.E., Dubé, M.G., 2012. A comparison of pixel-based and object-based image analysis with selected machine learning algorithms for the classification of agricultural landscapes using SPOT-5 HRG imagery. *Remote Sensing of Environment*. 118, 259-272.
DOI: <https://doi.org/10.1016/j.rse.2011.11.020>
- [32] Madhura, M., Venkatachalam, S., 2015. Comparison of supervised classification methods on remote sensed satellite data: An application in Chennai, South India. *International Journal of Science and Research*. 4(2), 1407-1411.
- [33] Rozenstein, O., Karnieli, A., 2011. Comparison of methods for land-use classification incorporating remote sensing and GIS inputs. *Applied Geography*. 31(2), 533-544.
DOI: <https://doi.org/10.1016/J.APGEOG.2010.11.006>
- [34] Kalra, K., Goswami, A.K., Gupta, R., 2013. A comparative study of supervised image classification algorithms for satellite images. *International Journal of Electrical, Electronics and Data Communication*. 1(10), 10-16.
- [35] Akgün, A., Eronat, A.H., Türk, N., 2004. Comparing different satellite image classification methods: an application in Ayvalik District, Western Turkey [Internet]. Available from: <https://www.isprs.org/PROCEEDINGS/XXXV/congress/comm4/papers/505.pdf>
- [36] Niknejad, M., Zadeh, V.M., Heydari, M., 2014. Comparing different classifications of satellite imagery in forest mapping (case study: Zagros forests in Iran). *International Research Journal of Applied and Basic Sciences*. 8(9), 1407-1415.
- [37] Ouchra, H., Belangour, A., Erraissi, A., 2022. A comprehensive study of using remote sensing and geographical information systems for urban planning *Internetworking Indonesia Journal*. 14(1), 15-20.
- [38] Landsat 8 Bands [Internet]. Landsat Science [cited 2023 Oct 26]. Available from: <https://landsat.gsfc.nasa.gov/satellites/landsat-8/landsat-8-bands/#>
- [39] Borra, S., Thanki, R., Dey, N., 2019. Satellite image analysis: Clustering and classification. Springer: Singapore.
- [40] Jayaswal, V., 2020. Performance Metrics: Confusion Matrix, Precision, Recall, and F1 Score [Internet]. Towards Data Science [cited 2023 Aug 10]. Available from: <https://towardsdatascience.com/performance-metrics-confusion-matrix-precision-recall-and-f1-score-a8fe076a2262>
- [41] Heydarian, M., Doyle, T.E., Samavi, R., 2022. MLCM: Multi-label confusion matrix. *IEEE Access*. 10, 19083-19095.
DOI: <https://doi.org/10.1109/ACCESS.2022.3151048>
- [42] Coefficient Kappa de Cohen (K) [Internet] [cited 2023 Aug 10]. Available from: <https://www.irdp.ch/institut/coefficient-kappa-cohen-2039.html>
- [43] Abbas, A.W., Minallh, N., Ahmad, N., et al., 2016. K-Means and ISODATA clustering algorithms for landcover classification using remote sensing. *Sindh University Research Journal-SURJ (Science Series)*. 48(2), 315-318.
- [44] Mfondoum, A.H.N., Etouna, J., Nongsi, B.K., et al., 2016. Assessment of land degradation status and its impact in arid and semi-arid areas by correlating spectral and principal component analysis neo-bands. *International Journal*. 5(2),

- 1539-1560.
- [45] NDBI—ArcGIS Pro [Internet] [cited 2023 May 19]. Available from: <https://pro.arcgis.com/en/pro-app/latest/arcpy/spatial-analyst/ndbi.htm>
- [46] Shafaey, M.A., Salem, M.A.M., Ebied, H.M., et al. (editors), 2018. Deep learning for satellite image classification. International Conference on Advanced Intelligent Systems and Informatics; 2018 Sep 1-3; Cairo, Egypt. Cham: Springer International Publishing. p. 383-391. DOI: https://doi.org/10.1007/978-3-319-99010-1_35
- [47] Warf, B., 2014. Supervised classification. Encyclopedia of Geography. Sage: Thousand Oaks, California. DOI: <https://doi.org/10.4135/9781412939591.n1101>
- [48] Würsch, L., Hurni, K., Heinimann, A., 2017. Google Earth Engine Image Pre-processing Tool: User Guide [Internet] [cited 2022 Dec 13]. Available from: https://www.cde.unibe.ch/e65013/e542846/e707304/e707386/e707390/CDE_Pre-processingTool-UserGuide_eng.pdf
- [49] El Imanni, H.S., El Harti, A., Bachaoui, E.M., et al., 2023. Multispectral UAV data for detection of weeds in a citrus farm using machine learning and Google Earth Engine: Case study of Morocco. Remote Sensing Applications: Society and Environment. 30, 100941. DOI: <https://doi.org/10.1016/J.RSASE.2023.100941>
- [50] Chen, H., Yunus, A.P., Nukapothula, S., et al., 2022. Modelling Arctic coastal plain lake depths using machine learning and Google Earth Engine. Physics and Chemistry of the Earth, Parts A/B/C. 126, 103138. DOI: <https://doi.org/10.1016/J.PCE.2022.103138>
- [51] Amani, M., Ghorbanian, A., Ahmadi, S.A., et al., 2020. Google earth engine cloud computing platform for remote sensing big data applications: A comprehensive review. IEEE Journal of Selected Topics in Applied Earth Observations and Remote Sensing. 13, 5326-5350. DOI: <https://doi.org/10.1109/JSTARS.2020.3021052>
- [52] Tassi, A., Vizzari, M., 2020. Object-oriented lulc classification in google earth engine combining snic, glcm, and machine learning algorithms. Remote Sensing. 12(22), 3776. DOI: <https://doi.org/10.3390/rs12223776>

Appendix

Table A1. Land cover evaluation metrics of each classifier.

SVM				
	PA	UA	OA	Kappa
Water_area	100	100		
Barren_area	100	77.35		
Forest_area	82.75	75	83	0.78
Built-up_area	69.23	81.81		
Cropped_area	50	86.66		
Cart				
	PA	UA	OA	Kappa
Water_area	100	100		
Barren_area	95.12	97.5		
Forest_area	89.65	81.25	91.50	0.89
Built-up_area	76.92	83.33		
Cropped_area	92.30	92.30		

Table A1 continued

RF				
	PA	UA	OA	Kappa
Water_area	100	100		
Barren_area	97.56	100		
Forest_area	93.10	90	95.42	0.94
Built-up_area	84.61	91.66		
Cropped_area	100	92.85		
GTB				
	PA	UA	OA	Kappa
Water_area	100	100		
Barren_area	97.56	100		
Forest_area	79.31	92	93.46	0.91
Built-up_area	88.46	79.31		
Cropped_area	100	92.85		
DT				
	PA	UA	OA	Kappa
Water_area	100	100		
Barren_area	95.12	97.5		
Forest_area	89.65	81.25	91.50	0.89
Built-up_area	76.92	83.33		
Cropped_area	92.30	92.30		
MD				
	PA	UA	OA	Kappa
Water_area	100	100		
Barren_area	95.12	100		
Forest_area	86.20	92.59	94.77	0.93
Built-up_area	92.30	88.88		
Cropped_area	100	89.65		



Tel: +65 65881289

E-mail: contact@bilpublishing.com

Website: <https://journals.bilpubgroup.com>

2661-3190



9 772661 319234